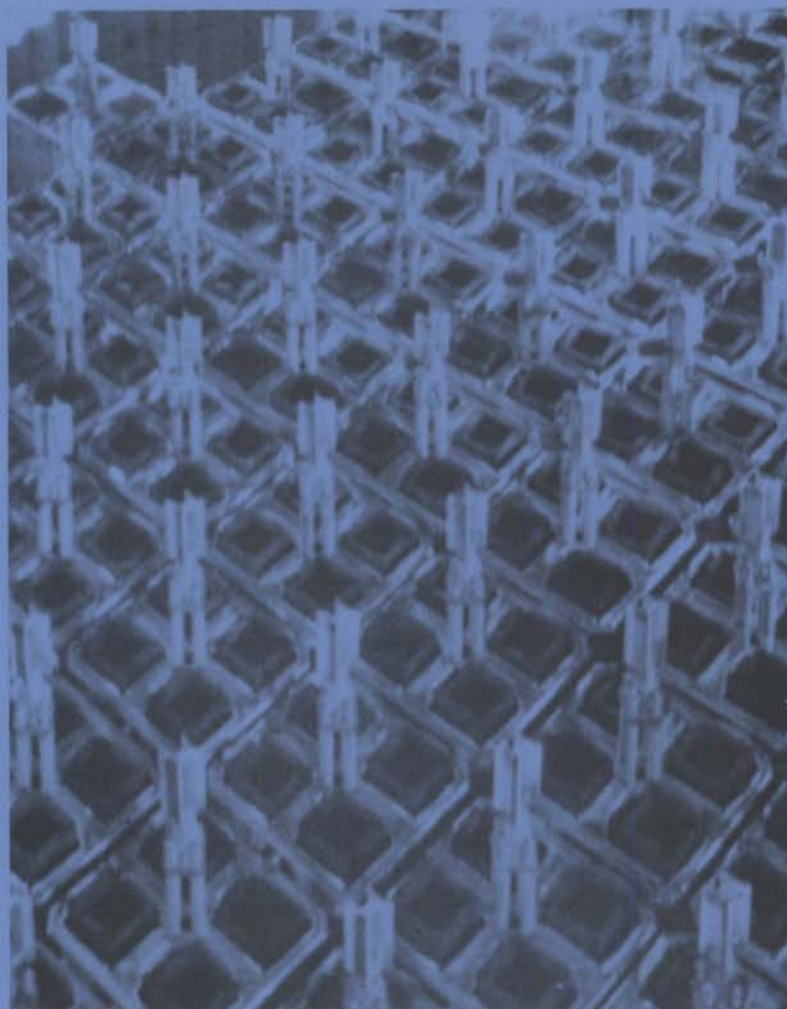


**BWR Spent Fuel Storage Cask Performance Test**

**Volume I**

2F

**Cask Handling Experience  
and Decay Heat, Heat Transfer,  
and Shielding Data**



**February 1986**

**Prepared for the U.S. Department of Energy  
under Contract DE-AC06-76RLO 1830**

**Pacific Northwest Laboratory  
Operated for the U.S. Department of Energy  
by Battelle Memorial Institute**



## DISCLAIMER

This report was prepared as an account of work sponsored by an agency of the United States Government. Neither the United States Government nor any agency thereof, nor any of their employees, makes any warranty, express or implied, or assumes any legal liability or responsibility for the accuracy, completeness, or usefulness of any information, apparatus, product, or process disclosed, or represents that its use would not infringe privately owned rights. Reference herein to any specific commercial product, process, or service by trade name, trademark, manufacturer, or otherwise, does not necessarily constitute or imply its endorsement, recommendation, or favoring by the United States Government or any agency thereof. The views and opinions of authors expressed herein do not necessarily state or reflect those of the United States Government or any agency thereof.

PACIFIC NORTHWEST LABORATORY  
*operated by*  
BATTELLE  
*for the*  
UNITED STATES DEPARTMENT OF ENERGY  
*under Contract DE-AC06-76RLO 1830*

Printed in the United States of America  
Available from  
National Technical Information Service  
United States Department of Commerce  
5285 Port Royal Road  
Springfield, Virginia 22161

NTIS Price Codes  
Microfiche A01

### Printed Copy

Pages	Price Codes
001-025	A02
026-050	A03
051-075	A04
076-100	A05
101-125	A06
126-150	A07
151-175	A08
176-200	A09
201-225	A010
226-250	A011
251-275	A012
276-300	A013

BWR SPENT FUEL STORAGE CASK PERFORMANCE TEST

VOLUME I

CASK HANDLING EXPERIENCE AND DECAY HEAT,  
HEAT TRANSFER, AND SHIELDING DATA

M. A. McKinnon  
J. W. Doman(a)  
J. E. Tanner  
R. J. Guenther  
J. M. Creer  
C. E. King(a)

February 1986

Prepared for  
the U.S. Department of Energy  
under Contract DE-AC06-76RLO 1830

Pacific Northwest Laboratory  
Richland, Washington 99352

---

(a) General Electric-Morris Operation, Morris, Illinois





## ACKNOWLEDGMENTS

The authors would like to acknowledge those individuals from the U.S. Department of Energy (DOE), the Pacific Northwest Laboratory (PNL), General Electric's Morris Operation (GE-MO), Nebraska Public Power District (NPPD), Los Alamos National Laboratory (LANL), Lawrence Livermore National Laboratory (LLNL), and the Electric Power Research Institute (EPRI) who contributed to the project.

Appreciation is extended to Jim Daily and Phil Craig of DOE's Richland Operations Office for sponsoring this work. Dale Oden, Jr., Darrell Newman, and Gordon Beeman of the Commercial Spent Fuel Management program office managed by PNL are acknowledged for their support and guidance during the study.

The authors would like to recognize the following GE personnel for their efforts: Gene Voiland and Eugene Ingels for management support at GE-MO; Ken Eger for analytical support; and the staff at GE-MO for test operations.

Appreciation is extended to NPPD for the use of the Cooper reactor spent fuel assemblies.

Thanks are extended to Phillip Rinard and Gene Bosler of LANL for providing their ION-1 system, which was used to obtain axial radiation profiles on each spent fuel assembly. Their assistance in setting up the instrument and in training the GE-MO staff in its operation was helpful.

Pretest decay heat, heat transfer, and shielding predictions provided by PNL staff were helpful in planning the test. Appreciation is extended to the involved staff members who have prepared Volume II, results of the pretest and post-test decay heat, heat transfer, and shielding analyses, of this document.

The efforts of Burt Johnson and Bob Gilbert of PNL in planning fuel integrity activities are acknowledged and greatly appreciated. Appreciation is extended to LLNL staff Dr. Charles F. Smith, Wayne Culham, and Dr. Virginia Oversby for the analyses of gas and particulate samples.

Appreciation is also extended to Ray Lambert and Bob Williams of EPRI for their interest in the program and for the work they funded to evaluate ORIGEN2 for predicting decay heat rates of BWR spent fuel assemblies to assist this DOE testing effort.



## EXECUTIVE SUMMARY

This report documents a heat transfer and shielding performance test conducted on a Ridihaigh, Eggers & Associates REA 2023 boiling water reactor (BWR) spent fuel storage cask. The experimental work was conducted for the U.S. Department of Energy's (DOE) Commercial Spent Fuel Management Program by the Pacific Northwest Laboratory (PNL) and General Electric at the latter's Morris Operation (GE-MO). The testing effort consisted of three parts: pretest preparations, performance testing, and post-test activities. Pretest preparations included conducting cask handling dry runs and characterizing BWR spent fuel assemblies from Nebraska Public Power District's Cooper Nuclear Station. The performance test matrix included 14 runs consisting of two loadings, two cask orientations, and three backfill environments. Post-test activities included calorimetry and axial radiation scans of selected fuel assemblies, in-basin sipping of each assembly, crud collection, video and photographic scans, and decontamination of the cask interior and exterior.

The REA 2023 spent fuel storage cask consists of a double containment design with silicone rubber O-rings for sealing the primary lid of the inner cavity and a welded final closure on the secondary cover. The cask has a smooth, painted, stainless steel outer skin; a lead/stainless steel gamma shield; and a water/glycol neutron shield. The fuel basket is constructed of stainless steel clad Boral for criticality control, copper plates to conduct heat to the cask wall, and stainless steel for structural strength. The loaded cask is approximately 5 m tall and 2.25 m in diameter, and weighs approximately 100 tons. The basket is configured to hold 52 BWR spent fuel assemblies. The test fuel assemblies were of the General Electric 7x7 rod design. The REA 2023 BWR spent fuel storage cask design and manufacturing rights have been acquired by Mitsubishi of Japan, and the cask model designation has been changed to MSF IV.

Dry runs of cask handling were performed prior to fuel being loaded in the cask and concurrent with fuel calorimetry. The objectives of the dry runs were to gain cask handling and loading experience and to finalize procedures. Each dry run was conducted successfully without significant problems. During the dry



dry runs, minor modifications were required to make the lifting yoke, yoke alignment guide, impact limiter, primary head bolts, neutron shield rupture disk, and the cask pressurizing device more functional.

The Cooper spent fuel assemblies were characterized using in-basin sipping, calorimetry, axial radiation scans, video scans, and 35-mm photography. The results of these methods revealed no indication of any failed fuel before or after the performance test. Gas sampling during testing did indicate a leak in a fuel rod after the cask was fully loaded. However, the leak was calculated to be extremely small, so small that its source was not identifiable by post-test sipping activities, video scans, or photography.

Based on pretest calorimetry, fuel assembly decay heat rates averaged ~310 W/assembly to produce a total initial heat load in the cask of ~15 kW (Table S.1). Assembly decay heat rates ranged from 250 W to 390 W. The hotter fuel assemblies were located in the center of the basket, and the cooler assemblies were in the outer basket locations.

Figures S.1 and S.2 show representative measured gamma and neutron axial profiles for the Cooper fuel assemblies. The profiles are typical of BWR assemblies, and indicate less activity in the upper region of the assembly active length. Lower activity levels in the upper ends of BWR fuel assemblies can be expected because steam-water voids in the upper region of a BWR core result in lower fuel assembly burnup values, which produce lower activity levels.

TABLE S.1. Cooper Spent Fuel Assembly Characteristics and Decay Heat Rates

Number of Assemblies	Burnup Range, GWd/MTU	Operating History, cycles in reactor <sup>(a)</sup>	Cooling Time, months	Measured Decay Heat, W
36	25-28	1,2,3,*,*,6,7	~28	265-390
8	24-25	1,2,*,*,5,6	~41	280-290
8	26	1,2,3,4,5,6	~41	250-280
Average				310

(a) The \* designates that the fuel assembly was out of the reactor for this cycle.

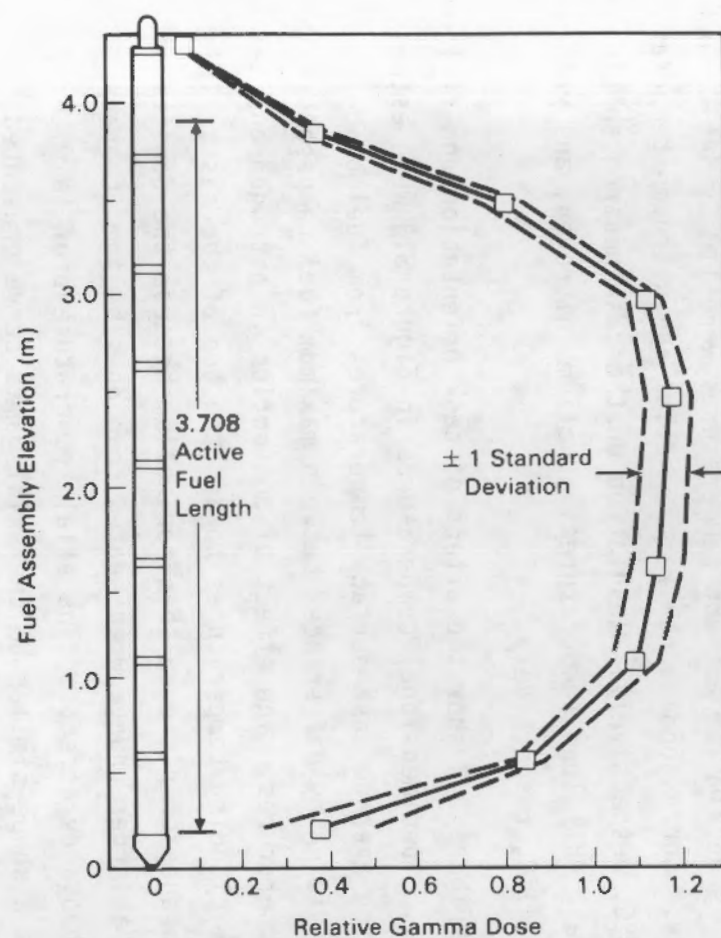


**FIGURE S.1.** Cooper Fuel Assembly Normalized Average Axial Gamma Dose Rate Profile

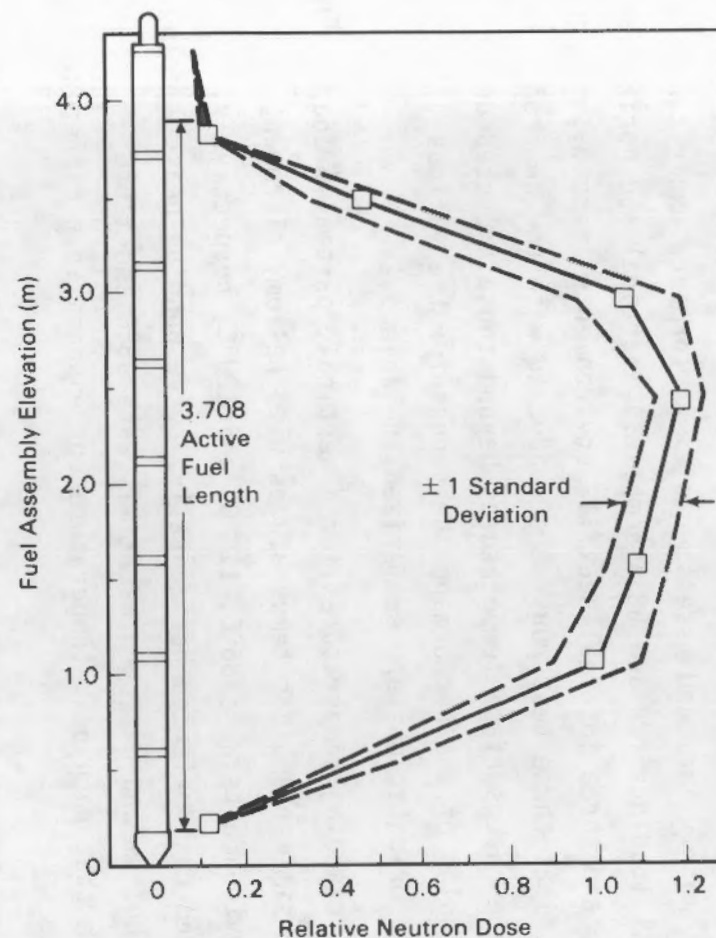


**FIGURE S.2.** Cooper Fuel Assembly Normalized Average Axial Neutron Dose Rate Profile

The cask test matrix included assessments of performance under conditions of partial and full loadings (28 and 52 assemblies), vertical and horizontal cask orientations, and three internal backfill environments (vacuum, nitrogen, and helium). The final three test runs were conducted with the neutron shield insulated to elevate cask surface temperatures beyond those expected during summer months. Results of the performance test runs for the various fill conditions and cask orientations are summarized in Table S.2.

Measured peak cladding temperatures for a vertical, partially loaded cask (28 assemblies) at similar ambient temperatures with helium, nitrogen, and vacuum backfill environments were 86°C, 118°C, and 170°C, respectively. With the partially loaded cask oriented horizontally, corresponding peak cladding temperatures with helium and nitrogen backfills were 93°C and 116°C, respectively. Note that each peak temperature corresponds to a different ambient temperature.

Measured peak cladding temperatures with the cask fully loaded were higher than partial load temperatures. Vertical helium, nitrogen, and vacuum peak cladding temperatures at similar ambient temperatures were 110°C, 146°C, and 200°C, respectively. Corresponding horizontal helium and nitrogen temperatures were 113°C and 164°C, respectively. Insulation on the cask neutron shield resulted in vertical, full load temperatures in helium, nitrogen, and vacuum of 185°C, 209°C, and 241°C, respectively.

The curves in Figure S.3 show the effect of cask orientation and fill gas on cask performance. Nondimensional temperatures in Figure S.3 were established by subtracting average cask surface temperatures from fuel cladding temperatures and dividing by differences between maximum fuel temperatures and average surface temperatures. The effect of convection in nitrogen and helium tends to shift peak cladding temperatures toward the top of the cask. This effect is more apparent for nitrogen than for helium because the density of nitrogen undergoes a larger change when heated than does helium, thereby producing greater buoyancy effects. The axial temperature profile with a vacuum backfill has a shape similar to the axial gamma curve presented in Figure S.1, indicating the absence of convection. The horizontal temperature profile was developed using temperature measurements with all three backfill



TABLE S.2. Cask Performance Test Run Summary

Cask Test Conditions			Total Decay Heat, kW	Wind Speed, m/sec	Solar Insolation, W	Ambient Temp, °C	Average Surface Temp, °C	Maximum Cladding Temp, °C
Loading <sup>(a)</sup>	Orientation	Backfill Environment						
Partial	Vertical	Vacuum	9.0	2.2	75	7	18	170
Partial	Vertical	Nitrogen	8.9	1.3	85	1	15	118
Partial	Horizontal	Nitrogen	8.9	3.6	95	-10	2	116
Partial	Horizontal	Helium	8.8	1.3	87	5	21	93
Partial	Vertical	Helium	8.8	3.6	21	-3	7	86
Partial	Vertical	Helium <sup>(b)</sup>	8.7	6.3	16	14	20	97
Full	Vertical	Vacuum	15.2	0.0	0	24	52	227
Full	Vertical	Vacuum <sup>(b)</sup>	15.2	3.6	65	-10	9	200
Full	Vertical	Nitrogen	15.1	3.1	43	-4	15	151
Full	Vertical	Nitrogen <sup>(b)</sup>	14.9	1.3	143	-17	12	146
Full	Horizontal	Nitrogen	15.0	2.0	48	-4	23	164
Full	Horizontal	Helium	14.8	4.2	127	-8	10	113
Full	Vertical	Helium	14.9	0.7	141	-14	15	110
Full	Vertical	Helium <sup>(b)</sup>	14.6	0.0	0	22	52	144
Full	Vertical	Helium <sup>(c)</sup>	14.4	0.0	0	20	101	185
Full	Vertical	Nitrogen <sup>(c)</sup>	14.4	0.0	0	22	100	209
Full	Vertical	Vacuum <sup>(c)</sup>	14.3	0.0	0	24	95	241

(a) Partial load had 28 fuel assemblies, full load had 52 fuel assemblies.

(b) Repeat run.

(c) Insulated run.

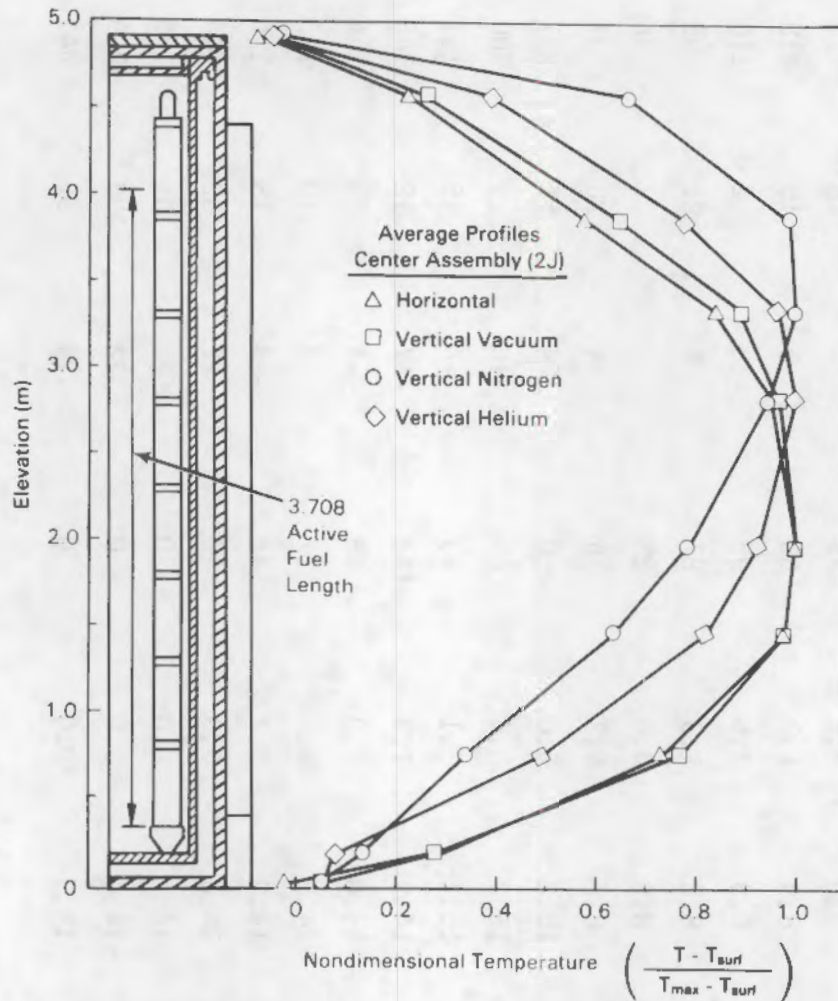


FIGURE S.3. Effects of Cask Orientation and Fill Gas

gases. The horizontal profile is similar to the gamma and vacuum curves and also shows the lack of convection due to the absence of an axial gravity head in the horizontal orientation.

Dose rate profiles on the surface of a fully loaded cask are shown in Figures S.4 through S.6. On the primary lid of the cask (Figure S.4), gamma dose rates were generally ~35 mrem/hr. A dose rate peak of ~70 mrem/hr was measured near the edge of the lid where a small window exists between the lead in the lid and the lead in the cask wall. Neutron dose rates on the lid were less than 15 mrem/hr.

Dose rate profiles on the side of the cask shown in Figure S.5 indicate peaks were measured near the top and bottom. A gamma dose rate peak of

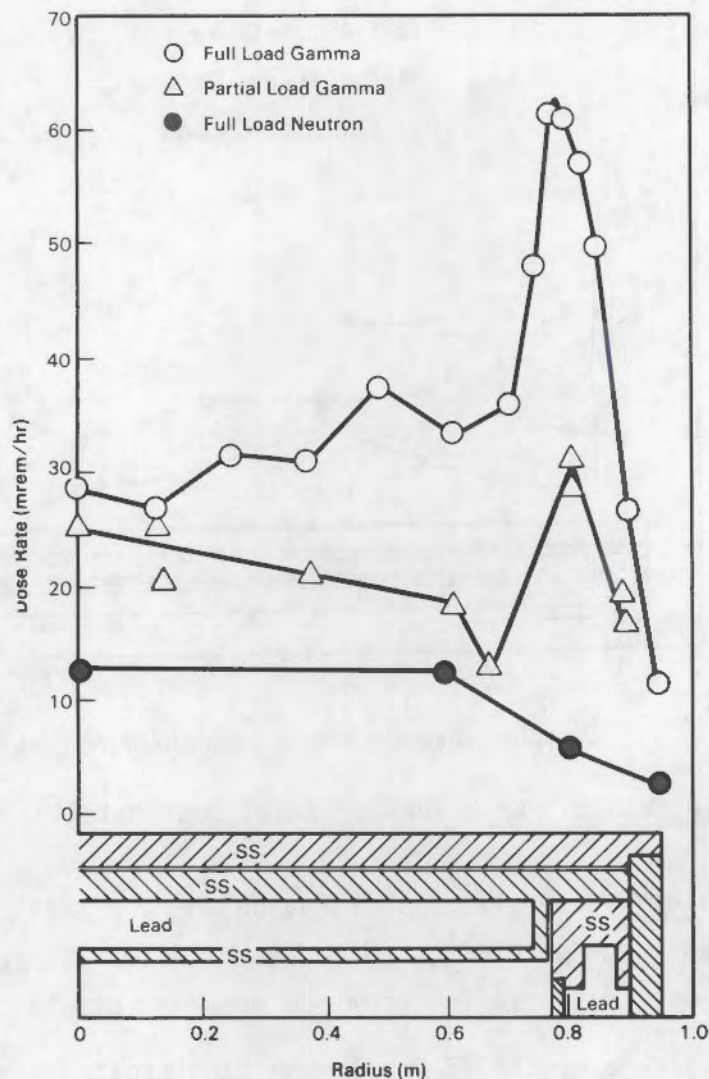


FIGURE S.4. Primary Lid Radial Dose Rate Profiles

~38 mrem/hr was measured near the top. A neutron dose rate peak of ~16 mrem/hr was measured near the bottom of the cask. Gamma and neutron dose rates on the side were generally 15 mrem/hr and 3 mrem/hr, respectively.

Combined gamma and neutron dose rates on the cask bottom (Figure S.6) were <100 mrem/hr with the exception of one small region at a radius of 0.5 m and an angle of 270 degrees where the dose rate was measured at 190 mrem/hr (dose rate not shown in Figure S.6). Post-fabrication quality assurance inspections of



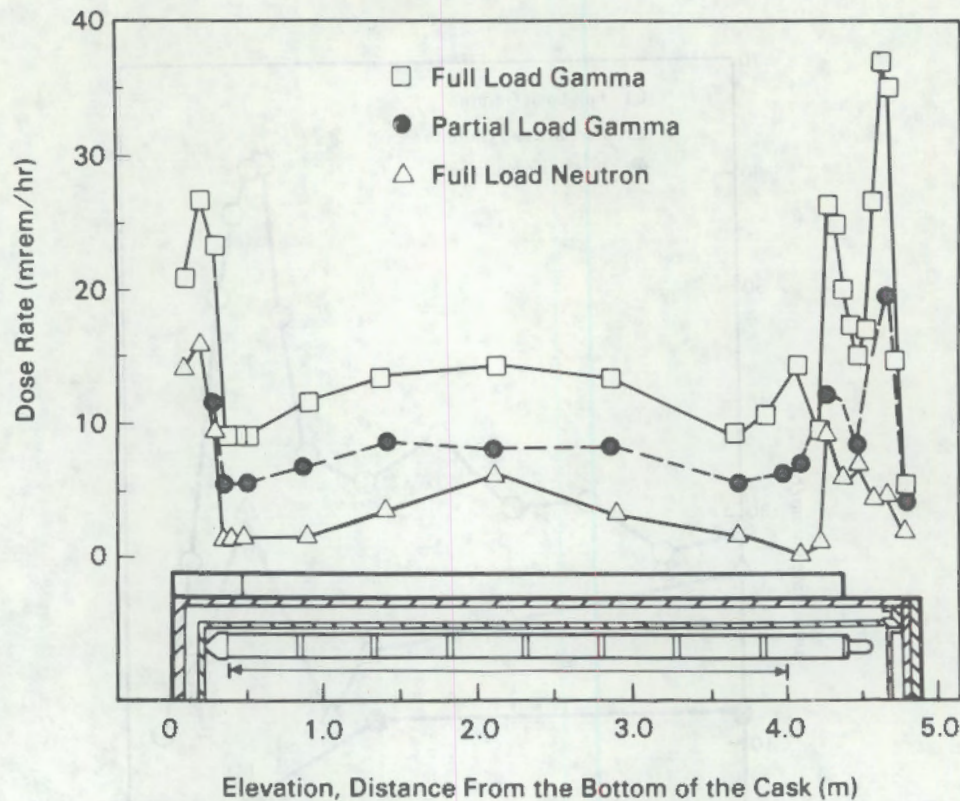
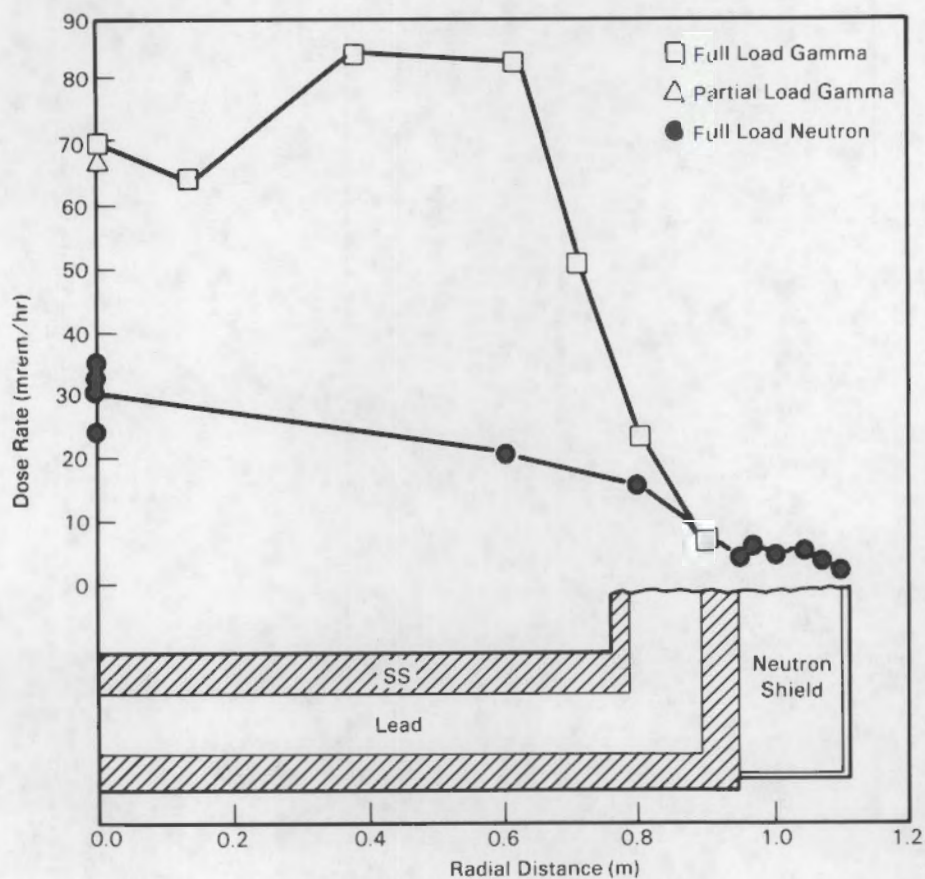


FIGURE S.5. Cask Surface Axial Dose Rate Profiles

the cask had previously identified this region where a small anomaly apparently exists in the lead gamma shielding. Other gamma dose rate peaks are ~85 mrem/hr; neutron dose rates varied from ~35 mrem/hr to a few mrem/hr.

Radiation exposure of the 28 people who participated in the cask performance test was relatively low, averaging 24 mrem per person over the 4-1/2-month testing period. During the testing period, the cask was loaded twice and rotated several times; gas sampling was routinely conducted, and radiation and smear surveys were performed. Personnel exposure at a storage facility in which a cask is loaded once and moved directly to a long-term storage facility will be considerably lower.

The cask performance test demonstrated that the cask could be handled and decontaminated satisfactorily. It was concluded that the heat transfer performance of the REA 2023 BWR cask was exceptionally good. Peak clad temperatures were relatively low for all orientations and backfill environments.



**FIGURE S.6. Cask Bottom Radial Dose Rate Profiles**

Although the shielding performance of the cask did not meet design expectations (20 mrem/hr), cask surface dose rates were manageable. With minor shielding modifications, dose rates of <50 mrem/hr can be established.



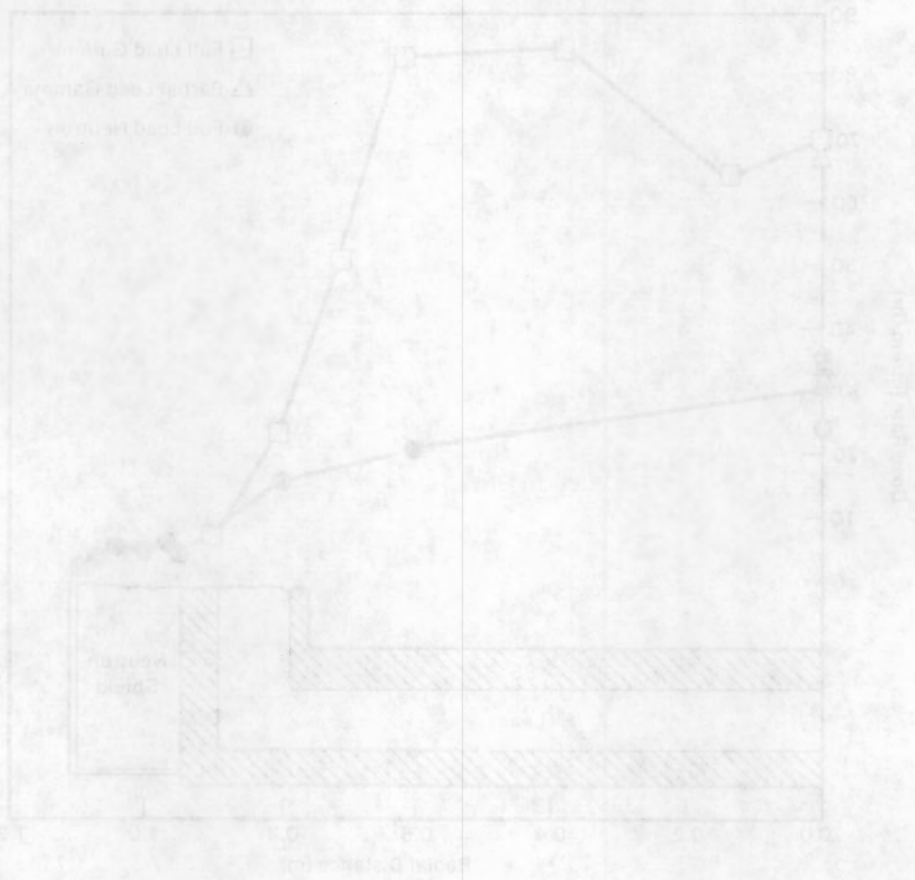


FIGURE 2.8. Cask Bottom Radial Dose Rate Profiles

Although the shielding performance of the cask did not meet design expectations (50 mSv/hr), cask surface dose rates were manageable. With minor shielding modifications, dose rates of 50 mSv/hr can be achieved.



## CONTENTS

ACKNOWLEDGMENTS .....	iii
EXECUTIVE SUMMARY .....	v
ABBREVIATIONS AND ACRONYMS .....	xxix
1.0 INTRODUCTION .....	1.1
2.0 CONCLUSIONS AND RECOMMENDATIONS .....	2.1
2.1 CONCLUSIONS .....	2.1
2.2 RECOMMENDATIONS .....	2.5
3.0 SPENT FUEL STORAGE CASK TESTING .....	3.1
3.1 CASK DESCRIPTION .....	3.1
3.1.1 Cask Body and Containment Vessel .....	3.1
3.1.2 Primary and Secondary Covers .....	3.3
3.1.3 Containment Vessel Penetrations and Internal Environment .....	3.4
3.1.4 Lifting Devices .....	3.5
3.1.5 Basket .....	3.7
3.2 GENERAL ELECTRIC-MORRIS OPERATIONS CASK TESTING FACILITY ....	3.8
3.2.1 Cask Receiving Area .....	3.12
3.2.2 Decontamination Area .....	3.12
3.2.3 Cask Unloading Basin .....	3.14
3.2.4 Cask Test Station .....	3.15
3.3 TEST PLAN .....	3.16
3.4 CASK HANDLING AND DECONTAMINATION PROCEDURES AND EXPERIENCE .....	3.20
3.4.1 Cask Removal from Rail Car .....	3.22

3.4.2	Cask Transfer from Receiving Area to Decontamination Pad .....	3.24
3.4.3	Loading Preparations .....	3.25
3.4.4	Cask Transfer to Unloading Basin .....	3.26
3.4.5	Cask Loading .....	3.27
3.4.6	Cask Return to Shelf and Decontamination Pad, Primary Head Torquing, and Helium Leak Checking .....	3.27
3.4.7	Vacuum Drying .....	3.31
3.4.8	Decontamination Area Operations Prior to Cask Return to Rail Car .....	3.33
3.4.9	Cask Placement on Rail Car for Performance Testing ...	3.34
3.4.10	Cask Rotation During Performance Testing .....	3.36
3.4.11	Gas Sampling/Changing During Performance Testing ....	3.36
3.4.12	Decontamination .....	3.39
3.4.13	Personnel Exposure .....	3.42
4.0	SPENT FUEL ASSEMBLY CHARACTERIZATION .....	4.1
4.1	SPENT FUEL ASSEMBLIES .....	4.1
4.2	DECAY HEAT RATES .....	4.7
4.2.1	Calorimeter Description and Operation .....	4.7
4.2.2	Decay Heat Data .....	4.10
4.3	AXIAL RADIATION PROFILES .....	4.14
4.3.1	ION-1/Fork Measurement System .....	4.14
4.3.2	Axial Radiation Profiles .....	4.16
4.4	SPENT FUEL INTEGRITY .....	4.18
4.4.1	In-Basin Sipping .....	4.19
4.4.2	Video and Photographic Examinations .....	4.23
4.4.3	Cask Cover Gas Sampling .....	4.24

4.4.4	Crud Sampling .....	4.30
4.4.5	Summary .....	4.31
5.0	CASK HEAT TRANSFER AND SHIELDING PERFORMANCE .....	5.1
5.1	THERMAL PERFORMANCE .....	5.1
5.1.1	Instrumentation .....	5.1
5.1.2	Temperature Data .....	5.4
5.2	SHIELDING PERFORMANCE .....	5.46
5.2.1	Gamma and Neutron Instrumentation .....	5.46
5.2.2	Shielding Data .....	5.46
REFERENCES	.....	Ref.1
APPENDIX A -	INSTRUMENTATION AND DATA ACQUISITION SYSTEM .....	A.1
APPENDIX B -	VACUUM DRYING/GAS SAMPLING SYSTEM .....	B.1
APPENDIX C -	CASK DECONTAMINATION .....	C.1
APPENDIX D -	DECAY HEAT MEASUREMENTS .....	D.1
APPENDIX E -	AXIAL RADIATION PROFILES .....	E.1
APPENDIX F -	IN-BASIN SIPPIING RESULTS .....	F.1
APPENDIX G -	CASK TEMPERATURE PERFORMANCE DATA .....	G.1
APPENDIX H -	CASK RADIATION MEASUREMENT DATA AND INSTRUMENTATION .....	H.1

## FIGURES

S.1	Cooper Fuel Assembly Normalized Average Axial Gamma Dose Rate Profile .....	vii
S.2	Cooper Fuel Assembly Normalized Average Axial Neutron Dose Rate .....	vii
S.3	Effects of Cask Orientation and Fill Gas .....	x
S.4	Primary Lid Radial Dose Rate Profiles .....	xi
S.5	Cask Surface Axial Dose Rate Profiles .....	xii
S.6	Cask Bottom Radial Dose Rate Profiles .....	xiii
3.1	REA 2023 BWR Spent Fuel Storage Cask .....	3.2
3.2	Quarter Section of REA 2023 Cask and BWR Spent Fuel Basket ....	3.2
3.3	Primary and Secondary Lids .....	3.4
3.4	Secondary Lid Clamp Ring .....	3.5
3.5	Instrument Ports with Instrument Leads Connected .....	3.6
3.6	Lifting Yoke with Short Arms .....	3.7
3.7	52-Assembly BWR Basket .....	3.8
3.8	General Electric-Morris Operation Fuel Storage Facility .....	3.10
3.9	General Electric-Morris Operation Fuel Storage Basin .....	3.11
3.10	Cask Rotation .....	3.13
3.11	Cask Test Station .....	3.16
3.12	REA 2023 Cask Load Pattern .....	3.18
3.13	REA Cask on Depressed-Center Rail Car .....	3.23
3.14	Use of Slings to Rotate Cask into Vertical Orientation .....	3.24
3.15	Preparation of Primary Head for Fuel Loading .....	3.26
3.16	Cask in Unloading Basin .....	3.28

3.17	TAD Installation in Unloading Basin .....	3.29
3.18	Pressurizing Device .....	3.32
3.19	Impact Limiter .....	3.34
3.20	REA Cask and Rail Car .....	3.35
3.21	Cask Rotation and Lifting .....	3.37
3.22	Pressurizing Device and Gas Sampling Equipment .....	3.38
3.23	Smear Survey Grid .....	3.40
4.1	Cooper Spent Fuel Assembly .....	4.2
4.2	Cooper Nuclear Station Operating History .....	4.6
4.3	Assembly CZ205 Operating History .....	4.7
4.4	General Electric-Morris Operations In-Basin Calorimeter and Associated Equipment .....	4.8
4.5	Repeatability of Calorimetry Measurements on Assembly CZ205 .....	4.14
4.6	Los Alamos ION-1 Spent Fuel Radiation Measurement Equipment .....	4.15
4.7	Normalized Average Axial Gamma Dose Rate Profile .....	4.17
4.8	Normalized Average Axial Neutron Dose Rate Profile .....	4.17
4.9	Comparison of Fuel and Hardware Characteristics Near the Bottom of Assembly CZ205 Before and After Testing in the REA Cask .....	4.25
4.10	Release of <sup>85</sup> Kr Fission Gas During Performance Test .....	4.28
4.11	Comparison of Krypton Gas Released During Performance Test and Fuel Temperature Test .....	4.29
5.1	Basket and Fuel Thermocouple Locations .....	5.2
5.2	External Thermocouple Locations .....	5.3
5.3	Cask Temperature Response to Ambient Conditions During Run 3 .....	5.5



5.4	Cask Temperature Response to Ambient Conditions During Run 10 .....	5.5
5.5	Relationship Between Wind Speed and Cask Surface-to-Ambient Temperature Differences .....	5.10
5.6	Axial Fuel and Surface Temperature Profiles for Vertical Vacuum Runs .....	5.12
5.7	Axial Fuel Temperature Profiles Referenced to Average Surface Temperatures for Vertical Vacuum Runs .....	5.13
5.8	Normalized Axial Fuel Temperature Profiles for Vertical Vacuum Runs .....	5.14
5.9	Radial Temperature Profiles for Vertical Vacuum Runs .....	5.15
5.10	Normalized Radial Temperature Profiles for Vertical Vacuum Runs .....	5.16
5.11	Diametrical Fuel Temperature Profiles for Vertical Vacuum Runs .....	5.17
5.12	Axial Fuel and Surface Temperature Profiles for Vertical Nitrogen Runs .....	5.19
5.13	Axial Fuel and Surface Temperature Profiles for Horizontal Nitrogen Runs .....	5.20
5.14	Axial Fuel Temperature Profiles Referenced to Average Surface Temperatures for Vertical and Horizontal Nitrogen Runs .....	5.21
5.15	Normalized Radial Temperature Profiles for Vertical Nitrogen Runs .....	5.22
5.16	Normalized Radial Temperature Profiles for Horizontal Nitrogen Runs .....	5.23
5.17	Diametrical Fuel Temperature Profiles for Vertical Nitrogen Runs .....	5.24
5.18	Diametrical Fuel Temperature Profiles for Horizontal Nitrogen Runs .....	5.25
5.19	Axial Fuel and Surface Temperature Profiles for Vertical Helium Runs .....	5.27
5.20	Axial Fuel and Surface Temperature Profiles for Horizontal Helium Runs .....	5.28

5.21	Axial Fuel Temperature Profiles Referenced to Average Surface Temperatures for Vertical and Horizontal Helium Runs .....	5.29
5.22	Normalized Radial Temperature Profiles for Vertical Helium Runs .....	5.30
5.23	Normalized Radial Temperature Profiles for Horizontal Helium Runs .....	5.31
5.24	Diametrical Fuel Temperature Profiles for Vertical Helium Runs .....	5.32
5.25	Diametrical Fuel Temperature Profiles for Horizontal Helium Runs .....	5.33
5.26	Normalized Axial Fuel Temperature Profiles for Vertical Nitrogen Runs .....	5.35
5.27	Normalized Axial Fuel Temperature Profiles for Vertical Helium Runs .....	5.35
5.28	Normalized Axial Fuel Temperature Profiles for Horizontal Nitrogen and Helium Runs .....	5.36
5.29	Normalized Axial Fuel Temperature Profiles Showing Effects of Fill Gas and Cask Orientation .....	5.36
5.30	Partial Load, Normalized Radial Fuel Temperature Profiles Showing Effects of Fill Gas and Cask Orientation .....	5.38
5.31	Full Load, Normalized Radial Fuel Temperature Profiles Showing Effects of Fill Gas and Cask Orientation .....	5.38
5.32	Axial Fuel and Surface Temperature Profiles for Insulated Vertical Runs .....	5.40
5.33	Circumferential Cask Surface Temperature Profiles .....	5.41
5.34	Partial Load Fuel and Ambient Temperature Transients .....	5.44
5.35	Full Load Fuel and Ambient Temperature Transients .....	5.45
5.36	Axial Surface Dose Rate Profiles .....	5.51
5.37	Surface Dose Rate Profiles on Cask Lid .....	5.52
5.38	Surface Dose Rate Profiles on Cask Bottom .....	5.53
5.39	Circumferential Surface Dose Rate Profiles at 2.23-m Elevation .....	5.54

5.40	PNL Survey Instrument Axial Radiation Profile on Side of Cask .....	5.55
5.41	Full Load GE-MO Survey Instrument Axial Gamma Radiation Profile on Side of Cask .....	5.56
5.42	Full Load GE-MO Survey Instrument Axial Neutron Radiation Profile on Side of Cask .....	5.57
A.1	REA Cask Data Acquisition System .....	A.2
A.2	Data Acquisition System .....	A.3
A.3	Method Used to Attach Thermocouples to Basket Bottom .....	A.4
A.4	Thermocouple Attachment Device for Inserting Thermocouples into Fuel Assemblies .....	A.5
A.5	View Showing TAD Installation Tool Attached to Basin Crane ....	A.6
A.6	TAD in Jaws .....	A.7
A.7	Installed TAD .....	A.8
A.8	TAD-Holder .....	A.9
A.9	Peripheral Mounted Thermocouple .....	A.11
A.10	Bail-Mounted Thermocouple .....	A.12
A.11	Thermocouple Termination Details .....	A.13
A.12	External Thermocouple Mounting Block .....	A.13
A.13	Data Acquisition System External Hardware .....	A.14
A.14	Weather Station .....	A.16
B.1	Vacuum Drying/Gas Sampling System .....	B.2
C.1	REA Cask - Top and South Side Maps .....	C.2
C.2	REA Cask - Bottom and North Side Maps .....	C.3
C.3	REA Cask Basket Radiation Survey .....	C.7
D.1	October 1984 Calorimeter Calibration Heat-Up Curves .....	D.3
D.2	October 1984 Calorimeter Calibration Curve .....	D.4

E.1	View Showing Los Alamos Fork Measurement System Detector Installed in Morris Basin .....	E.2
E.2	Electronics Instrument for ION-1 System .....	E.3
E.3	Gamma/Neutron Scan Locations .....	E.5
E.4	Influence of Fuel Assembly Spacers on Radiation Profile .....	E.10
G.1	Key to Temperature Measurement Locations .....	G.2
H.1	REA 2023 Spent Fuel Storage Cask Spectral Radiation Measurement Location .....	H.6
H.2	Cask Radiation Measurement Locations .....	H.10
H.3	Temperature Response of the Cutie Pie .....	H.15
H.4	<sup>3</sup> He Spectrometer Results .....	H.19

## TABLES

S.1	Cooper Spent Fuel Assembly Characteristics and Decay Heat Rates .....	vi
S.2	Cask Performance Test Run Summary .....	ix
3.1	Cask Performance Test Matrix .....	3.17
3.2	REA Cask Handling Equipment Used for Basin Handling and Fuel Loading .....	3.21
3.3	Comparison of Outgoing and Incoming Surveys for the REA Cask .....	3.41
4.1	Design Characteristics of Cooper BWR Fuel Rods and Assemblies .....	4.3
4.2	Cooper Fuel Assembly Burnup Data .....	4.4
4.3	Cooper Nuclear Station Operating History .....	4.5
4.4	Calorimeter Decay Heat Data Summary .....	4.11
4.5	Calorimeter Measurements of Assembly CZ205 .....	4.13
4.6	Repeatability of Radiation Scans (Assembly CZ331) .....	4.19
4.7	Normalized Radiation Profiles (Assembly CZ331) .....	4.20
4.8	Comparison of $^{137}\text{Cs}$ Levels Detected During Pretest and Post-Test Sipping of Cooper BWR Spent Fuel Assemblies .....	4.21
4.9	Cask Gas Sample Identification .....	4.26
4.10	Sample Composition and Radionuclide Concentration .....	4.27
4.11	Analysis of Crud Samples from REA Cask .....	4.31
5.1	Cask Thermal Performance Test Run Summary .....	5.8
5.2	Symmetry of Temperature Measurements .....	5.43
5.3	Partial Load Reference Neutron Dose Rate Measurements .....	5.48
5.4	Full Load Reference Neutron Dose Rate Measurements .....	5.49
5.5	Reference Gamma Dose Rate Measurements .....	5.50



B.1	Vacuum Drying Experience with the REA 2023 Cask .....	B.4
C.1	REA Cask Smearable Contamination Survey Results .....	C.4
D.1	October 1984 Calorimeter Calibration Data .....	D.5
E.1	Gamma Data Collection with the ION-1 .....	E.6
E.2	Neutron Data Collection with the ION-1 .....	E.8
F.1	Sipping Tests For Cooper Fuel Pre-Characterization, Basket B-85 .....	F.2
F.2	Sipping Tests For Cooper Fuel Pre-Characterization, Basket B-86 .....	F.2
F.3	Sipping Tests For Cooper Fuel Pre-Characterization, Basket B-88 .....	F.3
F.4	Sipping Tests For Cooper Fuel Pre-Characterization, Basket B-90 .....	F.3
F.5	Sipping Tests For Cooper Fuel Pre-Characterization, Basket B-91 .....	F.4
F.6	Sipping Tests For Cooper Fuel Pre-Characterization, Basket B-92 .....	F.4
F.7	Sipping Tests For Cooper Fuel Pre-Characterization, Basket B-93 .....	F.5
F.8	Sipping Tests For Cooper Fuel Post-Characterization, Basket B-85 .....	F.5
F.9	Sipping Tests For Cooper Fuel Post-Characterization, Basket B-86 .....	F.6
F.10	Sipping Tests For Cooper Fuel Post-Characterization, Basket B-88 .....	F.6
F.11	Sipping Tests For Cooper Fuel Post-Characterization, Basket B-90 .....	F.7
F.12	Sipping Tests For Cooper Fuel Post-Characterization, Basket B-91 .....	F.7
F.13	Sipping Tests For Cooper Fuel Post-Characterization, Basket B-92 .....	F.8

F.14	Sipping Tests For Cooper Fuel Post-Characterization, Basket B-93 .....	F.8
G.1	Vertical Vacuum Run .....	G.3
G.2	Vertical Nitrogen Run .....	G.4
G.3	Horizontal Nitrogen Run .....	G.5
G.4	Horizontal Helium Run .....	G.6
G.5	Vertical Helium Run .....	G.7
G.6	Vertical Helium Run .....	G.8
G.7	Vertical Vacuum Run .....	G.9
G.8	Vertical Vacuum Run .....	G.10
G.9	Vertical Nitrogen Run .....	G.11
G.10	Vertical Nitrogen Run .....	G.12
G.11	Horizontal Nitrogen Run .....	G.13
G.12	Horizontal Helium Run .....	G.14
G.13	Vertical Helium Run .....	G.15
G.14	Vertical Helium Run .....	G.16
G.15	Insulated Vertical Helium Run .....	G.17
G.16	Insulated Vertical Nitrogen Run .....	G.18
G.17	Insulated Vertical Vacuum Run .....	G.19
H.1	Thermoluminescent Dosimeter Results for the REA Spent Fuel Storage Cask (Partial Loading) .....	H.7
H.2	Thermoluminescent Dosimeter Results for the REA Spent Fuel Storage Cask (Full Loading) .....	H.8
H.3	REA Cask Radiation Survey Data Taken by General Electric .....	H.11
H.4	PNL Cutie Pie Measurements for REA Cask .....	H.14
H.5	PNL SNOOPY Measurement for REA Cask .....	H.16

H.6	Track Etch Dosimeter Results for the REA Spent Fuel Storage Cask (Full Loading) .....	H.17
H.7	Neutron Dose Rate Measurements at Partial Loading .....	H.18
H.8	Neutron Dose Rate Measurements at Full Loading .....	H.19



## ABBREVIATIONS AND ACRONYMS

BWR	boiling water reactor
cm	centimeter(s)
CRA	cask receiving area
CSF	cask service facility
CSFM	Commercial Spent Fuel Management
cc	cubic centimeter(s)
°C	degrees centigrade
Ci	curie(s)
DOE	U.S. Department of Energy
dpm	disintegration per minute
ft	foot, feet
gal	gallon(s)
GE-MO	General Electric-Morris Operation
GWd	gigawatt-day(s)
hr	hour(s)
in.	inch, inches
kPa	kilopascal
kW	kilowatt(s)
LLNL	Lawrence Livermore National Laboratory
L	liter(s)
LANL	Los Alamos National Laboratory
m	meter(s)
t	metric ton(s)
MTU	metric ton(s) of uranium



ABBREVIATIONS AND ACRONYMS (contd)

mrem	millirem(s)
m/s	multisphere
pCi	picocurie(s)
PNL	Pacific Northwest Laboratory
PRM	pocket rem meter
psig	pound-force per square inch gauge
PWR	pressurized water reactor
RTD	resistance temperature device
REA	Ridihalgh, Eggers & Associates
TC	thermocouple
TLD	thermoluminescent dosimeter
TAD	thermocouple attachment device
TEPC	tissue equivalent proportional counter
TED	track etch dosimeter
W	watt(s)

# BWR SPENT FUEL STORAGE CASK PERFORMANCE TEST

## VOLUME I

### CASK HANDLING EXPERIENCE AND DECAY HEAT, HEAT TRANSFER, AND SHIELDING DATA

#### 1.0 INTRODUCTION

The need for additional storage capacity for spent fuel from commercial nuclear power reactors is near-term (as few as 3 to 5 years) for some utilities. The consequences of failure to provide additional storage capacity could be significant if reactors are forced to terminate operations until required storage expansions can be provided. The storage capacity requirements can be expected to increase in the foreseeable future until reprocessing plants and/or repositories are established. Therefore, a proven method of interim dry storage of spent fuel is needed in the near term to avoid reactor shutdowns and, in the long term, to provide emergency storage capability in the event that implementation of reprocessing and/or a repository is delayed.

The U.S. Department of Energy (DOE) Commercial Spent Fuel Management (CSFM) Program<sup>(a)</sup> and operators of commercial nuclear power reactors have identified metal storage casks as one of the leading candidates among available dry storage concepts for interim spent fuel storage. It is anticipated that licensing of large, multi-assembly storage casks will be attempted. The number of casks needed could be very large, representing a substantial investment. Economics is, therefore, an important consideration, and every effort should be made to ensure that the chosen interim storage system provides the minimum cost commensurate with environmental and safety considerations. Therefore, performance tests are needed to 1) provide experimental data to support licensing efforts, 2) determine cask operating limits, 3) gain cask handling and

---

(a) The CSFM Program is managed by the Pacific Northwest Laboratory, which is operated for the U.S. Department of Energy by Battelle Memorial Institute.

decontamination experience, 4) identify candidate cask design improvements, and 5) evaluate computer codes required to perform future design and licensing analyses.

The primary objective of the study documented in this report was to performance-test a Ridihaugh, Eggers & Associates REA 2023 boiling water reactor (BWR) spent fuel storage cask. The work was conducted by the Pacific Northwest Laboratory (PNL) and General Electric for DOE's CSFM Program. The REA cask, tested at General Electric's Morris Operation (GE-MO), contained 52 BWR spent fuel assemblies from Nebraska Public Power District's Cooper Nuclear Station. The primary data to be obtained during the testing activities were peak fuel cladding temperatures and cask surface radiation dose rates for a cask filled with well-characterized BWR spent fuel. Secondary information to be obtained was cask handling and decontamination experience and fuel integrity data.

The work began with a revision to GE-MO's safety analysis documents, to permit loading of BWR spent fuel in the REA cask. Dry runs were required to finalize handling and operating procedures. The fuel assemblies were sipped in the GE-MO basin to ensure integrity, and calorimetered to determine decay heat rates before being loaded into the cask. The exterior surface and basket of the cask were instrumented with thermocouples, and the cask was incrementally loaded with spent fuel. Thermocouples were inserted into selected fuel assemblies during the first incremental loading, to monitor clad temperatures throughout the test. A test station was prepared, comprising a depressed-center rail car, a weather station, and a data acquisition system. A total of 14 runs, involving a combination of cover gases, fuel loadings, cask orientations, and cask surface boundary conditions, were performed during the test. The backfill environments used were vacuum, nitrogen, and helium, and they were sampled and analyzed to detect leaking fuel assemblies. Fuel loadings included a partial load of 28 assemblies and a full load of 52 assemblies. Both vertical and horizontal orientations were investigated; test runs were performed inside under controlled conditions and outside in the natural environment. Cask surface radiation dose rate measurements were taken as part of the test program. At the conclusion of testing, the cask was decontaminated and crud samples were collected and analyzed.

## 2.0 CONCLUSIONS AND RECOMMENDATIONS

The performance test of the REA 2023 BWR spent fuel storage cask was successfully conducted at GE-MO during the winter of 1984-85. The test demonstrated that the cask could be satisfactorily handled and decontaminated in a reactor-like facility, and demonstrated the heat transfer and shielding performance of the cask when loaded with 52 BWR spent fuel assemblies. The heat transfer performance of the cask was excellent, as indicated by relatively low ( $<250^{\circ}\text{C}$ ) peak cladding temperatures with a heat load of approximately 15 kW. Even though the shielding performance did not meet design expectations (20 mrem/hr), cask surface dose rates were manageable. With minor shielding modifications, dose rates of  $<50$  mrem/hr can be established.

The following sections present specific conclusions and recommendations noted during the testing effort.

### 2.1 CONCLUSIONS

The results of the performance test permit the following conclusions:

#### Cask Handling and Decontamination

- The cask can be satisfactorily handled in many reactor facilities with only minor modifications to the supplied handling equipment and procedures.
- The cask lifting yoke, yoke alignment guide, impact limiter, primary head bolts, and cask pressurizing device required modifications to function satisfactorily.
- The cask was awkward to rotate from a vertical to a horizontal orientation or vice versa.
- Occasional leaks of the neutron shield rupture disk during the test were attributed to selection of a less than optimal design and overtorquing of the disk.

- During the insulated cask test runs, the Carbolite silicone-based paint softened, and it was concluded that the paint had not been properly cured.
- The cask exterior can be decontaminated using soap and water in a manner similar to that used for transportation casks.
- Smear surveys taken during testing demonstrated that the painted cask surface does not leach smearable or otherwise detectable radioactive particles after long periods.
- Significant amounts of crud were not found in the cask after the fuel was unloaded.
- The cask interior can be decontaminated to below Class A licensing limits, even when a small leak is present in fuel rod cladding, by flushing it with water.
- Total personnel exposures during the cask testing effort were surprisingly low (670 mrem for 28 people) and will be even lower at a reactor where the cask will be loaded only once and not worked around continually.

#### Fuel Characterization and Integrity

- Results of pretest in-basin sipping of each Cooper spent fuel assembly indicated that no failed fuel was loaded in the REA cask.
- The average decay heat rate of each assembly was ~310 kW at the start of testing, which produced a total initial cask heat load of ~15 kW.
- Repeated calorimetry measurements of the decay heat rate of spent fuel assembly CZ205 resulted in a measurement standard deviation of  $\pm 14.1$  W.
- Krypton gas was found in gas samples taken from the cask after it was fully loaded. The size of the cladding penetration was estimated to be extremely small, and it had no adverse effects on the testing effort.



## Heat Transfer

- Peak cladding temperatures for an uninsulated, vertical cask with vacuum, nitrogen, and helium backfills were 200°C, 151°C, and 110°C, respectively. The respective average cask surface temperatures were 9°C, 15°C, and 15°C. Average cask surface temperatures were ~20°C above ambient temperatures.
- Peak cladding temperatures for an uninsulated, horizontal cask with nitrogen and helium backfills were 164°C and 113°C, respectively. The respective average cask surface temperatures were 23°C and 10°C.
- A maximum peak cladding temperature of 241°C occurred during a full load, vertical, vacuum run with an insulated neutron shield. The average surface temperature of the neutron shield was 95°C.
- Effects of fill gas on the thermal performance of the cask were apparent. The increased convection in a vertical cask filled with nitrogen shifted peak cladding temperatures near the top of the cask. Peak cladding temperatures showed some upward shift due to helium convection in a vertical cask. Temperature profiles in vertical vacuum runs showed that peak cladding temperatures occurred at an axial location where the axial decay heat rate peaked, indicating the absence of convection.
- Rotating the cask from a vertical to a horizontal orientation resulted in higher temperature differences between the peak cladding and ambient, i.e., the additional contact between fuel assemblies and the cask basket in the horizontal orientation was not sufficient to overcome the convection present in a vertical orientation. The axial location of the peak cladding temperatures corresponded to the location of the peak axial decay heat rate, indicating the absence of convection.
- Comparisons of temperature profiles across the diameter for vertical and horizontal orientations indicated a change in contact resistance between the basket and the cask due to the effects of gravity. This

change in contact resistance resulted in higher temperatures in the upper quadrants and lower temperatures in the lower quadrants of a horizontal cask.

- The REA 2023 BWR spent fuel storage cask has a thermal time constant of ~22 hours.
- Solar insolation does not appear to add to the total cask heat load in a significant or correlatable manner.

#### Shielding

- The average surface dose rate on the primary lid of the cask was ~50 mrem/hr (40 mrem/hr gamma, 10 mrem/hr neutron), with a peak of ~80 mrem/hr (70 mrem/hr gamma, 10 mrem/hr neutron) in the vicinity of the parting plane of the lid.
- The average surface dose rate on the side of the cask was ~20 mrem/hr (15 mrem/hr gamma, 5 mrem/hr neutron) with peaks of ~40 mrem/hr (35 mrem/hr gamma, 5 mrem/hr neutron) near the ends where the neutron and/or gamma shields ended.
- The dose rate profile on the bottom of the cask was relatively uniform, with an average value of ~110 mrem/hr (85 mrem/hr gamma, 25 mrem/hr neutron) and an anomaly of 195 mrem/hr at a radius of 0.5 m and 270°. This apparent anomaly in the gamma shield in a very localized area was also identified during post-fabrication quality assurance verification activities.
- With minor shielding modifications, total surface dose rates of <50 mrem/hr can be attained.

#### Pressure Monitoring

- The performance of the pressure transducer provided with the cask was unsatisfactory, and the transducer failed during the performance test.

## 2.2 RECOMMENDATIONS

The results and conclusions of this experimental work led to the following recommendations:

### Cask Handling and Decontamination

- The redundant cask lifting yoke was not used during the cask performance test. Dry runs should be performed with the yoke prior to using it with a loaded cask.
- Cask handling procedures are site-specific, and procedures should be developed for each site. The experience gained at GE-MO will be helpful in developing such procedures.
- The method required to rotate the cask from a horizontal to a vertical orientation or vice versa is awkward; the standard method of using a shipping cradle as a pivot base is recommended.
- The Carboline silicone base paint should be properly cured to minimize decontamination problems.

### Fuel Characterization and Integrity

- If better precision ( $<\pm 4.1$  W) is needed for measurements of relatively low spent fuel decay heat rates such as those planned for repositories, the in-basin calorimeter should be evaluated for potential methods of increasing precision.

### Heat Transfer

- The maximum decay heat load in the cask during testing was ~15 kW. The maximum cask heat load at allowable fuel temperatures or cask design limits should be determined [see Volume II (Wiles et al. 1986) for predictions of allowable cask heat loads].

### Shielding

- Additional shielding is needed to reduce dose rate peaks and meet design expectations (20 mrem/hr) on the cask side, above and below the neutron shield, and on the cask bottom.

### Pressure Monitoring

- A more reliable pressure monitoring device should be utilized on the cask.



### 3.0 SPENT FUEL STORAGE CASK TESTING

This section describes the REA 2023 BWR spent fuel storage cask and the GE-MO cask testing facility, discusses the test plan, and documents the cask handling procedures and experience.

#### 3.1 CASK DESCRIPTION

The cask tested at GE-MO is a prototype developed for DOE to demonstrate the dry storage of spent fuel. The cask, shown in Figure 3.1, was specifically designed for BWR fuel and specially instrumented for performance testing. Since the cask was built and tested, Mitsubishi Heavy Industries, Ltd. of Japan has obtained design and fabrication rights, and markets the cask as a MSF IV. The cask consists of a double containment design with silicone rubber O-rings for sealing the primary or inner cavity and a welded final closure on the secondary cover. The cask has a smooth, painted, stainless steel outer skin, a lead/stainless steel gamma shield, and a water/glycol neutron shield (Figure 3.2). The fuel basket is constructed of stainless steel clad Boral for criticality control, copper plates to conduct heat to the cask wall, and stainless steel for structural strength. The loaded cask holds 52 assemblies, is approximately 5 m (16 ft) tall and 2.5 m (8 ft) in diameter, and weighs approximately 100 tons. Cask components are described in greater detail in the following subsections; information reported was taken from the REA cask topical report (REA 1983) and is available through the Public Document Room of the U.S. Nuclear Regulatory Commission (NRC) as docket number M33.

##### 3.1.1 Cask Body and Containment Vessel

The structural design of the cask conforms, where applicable, to the ASME Boiler and Pressure Vessel Code, Section III, Division 1 for Class 1 components. Level A stress levels, i.e., stress levels less than 0.67 of minimum yield stresses, were used for normal operation, and Level D stress levels based on controlling deformation were used for accident analyses. The lifting devices, trunnions, and cover hooks are designed to ANSI N14.6 for special

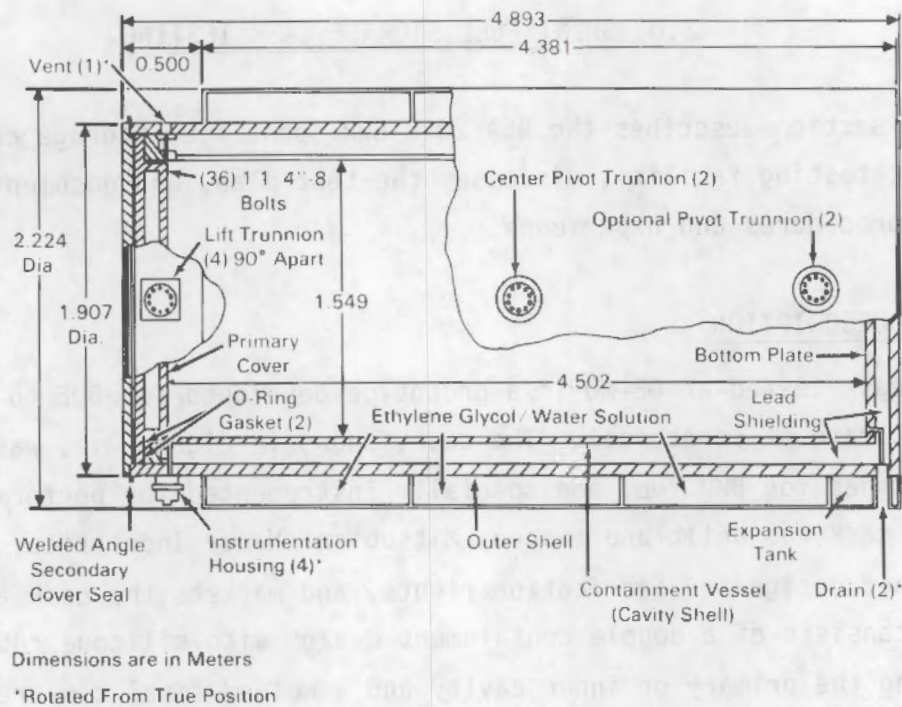


**FIGURE 3.1.** REA 2023 BWR Spent Fuel Storage Cask

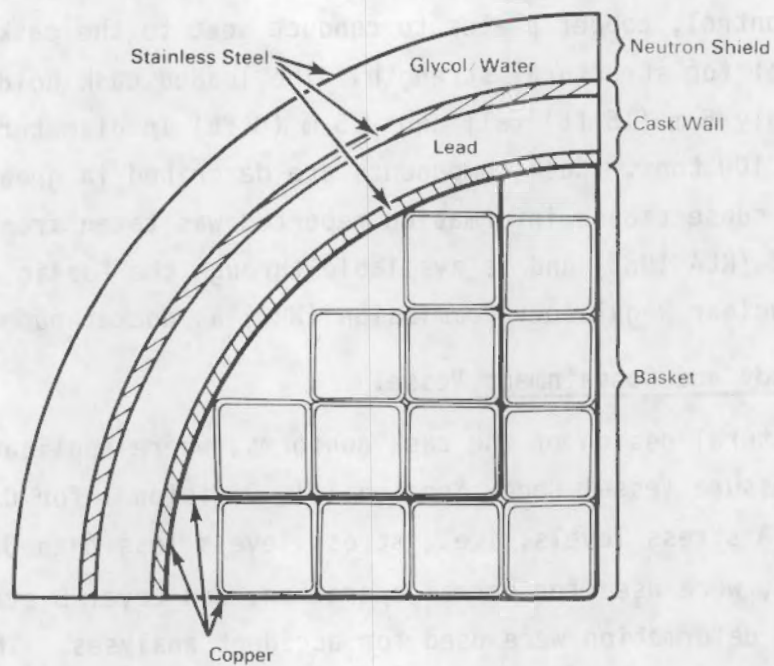


**FIGURE 3.2.** Quarter Section of REA 2023 Cask and BWR Spent Fuel Basket



lifting devices for shipping containers. Design safety factors of 3 and 5 based on minimum yield stresses and ultimate tensile strengths, respectively, were used.

The containment vessel, or cavity shell, is 1.91-cm (0.75-in.) hot-rolled and annealed 304 stainless steel (Figure 3.1). The cavity bottom plate is 5.08-cm (2-in.) stainless steel. The outer cylindrical shell and bottom plate are also 5.08-cm (2-in.) stainless steel. Thicknesses of lead shielding are 10.80 cm (4.25 in.) in the sidewall and 8.26 cm (3.25 in.) in the bottom.

The neutron shield is a 15.2-cm (6-in.) annular tank, divided into two sections and extending from the bottom of the cask to 50.8 cm (20 in.) below the top of the cask. The annular tank contains 3800  $\pm$  (1000 gal) of a 50/50 ethylene glycol/water solution. Within the neutron shield are the trunnion supports, to which the lifting trunnions may be externally bolted.

Vertically, the bottom section (expansion tank) begins 0.64 cm (0.25 in.) from the cask bottom and extends up 40 cm (15.75 in.). The adjoining top section (primary neutron shield cavity) is 398 cm (156.75 in.) long. The only connection between the two sections is a 1.91-cm (0.75-in.) schedule 40 stainless steel siphon pipe that runs from the top of the neutron shield cavity to the bottom of the expansion tank. The neutron shield cavity has top and bottom fill and drain plugs, and the expansion tank has a bottom drain plug.

### 3.1.2 Primary and Secondary Covers

The inner or primary cover (Figure 3.3) is constructed of a 2.5-cm (1.0-in.) stainless steel bottom plate and a 5.08-cm (2.0-in.) top plate, and contains 7.62 cm (3.0 in.) of lead between the two plates. It is secured to the cask body by 36 high-strength bolts 3.18 cm (1.25 in.) in diameter, and made of ASTM-A193, B7 steel. Sealing is obtained by two silicone rubber O-rings. A hole through the top plate, located between the O-rings, permits checking for leak tightness.

The outer or secondary cover is constructed of 5.08-cm (2.0-in.) stainless steel plate. It has a stainless steel angle welded around its periphery to mate with a similar angle at the top of the outer wall of the cask body.



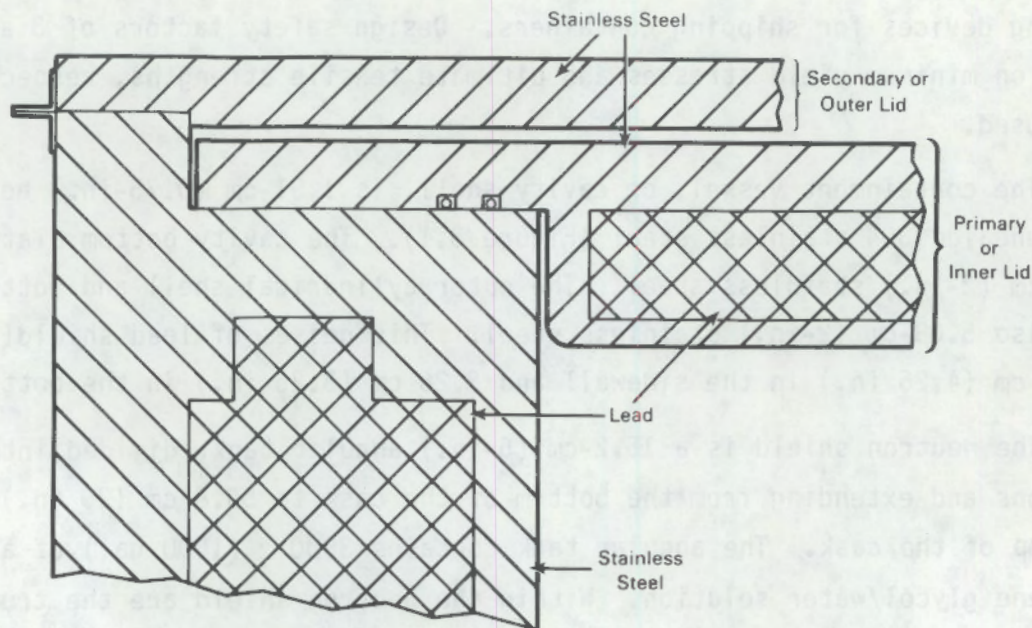


FIGURE 3.3. Primary and Secondary Lids

Normally these angles are seal-welded after loading, to provide high integrity, long-term leak tightness. During performance testing at GE-MO, a clamp ring was used for securing the outer head to the cask. The clamp ring can be seen in Figure 3.4.

Both the primary and secondary covers have holes drilled and tapped in them to facilitate eye-bolt installation for lifting the covers.

### 3.1.3 Containment Vessel Penetrations and Internal Environment

Two 1.27-cm- (0.5-in.-) diameter drain lines penetrate the cavity bottom plate and lead (Figure 3.2). These lines terminate at the outer wall of the cask where they are sealed by 1.27-cm (0.5-in.) pipe plugs in series with 1.91-cm (0.75-in.) pipe plugs. Both plugs are recessed into the neutron shield expansion tank. A 1.27-cm (0.5-in.) vent/sampling line penetrates the cavity wall and lead near the top of the cask, slightly below the primary cover. This line terminates with a dual plug arrangement at the outer wall of the cask, similar to that for the drain lines.



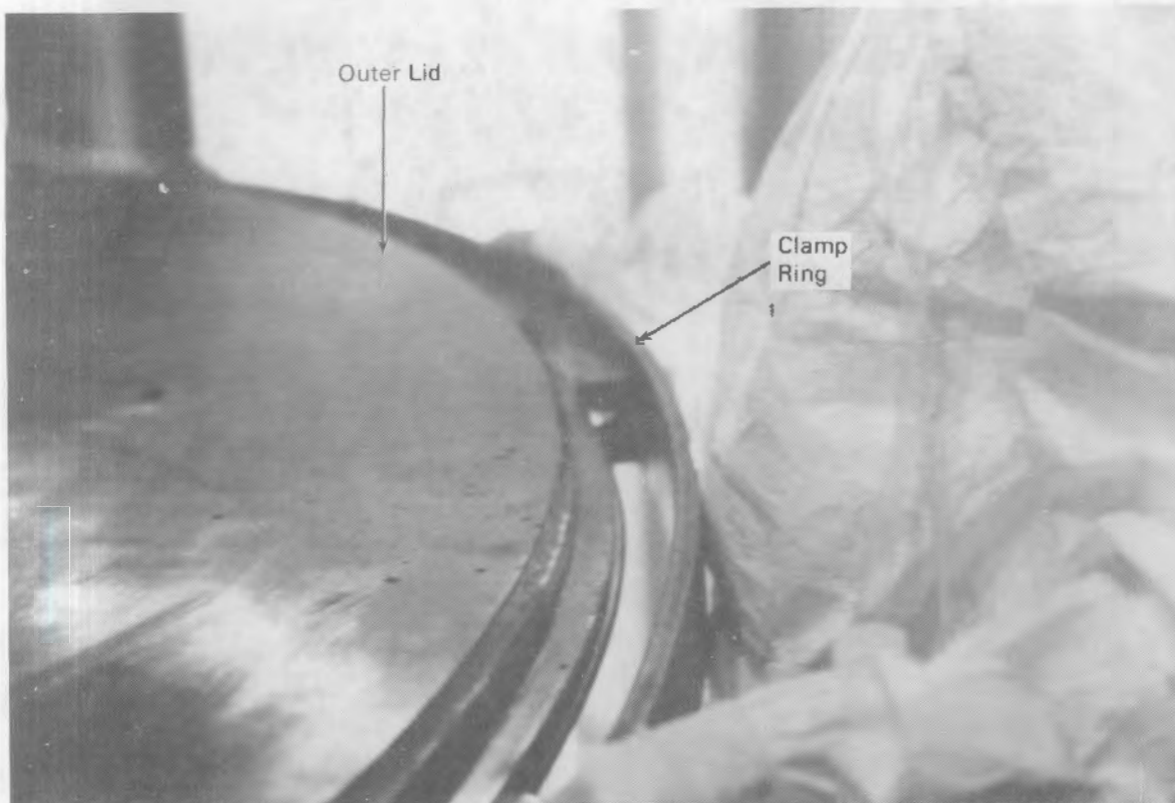


FIGURE 3.4. Secondary Lid Clamp Ring

The REA cask tested at GE-MO had four instrument ports located on its side, above the point where the neutron shield tank terminates (Figure 3.5). These instrument ports provided passthroughs for 38 internally located thermocouples and two pressure transducers.

The REA cask is designed to operate with nitrogen or helium backfill environments. The internal gas pressure should be positive with respect to the atmosphere, 50 to 70 kPa (7 to 10 psig). The pressure transducer mounted on the cask provides a means of detecting leaks during long-term storage.

#### 3.1.4 Lifting Devices

The cask body has eight attachment points or trunnion supports for bolt-on trunnions. Four of these are located near the top, spaced 90° apart, and are used for lifting the cask in the vertical position. Two trunnion supports, 180° apart, are at an elevation slightly above the center of gravity of the



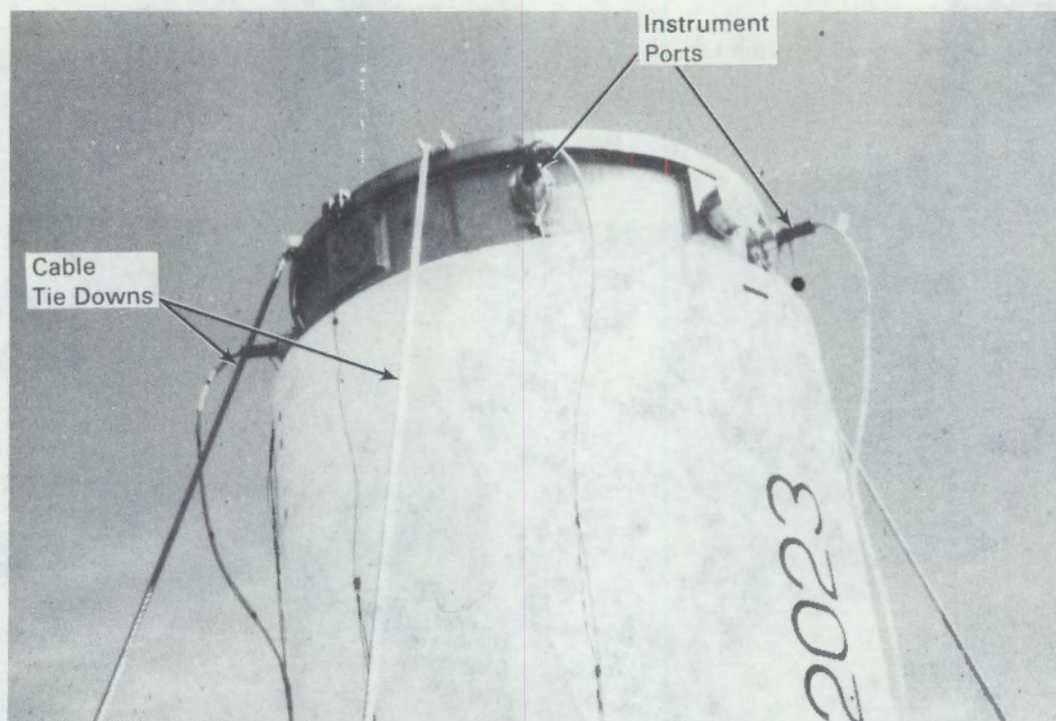


FIGURE 3.5. Instrument Ports with Instrument Leads Connected

cask. These trunnions are used when lifting the cask in the horizontal position, and for rotating the cask from a vertical to a horizontal position or vice versa. The other two trunnion supports are near the bottom of the cask and are located 180° apart. These supports were used for securing the impact limiter to the cask during testing at GE-MO.

A lifting yoke (rated at 109 t) is connected to the cask trunnions to lift the cask with a crane. The yoke has air-operated cylinders that extend or retract the lifting arms used to engage the trunnions. Two sets of lifting arms are used in conjunction with cask handling: a set of short arms (164 cm long) is used for lifting the cask in the vertical mode from the upper trunnions; a set of long arms (390 cm long) is used for rotating the cask on the center trunnions. Figure 3.6 shows the short arms on the lifting yoke.

The yoke consists of two separate components: a primary yoke and a redundant yoke. The redundant yoke fits below the primary yoke and engages the



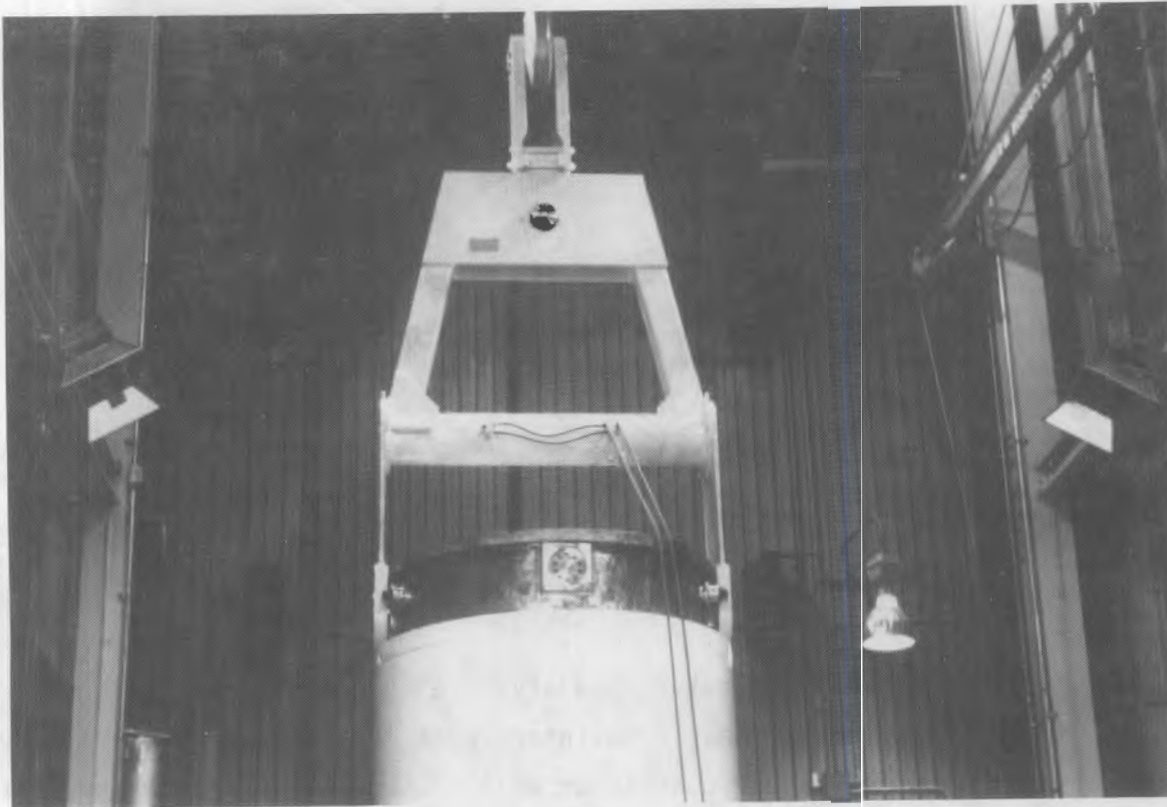


FIGURE 3.6. Lifting Yoke with Short Arms

second set of upper lifting trunnions. The yoke was designed for use with a crane having a redundant lift system, but a special "J" hook adapter was designed and procured for work done at GE-MO because the cask was not lifted in the redundant mode.

#### 3.1.5 Basket

The basket (Figure 3.7) was fabricated in four quadrants, which are placed in the cask cavity. Contact is made between the outer cylindrical copper shells of the basket quadrants and the inner wall of the cask, thus minimizing thermal resistance (Figure 3.2). Each quadrant has thirteen 15.2-cm (6-in.) square spent fuel tubes, each of which contains one fuel assembly. Each fuel tube consists of concentric inner and outer square shrouds, which integrally encapsulate Boral neutron absorber plates. The Boral plates extend above and below the active lengths of the fuel assemblies. These tubes are essentially identical to tubes currently licensed for use in spent fuel storage basins.



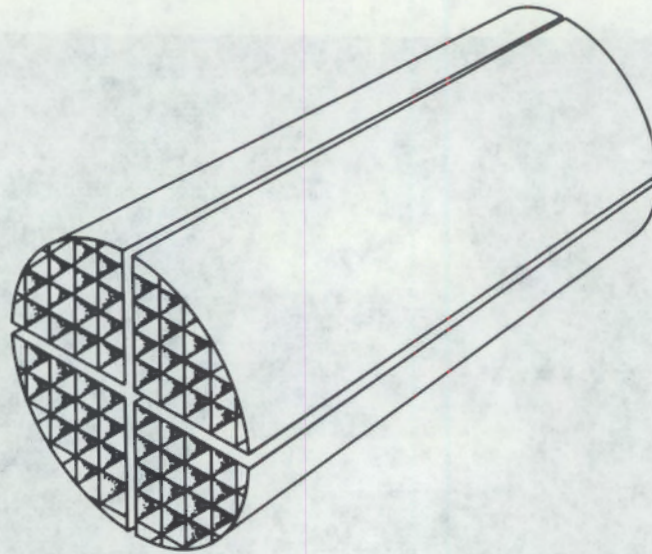


FIGURE 3.7. 52-Assembly BWR Basket

Copper strips are used as the outer boundary of each quadrant and as internal ribs to effectively transfer heat from inner spent fuel assemblies/fuel tubes to the outer copper shells and cask inner wall. Other structural members of the basket are made of stainless steel. The basket rests on the bottom of the cask and has cutouts on the bottom edge to permit water drainage and backfill gas circulation.

### 3.2 GENERAL ELECTRIC-MORRIS OPERATIONS CASK TESTING FACILITY

General Electric-Morris Operation is currently the only Independent Spent Fuel Storage Installation (ISFSI) licensed by the NRC under 10 CFR Part 72. General Electric owns and operates the facility, which is located approximately 50 miles southwest of Chicago. The facility receives and stores PWR and BWR fuel under NRC license SNM 2500 issued in May 1982. Prior to that date, fuel was received and stored under a 10 CFR Part 50 license. As of October 1, 1985, 350 PWR and 1455 BWR spent fuel assemblies were stored at GE-MO, for a total of 401 t of heavy metal.

The REA cask performance test was conducted at GE-MO under Section 35 of 10 CFR Part 72, which permits tests and experiments to be conducted without NRC



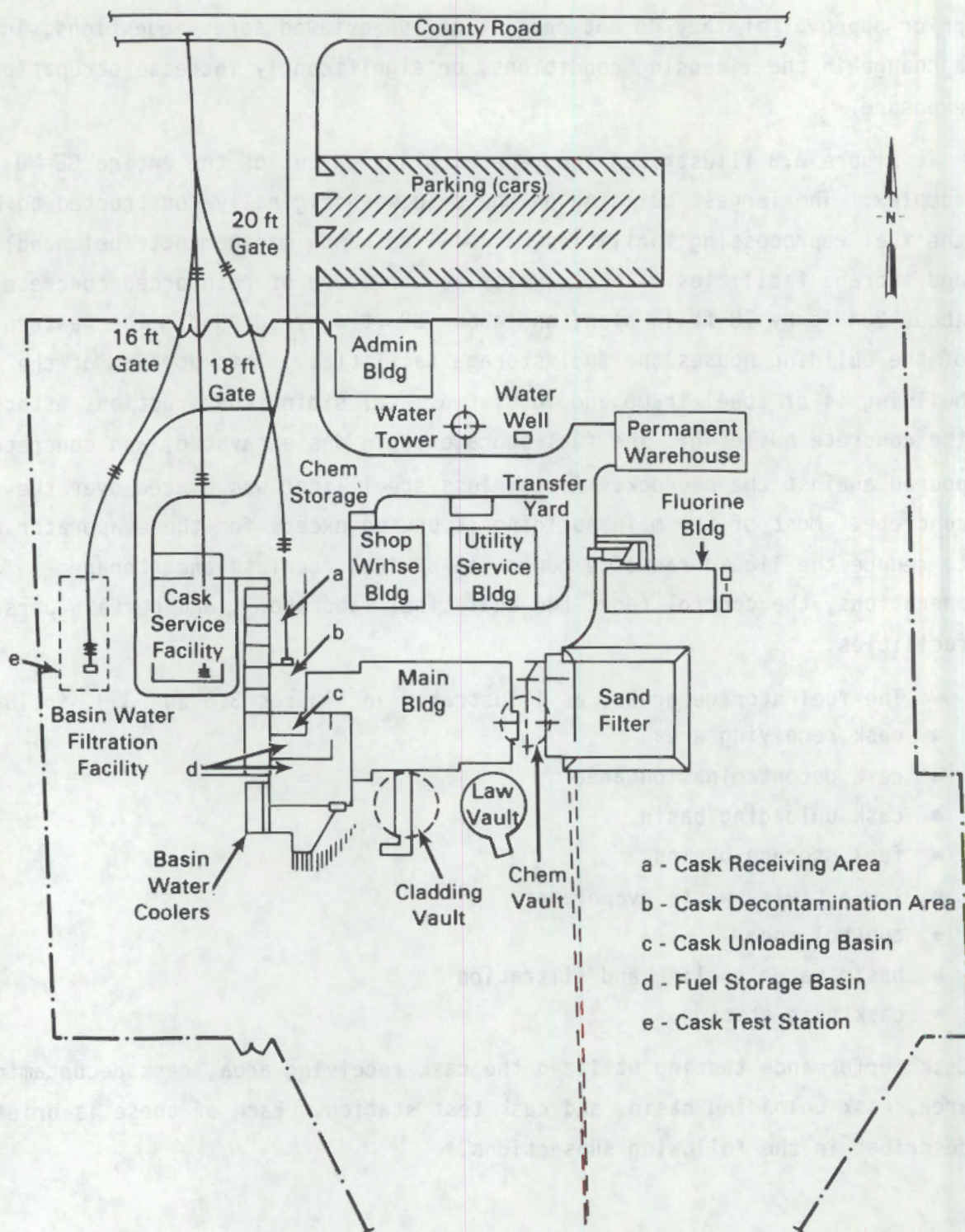
prior approval if they do not present any unreviewed safety questions, involve a change in the licensing conditions, or significantly increase occupational exposure.

Figure 3.8 illustrates the general plant layout of the entire GE-MO complex. The largest building on the site was originally constructed to house the fuel reprocessing facilities, as well as waste management, fuel handling, and storage facilities. It is a massive structure of reinforced concrete, about 204 ft by 78 ft in plan, and about 88 ft above ground. The western end of the building houses the fuel storage facilities. This portion of the building is of steel frame and insulated metal siding construction, attached to the concrete building. The fuel storage basin was excavated, and concrete was poured against the bedrock. A stainless steel liner was placed over the concrete. Most of the main building is unused except for the evaporator used to reduce the liquid radwaste generated by fuel receipts and storage operations, the control room, the analytical laboratory, and certain personnel facilities.

The fuel storage areas, as illustrated in Figures 3.8 and 3.9, include:

- cask receiving area
- cask decontamination area
- cask unloading basin
- fuel storage basins
- low-activity waste evaporator
- control room
- basin water cooling and filtration
- cask test station.

Cask performance testing utilized the cask receiving area, cask decontamination area, cask unloading basin, and cask test station. Each of these is briefly described in the following subsections.



**FIGURE 3.8.** General Electric-Morris Operation Fuel Storage Facility



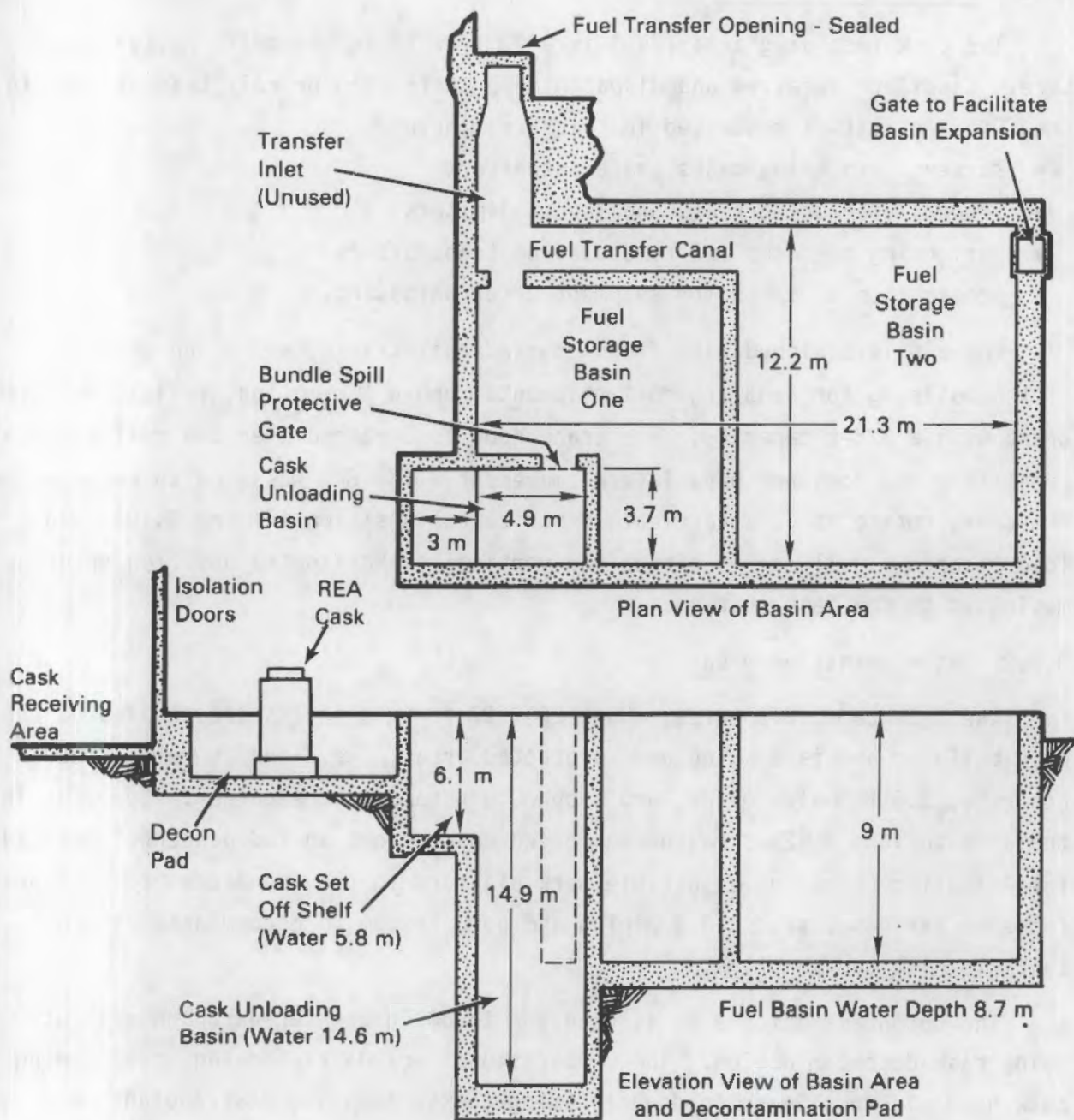


FIGURE 3.9. General Electric-Morris Operation Fuel Storage Basin



### 3.2.1 Cask Receiving Area

The cask receiving area (CRA) is a 20 ft x 69 ft minimally heated structure. Casks are received and dispatched on their road or rail transporters in the CRA. Activities conducted in this area include:

- survey of incoming casks and transporters
- removal of cask barriers and impact limiters
- uprighting of casks and removal from transporters
- preparation of casks for shipment after unloading.

The CRA is equipped with flush-mounted rail tracks, which run the length of the building for handling rail shipments, and a two-motion, radio-controlled crane with a 125-t capacity. The crane hook is centered over the rail track centerline and does not have lateral movement. The CRA was used to receive the REA cask, rotate it to a vertical or horizontal position (Figure 3.10), and load it onto a rail car in either the vertical or horizontal position prior to moving it to the test station.

### 3.2.2 Decontamination Area

The decontamination area, about 20 x 27 ft in plan, is located inside the main building and is a safeguards protected area. The floor is reinforced concrete, 3.5 ft below grade, and sloped to a sump in one corner. Services in the area include a 125-t radio-controlled cask crane; an independent, overhead fuel-handling crane; an adjustable work platform to provide access to all surfaces of various casks; and a piping and pump system to accommodate internal cask flushing and sampling.

The decontamination area is used for incoming cask preparation and outgoing cask decontamination. These operations include tightening or loosening cask head closures, washing down incoming casks, sampling cask coolant, and decontaminating casks. The area is used for other activities involving maintenance of contaminated equipment and preparation of solid radioactive waste for shipment.



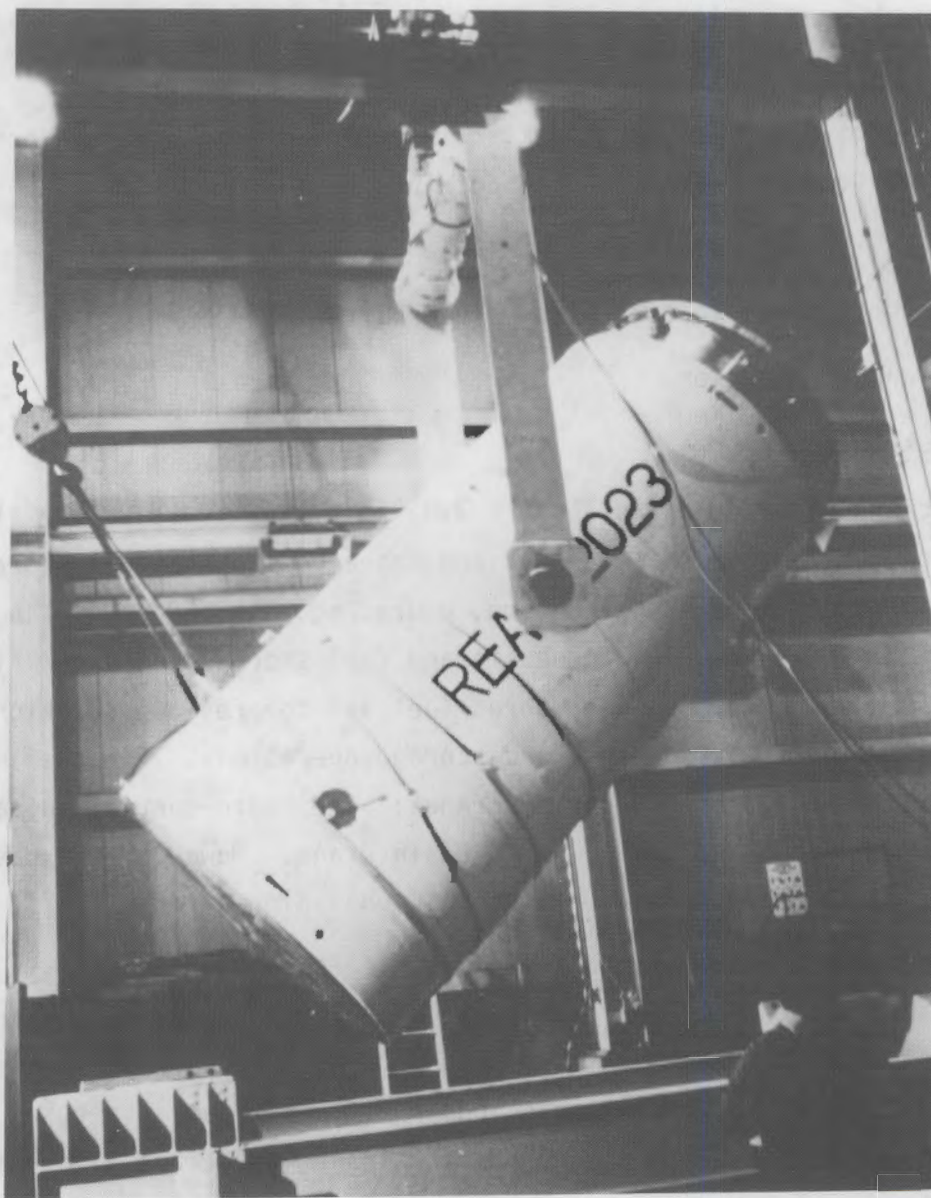


FIGURE 3.10. Cask Rotation

This area was used to accomplish the following activities associated with the REA cask performance test:

- installation and orientation of all internal cask thermocouples prior to fuel loading
- torquing and untorquing of cask head bolts



- all cask preparations required before the empty cask was placed in the unloading basin
- removal of water from the cask, cask vacuum-drying, cavity inerting, and leak-checking after cask loading
- cask cavity gas sampling
- cask performance testing with vacuum backfill
- cask decontamination.

### 3.2.3 Cask Unloading Basin

The cask unloading basin (Figure 3.9) is a two-level, water-filled basin adjacent to the decontamination area and connected to the fuel storage basins. It is a reinforced concrete structure, poured against bedrock, with a stainless steel liner. The cask unloading basin and fuel storage basin are filled with demineralized water to cool the stored fuel and to provide radiation shielding during fuel unloading, transfer, and storage operations. The cask unloading basin is serviced by three facility cranes: the radio-controlled cask-handling crane, the fuel-handling crane, and a basin crane. However, the basin crane services only the deep portion of the cask unloading basin.

The primary purpose of the set-off shelf (shown in Figure 3.9) is to provide a place to set casks while changing the lifting hardware. When an extension hook is installed between the crane hook and the cask lifting yoke, the cask can be lowered to the unloading basin floor without submerging the crane hook and block. This eliminates contamination of the crane with basin water.

The deep unloading basin provides sufficient shielding when spent fuel is removed from a cask and placed in storage baskets. Storage of the baskets is then possible in shallower fuel storage basins.

The floors of the set-off shelf and the cask unloading basin are provided with devices to dissipate impact loads from a cask-drop accident. However, in the case of the REA cask, an impact limiter had to be attached to the cask base to provide additional protection for the cask.



The unloading basin was used during the cask performance test for:

- taking radiation profiles (gamma and neutron) of the fuel assemblies with a detector loaned to GE-MO by Los Alamos National Laboratory (LANL)
- obtaining decay heat generation rates of the test fuel assemblies in an in-basin calorimeter
- instrumenting of selected fuel assemblies with thermocouples during loading into the REA cask
- loading and unloading of the REA cask.

#### 3.2.4 Cask Test Station

A cask test station was constructed at the end of the west railroad spur (Figure 3.8). As shown in Figure 3.11, the test station consisted of the end of the railroad spur, a depressed-center rail car, a weather station, and a chainlink fence. The end of the rail spur was selected to minimize interference with ongoing fuel receipts, locate the test area away from generally occupied personnel areas, and perform the cask performance test near a building (cask service facility shown in Figure 3.8) in which the data acquisition system could be housed.

The depressed-center rail car was rated at 150 t and was constructed entirely of metal. The depressed center was 0.6 m above ground and was advantageous when lifting or working with the REA cask. The cask remained on the rail car in either a vertical or horizontal orientation throughout cask performance testing. When in the horizontal orientation, the shipping cradle was used to support the cask.

The fenced enclosure limited access to the cask to those people working on the testing activity, and served as a reminder to other personnel not to linger too long near the cask because of potential radiation exposure. Because the cask test station was within the GE-MO perimeter fence, the test station fence served no security function.



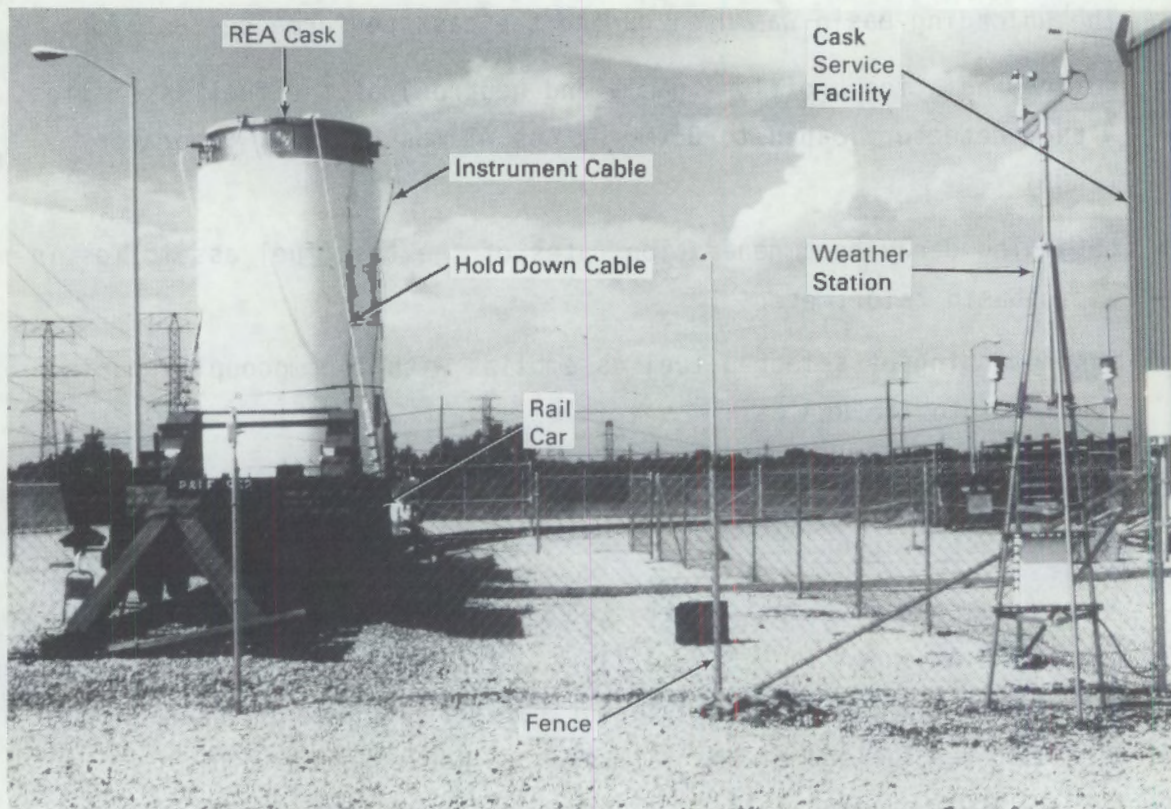


FIGURE 3.11. Cask Test Station

### 3.3 TEST PLAN

The cask performance test consisted of the 14 runs indicated in Table 3.1. The test runs involved two loadings, three backfill environments, and two cask orientations. A test plan specified the order of the runs, spent fuel assembly load patterns, instrument/measurement locations, calibration requirements, and gas and crud sampling intervals. The test plan also addressed cask handling and fuel assembly characterization activities that were required prior to and after performance testing.

The test plan required gas samples to be taken each time the cask was loaded and each time the fill gas was changed. The samples taken are indicated in Table 3.1.

The load pattern used for the partial and full loads is shown in Figure 3.12. The shaded areas represent the load pattern specified for the partial load. Fuel assembly locations were selected based on pre-test thermal



TABLE 3.1. Cask Performance Test Matrix

Run Number	Loading, Number of Spent Fuel Assemblies	Total Decay Heat, kW	Fill Gas	Cask Orientation
1(a)	28	9.0	Vacuum	Vertical
2	28	8.9	Nitrogen <sup>(c)</sup>	Vertical
3	28	8.9	Nitrogen <sup>(c)</sup>	Horizontal
4	28	8.8	Helium <sup>(c)</sup>	Horizontal
5	28	8.8	Helium <sup>(c)</sup>	Vertical
6(a)	52	15.2	Vacuum	Vertical
7	52	15.1	Nitrogen <sup>(c)</sup>	Vertical
8(b)	52	14.9	Nitrogen	Vertical
9	52	15.0	Nitrogen <sup>(c)</sup>	Horizontal
10	52	14.8	Helium <sup>(c)</sup>	Horizontal
11	52	14.9	Helium	Vertical
12(a)	52	14.4	Helium <sup>(c)</sup>	Vertical-Insulated
13(a)	52	14.4	Nitrogen <sup>(d)</sup>	Vertical-Insulated
14(a)	52	14.3	Vacuum	Vertical-Insulated

(a) Run inside the cask service facility (CSF).

(b) Rerun of Run 7 after cask was rotated to a horizontal orientation and returned to the vertical.

(c) Gas sample taken.

(d) Two gas samples taken.

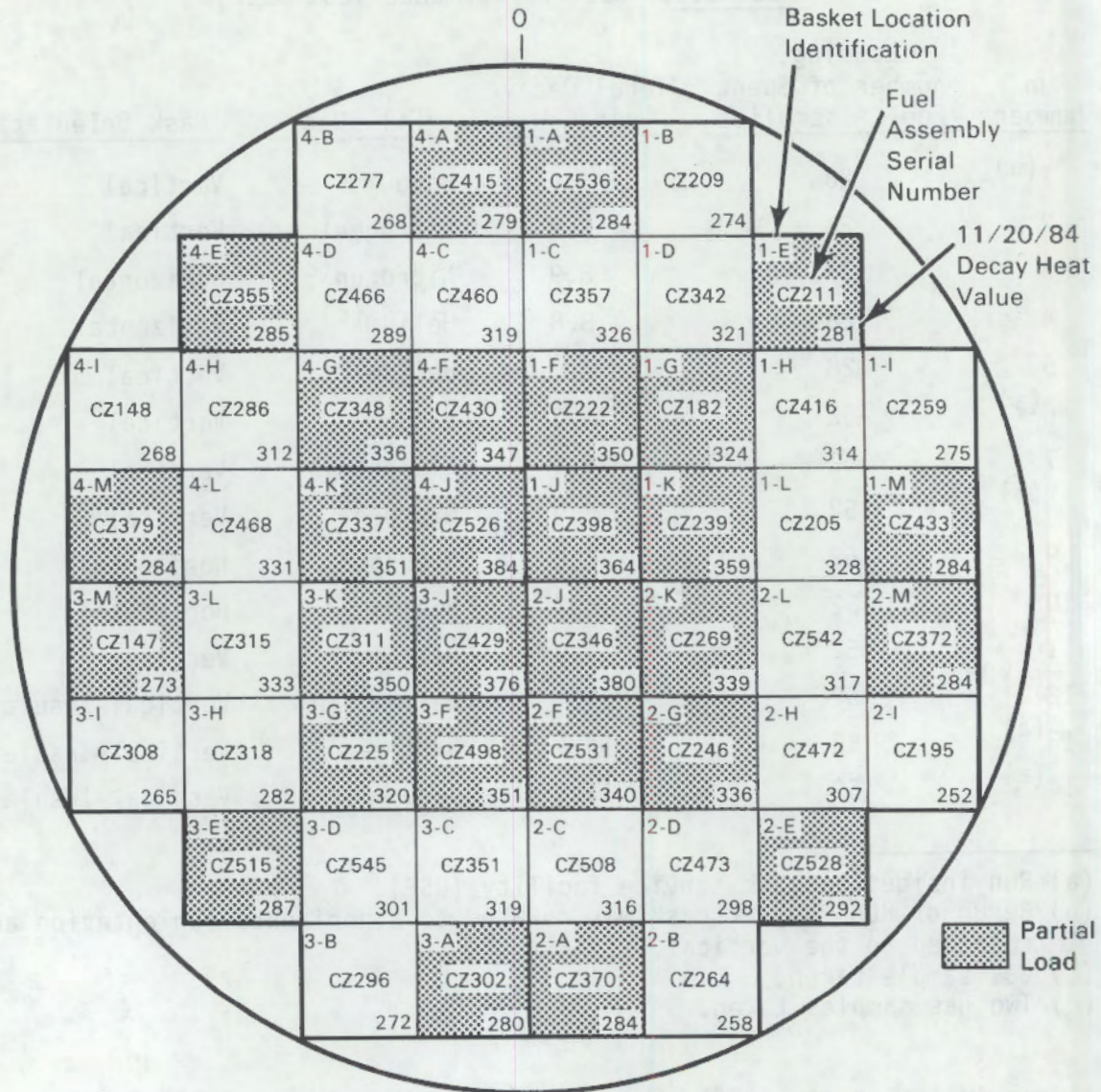
analyses (Wiles et al. 1986), the results of calorimetry, combined with a desire to locate the hottest fuel assemblies in the center of the cask and to maintain 1/8 symmetry in the cask to ease the analytical modeling effort. In addition to location, Figure 3.12 gives the decay heat output of each fuel assembly adjusted to a common date. The adjustment is based on calorimetry data and predicted daily rates of decay.

Cask thermal instrumentation consisted of 70 type K thermocouples, six weather station inputs, and two pressure transducers. The location of each thermal measurement was specified in the test plan and is described in



Quadrant #4

Top of Cask



Quadrant #3

Quadrant #2

FIGURE 3.12. REA 2023 Cask Load Pattern

Section 5.1.1. Likewise, the radiation dose rate measurement instrumentation used and the measurement locations on the cask are described in Section 5.2.1.

The spent fuel assemblies used in the performance test were well characterized prior to their use. ORIGEN2 predictions (Wiles et al. 1986) were used in the initial selection of spent fuel assemblies. The selected fuel assemblies were obtained in a shipment from the Cooper reactor to GE-MO. After the



selected fuel assemblies were received at GE-MO, each was subjected to in-basin sipping, axial radiation scans, and calorimetry. Five fuel assemblies were visually inspected by videotaping and by use of underwater 35-mm photography.

The test plan formed the basis for GE-MO development of a set of procedures that addressed the specific requirements of the performance test. The procedures resulted in the data reported herein and consisted of:

- instrument identification and placements
- instrument and data acquisition system calibrations, checkout, and continuity checks
- placement of thermocouples on the cask exterior
- development and testing of the fuel thermocouple attachment device (TAD)
- placement of thermocouples on the fuel and cask basket
- operation and calibration of the calorimeter
- radiation measurements associated with the cask and the fuel
- loading patterns and fuel assembly placements within the cask
- fuel integrity checks through in-basin sipping and calorimeter water sampling
- dry runs of the REA cask
- vacuum drying
- performance of cask test runs
- collection and identification of crud and gas samples
- decontamination of the cask
- video and 35-mm documentation of the fuel, cask, and performance testing.



### 3.4 CASK HANDLING AND DECONTAMINATION PROCEDURES AND EXPERIENCE

Handling a 100-t cask in a nuclear facility is not easy. The sheer size and mass of a large storage cask create unique handling problems that differ from those for standard transportation casks. This section describes the procedures used at GE-MO to safely handle the REA 2023 cask during the performance test, as well as the experience gained. The procedures developed were similar to existing cask loading and unloading procedures used by utilities. It should be noted that the procedures and experience are specific to the GE-MO facility, and will be only partially applicable to other facilities. Equipment needs will vary, depending upon the need for redundant lifting and because of differences in physical sizes of basins, cask receiving areas, and decontamination areas.

Before the REA cask was handled at GE-MO, a dimensional check and interface study were performed to determine the presence of any critical minimum clearances through which the cask would not fit. Elevations were checked to ensure that the fuel could be loaded into the cask, and that the cask would clear facility structures when lifted. Crane capacities and lifting hardware capacities had to be checked to make sure that the equipment was capable of handling the cask.

The required cask-handling equipment either existed at GE-MO or was obtained. Table 3.2 provides a list of equipment that was used at GE-MO; similar equipment would be required at other facilities.

Of utmost importance in handling any new cask at any facility is the performance of a "dry run" before the cask is loaded. No matter how thorough the interface study or how many times the cask has been used before, it is imperative that a dry run be performed before a cask is initially used at a facility. A dry run was especially important at GE-MO because this was the first time the REA cask had been handled.

The handling procedures summarized in the following subsections were developed using the generic REA procedures (REA 1983), handling experience



TABLE 3.2. REA Cask Handling Equipment Used For Basin Handling and Fuel Loading

Item	Use
125-ton overhead crane	Handling cask
5-ton auxiliary crane	Removing head and handling fuel
7-1/2-ton mobile crane	Rotating cask
Yoke alignment guide	Mating yoke with cask
Primary lifting yoke	Lifting cask
Secondary (redundant) lifting yoke	If redundant lift required
Over-the-shelf yoke hanger(s)	Storing yoke
Long lifting arms	Rotating cask
Short lifting arms	Vertical lifting
7-in.-diameter pin for REA yoke	Connecting "J" hook adapter to yoke
"J" hook adapter	Connecting yoke to crane
Extension hook	Placing cask on basin bottom
Impact limiter	Drop protection
Decontamination pad scaffolding	Decontaminating cask
Over-the-shelf scaffolding	Working on cask when on unloading basin shelf
Cask flush system	Pumping water from cask
Helium leak detector	Leak-checking cask
Vacuum drying system	Drying cask
High purity gas fill-station	Backfilling cask
Miscellaneous torque wrenches	Torquing trunnions and primary head
Miscellaneous slings	Moving equipment
Miscellaneous spare parts	Replacing parts as necessary

gained by Allied General Nuclear Services in Barnwell, North Carolina, and dry runs performed at GE-MO as part of the performance test. The procedures encompassed:

- cask removal from rail car
- cask transfer from CRA to decontamination pad
- loading preparations

- cask transfer to unloading basin
- cask loading
- cask return to shelf and decontamination pad, primary head torquing, and helium leak checking
- vacuum drying
- decontamination area operations prior to return of cask to rail car
- cask placement on rail car for performance testing
- cask rotation during performance testing
- gas sampling/changing during performance testing
- cask decontamination
- personnel exposure monitoring.

#### 3.4.1 Cask Removal from Rail Car

Removing the cask from the rail car required removing the shipping restraints, installing the trunnions and lifting arms, and lifting the cask from the rail car and placing it on the impact limiter. The steps followed to accomplish these tasks were:

- Remove front and rear shipping spacers and hold-down bands (Figure 3.13).
- Place lifting yoke on crane and attach long lifting arms to yoke.  
NOTE: A crane of at least 109-t capacity is needed.
- Position impact limiter in CRA. Place several sheets of 1.9-cm (0.75-in.) plywood under impact limiter to level.
- Move rail car into CRA and secure. Brake end of rail car must be north so cask will clear hand brake when being moved to decontamination pad.
- Install center trunnions.
- Using cask crane, position primary yoke and long arms on center lifting trunnions, and engage trunnions.



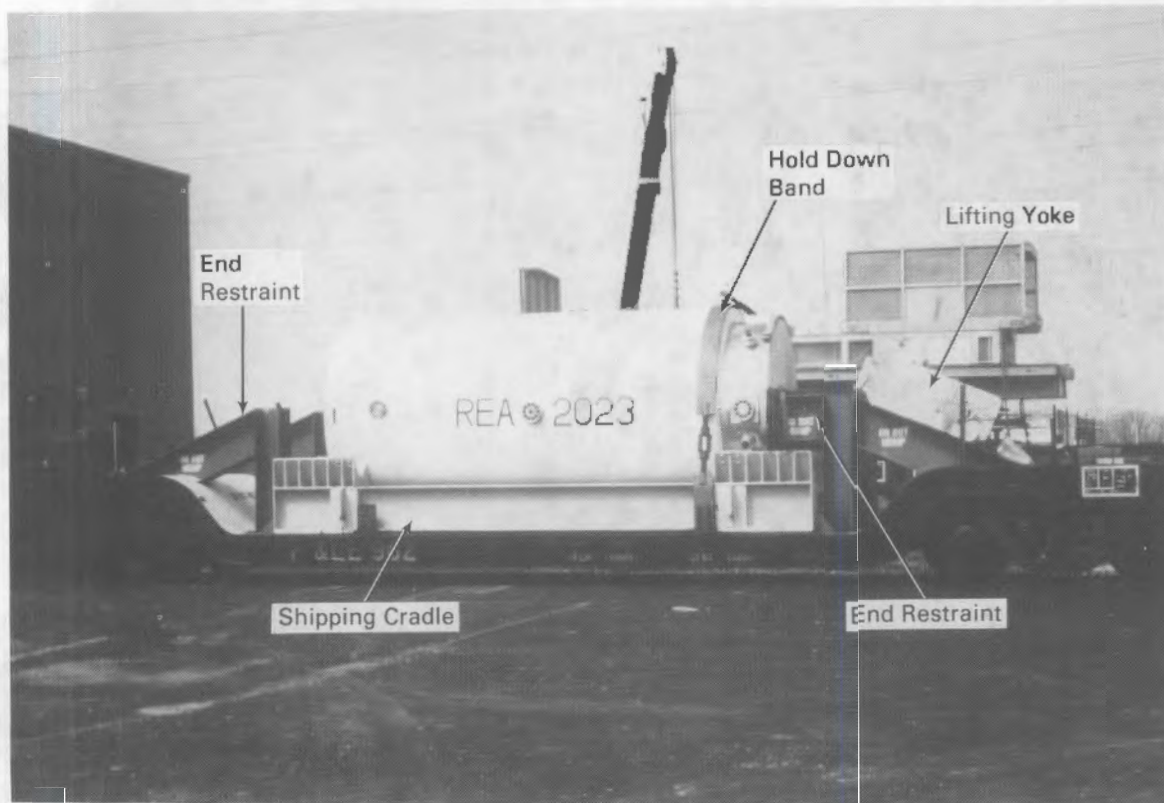


FIGURE 3.13. REA Cask on Depressed-Center Rail Car

- Lift cask in horizontal position. (If cask is empty, it will balance and can be lifted without resorting to two-point pick. If cask contains fuel, it will be bottom-heavy, and two-point pick method described in Section 3.4.9 must be used.)
- After cask is lifted and rail car removed, rotate cask to vertical position. Use fork truck and two slings to pull cask into vertical position (Figure 3.14).
- Position cask over impact limiter. Lower cask onto impact limiter and secure to cask lower trunnions.

The method used to rotate the cask from a horizontal to a vertical orientation was found to be awkward. The empty cask was well balanced and did not rotate when it was lifted by the center trunnions. Pulling the cask to a vertical position with a fork truck was not a normal procedure at GE-MO and required practice.

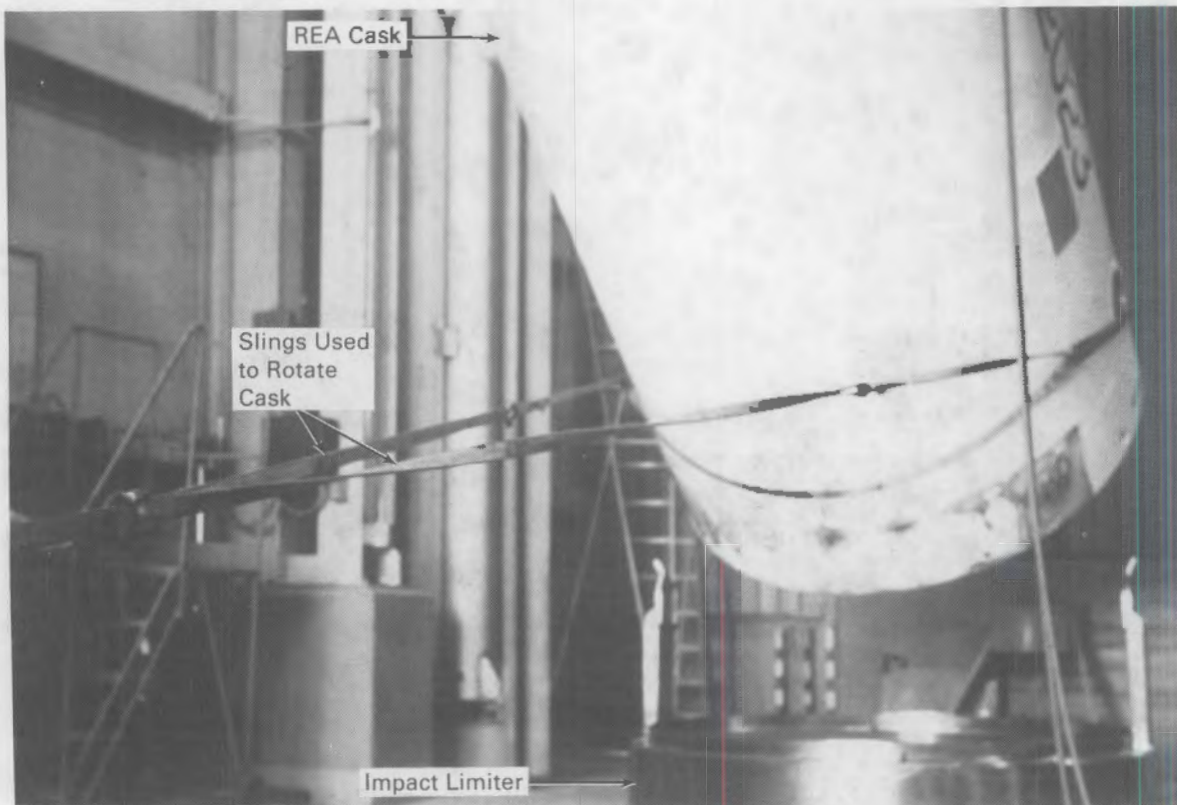


FIGURE 3.14. Use of Slings to Rotate Cask into Vertical Orientation

Once the cask was placed on the impact limiter, the limiter attachment arms had to be field-welded to the limiter to ensure proper fitup with the cask lower lifting trunnion bolt holes.

#### 3.4.2 Cask Transfer from Receiving Area to Decontamination Pad

The transfer of the cask from the CRA to the decontamination pad required changing the arms of the yoke, engaging the trunnions, and moving the cask to the pad. The steps involved were as follows:

- Disengage yoke from cask.
- Remove long lifting arms and install short arms.
- Remove center trunnions from the cask.



- Install upper trunnions and engage them with short lifting arms. Verify that yoke is properly engaged to upper trunnions.
- Raise cask and move to decontamination pad.

### 3.4.3 Loading Preparations

After the cask was placed on the decontamination pad, scaffolding was assembled to facilitate working on the cask. Preparations prior to loading included removal and storage of the heads, inspection of cask components, and preparations for installation of internal instrumentation. The steps followed were:

- Assemble special scaffolding.
- Remove secondary head clamp ring and note each half's orientation relative to cask.
- Install four eye-bolts in secondary head, attach four cable lifting slings, and remove secondary head.
- Loosen primary head by removing thirty-six 3.17-cm (1-1/4-in.) bolts. Attach biological shield to primary head; then position and attach yoke alignment guide to biological shield as shown in Figure 3.15. Attach lifting bail and yoke alignment guide to biological shield; then remove primary head.
- Inspect primary head O-rings located on underside of head.
- Inspect cask and cavity.
- Install all internal thermocouples and pressure transducers for performance testing.
- Remove and inspect inner and outer plugs at vent and drain ports.
- Fill cask with basin water.

Some modification work was required on the yoke alignment guide used to align the lifting yoke(s) with the trunnions. This guide is very important when the yoke must be re-engaged to the cask under water. The yoke alignment guide was shortened so that it did not interfere with closure of the lifting



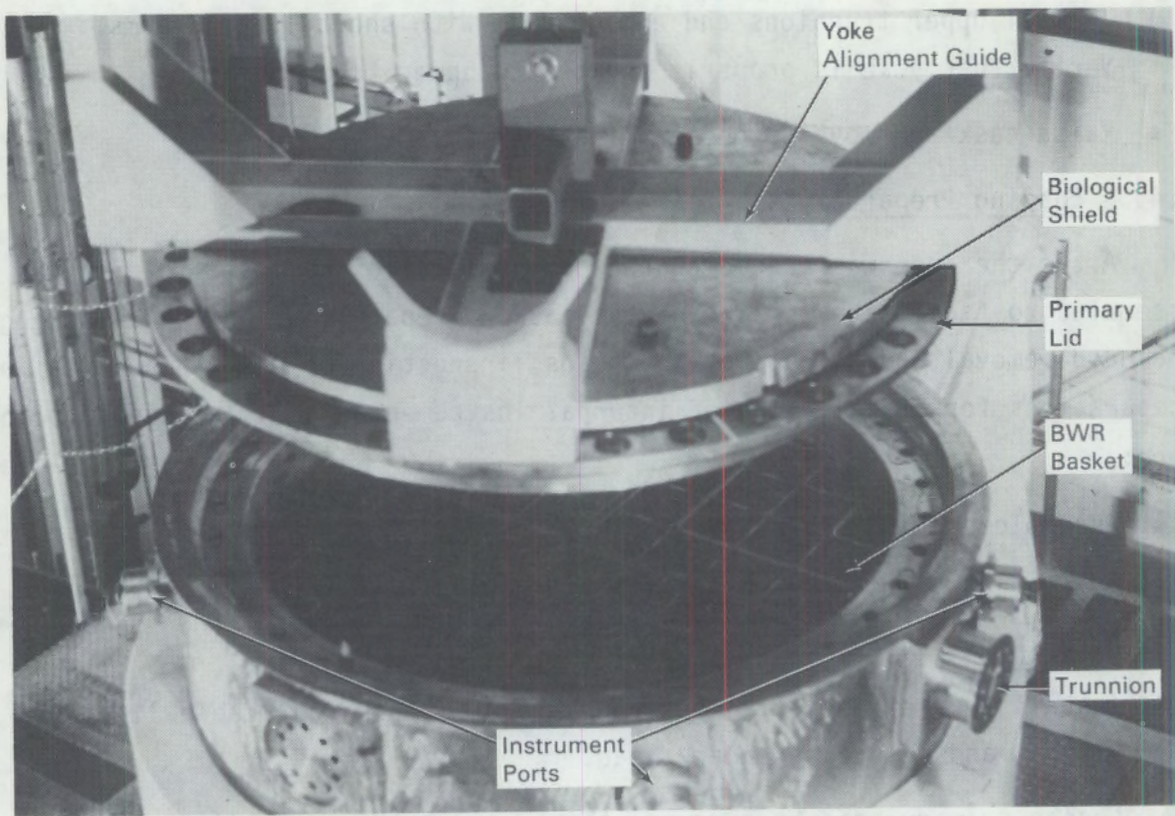


FIGURE 3.15. Preparation of Primary Head for Fuel Loading

arms. The guide cradle rests were adjusted so they did not interfere with the yoke antirotation arm, and a lifting bail was installed so the primary head could be more easily installed on the REA cask by means of a "J" hook.

#### 3.4.4 Cask Transfer to Unloading Basin

Moving the cask to the unloading basin was a two-part process. First, the cask was picked up and placed on the shelf ~6 m (20 ft) under water in the unloading basin. Then, after the lifting hardware was changed, the cask was placed on the floor of the unloading basin ~15 m (49 ft) under the water surface. The steps used were as follows:

- Engage primary yoke to cask. Observe both trunnions to verify proper engagement of yoke.
- Move cask to unloading basin.
- Open drain and vent fittings before cask enters water.



- Wet cask down with demineralized water as it is lowered into unloading basin.
- Secure yoke in an upright position using cable hangers after cask is placed on unloading basin shelf ~6 m (20 ft) below water surface.
- Pick up extension hook and re-engage primary yoke.
- Using overhead crane, slowly move cask through extension hook hangers and lower to unloading basin floor ~15 m (49 ft) below water surface (Figure 3.16).
- Disengage yoke from cask, and raise yoke to full up position.
- Place yoke on special over-the-shelf yoke hanger, and disengage crane.
- Move extension hook and cask crane to full north position.

#### 3.4.5 Cask Loading

Fuel assemblies were loaded into the REA cask in a manner similar to that used to load fuel into a transportation cask. Seven of the fuel assemblies were instrumented with thermocouples as they were loaded into the cask (Figure 3.17). The thermocouple attachment device (TAD) and the method used to install the thermocouples are described in detail in Appendix A.

#### 3.4.6 Cask Return to Shelf and Decontamination Pad, Primary Head Torquing, and Helium Leak Checking

Once loaded with spent fuel, the cask was removed from the unloading basin in preparation for cask performance testing. The steps required to execute this procedure were as follows:

- Clean seal surface of cask by wiping with soft cloth or sponge attached to long pole.
- Using fuel-handling crane and special lifting hook, lift primary head assembly (head, biological shield, yoke alignment guide, and lifting bail) from decontamination pad.
- Install head assembly on cask and verify proper seating and correct orientation.

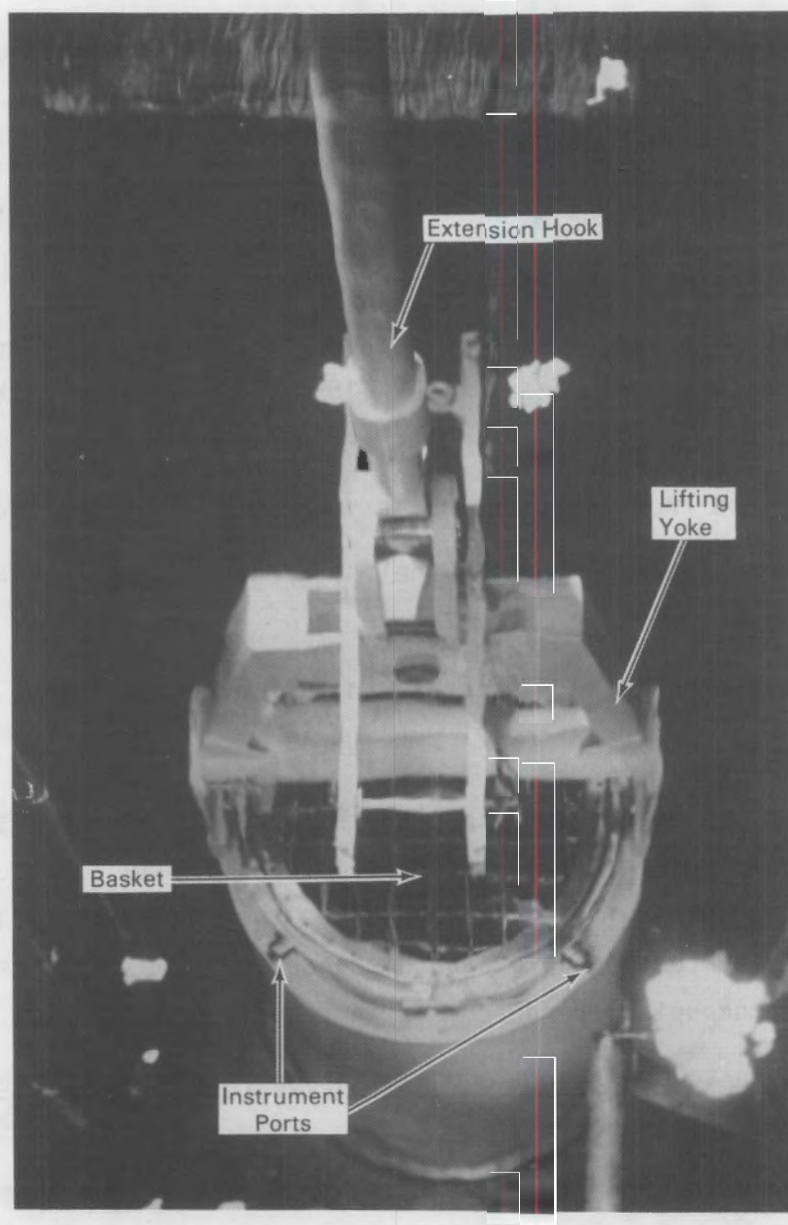


FIGURE 3.16. Cask in Unloading Basin

- Engage yoke to cask and verify that trunnions are properly engaged.
- Slowly lift cask and observe possible misalignment of yoke on lifting trunnions.
- Take dose rate readings over top of cask as it is moved to shelf area.
- Set cask on shelf and hang up extension hook.



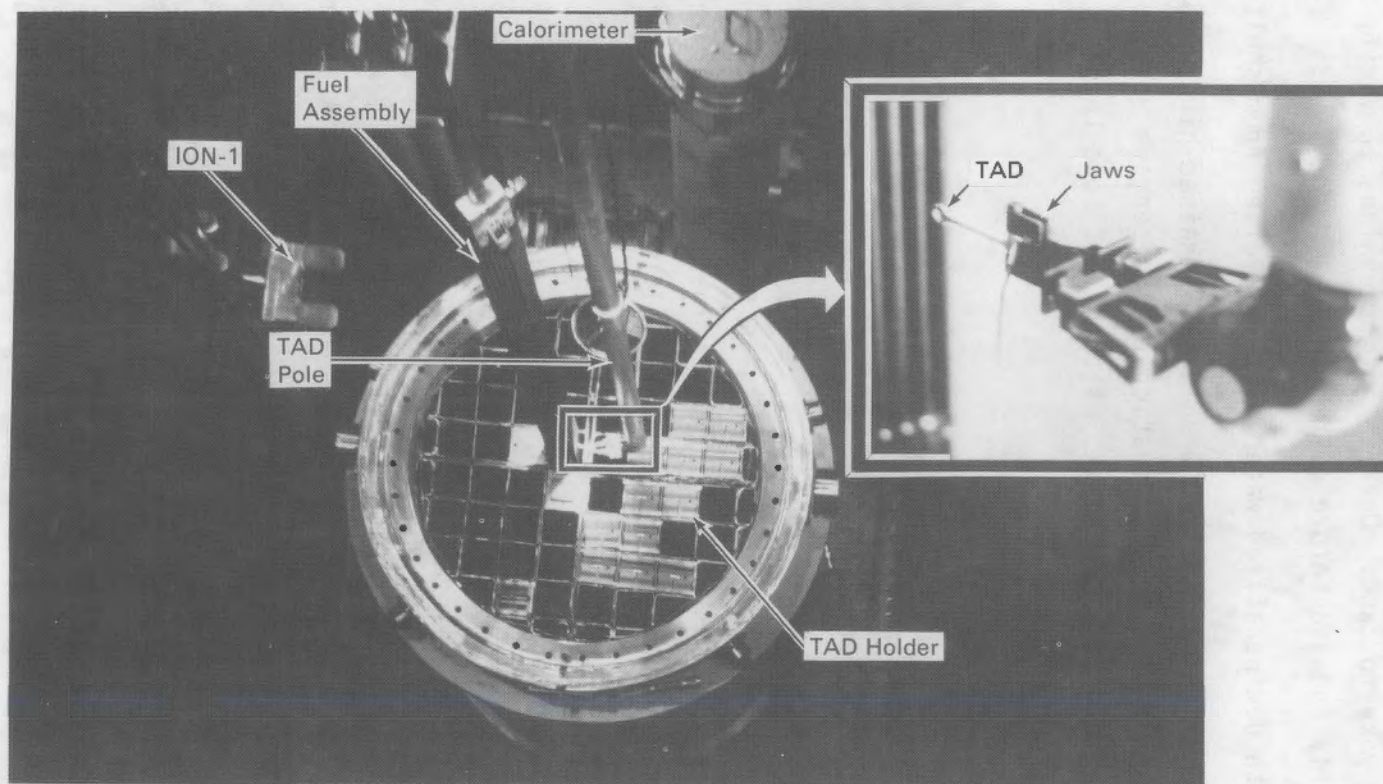


FIGURE 3.17. TAD Installation in Unloading Basin



- Install four reasonably evenly spaced primary head bolts.
- Remove yoke alignment guide and lifting bail.
- Re-engage REA yoke to cask. Observe both trunnions to verify that yoke is properly engaged before lifting.
- Rinse cask with demineralized water as it is raised from shelf.
- Close vent and drain port valves when cask is raised high enough to do so; transfer cask to decontamination pad, disengage yoke, and reassemble scaffolding around cask. Attach vent hose to cask, and vent cask.
- Connect data acquisition system.
- Vacuum water from head area and clean with wipes. After the water has been removed from primary head and bolt holes, secure primary head.
- Connect helium purge line to cask vent adapter and displace ~0.6 m (2 ft) of water from cask. Perform preliminary helium leak check around primary head and instrument ports. If no leak larger than  $1.0 \times 10^{-6}$  cc/sec is observed, proceed.
- Hook vent and drain hoses to cask, and drain water from cask using helium to displace water. Purge cask cavity with helium for 2 hours after water has been removed.
- Remove hoses and install plugs. Perform final helium leak check of cask. Check head seal area, instrument ports, and drain plugs.

The REA-supplied lifting yoke arms were activated by means of reversible air cylinders. During the dry runs, it was found that the hydrostatic pressure at the bottom of the unloading basin could become great enough to close the arms. This was a problem whenever the cask had to be removed from the bottom of the unloading basin. The problem was solved by venting the center of the yoke (air cylinder location) so pressures could equilibrate between the inner region of the yoke and the basin.



During dry runs and after the primary head was installed under water and the head bolts torqued, it was discovered that the bolts, even though tightened to 27.7 kg-m (200 ft-lb), would loosen over time. The problem was traced to water trapped in the ends of the bolt holes, making the bolts behave as if they had bottomed out during torquing. When the cask sat for a period of time, the water leaked out through the threads and the bolts loosened. New bolts were procured with holes drilled in the centers to relieve the hydrostatic pressure. This solved the bolt-loosening problem, but left a vacuum-drying problem. The water remaining in the bolt threads during the vacuum-drying process was sufficient to corrode the bolts. The problem was finally solved by removing the cask completely from the water and drying the bolt holes, one at a time with each bolt removed, before finally installing the bolts. Personnel exposure (both neutron and gamma) associated with torquing the head in air on the decontamination pad did not differ significantly from that associated with torquing the head under water, because less time was needed to torque the head in air.

#### 3.4.7 Vacuum Drying

After the cask was leaktight, it was vacuum-dried to remove residual moisture. The vacuum-drying procedure that follows was designed to remove moisture from the cask in such a way that ice was not formed. No effort was required to minimize the vacuum-drying time because of the relatively low heat load in the cask. The steps used to vacuum-dry the cask are as follows:

- Remove vent adapter and install pressurizing device. (Refer to Figure 3.18 for a cross-sectional view of pressurizing device. Refer to Appendix B for equipment associated with vacuum-drying system.)
- Verify data acquisition system hook-up, and monitor fuel internal temperatures during vacuum drying. NOTE: Hottest fuel pin temperatures may be reached during vacuum drying.
- Attach vacuum hose to pressurizing device, evacuate cask to 4 kPa (30 mm Hg), and valve out vacuum pump. Monitor pressure buildup for 1 hour. Repeat evacuation and monitoring steps until cask pressure remains at 4 kPa.



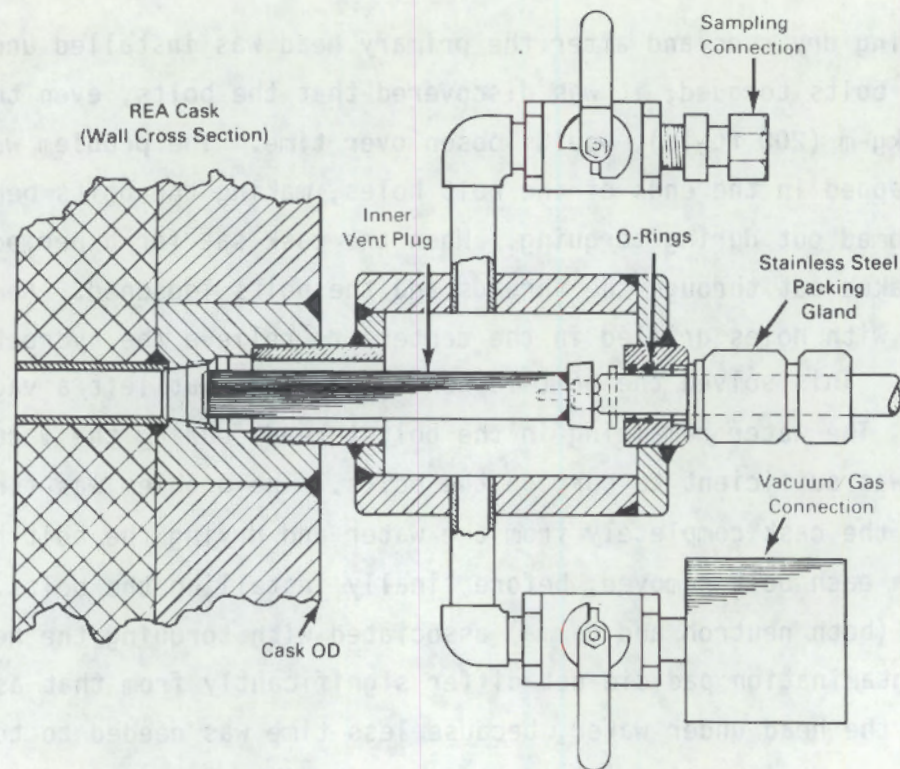


**FIGURE 3.18.** Pressurizing Device

- Evacuate cask to 0.27 kPa (2 mm Hg). Observe rate of pressure decrease at 0.9 kPa (7 mm Hg). Hesitancy in the rate of decrease around 0.9 kPa may mean formation of ice. If necessary, repressurize cask to 1.3 kPa (10 mm Hg) with helium, and repeat evacuation until no hesitancy is observed.
- Once cask is at 0.27 kPa (2 mm Hg), valve out vacuum pump and monitor cask pressure for 6 hours. Any pressure increase over 6-hour period indicates residual water or leak.
- Repeat pumpdown to 0.27 kPa and 6-hour monitoring sequence until there is no observed increase in pressure over 6-hour period.
- Once cask cavity has been successfully vacuum-dried, repeat procedure to vacuum-dry area between two O-rings on primary head.



#### 3.4.8 Decontamination Area Operations Prior to Cask Return to Rail Car

Before the cask was placed on the rail car, it was filled with gas, and the exterior surface was decontaminated. The steps used to accomplish these tasks are as follows:

- Fill cask to 50 kPa (7.5 psig) with designated storage gas. Evacuate cask, and refill to 50 kPa with designated storage gas.
- Sample storage gas. (Refer to Section 3.4.11 for details of gas sampling.)
- Install inner vent plug. Remove pressurizing device and install outer vent plug.
- Decontaminate cask using standard procedures with soap and water. (Details are found in Section 3.4.12 and Appendix C.)
- Install secondary head on cask. Secure the secondary head to the cask with special clamp rings. Apply silicone sealant to top surface of cask before installing secondary head to form gasket.
- After gasket sealant on secondary head has dried sufficiently, vacuum-dry space between two heads.
- Attach impact limiter to cask per Section 3.3.1 (Figure 3.19).

The REA cask used for cask performance testing was designed to have a removable outer head. Normally the outer head would be seal-welded in place, leak-checked, and vacuum-dried. However, during the performance test the outer head was secured to the cask by means of a clamp ring instead of being seal-welded. Because of the uneven top surface of the cask, it was impossible to achieve a leak-free seal; consequently, the space between the two heads could not be easily vacuum-dried. Several different types of gaskets and sealants were tried, but did not work. This problem is unique to the performance test where the secondary head was not welded in place.



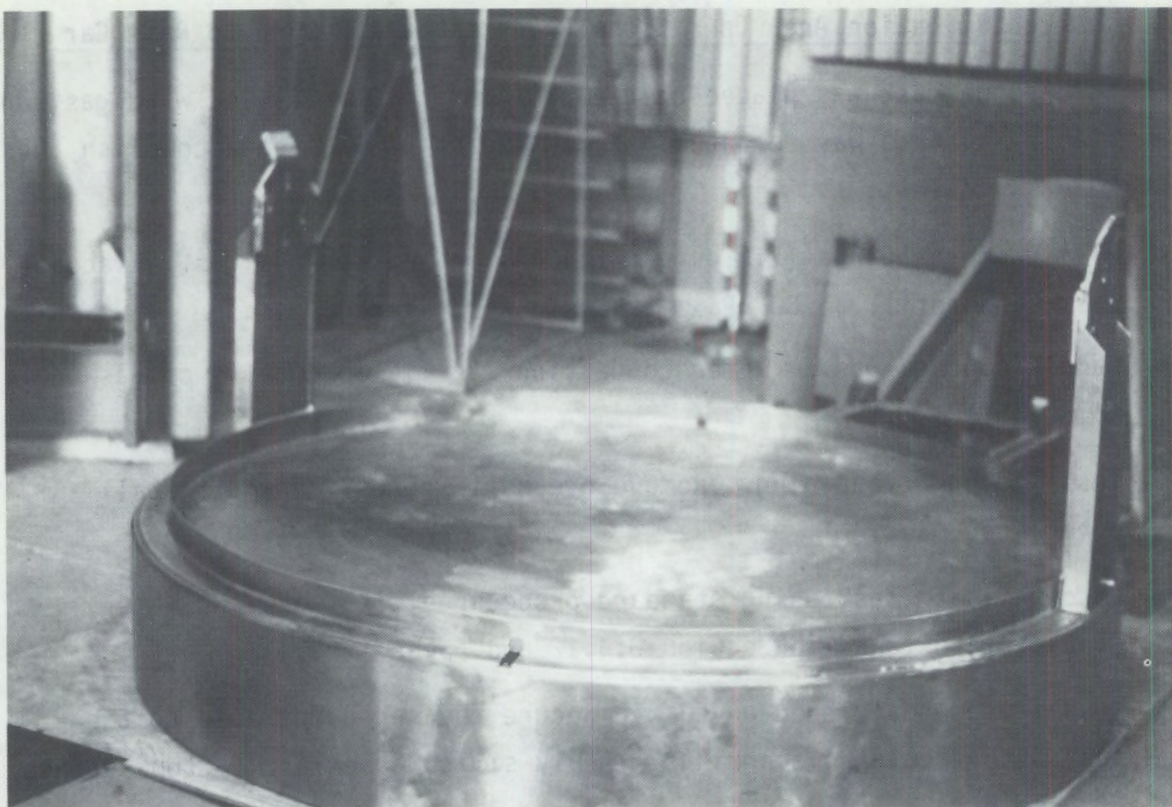


FIGURE 3.19. Impact Limiter

#### 3.4.9 Cask Placement on Rail Car for Performance Testing

The cask was placed on the rail car in the vertical position prior to being moved to the test station. The following steps were used:

- Raise cask, with impact limiter attached, and transfer it to CRA.
- Set cask down on plywood supports and remove impact limiter.
- Raise cask until it is high enough to clear rail car structure.
- Move rail car under suspended cask, and lower cask onto center of depressed-center rail car. Position plywood sheets on rail car bed to prevent damage to bottom of cask.
- Disengage lifting yoke from upper cask trunnions.
- Using an auxiliary jib crane, position cable crossover fixture on top of cask.



- Secure two 2.54-cm (1-in.) steel cables over top of cask, and secure cables to rail car with clevises (Figure 3.20). Move cask to test station.

Once the cask was at the test station, the instrumentation cables were connected and test runs in accordance with Section 3.2 were performed. The pressure transducer supplied to monitor the internal cask pressure did not perform satisfactorily. The output signal was very sensitive to temperature, and resulted in erroneous pressure measurements. During testing, the transducer failed; the test was completed using a backup sensor installed at the start of the performance test.

Three rupture disk failures occurred, one prior to loading fuel into the cask and two during the insulated test runs. The failures were most likely associated with improper selection and damage (overtorquing) to the disks during installation. To solve this problem, the standard rupture disks supplied with the cask were replaced with rupture disks using a vacuum support and a protective ring. No failures occurred after this change was made.

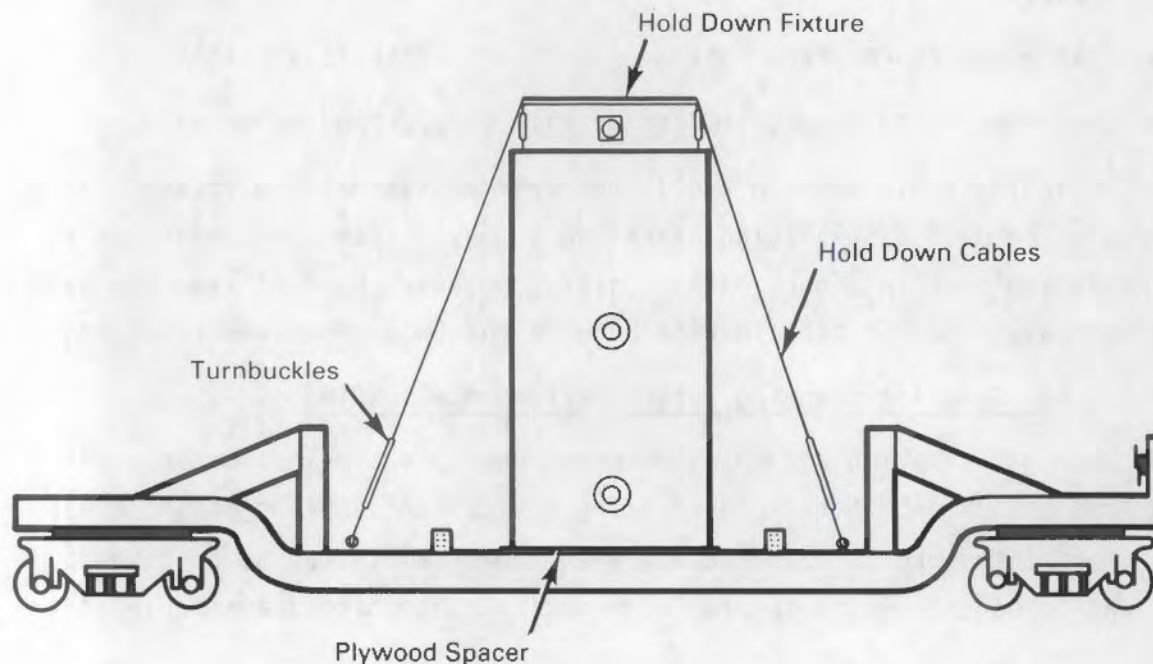


FIGURE 3.20. REA Cask and Rail Car

#### 3.4.10 Cask Rotation During Performance Testing

The steps used to rotate the cask from the horizontal to the vertical position were as listed below. Rotation from the vertical to the horizontal position was done in a similar manner.

- Install center trunnions.
- Using cask crane, position yoke and long arms on center lifting trunnions. Verify that lifting arms are properly engaged on trunnions.
- Position mobile crane as close to rail car as possible.
- Using one 6-m (20-ft) and two 4.5-m (15-ft) nylon slings, connect choker to bottom of cask. Attach other end of choker to mobile crane.
- Slowly raise both cask crane and mobile crane, using care to keep cask horizontal. Refer to Figure 3.21.
- Slowly begin lowering bottom of cask by letting out line from mobile crane.
- Disconnect choker from bottom of cask once cask is vertical.
- Lower cask onto impact limiter or rail car, depending on need.

As indicated in Section 3.4.1, the cask was awkward to rotate. When full of fuel, the main cask-lifting crane and a mobile crane were required to maintain the cask in a horizontal position because the fuel made the cask bottom-heavy. Smooth coordination between the two cranes was required.

#### 3.4.11 Gas Sampling/Changing During Performance Testing

Both gas sampling and changing were done in a similar manner. Both required attachment of the pressurizing device. A sampling manifold was attached to the pressurizing device when a gas sample was to be taken. If the gas was to be changed, a special high purity gas manifold available in the CRA



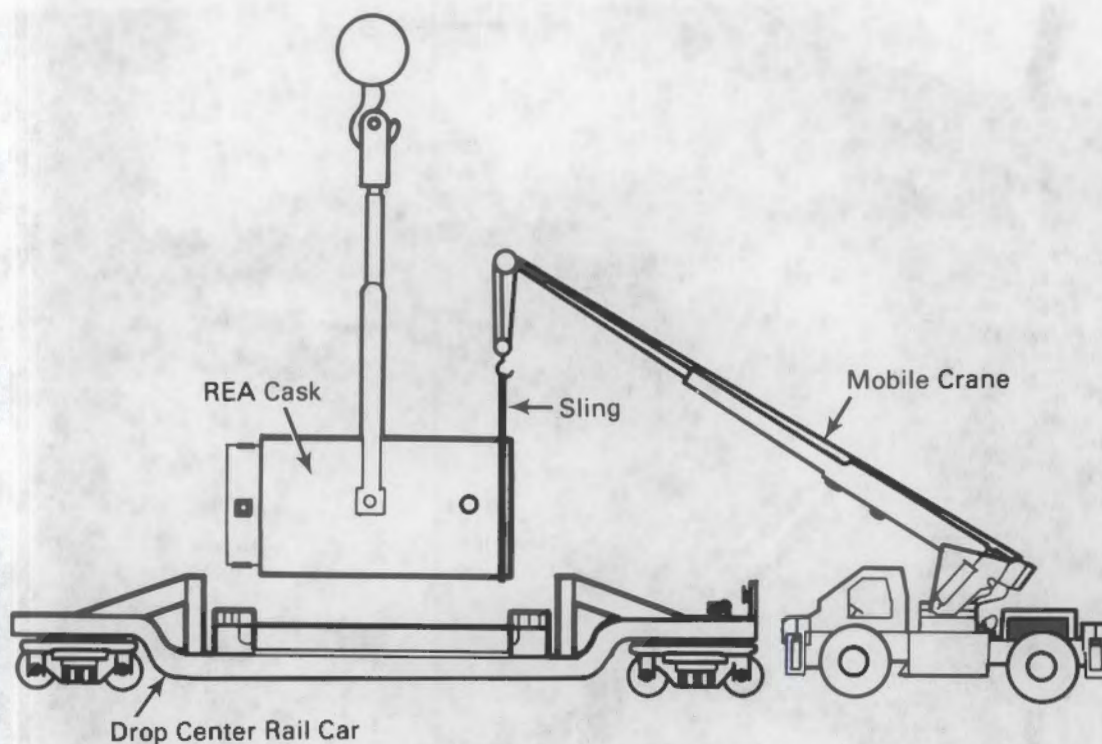
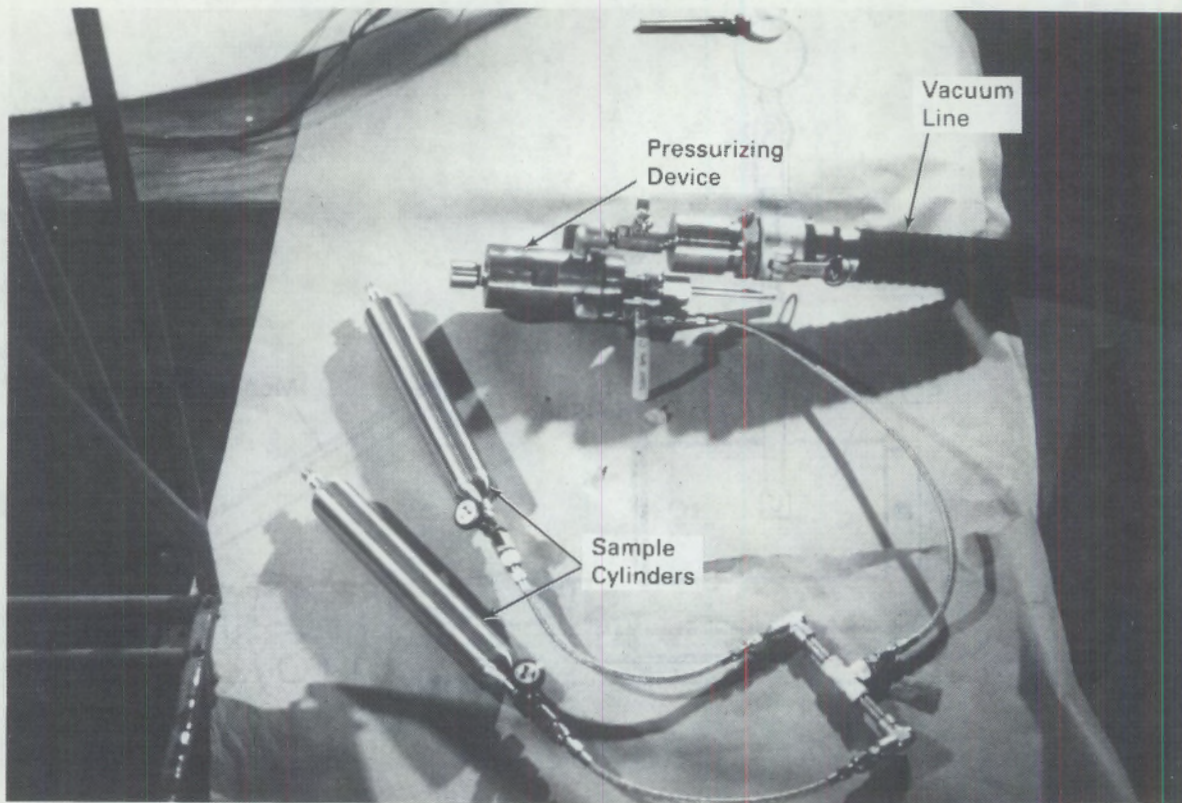


FIGURE 3.21. Cask Rotation and Lifting

was valved into the evacuation manifold, and the cask was evacuated and backfilled with the desired gas. The following steps were used to take gas samples:

- Remove outer 1.9-cm (0.75-in.) plug of vent port and install pressurizing device into vent port.
- Start vacuum pump.
- Attach two 500-cc gas bottles to sampling manifold on pressurizing device.
- Attach connecting vacuum hose to pressurizing device. (Refer to Figure 3.22.)
- Evacuate manifold and sample bottles.
- Check leak rate of manifold. The manifold should hold  $<2.7$  kPa (5 torr) for 15 minutes. Proceed when leak rate is below acceptable minimum.





**FIGURE 3.22.** Pressurizing Device and Gas Sampling Equipment

- Valve out vacuum pump and remove inner plug using pressurizing device.
- Fill both cylinders if taking a gas sample.
- Replace inner plug and close cylinder valves.
- Evacuate manifold.
- Repressurize with air; then remove sample cylinders.
- Remove pressurizing device and replace outer 1.9-cm (0.75-in.) plug.

The pressurizing device (Figure 3.18) supplied and used for gas sampling/ changing did not allow consistently high quality gas samples to be obtained. The sealing mechanism on the shaft of the device allowed air to leak into gas samples. The problem was corrected by adding an O-ring seal around the shaft of the plug removal rod. Elbows were used to attach the gas bottle manifold



and vacuum line to the pressurizing device, to prevent interference between the pressurizing device and the secondary trunnion mounting block.

#### 3.4.12 Decontamination

Methods used to decontaminate both the external surface of the cask and the internal cavity are discussed in the following subsections. Experience gained during decontamination activities is presented.

##### 3.4.12.1 External Surface

The cask external surface was decontaminated each time it was removed from the basin. Cask decontamination was done to remove smearable surface contamination that accumulated on the cask surface during underwater loading and unloading in the basin. The method used to decontaminate the cask was simply manual scrubbing with a detergent and water solution, followed by rinsing and drying.

After the cask was decontaminated, smear surveys were made of the cask surface to verify that the removable contamination was less than 20 dpm/cm<sup>2</sup> for beta-gamma emitting isotopes. To evaluate the possibility of radioactive contamination leaching from the cask surface, the cask was surveyed when it was delivered to the storage area (outgoing survey) and when it was returned to the basin area (incoming survey). Any increase in smearable activity over this duration was indicative of leaching of radioactive material out of the surface.

The cask was sectioned into 96 different areas (see Appendix C) to permit taking representative smear surveys and allow easy identification of the smears (Figure 3.23). Each area on the side of the cask was approximately 0.6 m x 0.9 m (2 ft x 3 ft). Smaller areas were marked off on the top and bottom of the cask and around the outer head closure area. Surveys were made by wiping a 100-cm<sup>2</sup> area from each designated area of the cask with a paper planchet.

A comparison of the outgoing to incoming smear surveys was made to assess the leaching of radioactive contamination from the surface. As can be seen in Table 3.3, the incoming surveys were very similar to the outgoing surveys (see Appendix C for additional surveys). This indicates that the cask surface



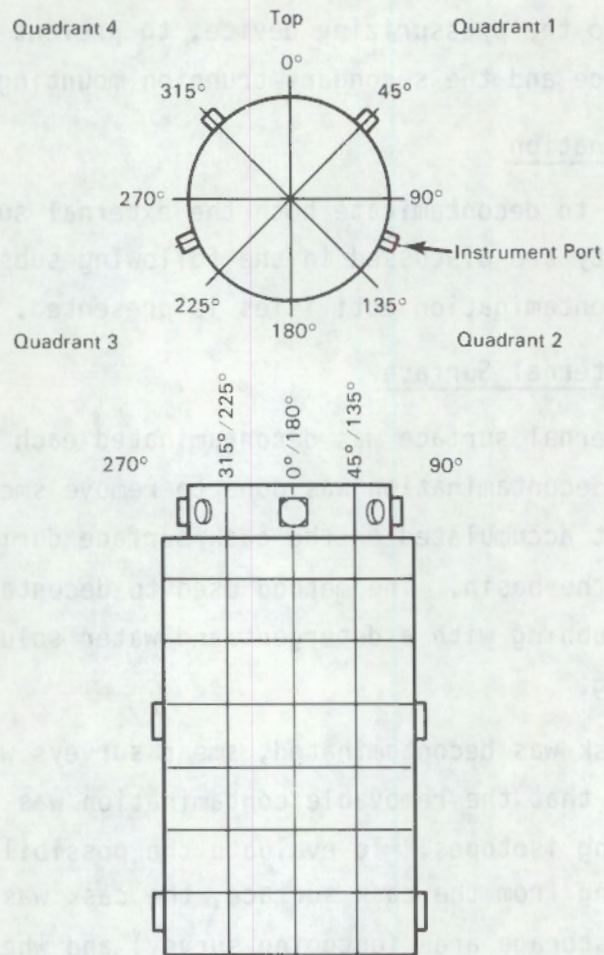


**FIGURE 3.23.** Smear Survey Grid

exhibited very little tendency to leach (or hold) radioactive contamination. The time between incoming and outgoing smear surveys was 45 days for the partial load and 91 days for the full load.

The outer surface of the cask is made entirely of stainless steel; that portion of the cask comprising the neutron shield tank is painted. This was done to ease the decontamination effort and to improve the emissivity of the surface. The painted area of the cask could usually be decontaminated with a reasonable effort, except when the paint softened as a result of higher surface temperatures. During insulated cask test runs, the paint became very soft and the insulation stuck to the paint. From conversations with Carboline, the paint is supposed to be hard and stable to over 235°C when properly cured.

**TABLE 3.3.** Comparison of Outgoing and Incoming Surveys  
for the REA Cask

Load Condition	Measured Surface Contamination, dpm/100 cm <sup>2</sup> (a)	
	Outgoing	Incoming
Partial Load	393	156
	409	206
	773	704
	351	321
	635	469
	659	356
	813	454
	556	456
	746	327
	581	603
Full Load	137	147
	453	875
	953	957
	1215	913
	924	325
	946	219
	762	302
	869	261
	941	328
	1213	965

(a) Each value listed is the average (mean) of  
10 smears.

Apparently, the paint was not properly cured and, because the cask was wrapped with insulation, the insulation adhered to the surface. When the insulation was removed, it separated, and part of it remained embedded in the paint. This made the surface fuzzy, and it had to be hand-scraped with razor blades several



times to remove the fuzz. However, the cask was successfully decontaminated after it was finally unloaded, without having to remove the paint.

Decontamination times for the REA cask after the partial and full loadings were not excessive, and generally required three to four shifts to complete.

#### 3.4.12.2 Internal Cavity

The cask's potential to retain radioactive material within the internal cavity was assessed. Dose rates were measured above the cask cavity prior to loading fuel into the cask and upon termination of the test program after all the fuel was unloaded. The post-test radiation readings (25 mrem/hr to 50 mrem/hr) were taken after the cask was returned to the decontamination pad and the water drained out. No dose rate measurements were taken below the top of the cask basket, and the cavity was not rinsed or flushed.

An attempt was made to obtain crud samples from the inside of the REA cask; however, because the cask contained very little observable crud, this was impossible. Instead, smears were taken of the reddish film that was present at some locations on the inside surface of the fuel tubes.

The last 2 in. of water pumped from the cask cavity was filtered by passing it through a cloth filter. Again, very little observable material was obtained, although the cloth filter read upward of 25 mrem/hr. Small specks of dirt or other hard material were obtained and included as samples. The cloth filter was cut up and pieces of it included among samples sent to LLNL for analysis. The results of these analyses are included in Section 4.4.4 of this report.

#### 3.4.13 Personnel Exposure

Gamma and neutron readings were taken on the cask as soon as it came out of the water, to assess expected personnel exposure. The decision to torque the head on the decontamination pad (in air) was based upon the lower than expected gamma readings at the top of the cask. Contact readings directly above the bolt holes ran as high as 250 mrem/hr; however, in the general work area where a technician would stand while torquing the head, the dose rates were only 40 to 45 mrem/hr. Utilization of a biological shield (2-in.-thick stainless steel plate) helped reduce personnel exposure during torquing and



helium leak-checking activities. Total exposure received while torquing the head on the decontamination pad ran about 100 mrem.

Total beta/gamma exposure to GE-MO personnel who worked on or around the cask ran 671 mrem over the 4-1/2-month test program. A total of 28 people had close contact with the cask during this period. Assuming an equal distribution of exposure among the 28 different people who worked on the cask, an average dose of 24 mrem was determined.

Personnel working on or around the REA cask were also provided with extended energy range neutron badges, referred to as "Neutrack E.R.s". A total personnel neutron exposure of 160 mrem was obtained by these employees. The highest neutron exposure by any individual was 50 mrem. The minimum readable neutron dose was 20 mrem.

Utilization of these reported exposure values for future operations involving the REA cask must be done carefully. It should be noted that GE-MO personnel spent more time in proximity to the cask because of the test program. The cask had to be loaded twice (extra handling and decontamination time), moved to the CRA for cask rotation or gas sampling (extra time spent near the cask), and special radiation and smear surveys taken (again, extra time spent near the cask). If this had been a routine loading with only one move to a storage area, personnel exposure would have been considerably lower.

minimum acceptable activity. Total exposure received while working was  
less than the recommended limit of 50 mrem.

Total plutonium exposure to 50 mrem (period) was worked on or around the  
case for 21 hours over the 4-12 month test period. A total of 28 people had  
close contact with the case during this period. Assigned in equal proportion  
of exposure among the 28 people, each person who worked on the case, on average,  
received 1.8 mrem.

Personnel working on or around the RCA case were also provided with  
secondary barrier range monitors. No test results were obtained for these  
personnel because exposure of the area was limited by these monitors. The  
highest radiation exposure by any individual was 50 mrem. The minimum possible  
radiation dose was 50 mrem.

Information of these recorded exposure values for future operations  
involving the RCA case must be given priority. It should be noted that 50 mrem  
personnel exposure was in proximity to the case because of the case  
program. The case had to be loaded (into a handling and decontamination  
area) moved to the RCA for risk reduction and then during this time spent  
near the case, and special radiation and safety survey taken (gamma, beta,  
neutron, etc.). This was done in a routine fashion with only one  
move to a storage area. Personnel exposure would have been considerably lower.

#### 4.0 SPENT FUEL ASSEMBLY CHARACTERIZATION

All 52 spent fuel assemblies used in the performance test were obtained from the Nebraska Public Power District's Cooper Nuclear Station. The fuel assemblies were characterized by in-basin sipping, calorimetry, axial radiation scans, and limited video and 35-mm photography. This section describes the characterization effort. Section 4.1 describes the fuel assemblies, fuel characteristics, and operating histories. The calorimeter and decay heat measurements taken are described in Section 4.2. Axial radiation measurements are discussed in Section 4.3. Section 4.4 describes the assessment of fuel integrity.

##### 4.1 SPENT FUEL ASSEMBLIES

The spent fuel assemblies used in the cask performance test are of the GE 7x7 rod design as shown in Figure 4.1. Their design specifications are given in Table 4.1. The upper and lower tie plates are 304 stainless steel castings. The lower tie plate has a nose-piece that supports the fuel assembly in the reactor. The upper tie plate has a handle for transferring the fuel assembly.

In addition to having standard BWR fuel rods, each assembly has eight tie rods that thread into the lower tie plate casting. The upper ends of the tie rods extend through and are fastened to the upper tie plate with stainless steel hexagonal nuts and locking tabs. These tie rods support the weight of the assembly during fuel-handling operations when the assembly hangs by the handle. The center rod of each fuel assembly has been designed to maintain the position of the fuel rod spacers. It is inserted into the fuel assembly and rotated to lock the spacers into their respective locations. The spacers have Inconel-X springs to maintain rod-to-rod spacing. The fuel rods are pressurized with helium and sealed by welding end plugs on each end.

Additional information on the Cooper fuel assemblies is found in Tables 4.2 and 4.3 and in Figure 4.2. Table 4.2 lists assembly burnup values obtained from two different accounting methods. One method is used to meet fuel storage requirements and lists only the final total burnup. This method is referred to as Form 30. The other method contains end-of-cycle (EOC) burnup



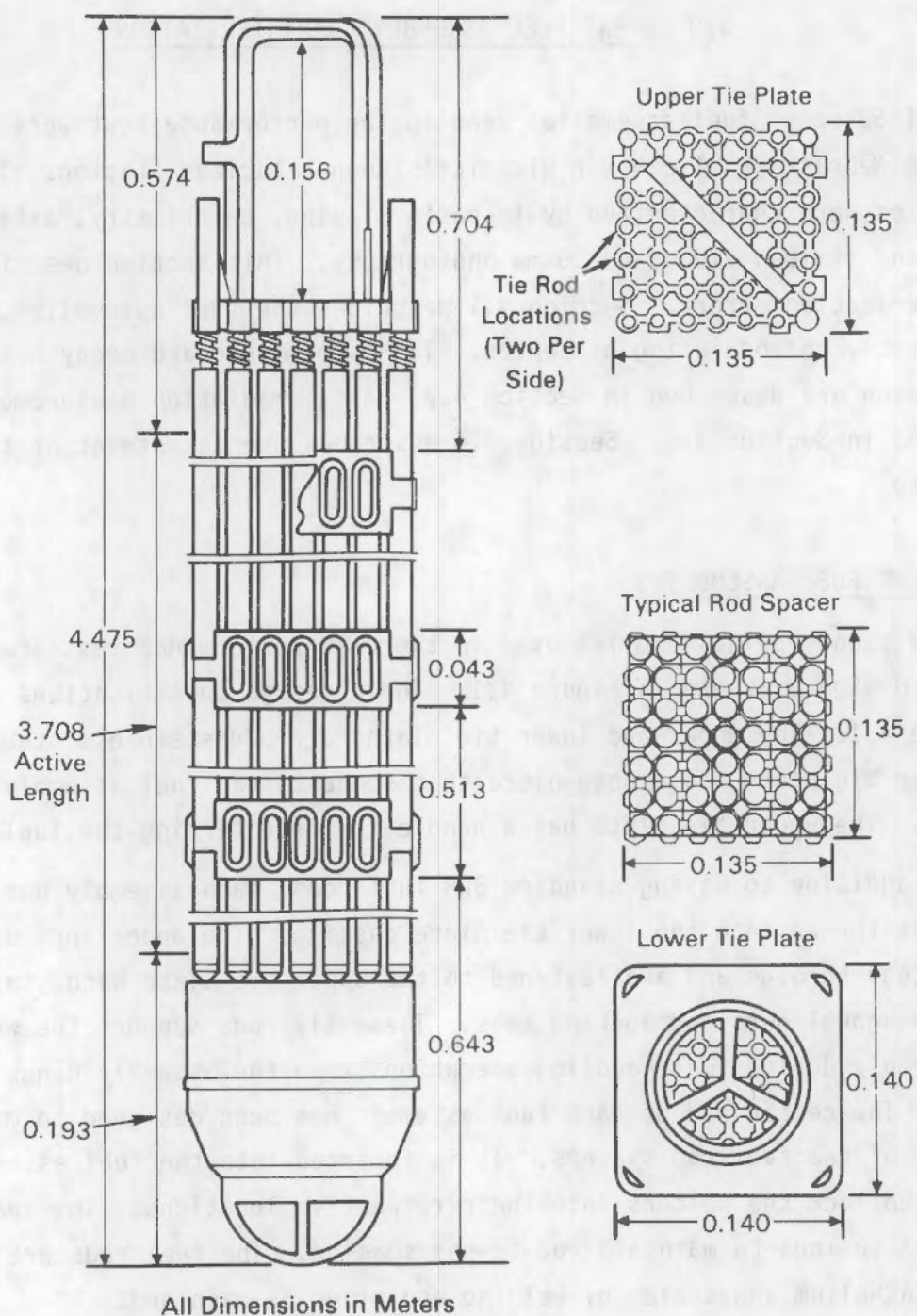


**FIGURE 4.1.** Cooper Spent Fuel Assembly

TABLE 4.1. Design Characteristics of Cooper BWR Fuel Rods and Assemblies

Fuel Assembly Data

Overall length	4.47 m	(175.83 in.)
Nominal active fuel length	3.71 m	(144 in.)
Fuel rod pitch	1.87 cm	(0.738 in.)
Space between fuel rods	0.445 cm	(0.175 in.)
Fuel bundle heat transfer area	8.04 m <sup>2</sup>	(86.52 ft <sup>2</sup> )
Fuel rod array	7 x 7	
Zr-2 weight	48.000 kg/ass.	(105.8 lb/ass.)
304 stainless steel	8.600 kg/ass.	(18.96 lb/ass.)

Fuel Rod Data

Average linear rod power	23.2 kW/m	(7.079 kW/ft)
Outside diameter	1.43 cm	(0.563 in.)
Cladding thickness	0.081 cm	(0.032 in.)
Pellet outside diameter	1.24 cm	(0.487 in.)
Fission gas plenum length	40.6 cm	(16 in.)
Pellet immersion density	10.42 g/cc	
Cladding material	Zircaloy-2	
Helium fill gas pressure	1 atm.	
Fuel	UO <sub>2</sub>	

values and is referred to as a Cycle Summary. Table 4.2 also lists the weight of uranium in each assembly, with each assembly initially enriched to 2.5 wt% <sup>235</sup>U averaged over all rods in the assembly.

The Cooper reactor power history for the first seven operating cycles is listed in Table 4.3 and shown in Figure 4.2. The specific powers shown in Table 4.3 are based on a design core power of 22.1 MW/MTU when the reactor is operated at its full thermal power of 2381 MWt. All the assemblies used in the performance test were discharged from the reactor at EOC 6 or 7, April 21, 1981, or June 1, 1982, respectively. Cooling times can be calculated from those dates.

The information contained in Tables 4.2 and 4.3 can be combined to produce an operating history for each fuel assembly. An example is shown in Figure 4.3 for assembly CZ205. This example was produced by using the burnup information from Table 4.2 to calculate the delta burnup for each cycle. The delta burnup



TABLE 4.2. Cooper Fuel Assembly Burnup Data

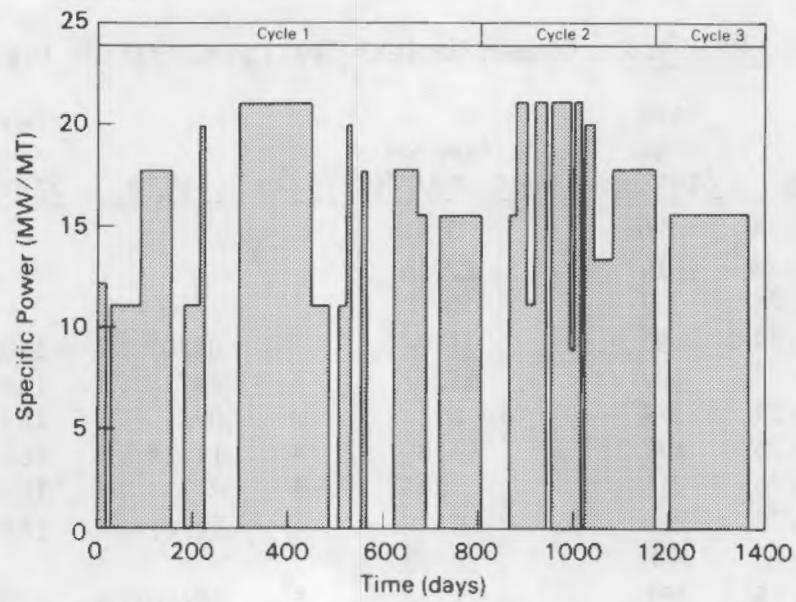
Assembly No.	<sup>235</sup> U, kg	Cycle Summary Burnup, Gwd/M <sup>1</sup>						Cycle Summary Total, Gwd/MTU	Form 30 Total, Gwd/M <sup>1</sup> U
		EOC 2	EOC 3	EOC 4	EOC 5	EOC 6	EOC 7		
CZ147	190.2	9.698	12.603	19.835	21.880	24.952		24.952	26.709
CZ148	190.2	9.570	12.495	19.739	21.786	24.868		24.868	26.310
CZ182	190.2	18.069	21.123			23.996	26.092	26.092	26.824
CZ195	190.2	9.343	11.432	19.392	21.364	23.906		23.906	26.392
CZ205	190.2	17.993	21.066			22.962	25.792	25.792	25.344
CZ209	190.2	20.389	21.144			23.423	25.056	25.056	25.383
CZ211	190.2	9.672	12.593	19.829	21.879	24.958		24.958	26.679
CZ222	190.2	18.434	21.498			23.736	26.665	26.665	26.692
CZ225	190.2	18.432	21.546			23.588	25.905	25.905	25.796
CZ239	190.2	16.915	21.086			24.306	27.130	27.130	27.246
CZ246	190.2	18.444	21.528			23.535	26.761	26.761	27.363
CZ259	190.2	9.149	11.682	19.376	21.335	23.930		23.930	26.466
CZ264	190.2	10.264	11.465	19.199	21.170	23.767		23.767	26.496
CZ277	190.2	9.331	11.627	19.334	21.294	23.891		23.891	26.478
CZ286	190.2	18.443	21.519			24.132	26.065	26.065	27.141
CZ296	190.2	9.708	12.609	19.846	21.228	24.973		24.973	26.388
CZ302	190.5	19.893			22.039	26.432		26.432	26.594
CZ308	190.5	19.554	20.939			23.056	24.817	24.817	25.815
CZ311	190.5	18.664	21.559			24.447	26.455	26.455	27.392
CZ315	190.5	18.793	21.561			23.434	25.685	25.685	26.881
CZ318	190.5	18.871	21.804			23.962	25.600	25.600	26.568
CZ337	190.5	18.662	21.538			23.780	26.691	26.691	26.720
CZ342	190.5	18.841	21.904			23.724	26.018	26.018	27.066
CZ346	190.5	18.807	21.537			24.762	27.559	27.559	28.048
CZ348	190.5	18.633	21.709			24.257	26.910	26.910	27.481
CZ351	190.5	18.705	21.552			24.156	26.074	26.074	25.753
CZ355	190.5	19.559	20.948			23.048	24.803	24.803	25.419
CZ357	190.5	18.723	21.562			24.456	26.528	26.528	27.140
CZ369	190.5	18.550	20.947			22.861	25.679	25.679	26.576
CZ370	190.5	19.818			21.967	26.367		26.367	26.342
CZ372	190.5	19.671			22.464	26.748		26.748	25.848
CZ379	190.5	18.804	21.530			23.830	25.438	25.438	25.925
CZ398	190.5	18.816	21.655			23.885	26.789	26.789	27.478
CZ415	190.5	19.674			22.472	26.752		26.752	25.863
CZ416	190.5	18.901	21.752			23.789	26.077	26.077	27.461
CZ429	190.5	18.674	21.568			24.793	27.585	27.585	27.641
CZ430	190.5	18.546	21.646			24.198	26.848	26.848	26.825
CZ433	190.5	19.802			21.950	26.351		26.351	25.977
CZ460	190.5	18.598	21.698			24.301	26.222	26.222	26.512
CZ466	190.5	18.361	21.472			23.547	25.280	25.280	26.077
CZ468	190.5	18.552	20.936			23.837	25.932	25.932	26.757
CZ472	190.5	18.741	21.449			23.364	26.171	26.171	25.957
CZ473	190.5	18.629	21.507			23.770	25.379	25.379	26.519
CZ498	190.5	18.792	21.506			23.743	26.660	26.660	26.482
CZ508	190.5	18.684	21.526			23.580	25.882	25.882	26.357
CZ515	190.5	19.653			22.448	26.727		26.727	25.737
CZ526	190.5	18.756	21.481			24.711	27.511	27.511	27.596
CZ528	190.5	19.673			22.471	26.747		26.747	25.715
CZ531	190.5	18.749	21.461			24.022	26.686	26.686	26.699
CZ536	190.5	19.922			22.060	26.473		26.473	26.589
CZ542	190.5	18.393	21.465			24.048	25.969	25.969	26.691
CZ545	190.5	18.629	21.713			23.800	25.535	25.535	26.668

Note: If the End of Cycle burnup did not increase from one cycle to the next, the assembly was out-of-reactor for the cycle; this condition is denoted by a blank entry.

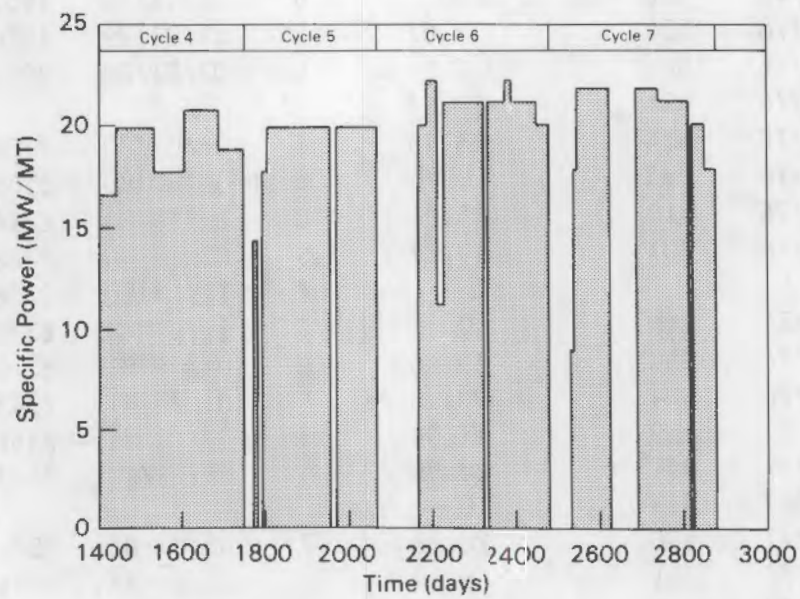


TABLE 4.3. Cooper Nuclear Station Operating History

Cycle	Date	Days From Startup	Core Average Power, MW/MTU	Cycle	Date	Days From Startup	Core Average Power, MW/MTU
1	07/03/74	0	0				
1	07/22/74	19	12.15				
1	07/30/74	27	0				
1	10/01/74	90	11.04	4	05/05/78	1402	0
1	12/07/74	157	17.67	4	06/12/78	1440	16.57
1	12/24/74	174	0	4	09/13/78	1533	19.88
1	01/01/75	182	11.04	4	11/25/78	1606	17.68
1	02/03/75	215	19.88	4	02/15/79	1688	20.76
1	02/13/75	225	0	4	04/07/79	1749	18.78
1	04/25/75	296	20.99				
1	09/27/75	451	11.04	5	05/10/79	1772	0
1	11/01/75	486	0	5	05/21/79	1783	14.36
1	11/20/75	505	11.04	5	05/30/79	1792	0
1	12/10/75	525	19.88	5	06/12/79	1805	17.67
1	12/17/75	532	0	5	11/11/79	1957	19.88
1	01/08/76	554	17.67	5	11/24/79	1970	0
1	01/20/76	566	0	5	03/01/80	2068	19.88
1	03/15/76	621	17.67				
1	05/07/76	674	15.46	6	06/07/80	2166	0
1	05/26/76	693	0	6	06/30/80	2189	19.88
1	06/20/76	718	15.46	6	07/25/80	2214	22.09
1	09/17/76	807	17.67	6	08/08/80	2228	11.04
				6	11/14/80	2326	20.99
2	11/15/76	866	0	6	11/23/80	2335	0
2	11/29/76	880	15.46	6	01/04/81	2377	20.99
2	12/23/76	904	20.98	6	01/20/81	2393	22.09
2	01/07/77	919	11.04	6	03/20/81	2452	20.99
2	02/02/77	945	20.99	6	04/20/81	2483	19.88
2	02/10/77	953	0				
2	03/25/77	996	20.99	7	06/07/81	2531	0
2	03/30/77	1001	8.84	7	06/15/81	2539	8.84
2	04/15/77	1017	20.99	7	06/24/81	2548	17.67
2	04/20/77	1022	0	7	09/11/81	2627	21.64
2	05/12/77	1044	19.88	7	11/11/81	2688	0
2	06/20/77	1083	13.25	7	01/05/82	2743	21.64
2	09/17/77	1172	17.67	7	03/20/82	2817	20.99
				7	03/25/82	2822	0
3	10/18/77	1203	0	7	04/25/82	2853	19.88
3	03/31/78	1367	15.46	7	05/21/82	2879	17.67



a. Cycles 1 through 3



b. Cycles 4 through 7

FIGURE 4.2. Cooper Nuclear Station Operating History



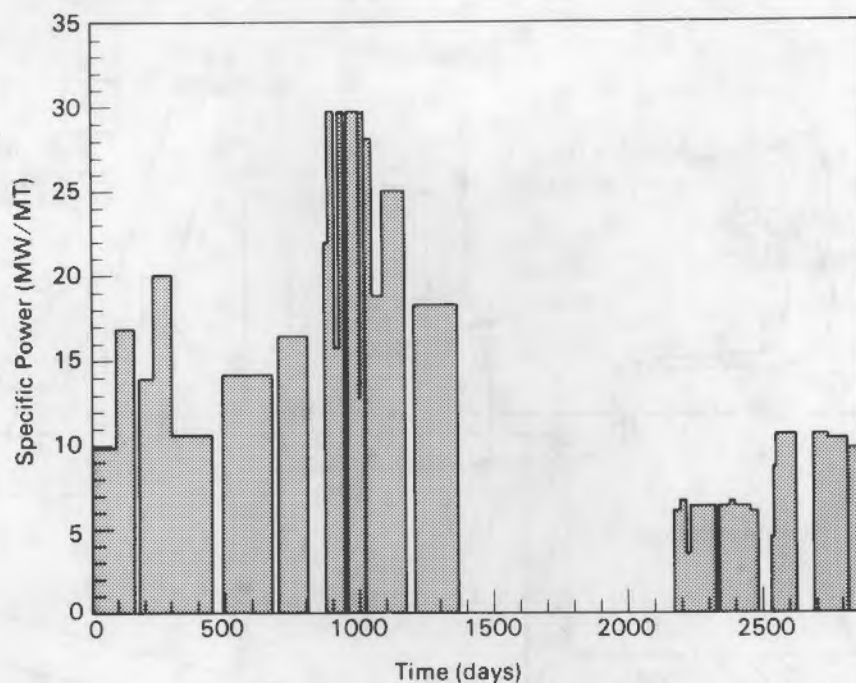


FIGURE 4.3. Assembly CZ205 Operating History

was then used to scale the reactor operating history shown in Figure 4.2 to arrive at the fuel history shown in Figure 4.3.

## 4.2 DECAY HEAT RATES

In this section the in-basin calorimeter used to obtain decay heat measurements at GE-MO is described, and calorimetry results are presented. A description of the calibration of the calorimeter and calorimetry data are found in Appendix D.

### 4.2.1 Calorimeter Description and Operation

The in-basin calorimeter used at GE-MO for decay heat measurements was designed to be compatible with routine underwater handling procedures (Judson et al. 1982; McKinnon et al. 1985). The calorimeter is shown schematically in Figure 4.4. The calorimeter is 460 cm (15 ft) long from base to top (excluding the head) and is composed of two concentric pipes. An inner 41-cm- (16-in.-) diameter stainless steel pipe forms the test chamber, and an outer carbon steel pipe forms the structural skin. The annular space between the two pipes is filled with urethane insulation and serves to reduce heat transfer from the



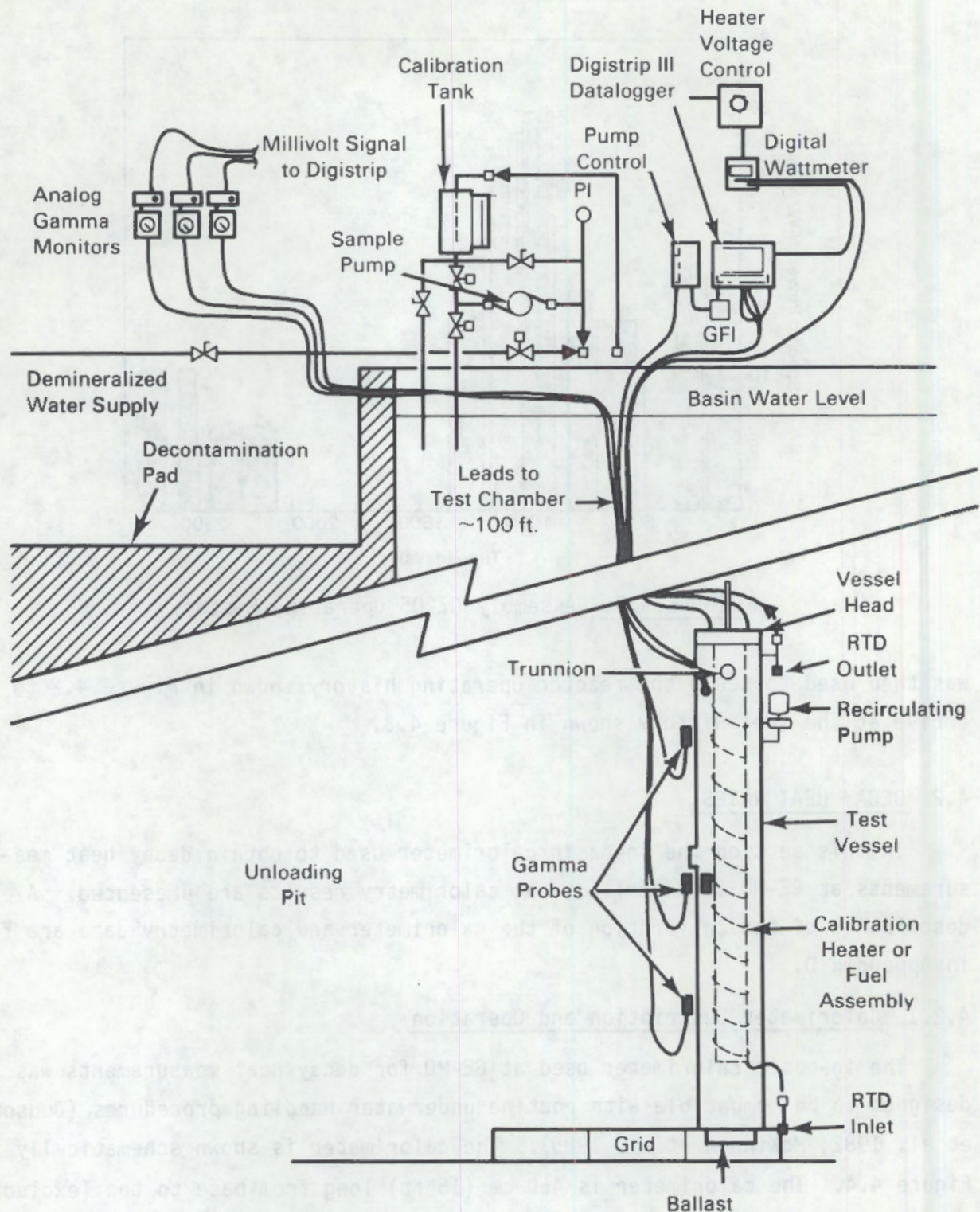


**FIGURE 4.4.** General Electric-Morris Operation In-Basin Calorimeter and Associated Equipment

Source: Judson et al. (1982)



calorimeter to the basin water. The calorimeter has a detachable head, which is secured to the vessel by engaging and rotating six captive bolts fitted with rotating clamping blocks.

Fuel is placed in the calorimeter in a method very similar to that used in loading a fuel transfer cask. The calorimeter cavity contains a fixed insert for PWR fuel and a removable insert for BWR fuel. These calorimeter inserts maintain the fuel assembly in a centered vertical position.

A magnetically-driven recirculation pump mixes the water in the calorimeter cavity. This maintains a homogeneous cavity temperature and results in consistent calorimeter measurements. An ammeter indicates operation of the pump, and a watt transducer has been installed to record the amount of power being supplied to the pump.

Platinum resistance temperature detectors (RTDs) are used to measure temperatures. Four RTDs are mounted on the PWR insert to measure inside water temperature. Two RTDs, one on the inside surface and one on the outside surface of the calorimeter, measure the temperature drop across the wall. Another RTD measures basin water temperature. Two other RTDs monitor the temperature of water entering and leaving the cavity. All RTDs were factory-supplied with continuous leads of sufficient length to reach the signal conditioning and readout instrumentation.

Gamma radiation monitors are installed on the calorimeter to quantify the amount of radiation that passes through the walls of the calorimeter. Three gamma sensors are located at different elevations ( $1/6$ ,  $1/2$ , and  $5/6$  of the height) on the exterior surface of the vessel. A fourth sensor is located on the interior surface of the outer shell (at  $1/2$  of the height). These sensors are used to assess the gamma radiation absorbed in the outer liner of the calorimeter and to estimate the axial gamma profile of the fuel assemblies.

Figure 4.4 also shows the instrumentation and related equipment used in calibrating and operating the calorimeter. During calorimetry, the system utilizes a Digistrip datalogger, a calibration tank, a sample pump, a purge system, a valve control panel, and gamma sensor readout devices. A heater power controller and a digital wattmeter are used during calibrations, but are not part of the normal equipment used during calorimetry.



All calorimeter data reported in this document is referenced to an October 1984 calibration of the calorimeter. The calibration was performed just before most of the calorimetry runs, and involved putting a known amount of electric energy into the calorimeter and observing the increase in internal water temperature with time. Six calibration runs were obtained over the range of 0 to 500 watts. The 1984 calibration is described in greater detail by McKinnon et al. (1985).

The calibration tank is a small vessel 0.3 m (12 in.) in diameter and 0.6 m (24 in.) in height. It is used to prevent pressurization of the calorimeter, to leak-check the calorimeter after the fuel is loaded, and to collect calorimeter water samples. The water samples help to determine fuel integrity.

The water in the calorimeter is purged between calorimeter runs, to cool off the vessel and to remove contaminated water that might bias subsequent in-calorimeter sipping results. When purging, demineralized basin water is pumped to the bottom of the calorimeter via 1.9-cm (0.75-in.) Tygon tubing. Purging is performed only when the vessel is empty and when the head is removed.

#### 4.2.2 Decay Heat Data

Table 4.4 is a summary of the calorimeter decay heat data; a more complete listing of the data is found in Appendix D. All the assemblies were calorimeted prior to the performance test. During pretest calorimetry, pretest predictions were compared to measurements of decay heat. Post-test calorimetry was designed to confirm or clear up questionable differences between repeat pretest decay heat measurements and pretest decay heat measurements and predictions. Assembly CZ259 exemplifies an assembly that was selected for post-test calorimetry because of the substantial difference between two measurements made on this assembly during pretest calorimetry. Comparisons between pretest predictions and measurements are discussed in Volume II of this report.

Assembly CZ205 was selected as a control or reference assembly. Repeat measurements were routinely taken on this assembly to confirm that the calorimeter was measuring properly. Repeatability of the data can be assessed from the 14 calorimetry runs made on fuel assembly CZ205 presented in Table 4.5.



TABLE 4.4. Calorimeter Decay Heat Data Summary

Assembly ID	Pretest Measurements		Post-Test Measurements	
	Date	Calorimetry Decay Heat, W	Date	Calorimetry Decay Heat, W
CZ147	11/04/84	276.7		
CZ148	10/23/84	273.5		
CZ182	09/27/84	342.6		
CZ195	10/29/84	255.5		
CZ205(a)	09/24/84	324.0	05/13/85	289.7
CZ205(a)	10/04/84	361.5	05/28/85	307.9
CZ205(a)	10/08/84	343.5		
CZ205(a)	10/09/84	352.9		
CZ205(a)	10/22/84	331.7		
CZ205(a)	10/24/84	338.6		
CZ205(a)	10/29/84	327.4		
CZ205(a)	11/02/84	313.0		
CZ205(a)	11/05/84	311.3		
CZ205(a)	12/05/84	314.0		
CZ205(a)	12/11/84	331.1		
CZ205(a)	12/21/84	317.2		
CZ209(a)	10/28/84	279.5		
CZ211	10/01/84	296.0	05/20/85	240.3
CZ222	11/04/84	355.7		
CZ225	10/02/84	327.3		
CZ239	10/30/84	366.5		
CZ246	11/02/84	320.9		
CZ246	11/05/84	341.7		
CZ259	10/29/84	247.7	05/14/85	254.1
CZ259	12/20/84	288.5		
CZ264	10/23/84	263.9		
CZ277	10/27/84	262.7	05/26/85	243.0
CZ286	12/06/84	278.4	05/28/85	284.2
CZ296	11/03/84	256.7	05/21/85	251.9
CZ302	10/24/84	285.6		
CZ308	11/01/84	269.7		
CZ311	10/26/84	356.9		
CZ315	12/07/84	328.0		

(a) The decay heat measurements of these assemblies were performed under EPRI sponsorship (McKinnon et al. 1985)

TABLE 4.4. (contd)

Assembly ID	Pretest Measurements		Post-Test Measurements	
	Date	Calorimetry Decay Heat, W	Date	Calorimetry Decay Heat, W
CZ318	12/07/84	277.6		
CZ337	11/01/84	347.7	05/24/85	300.4
CZ342	12/06/84	280.1	05/26/85	300.0
CZ346	10/27/84	388.7		
CZ348	10/31/84	342.8		
CZ351	12/09/84	313.8		
CZ355	10/28/84	290.5		
CZ357	12/08/84	320.3		
CZ369(a)	10/25/84	347.7		
CZ370	09/28/84	288.1		
CZ372	09/26/84	288.7		
CZ379	11/03/84	287.4		
CZ398	10/27/84	372.0		
CZ415	09/26/84	289.3		
CZ416	10/31/84	319.8		
CZ429(a)	10/26/84	385.6		
CZ430	10/30/84	353.3		
CZ433	09/25/84	287.4	05/21/85	256.7
CZ460	12/09/84	313.5		
CZ466	09/28/84	302.1		
CZ468	12/11/84	325.3		
CZ472	09/26/84	325.0		
CZ473	12/10/84	293.2		
CZ498	10/24/84	359.4		
CZ508	12/09/84	310.0		
CZ515(a)	09/25/84	294.0		
CZ515(a)	10/25/84	296.0		
CZ526(a)	10/01/84	395.3	05/21/85	321.8
CZ528(a)	10/25/84	297.6		
CZ531	10/30/84	347.2		
CZ536	09/27/84	295.2		
CZ542	12/08/84	311.9		
CZ545	12/11/84	295.2		

(a) The decay heat measurements of these assemblies were performed under EPRI sponsorship (McKinnon et al. 1985).

TABLE 4.5. Calorimeter Measurements of Assembly CZ205

Measurement	Date (a)	Measured Decay Heat, W	Calculated Decay Heat, W <sup>(b)</sup>	% Deviation
1	09/24/84	324.0	337.7	+4.0
2	10/04/84	361.5	335.9	-7.6
3	10/08/84	343.5	335.2	-2.5
4	10/09/84	352.9	335.0	-5.4
5	10/23/84	331.7	332.6	+0.2
6	10/24/84	338.6	332.4	-1.9
7	10/29/84	327.4	331.6	+1.2
8	11/02/84	313.0	330.9	+5.4
9	11/05/84	311.3	330.3	+5.7
10	12/06/84	314.0	324.9	+3.4
11	12/12/84	331.1	323.9	-2.3
12	12/21/84	317.2	322.2	+1.6
13	05/13/85	289.7	297.2	+2.5
14	05/28/85	307.9	294.8	-4.5

Standard Deviation +14.1 W (~4%)

(a) The 1984 decay heat measurements of assembly CZ205 were performed under EPRI sponsorship (McKinnon et al. 1985).

(b) Calculated based on a linear least-square fit to the measured data.

Figure 4.5 is a plot of the calorimetry measurements on CZ205. All but two of the measurements on CZ205 were performed under EPRI sponsorship (McKinnon et al. 1985). The solid line represents a linear least-squares fit to the data. The equation describing this line is

$$\text{Decay heat} = 337.7 - 0.174(\text{days})$$

where the days were counted from September 24, 1985. The standard deviation of the data about this line is  $\pm 14.1$  W.



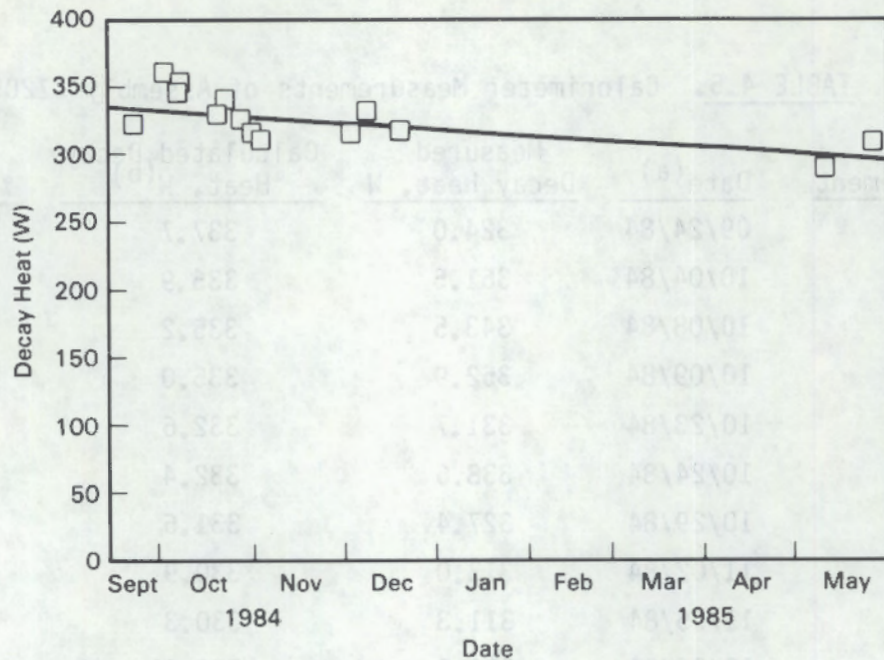


FIGURE 4.5. Repeatability of Calorimetry Measurements on Assembly CZ205

#### 4.3 AXIAL RADIATION MEASUREMENTS

This section includes a brief description of the ION-1/fork measurement system (Halbig 1985) used to obtain axial gamma and neutron radiation measurements of each of the spent fuel assemblies. Calibration of the ION-1 and a discussion of the data are also included.

##### 4.3.1 ION-1/Fork Measurement System

Gamma and neutron axial profile readings were taken on each of the fuel assemblies with the LANL portable spent-fuel detector, known as the ION-1/fork measurement system. Basically, the LANL ION-1 system shown in Figure 4.6 consists of underwater sensors and an above-water electronics unit that monitors and displays the measured radiation.

The underwater unit was located on the edge of the fuel unloading basin about 9 m (30 ft) below the water surface. It consists of two forked tines made of polyethylene. Each tine contains a cadmium-covered fission chamber,





**FIGURE 4.6.** Los Alamos ION-1 Spent Fuel Radiation Measurement Equipment

a noncovered fission chamber, and an ion chamber. The opening between the tines was about 1.27 cm (0.50 in.) greater than that of a typical 7x7 BWR spent fuel assembly. Electrical leads from the underwater unit were connected to a preamplifier above the water that was, in turn, connected to the signal conditioning equipment and a computer. The small portable computer provided a hard copy output of the data and a magnetic tape interface.

Gamma and neutron radiation measurements were made at nine axial locations on each fuel assembly. Before any radiation measurements were taken, the fuel grapple was indexed so that the bottom of the fuel assembly was at the exact center of the tines when the reference mark on the grapple read zero elevation. Corresponding marks were then made for each of the nine axial measurement locations. When a fuel assembly was scanned, it was grappled from a fuel storage basket and moved through the tines of the detector. Readings were taken at



each desired elevation. At each measurement location, a count time of 10 seconds was used before the assembly was moved to the next position.

#### 4.3.1.2 ION-1 Calibration

The measurements obtained with the ION-1 were intended to give sufficient information to establish the axial decay heat profile for each of the fuel assemblies. Consequently, it was not necessary to have an absolute radiation reading at each point. It was important to be able to compare ION-1 readings and obtain relative magnitudes between readings.

In preparation for using the ION-1 at GE-MO, various preliminary neutron and gamma measurements were made to test the equipment and to determine the detector response for well-defined source-detector configurations. Neutron measurements were made in water with a  $^{252}\text{Cf}$  source of known strength. The source was centered between the arms of the fork. For a lower-level discriminator setting of 25 on the ION-1, the efficiency for the cadmium-covered detector was  $2.68 \times 10^{-5}$ ; for the bare detectors it was  $5.2 \times 10^{-5}$ . The ion chambers were calibrated in air using a  $^{60}\text{Co}$  source. The average linear response of the two ion chambers is 70 R/hr per ION-1 reading. These measurements verified that the equipment was functioning properly. However, direct correlations between the source measurements and actual fuel assembly measurements were not possible within the scope of this project. Such correlations may be approximated through extensive Monte Carlo calculations.

#### 4.3.2 Axial Radiation Profiles

Figures 4.7 and 4.8 show representative gamma and neutron radiation profiles for the 52 Cooper spent fuel assemblies (see Appendix E for data). The center curve represents the average of the normalized data where the data has been normalized to an average of 1 over the active length of the fuel assembly. The active length of the fuel assembly is 3.708 m (146 in.). The other two curves represent data within one standard deviation of the normalized average.

Several measurements were made with the ION-1 system to determine its repeatability and to determine its sensitivity to positioning, count times, and signal conditioning equipment settings. Assembly CZ331 (not used in the cask tests but used as the reference assembly) was scanned a total of six times; the



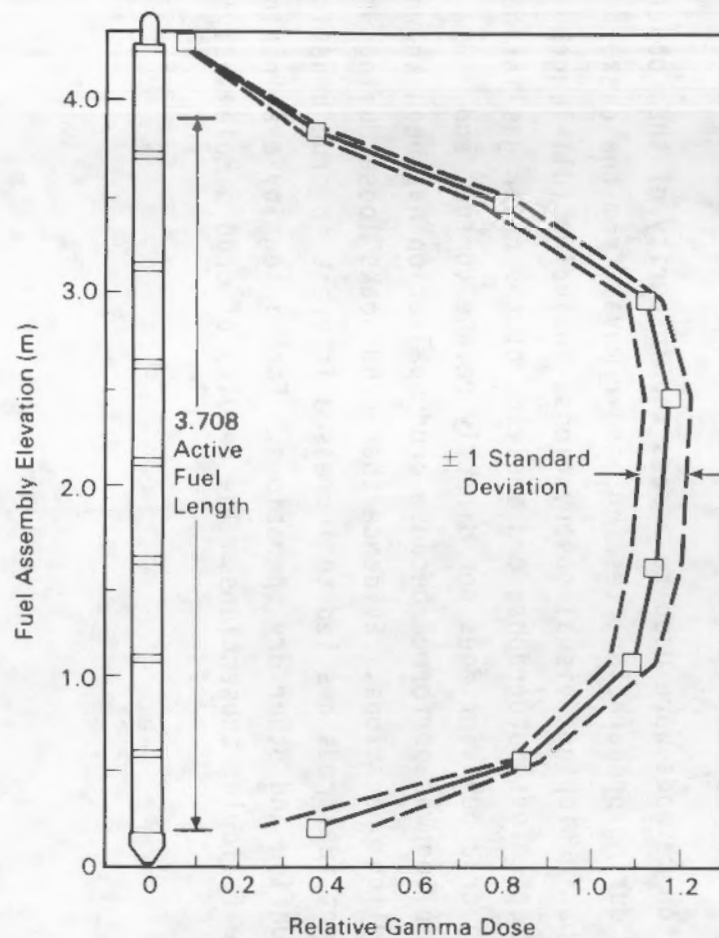


FIGURE 4.7. Normalized Average Axial Gamma Dose Rate Profile

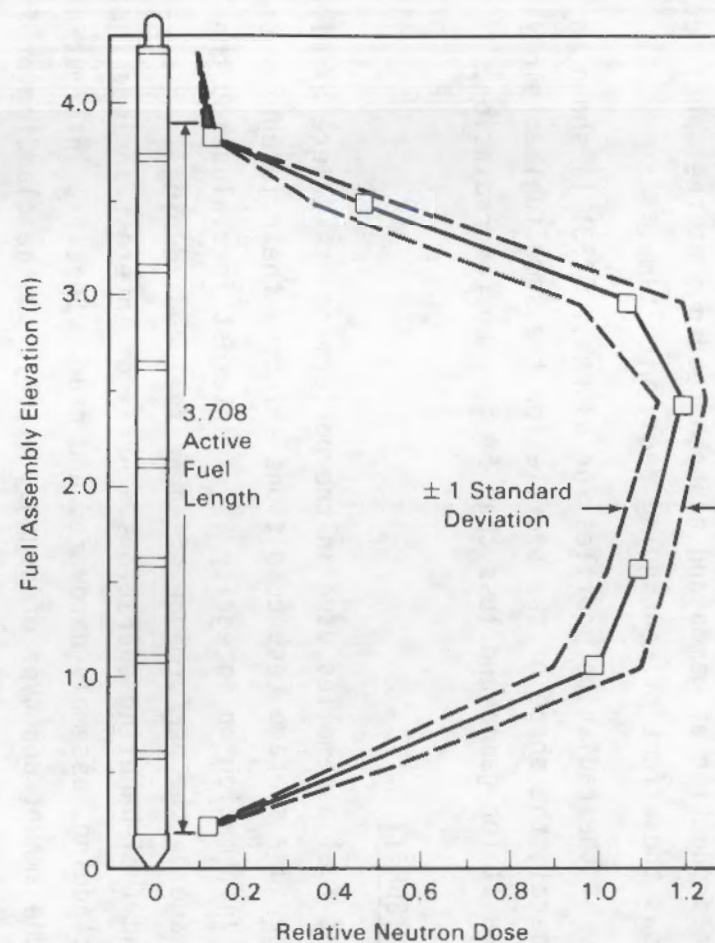


FIGURE 4.8. Normalized Average Axial Gamma Dose Rate Profile

results are listed in Table 4.6. Examination of the data in Table 4.6 indicates consistent reproduction of gamma and neutron readings at the specified elevations and shows the effect of continuing decay with time.

Repeatability of the radiation profiles for assembly CZ331 is shown in Table 4.7. In general, the shape of the profile for the same fuel assembly varies by less than 1% for gamma and less than 5% for neutron radiation.

#### 4.4 SPENT FUEL INTEGRITY

Selected spent fuel assemblies used in the performance test were examined to determine whether dry storage test conditions affected their integrity or characteristics. Information on integrity is of interest in evaluating the impact of dry storage on the performance of spent fuel rods during long dry-storage periods and fuel-handling operations. Areas of interest include the condition of the cladding, assembly hardware, and crud. Specific information desired included the amount and type of damage, if any, to the cladding or fuel assembly hardware during fuel handling or dry storage; fission gas release during testing; and changes in the crud characteristics, particularly any increase in crud spallation.

Four examination methods were used to assess the integrity of the Cooper fuel assembly rods during preparation, testing, and removal from the cask. These included in-basin sipping; visual observations, including full-length videos and underwater color photographs; and analyses of the cover gas in the REA cask. Although crud behavior does not directly relate to fuel rod integrity, crud sampling was performed because crud spallation has been known to impact fuel-handling operations. Evidence that crud soaks loose during wet storage of some spent fuel rods has led to increased interest in crud behavior during rod consolidation and other dry operations. Each integrity examination is discussed in the following subsections. The results of crud sample analyses are also discussed.



TABLE 4.6. Repeatability of Radiation Scans (Assembly CZ331)

Date <sup>(a)</sup>	Elevation from Bottom of Fuel Assembly, m								
	0.19	0.55	1.06	1.57	2.47	2.98	3.49	3.85	4.31
Gamma									
11/02/84	84.3	134.9	162.5	164.3	163.7	166.8	127.4	66.3	18.8
11/28/84	83.0	132.3	160.0	162.5	161.2	163.7	126.2	66.1	18.7
11/30/84	83.0	132.3	159.4	161.2	160.6	168.7	125.6	65.8	18.6
05/22/85	79.4	123.7	152.2	153.7	153.7	155.6	120.1	63.3	17.7
05/23/85	80.2	123.4	152.2	154.4	153.7	156.2	122.4	63.8	18.1
05/23/85	79.7	124.1	152.5	155.0	155.6	158.1	123.4	65.5	18.1
Neutron									
11/02/84	1.6	40.3	87.6	97.9	112.7	134.0	59.8	3.1	0.0
11/28/84	2.5	38.9	87.3	100.8	115.8	132.6	64.8	4.0	0.1
11/30/84	3.6	41.2	84.9	101.4	116.4	127.1	61.3	4.9	0.0
05/22/85 <sup>(b)</sup>	1.6	16.8	41.9	50.5	58.2	63.7	31.8	2.5	0.0
05/23/85	0.8	14.5	44.1	50.2	53.1	65.7	33.5	2.0	0.0
05/23/85	1.0	22.2	44.7	52.6	61.5	65.4	34.9	3.3	0.0

(a) The 1984 measurements were performed under EPRI sponsorship (McKinnon et al. 1985).

(b) Measurements obtained with different ION-1 unit. Neutron response is about half of previous measurements.

#### 4.4.1 In-Basin Sipping

The 52 fuel assemblies used in the performance test were sipped "in-basin" and "in-vessel" to investigate fuel rod integrity before dry storage and to determine whether any of the fuel rods developed leaks during testing.

In-basin sipping was conducted in the fuel storage basin, while in-vessel sipping was conducted in the calorimetry vessel located in the smaller unloading basin. The assemblies were sipped both before and after testing, and assembly CZ205 was resipped each time fuel assemblies from a new basket were sipped, to ensure appropriate consistency. In-basin sipping consisted of placing a hood over the selected assembly and analyzing the water that was



TABLE 4.7. Normalized Radiation Profiles (Assembly CZ331)

Date (a)	Elevation from Bottom of Fuel Assembly, m								
	0.19(b)	0.55	1.06	1.57	2.47	2.98	3.49	3.85	4.31(c)
Gamma									
11/02/84	0.558	0.894	1.077	1.088	1.084	1.105	0.844	0.439	0.125
11/28/84	0.558	0.889	1.075	1.092	1.083	1.100	0.848	0.444	0.126
11/30/84	0.557	0.888	1.070	1.082	1.078	1.132	0.843	0.442	0.125
05/22/85	0.562	0.876	1.077	1.088	1.088	1.101	0.850	0.448	0.125
05/23/85	0.565	0.870	1.073	1.089	1.084	1.101	0.863	0.450	0.128
05/23/85	0.557	0.868	1.067	1.084	1.088	1.106	0.863	0.458	0.127
Average	0.560	0.881	1.073	1.087	1.084	1.108	0.852	0.447	0.126
Sigma	0.003	0.010	0.004	0.003	0.003	0.011	0.008	0.006	0.001
Neutron									
11/02/84	0.019	0.487	1.058	1.182	1.361	1.619	0.722	0.037	0.000
11/28/84	0.030	0.462	1.036	1.196	1.374	1.574	0.769	0.047	0.001
11/30/84	0.043	0.494	1.018	1.216	1.396	1.524	0.735	0.059	0.000
05/22/85	0.039	0.407	1.015	1.223	1.409	1.542	0.770	0.061	0.000
05/23/85	0.020	0.356	1.084	1.234	1.305	1.615	0.823	0.049	0.000
05/23/85	0.023	0.505	1.016	1.196	1.398	1.486	0.793	0.075	0.000
Average	0.029	0.452	1.038	1.208	1.374	1.560	0.769	0.055	0.000
Sigma	0.009	0.053	0.026	0.018	0.035	0.048	0.034	0.012	0.000

(a) The 1984 measurements were performed under EPRI sponsorship (McKinnon et al. 1985).

(b) Start of active length (active length was 3.7 m).

(c) Upper tie plate.

drawn off the top of the assembly. All of the sipping data was compared to background readings to assess fuel integrity.

Detailed results for the in-basin sipping are given in Appendix F. Data are provided on the date, time, basin temperature, and background radiation levels for both  $^{137}\text{Cs}$  and  $^{60}\text{Co}$ . The  $^{137}\text{Cs}$  levels detected during pretest and post-test sipping are summarized in Table 4.8. The concentrations listed in Table 4.8 were obtained by subtracting the  $^{137}\text{Cs}$  content obtained from under the hood from the background  $^{137}\text{Cs}$  content in the basin. Although there is



TABLE 4.8. Comparison of  $^{137}\text{Cs}$  Levels Detected During Pretest and Post-Test Sipping of Cooper BWR Spent Fuel Assemblies

GE Basket	Assembly No.	Delta Concentration in $^{137}\text{Cs}$ (a)	
		Pretest	Post-Test
B91	CZ460	4.11	-0.94
	CZ351	4.18	-0.88
	CZ415	2.14	-3.43
	CZ473	2.85	1.39
	CZ472	1.93	0.49
	CZ468	-2.72	1.73
	CZ545	5.6	3.1
	CZ372	9.3	3.1
	CZ536	13.5	NA <sup>(c)</sup>
B85	CZ302	0.57	3.2
	CZ259	0.73	2.2
	CZ264	0.15	0.81
	CZ205 <sup>(b)</sup>	-0.64	(b)
	CZ286	-0.76	1.33
	CZ148	-1.03	1.38
	CZ195	-0.09	2.76
B90	CZ342	3.31	3.79
	CZ318	6.16	4.99
	CZ315	-3.08	3.49
	CZ182	4.63	4.09
	CZ370	1.17	NA
	CZ357	0.83	1.93
	CZ542	1.14	3.27
	CZ508	1.64	3.59
B88	CZ466	0.56	2.05
	CZ239	-1.34	0.97
	CZ531	-1.07	-0.65
	CZ430	-1.14	1.28
	CZ416	-0.64	0.01

(a) All values should be multiplied by  $10^{-5}$   $\mu\text{Ci}/\text{ml}$  to obtain the actual value. Values were obtained by subtracting basin water background activity from the  $^{137}\text{Cs}$  level measured during sipping.

(b) CZ205 was measured several times as noted in text.

(c) Not available.

TABLE 4.8. (contd)

GE Basket	Assembly No.	Delta Concentration in $^{137}\text{Cs}$ (a)	
		Pretest	Post-Test
B88	CZ348	-1.05	0.17
	CZ337	-0.99	0.22
	CZ308	-0.07	-1.00
	CZ246	7.15	NA <sup>(b)</sup>
	CZ222	1.97	NA
B93	CZ249	-0.13	2.01
	CZ311	-0.17	1.09
	CZ398	0.81	4.21
	CZ346	5.12	NA
	CZ277	3.09	2.41
	CZ355	0.23	3.31
	CZ209	0.82	1.21
B92	CZ515	5.09	3.80
	CZ370	NA	2.90
	CZ526	NA	-0.23
	CZ536	NA	0.18
	CZ222	NA	-0.10
	CZ346	NA	-0.45
	CZ528	NA	0.01
	CZ246	NA	-0.17
	CZ433	4.35	0.98
B86	CZ296	1.61	3.11
	CZ225	3.06	0.55
	CZ526	0.01	NA <sup>(b)</sup>
	CZ379	4.88	-2.45
	CZ147	4.68	-2.69
	CZ369	1.65	-2.42
	CZ528	0.32	NA
	CZ498	1.44	-4.32
	CZ211	0.40	1.61

(a) All values should be multiplied by  $10^{-5}$   $\mu\text{Ci/ml}$  to obtain the actual value. Values were obtained by subtracting basin water background activity from the  $^{137}\text{Cs}$  level measured during sipping.

(b) Not available.



some variation in the differences between the pretest and post-test radio-nuclide concentrations, the values would be substantially higher if an assembly contained leaking fuel rods. The sipping results did not indicate any leaking fuel rods in any of the fuel assemblies used in the cask either before or after cask testing.

#### 4.4.2 Video and Photographic Examinations

Visual examinations were conducted to establish the general condition of the fuel assemblies prior to and after testing in the REA cask. Two kinds of visual examinations were used: black and white videos of five fuel assemblies, and color photography of one fuel assembly. The test plan specified that assemblies with possible leakers and those with unusual characteristics also be scanned.

A composite picture (split screen) for each assembly was made from the videos to facilitate comparison of the appearance of the rods before and after testing. Video scans were made on each of the four sides of assemblies CZ526, CZ205, CZ318, CZ415, and CZ277. The assembly number and side were inscribed on plates that were placed in a holder that was temporarily placed on top of the fuel assembly being examined. This procedure ensured that each fuel assembly was scanned in the same orientation before and after testing in the REA cask.

The black and white videos did not provide sufficient detail to characterize the crud or very small features on the fuel rods; however, there were no indications of significant variations in the fuel rods as a result of the cask testing. One lower end nozzle was slightly deformed; nevertheless, all of the fuel assemblies were easily retrieved for reinsertion in the basin. One fuel assembly had a white region on the upper end of a fuel rod. Closer visual examination of this location suggested that the coloration was not related to fuel rod integrity.

Color photographs were taken at three levels on each of the four sides of fuel assembly CZ205 before and after cask testing. A typical orange/reddish crud (probably  $\text{Fe}_2\text{O}_3$ ) was evenly deposited on all of the Zircaloy-2 cladding and fuel assembly hardware. The color pictures taken of CZ205 were used to determine any change in the condition or adherence of the crud as a result of



cask testing. Views near the bottom of fuel assembly CZ205 before and after testing in the REA cask are shown in Figure 4.9. There were no noticeable changes in the characteristics or adherence of the crud. Some scratches and worn spots were apparent on the spacer and the fuel rods, but these features did not change as a result of handling or testing. In general, the fuel rods were in excellent condition, with a very adherent crud layer.<sup>(a)</sup>

#### 4.4.3 Cask Cover Gas Sampling

The cask cover gas was sampled several times during the cask test to evaluate the integrity of the spent fuel rods. Duplicate gas samples were taken as indicated in Table 4.9. Each sample was collected in a separate 500-cc stainless steel cylinder equipped with a bellows seal valve. The cylinders were checked for leaks prior to sampling. Samples were taken by connecting two cylinders to a gas manifold. The sample pressures shown in Table 4.9 were determined by assuming the sample bottle was 500 cc, expanding the gas sample into a known volume, and measuring the pressure in the expanded volume. Pressure values given in Table 4.9 have been reduced to the equivalent pressure at 0°C and may be corrected to the pressures at sampling time when corrected for cask and system temperatures and expansion volumes during sampling. The overall accuracy of the pressure measurement is about  $\pm 1\%$ .

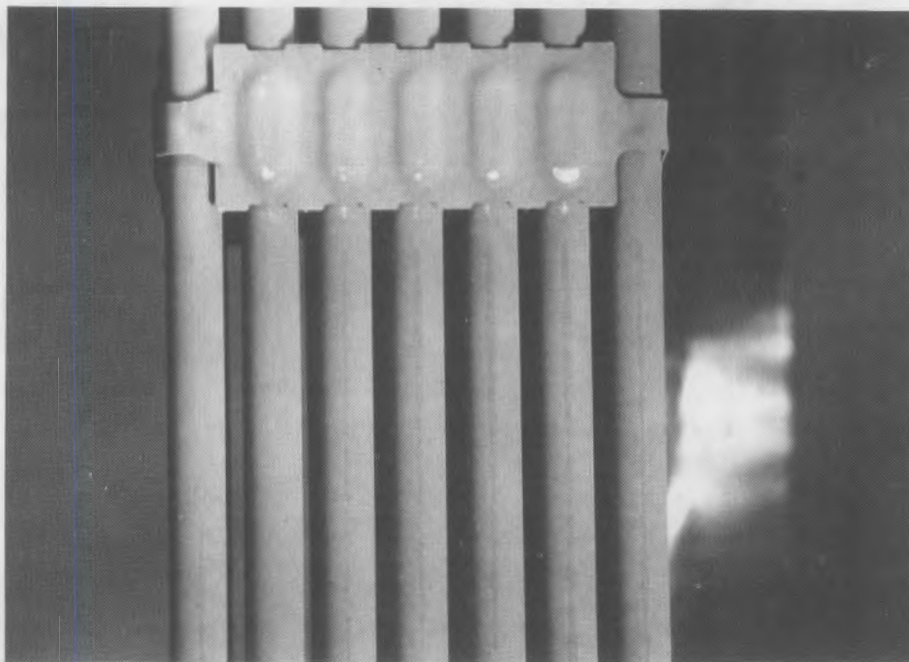
Three types of gas analyses were performed at Lawrence Livermore National Laboratory (LLNL): sample pressure, mass spectra, and radionuclide concentration. Results of the gas analyses made at LLNL are presented in Table 4.10.

Mass spectra were analyzed for a variety of gases with masses less than 100. Only O<sub>2</sub>, N<sub>2</sub>, and He concentrations above 0.01% are detected in the samples. The accuracy of the mass spectra measurements is noted in Table 4.10. Water was present in nine of the 22 samples; seven samples had 0.01 vol% and two had 0.04 vol%. These moisture levels are very low and are estimated to be

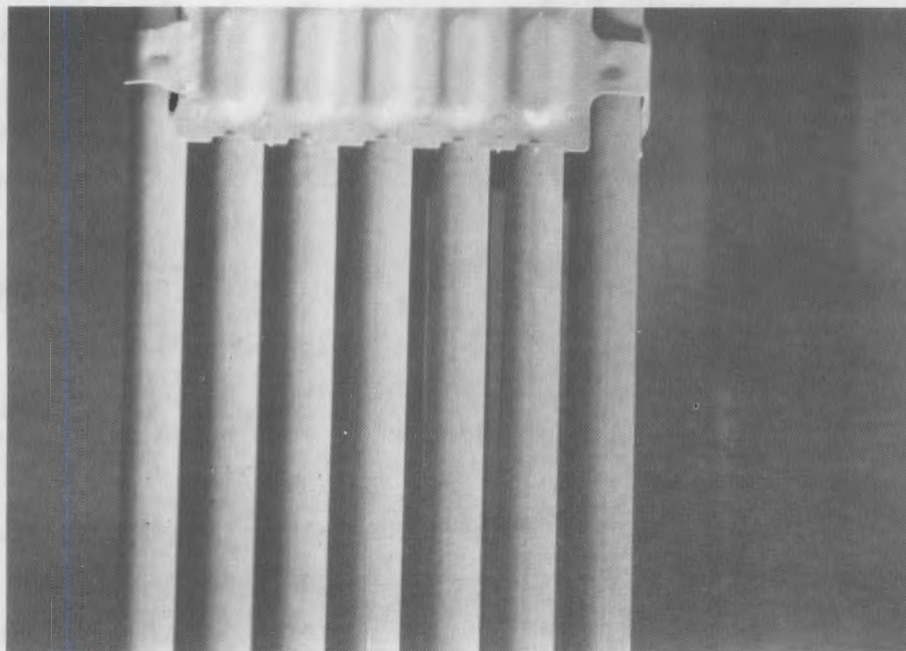
---

(a) Crud from several BWR and PWR reactors has tended to loosen during wet storage. The phenomenon has been observed with spent fuel rods stored for 8 years or longer. There is also evidence that certain dry storage conditions cause crud to loosen (Einziger et al. 1982). The Cooper spent fuel rods had been in pool storage only 2 or 3 years prior to the short-term cask test.





a. Before Testing - Side A Near the Bottom of CZ205



b. After Testing - Side A Near the Bottom of CZ205

**FIGURE 4.9.** Comparison of Fuel and Hardware Characteristics Near the Bottom of Assembly CZ205 Before and After Testing in the REA Cask



TABLE 4.9. Cask Gas Sample Identification

GE No. (a)	Sampling Date	Cask Backfill	Cask Test Run	Pressure, kPa (torr) (b)
1A, 1B	11/27/84	Nitrogen	Beginning of Run 2	142 (1065)
2A, 2B	12/08/84	Nitrogen	End of Run 3	128 (967)
3A, 3B	12/08/84	Helium	Beginning of Run 4	140 (1050)
4A, 4B	01/02/85	Helium	End of Run 5	133 (995)
5A, 5B	01/21/85	Nitrogen	Beginning of Run 7	142 (1067)
6A, 6B	02/05/85	Nitrogen	End of Run 9	127 (970)
7A, 7B	02/05/85	Helium	Beginning of Run 10	138 (1035)
8A, 8B	03/12/85	Helium	End of Run 11	151 (1135)
13A, 13B	03/12/85	Nitrogen	Beginning of Run 13	131 (980)
13C, 13D	03/15/85	Nitrogen	End of Run 13	131 (980)
14A, 14B	04/11/85	Helium	Prior to cask unloading	112 (838)

(a) Samples 9 to 12 do not exist.

(b) Sample bottle pressure at 0°C.

equivalent to 3 g of water in the cask at a moisture level of 0.04 vol%, and to 0.8 g of water in the cask at a 0.01 vol% moisture level, assuming a cask free volume of 5380 L.

The radionuclide concentrations ( $^{85}\text{Kr}$ ,  $^{14}\text{CO}_2$ , and  $^{14}\text{CO}$ ) were determined in two stages. The first stage involved screening the samples for activity greater than 1 nCi/ml. The activity can be measured as low as 1 pCi/ml. The second stage involved elution chromatography to obtain the pure gases for radioassay. The separated krypton gas was analyzed either by thin window beta counting for high levels or by internal proportional counting for low levels. Carbon-14 was measured as  $^{14}\text{CO}_2$  by internal proportional counting. The CO was separated from the gas sample, converted to  $\text{CO}_2$  over CuO at 500°C, and also analyzed by internal proportional counting. Typically, activities above 0.02 pCi/ml can be detected by this method.

Krypton-85 was detected in several gas samples. Low levels of krypton gas were indicated in samples 1A and 2A; however, analyses of the "B" samples



TABLE 4.10. Sample Composition and Radionuclide Concentration

GE No.	Volume Percent <sup>(a)</sup>			Radionuclide Concentration pCi/ml <sup>(STP)</sup> (1/1/85) <sup>(b)</sup>			
	N <sub>2</sub>	O <sub>2</sub>	He	Screening Analysis	<sup>85</sup> Kr	<sup>14</sup> CO <sub>2</sub>	<sup>14</sup> CO
1A	99.96	0.018	-	<1	0.11 ± 0.02 <sup>(c,e)</sup>	-	-
1B	99.97	0.017	-	<1	<0.02	<0.02	-
2A <sup>(f)</sup>	99.98	-	-	<1	0.19 ± 0.01 <sup>(c)</sup>	<0.08	-
2B	99.99	-	-	<1	<0.02	<0.02	-
3A <sup>(f)</sup>	0.25	0.06	99.68	<1	<0.06	0.08 ± 0.01	-
3B <sup>(f)</sup>	0.24	0.05	99.70	<1	-	-	-
4A <sup>(g)</sup>	0.20	0.04	99.75	<1	<0.02	<0.02	-
4B <sup>(g)</sup>	0.17	0.04	99.77	<1	-	-	-
5A <sup>(f)</sup>	99.98	-	-	20.1 ± 0.3	18.7 ± 0.2	<0.02	-
5B	99.98	0.01	-	20.6 ± 0.3	-	-	-
6A	99.99	-	-	14680 ± 160	14680 ± 170	0.28 ± 0.01 <sup>(d)</sup>	0.11 ± 0.03
6B <sup>(f)</sup>	99.99	-	-	14680 ± 160	-	-	-
7A	0.31	0.07	99.61	17.0 ± 0.2	12.9 ± 0.2	0.2 ± 0.01 <sup>(e)</sup>	-
7B	-	-	99.99	17.2 ± 0.2	-	-	-
8A	0.02	-	99.98	35600 ± 400	34600 ± 400	<0.02	0.031 ± 0.005
8B	0.02	-	99.97	35500 ± 500	-	-	-
13A	99.99	-	-	19.6 ± 0.2	15.8 ± 0.1	-	-
13B	99.99	-	-	19.0 ± 0.4	-	-	-
13C	99.98	0.01	-	3360 ± 40	3220 ± 60	0.06 ± 0.01 <sup>(d)</sup>	-
13D <sup>(f)</sup>	99.98	0.02	-	3310 ± 40	-	-	-
14A	0.05	-	99.93	36040 ± 630	35670 ± 390	<0.03	0.736 ± 0.004
14B	0.06	-	99.92	36080 ± 440	-	-	-

(a) Species present in mass spectra at 0.01% or more. Accuracy of these measurements is ±0.2% or ±1 unit in the least significant digit.

(b) Picocuries per milliliter of sample at 760 torr, 0°C decay corrected to 1/1/85. Indicated errors are one standard deviation of the mean of replicate measurements.

(c) Probable contamination by external krypton-85 during analysis. Companion samples contained no detectable radioactivity.

(d) Probable contamination by external krypton-85 during analysis. Should be considered as a limit value.

(e) Marginally detectable. Detection limit defined as a sample count rate greater than 20% that of the detector background.

(f) Moisture at 0.01% detected.

(g) Moisture at 0.04% detected.

indicated no krypton gas. The low levels of krypton gas in samples 1A and 2A are believed to have resulted from contamination from residual gas in the LLNL separation system from previous analyses.

Krypton gas was found in samples 6A, 6B, 8A, 8B, 14A, and 14B (see Tables 4.9 and 4.10). The 6A and 6B samples were taken (15 days) after testing with  $N_2$  gas while the cask was loaded with 52 assemblies, i.e., fully loaded. The 8A and 8B samples were taken (35 days) after testing with the fully loaded cask, but at the end of a subsequent phase using He gas in the cask. Sample  $^{13}C$  was taken at the end of a 3-day test in nitrogen gas. Samples 14A and 14B were taken (27 days) after testing with He gas during a higher temperature period. The estimated amount of  $^{85}Kr$  released to the cask during each sample period was determined. These amounts were accumulated and plotted as a function of total cask storage time as shown in Figure 4.10. The release of  $^{85}Kr$  to the cask was essentially linear during the 2.5 months of testing and indicates that the defect in the cladding was very small.

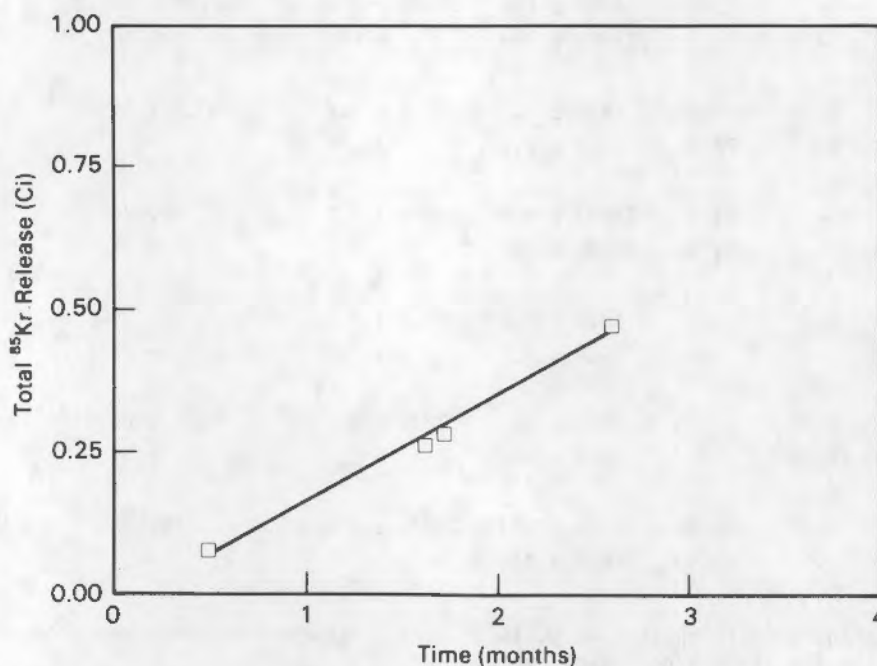


**FIGURE 4.10.** Release of  $^{85}Kr$  Fission Gas During Performance Test



The krypton releases during the cask test are compared in Figure 4.11 with the  $^{85}\text{Kr}$  releases observed in assembly B02 in the Fuel Temperature Test (FTT) (Johnson and Gilbert 1983) that was conducted to assess dry storage of spent fuel. The background level ( $3.086 \times 10^{-8}$  Ci) in the FTT, 1% release of the  $^{85}\text{Kr}$  produced in a single fuel rod, and 20% release of the  $^{85}\text{Kr}$  produced in a single fuel rod are plotted in Figure 4.11 for comparison with the release observed in the cask test. The krypton levels observed in the cask test are less than that expected for a single fuel rod with 20% release of  $^{85}\text{Kr}$  from the fuel. The krypton levels in the FTT were less than that from a fuel rod with 1% release. The higher release of  $^{85}\text{Kr}$  during the cask test would be expected from failure of a corner rod that probably experienced higher power during reactor operation. If the background level from the FTT is also used with the cask test data, it appears that the release of fission gas from both tests would have similar behaviors. With increasing time, the release of krypton in the cask would probably have decreased as indicated by the curve for the FTT

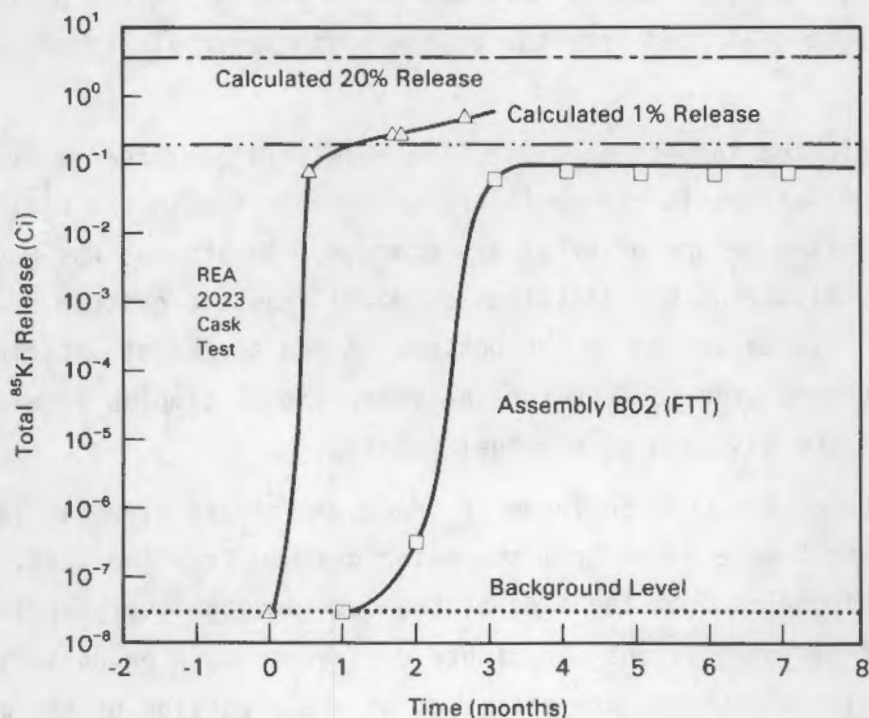


FIGURE 4.11. Comparison of Krypton Gas Released During Performance Test and Fuel Temperature Test



data. The difference in release rates during the first few months of testing in the REA cask and the FTT may have resulted from difference in the size of the defects or in the number of failed rods.

There was no confirmation of a leaking fuel rod either by visual inspection or sipping of the fuel assemblies after the cask test. It is believed that an extremely small defect may have opened up, perhaps at a previous cladding crack. The LLNL gas analyses provided the only indication of a leaking fuel rod. In any event, there has been no impact of any fuel rod failures on the basin operation or handling of the fuel assemblies subsequent to the cask test.

#### 4.4.4 Crud Sampling

The crud from the fuel bundles was sampled to establish the characteristics of the crud. In the event that crud spallation occurred during fuel movement, testing, or in the basin after testing, then the characteristics of the crud might provide useful information in evaluating the performance data. Crud was to be collected from the bottom of the cask if any residue was available.

As indicated in Section 4.2.2, the reddish/brown crud was very adherent. There was no noticeable change in the amount of crud in the basin or the basin filtering system before or after dry storage. An attempt was made to collect a sample by filtering the last inch of water from the cask to remove any crud that might have collected in the bottom. A few specks of material and the filter element were sent to LLNL for analyses. Smear samples were also taken from the side of the cask and on one fuel bundle.

Results of the LLNL analyses of crud samples are given in Table 4.11. Samples 1 and 3 were taken from the water drained from the cask. Samples 2 and 4 are smear samples from the side of the cask and the fuel bundles. Data are in units of disintegrations per minute decayed to noon on January 1, 1985. The values in parentheses are estimates of the precision of the measurement expressed as a percentage.



TABLE 4.11. Analysis of Crud Samples from REA Cask

Element	Activity in Samples from REA Cask, $10^4$ dpm			
	Sample 1	Sample 2	Sample 3	Sample 4
$^{54}\text{Mn}$	11.2 (7%)	112 (2%)	102 (6%)	570 (2%)
$^{60}\text{Co}$	1540 (1%)	3170 (1%)	9020 (2%)	9920 (1%)
$^{65}\text{Zn}$	12.9 (45%)	---	84.7 (30%)	102 (30%)
$^{125}\text{Sb}$	---	7.66 (16%)	---	17.6 (29%)
$^{134}\text{Cs}$	3.86 (9%)	7.95 (9%)	---	16.9 (16%)
$^{137}\text{Cs}$	121 (1%)	238 (1%)	111 (3%)	452 (1%)

#### 4.4.5 Summary

Examinations of the Cooper BWR spent fuel bundles used in the performance test indicate that there were no significant changes in the characteristics of integrity of the fuel rods. These examinations consisted of sipping, photography, and cask cover gas analyses.

Sipping and visual examinations of the fuel bundles before and after testing in the performance test indicate that the fuel rods were unaffected by the dry storage test. Features observed prior to testing, such as scratches and worn spots on the fuel rods and spacers, were unaffected by the handling operations or the dry storage test. A typical orange/reddish deposit of adherent crud ( $\text{Fe}_2\text{O}_3$ ) was found on all the fuel rods and the hardware. There were no noticeable changes in the characteristics or adherence of the crud as a result of the dry storage test or handling operations. The bottom of one lower-end nozzle was slightly deformed; however, all fuel assemblies were easily retrieved for reinsertion in the basin.

The gas analysis indicated that a small amount of krypton gas was released from the cask interior; however, this was not confirmed by either visual inspection or sipping of the fuel assemblies after the test. The rate of krypton release in the REA cask was approximately linear during the 2 to 3 months of testing, which suggests a very small cladding defect. Comparison of the gas release in the performance tests with gas release data for assembly B02 in the Fuel Temperature Test suggests that the release of fission gas would

eventually decrease with continued storage. It is believed that a small crack may have opened up at a previous cladding defect in one, or possibly a few, of the Cooper fuel rods.

Small amounts of water were detected in 9 of the 22 gas samples taken from the REA cask. Two of the gas samples had moisture content of 0.04 vol%, which is estimated to be equivalent to 3 g or less of water in the cask during testing.



## 5.0 CASK HEAT TRANSFER AND SHIELDING PERFORMANCE

Thermal and shielding performance of the REA 2023 BWR spent fuel storage cask are discussed in this section. The instrumentation used in collecting data, the measurement locations, and the measurement results are presented.

### 5.1 THERMAL PERFORMANCE

The placement of thermal instrumentation and the measurement results are described in this section.

#### 5.1.1 Instrumentation

Three types of instrumentation were used during the cask performance test: 1) Type K thermocouples for measuring cask and fuel temperatures, 2) pressure transducers for monitoring internal cask pressures, and 3) a weather station for determining the external cask boundary conditions.

##### 5.1.1.1 Temperature Measurements

Seventy Type K thermocouples (TCs) were used to monitor temperatures of the cask and fuel. Thirty-eight of these TCs were located inside the cask; the remaining 32 were mounted on the surface of the cask. The 1.6-mm (1/16-in.) metal-sheathed TCs were placed at eight axial locations in the basket and in seven fuel assemblies using several attachment methods. The internal measurement locations are shown in Figure 5.1; the thermocouple attachment methods are described in Appendix A. The placement of the internal thermocouples provided data for axial and radial temperature profiles when the cask was in a vertical orientation and axial and diametrical profiles when the cask was in a horizontal orientation.

Figure 5.2 shows the location of externally mounted thermocouples. The axial locations were selected to correspond to the elevation of the internal thermocouples. In addition to complementing the internal temperature measurements, the external thermocouple placements provided circumferential temperature profiles at three elevations and an axial surface temperature profile at 135 degrees.

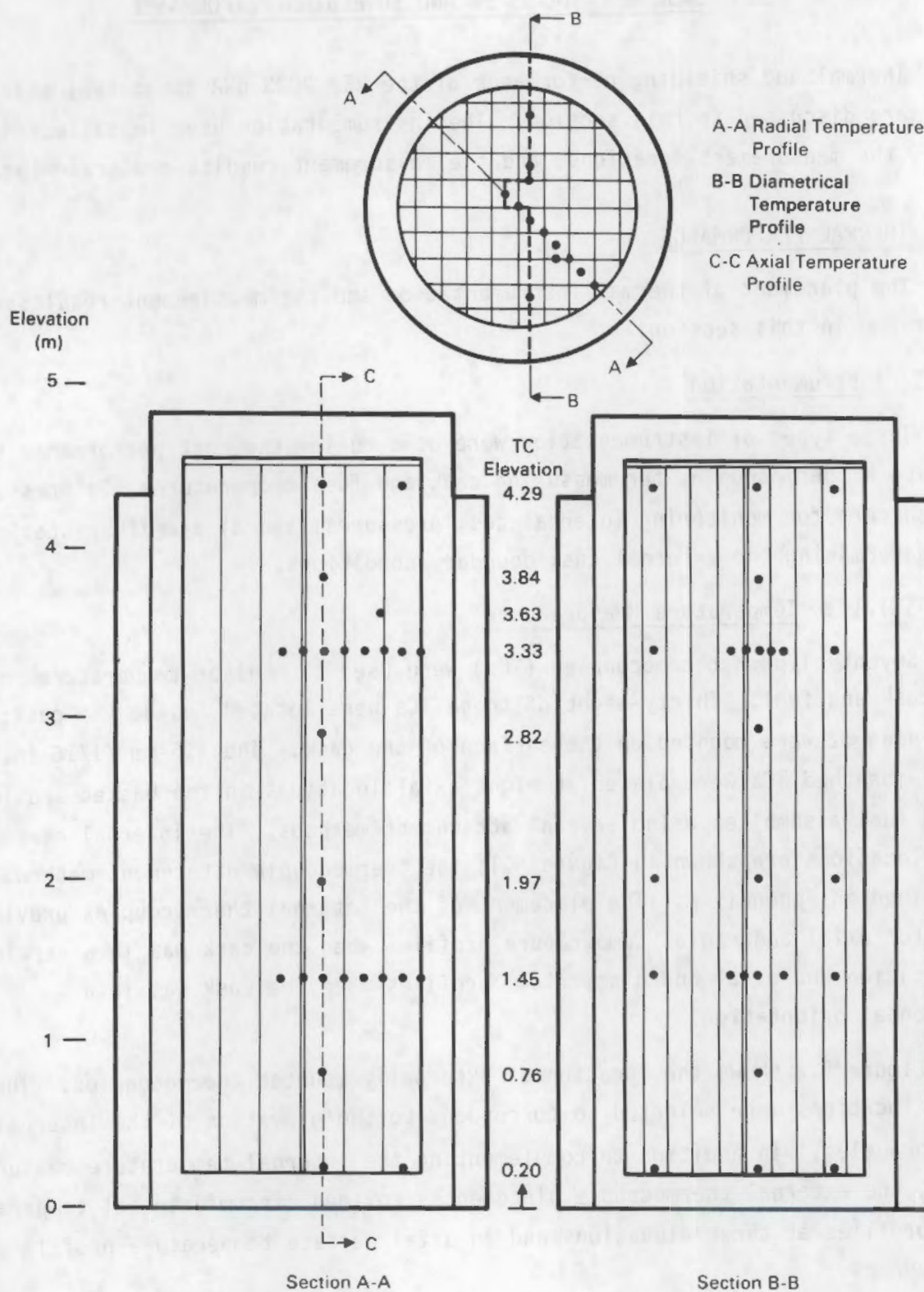


**FIGURE 5.1. Basket and Fuel Thermocouple Locations**



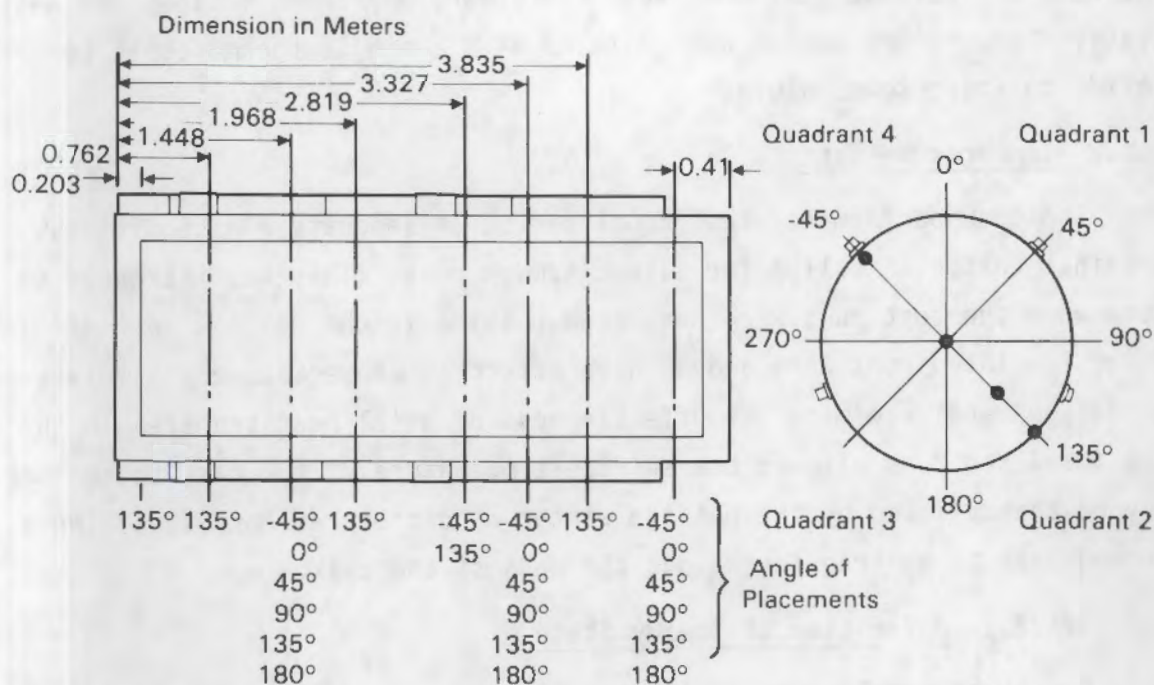


FIGURE 5.2. External Thermocouple Locations

#### 5.1.1.2 Pressure Instrumentation

In addition to the 38 internal thermocouples, two miniature pressure transducers were used to monitor internal cask pressures. One of the transducers was manufactured by Kulite and the other by Sensotec. Each pressure transducer was mounted in an instrument housing. The Kulite transducer was very temperature-sensitive and failed during the cask performance test. When the Kulite transducer was operational, its readings were difficult to interpret because it was difficult to separate actual cask pressure changes from apparent pressure changes due to transducer temperature changes. The Sensotec transducer performed reasonably well during the cask performance test.

#### 5.1.1.3 Weather Station

The weather station consisted of a temperature sensor, wind speed module, wind direction module, a star pyrometer (solar insolation), and a rain gage. The station was used to obtain the external boundary conditions experienced by



the cask at the test station. When tests were performed inside, the weather station temperature sensor was replaced with a single thermocouple to record inside building temperature.

#### 5.1.2 Temperature Data

The cask performance test consisted of 14 separate run conditions. The original test plan called for 11 hot summer runs. This was increased to 14 runs when the test runs were conducted outside in the coldest part of winter. Three insulated runs were added in an effort to conservatively simulate summer conditions and determine the effectiveness of axial heat transfer in the cask. The insulated runs allowed the surface temperature of the cask to be increased beyond that allowed by the outside winter conditions at Morris, Illinois, and forced heat to be transferred out the ends of the cask.

##### 5.1.2.1 Definition of Steady State

One of the challenges of testing was to determine when steady state had been achieved. If Mother Nature had cooperated and supplied steady ambient conditions, it would have been easy to select a steady-state run condition. Since this was not the case, a quasi-steady-state condition was selected for each run. The method for selecting this quasi-steady-state condition was to take a 24-hour average of the selected cask temperatures and weather conditions, and to select a time at which these averages remained nearly constant.

The rationale for selecting a 24-hour average was based on a desire to make it longer than the time constant of the cask and to dampen out day/night variations of solar insolation. Examination of the weather station data and cask temperatures presented in Figures 5.3 and 5.4 suggests that it takes from 14 to 22 hours for ambient temperature or wind disturbances to influence cask internal temperatures. Figure 5.3 is one of the more graphic examples of the time delay between cask surface disturbances and internal cask response. This figure represents the cask conditions between runs 2 and 3. In run 2 the cask was filled with nitrogen and in a vertical orientation. About 56 hours after the cask had been turned from vertical to horizontal, the ambient temperature



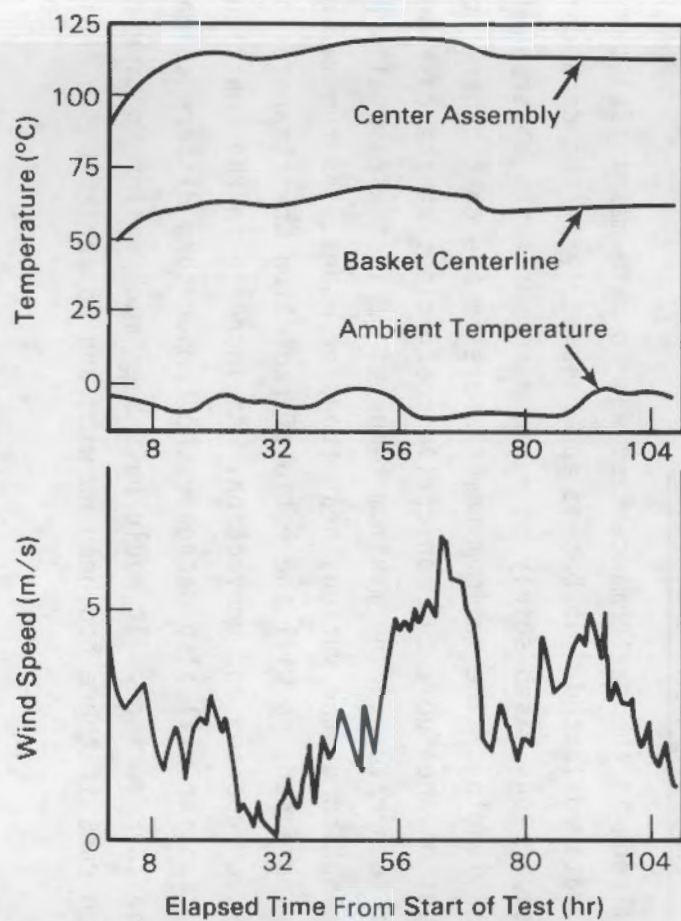


FIGURE 5.3. Cask Temperature Response to Ambient Conditions During Run 3

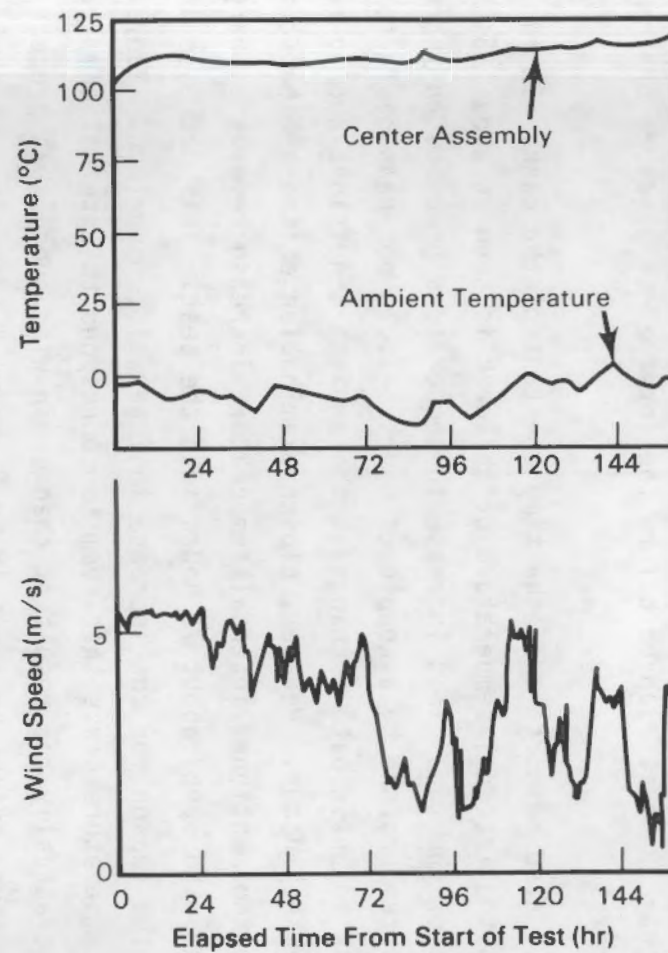


FIGURE 5.4. Cask Temperature Response to Ambient Conditions During Run 10

dropped 10°C and the wind speed increased from approximately 1.8 m/s to over 5 m/s. More than 12 hours elapsed before the internal temperature of the cask began to decrease.

Figure 5.4 also helps to show the time constant of the cask. In run 10, an increase in the internal temperature of the cask is seen at about 96 hours from the start of the run. This increase in temperature precedes an increase in the ambient temperature by a couple of hours. It is not reasonable to expect the cask to anticipate a change in the ambient conditions and to react to them before they occur. However, closer examination of the ambient conditions prior to the mentioned internal temperature increase reveals a sharp decrease in the wind speed about 73 hours into the test. This decrease in wind speed is the reason for the increase in internal temperature. Many of the internal temperature peaks that seem to correspond to external temperature spikes are actually the result of changes in wind speed that precede the internal temperature spikes by about 18 to 20 hours. Averaging the data over 24 hours accounts for time lags and variations in the ambient conditions. The numerical values of the averaged temperatures are given in Appendix G.

#### 5.1.2.2 Thermal Performance Overview

A big challenge in the performance test was to make meaningful comparisons of the thermal data collected. It became apparent early in the data comparison process that comparisons based solely on maximum temperatures observed in the cask could be misleading. The maximum temperature in the cask depends on the decay heat output of the fuel, the convective coefficient at the cask surface, and the ambient temperature. The maximum temperature in the cask also determines the contribution of the various heat transfer modes. As the maximum temperature is increased, so will the ratio of radiation heat transfer to the other two modes, conduction and convection. An increase in the contribution of radiation heat transfer will also decrease the temperature difference between the fuel and the cask surface. It would have been much easier to make comparisons between runs if there had been no wind and no variation in ambient temperature.

The test runs were designed to show the effect of loading, fill gas, and cask orientation on the thermal performance of the cask. The first set of test



runs was performed with a partial load of 28 fuel assemblies in the cask. This condition was used primarily to eliminate questions concerning safety by demonstrating the performance at a partial load and verifying pretest predictions (Wiles et al. 1986). Cask orientations consisted of horizontal and vertical positions. The fill gases included nitrogen, helium, and vacuum. Except for the repeat of runs 6 and 11, the first eleven runs were conducted outside. The repeats of runs 6 and 11 allowed higher cask surface temperatures in a more controlled inside environment. Near the conclusion of testing, the neutron shield was insulated. This provided still higher cask temperatures during runs 12, 13, and 14, that were more typical of summertime operation. The test matrix is summarized in Table 5.1, which shows maximum internal temperatures, average cask surface temperatures, average ambient temperatures, and average wind speeds and solar insolation for each of the performance test runs.

In Table 5.1 the maximum temperature in the cask was estimated based on the temperatures recorded in two center assemblies. One of the assemblies had eight temperature measurement locations that were used to determine the shape of the axial temperature profile. The other center assembly had only two TCs. When the temperatures from the two TCs exceeded temperatures at corresponding elevations in the well-instrumented assembly, they were used as the basis for extrapolating to the maximum temperature. The estimated maximum temperatures listed in Table 5.1 reflect this extrapolation.

The most apparent effect observed from Table 5.1 is that of the different fill conditions. The vacuum runs are about 50°C hotter than the nitrogen runs, and the nitrogen runs are about 35 to 40°C hotter than the helium runs.

Peak cladding temperatures for an uninsulated vertical cask with vacuum, nitrogen, and helium backfills were 200°C, 151°C, and 110°C, respectively. The respective average cask surface temperatures were 9°C, 15°C, and 15°C. Average cask surface temperature were about 20°C above ambient temperatures. The horizontal runs are generally hotter than the vertical runs. Peak cladding temperatures for an uninsulated horizontal cask with nitrogen and helium backfill were 164°C and 113°C, respectively. The respective average cask surface temperatures were 23°C and 10°C. There appears to be less than a 10°C difference between runs due to cask orientation. This indicates that increased contact

TABLE 5.1. Cask Thermal Performance Test Run Summary

Run No.	Cask Test Conditions			Total Decay Heat, kW	Wind Speed, m/sec	Solar Insol., W/m <sup>2</sup>	Ambient Temp, °C	Average Surface Temp, °C	Max. Clad Temp, °C	Max. Ambient Temp, °C	Max. Surface Temp, °C
1	Part.	Vert.	Vac.	9.0	2.2	75	7	18	170	163	152
2	Part.	Vert.	Nitr.	8.9	1.3	85	1	15	118	117	103
3	Part.	Horiz.	Nitr.	8.9	3.6	95	-10	2	116	126	114
4	Part.	Horiz.	Hel.	8.8	1.3	87	5	21	93	88	72
5A	Part.	Vert.	Hel.	8.8	3.6	21	-3	7	86	89	79
5B	Part.	Vert.	Hel.	8.7	6.3	16	14	20	97	83	77
6A	Full	Vert.	Vac.	15.2	0.0	0	24	52	227	203	175
6B	Full	Vert.	Vac.	15.2	3.6	65	-10	9	200	210	191
7	Full	Vert.	Nitr.	15.1	3.1	43	-4	15	151	155	136
8	Full	Vert.	Nitr.	14.9	1.3	143	-17	12	146	162	134
9	Full	Horiz.	Nitr.	15.0	2.0	48	-4	23	164	168	141
10	Full	Horiz.	Hel.	14.8	4.2	127	-8	10	113	121	103
11A	Full	Vert.	Hel.	14.9	0.7	141	-14	15	110	124	95
11B	Full	Vert.	Hel.	14.6	0.0	0	22	52	144	122	92
12 <sup>(a)</sup>	Full	Vert.	Hel.	14.4	0.0	0	20	101	185	165	84
13 <sup>(a)</sup>	Full	Vert.	Nitr.	14.4	0.0	0	22	100	209	187	109
14 <sup>(a)</sup>	Full	Vert.	Vac.	14.3	0.0	0	24	95	241	217	146

(a) Neutron shield was insulated.



between fuel assemblies and the basket in the horizontal orientation cannot compensate for convection in the vertical orientation with either nitrogen or helium. In general, the heat transfer performance was excellent, with a maximum temperature of  $241^{\circ}\text{C}$  observed for an insulated vertical cask with about 15 kW of decay heat output.

Runs 7 and 8 were performed to show the effect of shifting the position of the fuel assemblies in the basket on cask and fuel temperatures. Prior to run 7 the cask had been horizontal (during the partial load), and all the instrumented assemblies had the opportunity to shift to one side of the fuel tubes. Between runs 7 and 8 the cask was rotated to horizontal in the opposite direction so the fuel assemblies would shift to the other side of the fuel tube. The effect of this shift on measured temperatures was insignificant and less than  $5^{\circ}\text{C}$ .

The effect of radiation in the cask can be seen by looking at vacuum runs 6A and 6B. The increased surface temperature of 6A over 6B resulted in higher internal cask temperatures. The resultant higher internal temperatures in the cask increased the contribution of radiation heat transfer. This was seen as a lower temperature drop between the inside of the cask and the cask surface. In run 6A the maximum fuel-to-surface temperature drop was  $175^{\circ}\text{C}$  whereas in 6B it was  $190^{\circ}\text{C}$ , a difference of about  $15^{\circ}\text{C}$  between the two cases for a difference in maximum fuel temperatures of  $27^{\circ}\text{C}$ .

A lesser effect of radiation was seen when the cask was filled with helium, in runs 11A and 11B. Again, the radiation effect is seen by comparing the difference between maximum cask internal temperatures and average surface temperatures for the two cases. Here, the apparent radiation effect is on the order of  $3^{\circ}\text{C}$  for a maximum internal temperature difference of  $35^{\circ}\text{C}$ . The radiation heat transfer effect was less than for the vacuum runs due to the dominance of conduction heat transfer in the helium. In the vacuum runs, specifically 6A and 6B, conduction and convection heat transfer were minimal. In general, as the temperature of the cask increased, the contribution of radiation heat transfer increased. As a result, the temperature drop from the center of the cask to the cask wall decreased.



Figure 5.5 shows the effect of wind speed on surface temperatures. From heat transfer considerations, the cask decay heat output divided by the surface-to-ambient temperature difference is proportional to the convective heat transfer coefficient. This coefficient, in turn, is proportional to the Reynolds number. For small changes in temperature and for a cask of fixed dimensions, the Reynolds number will be proportional to the wind velocity. Therefore, the cask decay heat divided by the surface-to-ambient temperature difference should be proportional to some power of the wind velocity. A minimal effort was made to correlate the data in Figure 5.5 to this type of function, but the data did not correlate well. Further effort to develop a correlation was beyond the scope of this study.

An effort was made to correlate the solar insolation data to the thermal performance of the cask. However, it was not possible to separate the effect

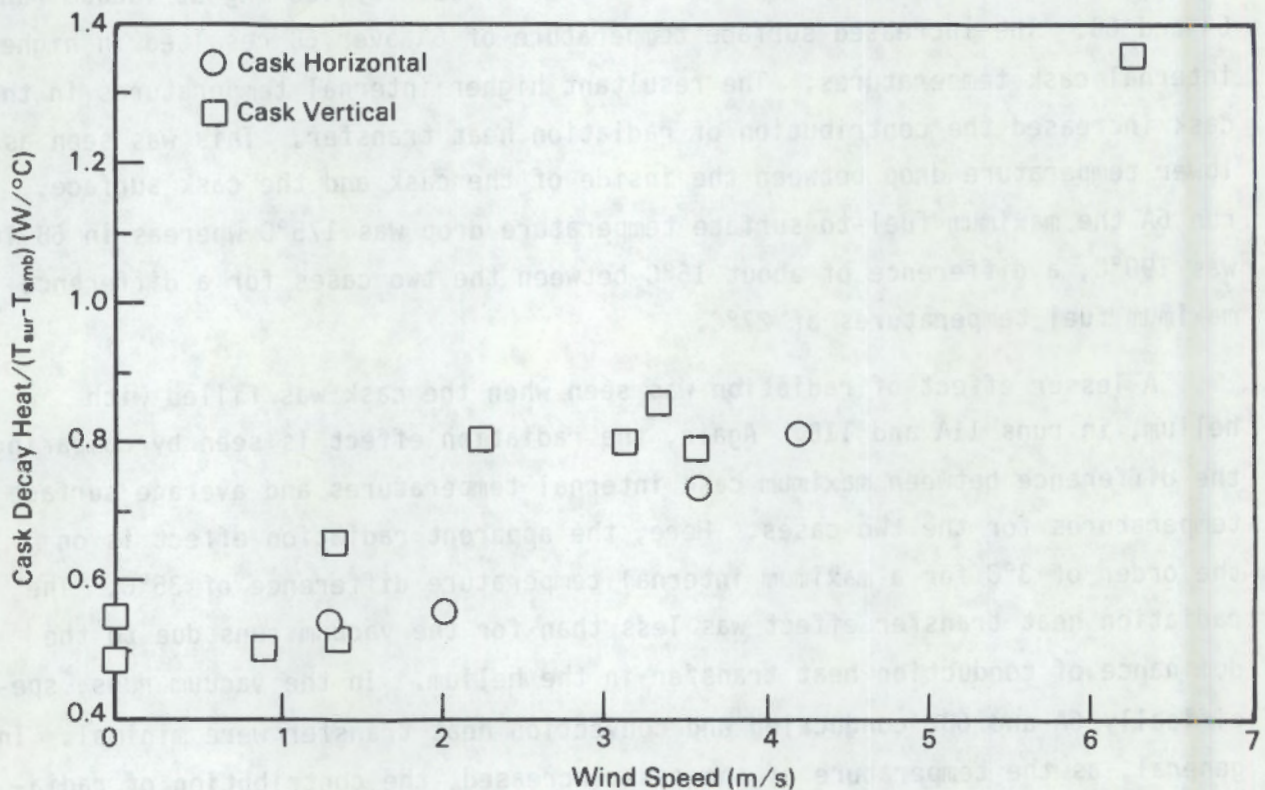


FIGURE 5.5. Relationship Between Wind Speed and Cask Surface-to-Ambient Temperature Differences



of ambient temperature from those of solar insolation. It appears that the effect of solar insolation is accounted for by considering the effect of cyclic ambient temperature. Solar insolation does not appear to add to the total cask heat load in a significant or correlatable manner.

In summary, correlations based on maximum fuel temperature must consider the effects of ambient temperature, wind speed, and absolute temperature magnitudes. Orientation did not significantly change the maximum temperature in the cask. The magnitude of the temperature in the cask affected the magnitude of the radiation heat transfer, which, in turn, affected the cask surface-to-maximum fuel temperature difference. Wind speed affected the temperature drop at the cask surface. Finally, there does not seem to be a correlation between solar insolation and cask temperature.

#### 5.1.2.3 Vacuum Runs

Four vertical vacuum runs were conducted; the results of the three uninsulated runs will be presented in this section. The results of the insulated vacuum run are presented in Section 5.1.2.7 of this report. The placement of the internal and external TCs allowed three types of temperature profiles to be obtained. They were 1) axial plots of temperatures on the surface of the cask and at the centerline of what was expected to be the hot assembly, 2) radial profiles of the temperatures along a diagonal (135 degrees circumferential orientation) at two elevations, and 3) diametrical temperature profiles taken across the basket from 0 to 180 degrees.

The axial temperature profiles obtained during the vertical vacuum runs of the performance test are shown in Figure 5.6. These profiles show the surface temperatures and center fuel assembly temperatures during runs 1, 6A, and 6B. These profiles show that the peak temperatures for the vacuum runs occurred in the lower portion of the cask at an elevation of about 2 m. The profile is quite similar to the gamma profile presented in Section 4, indicating the absence of axial convection. Run 6A had higher surface temperatures because it was run indoors on the decontamination pad; the other two runs were conducted outside at the test station.

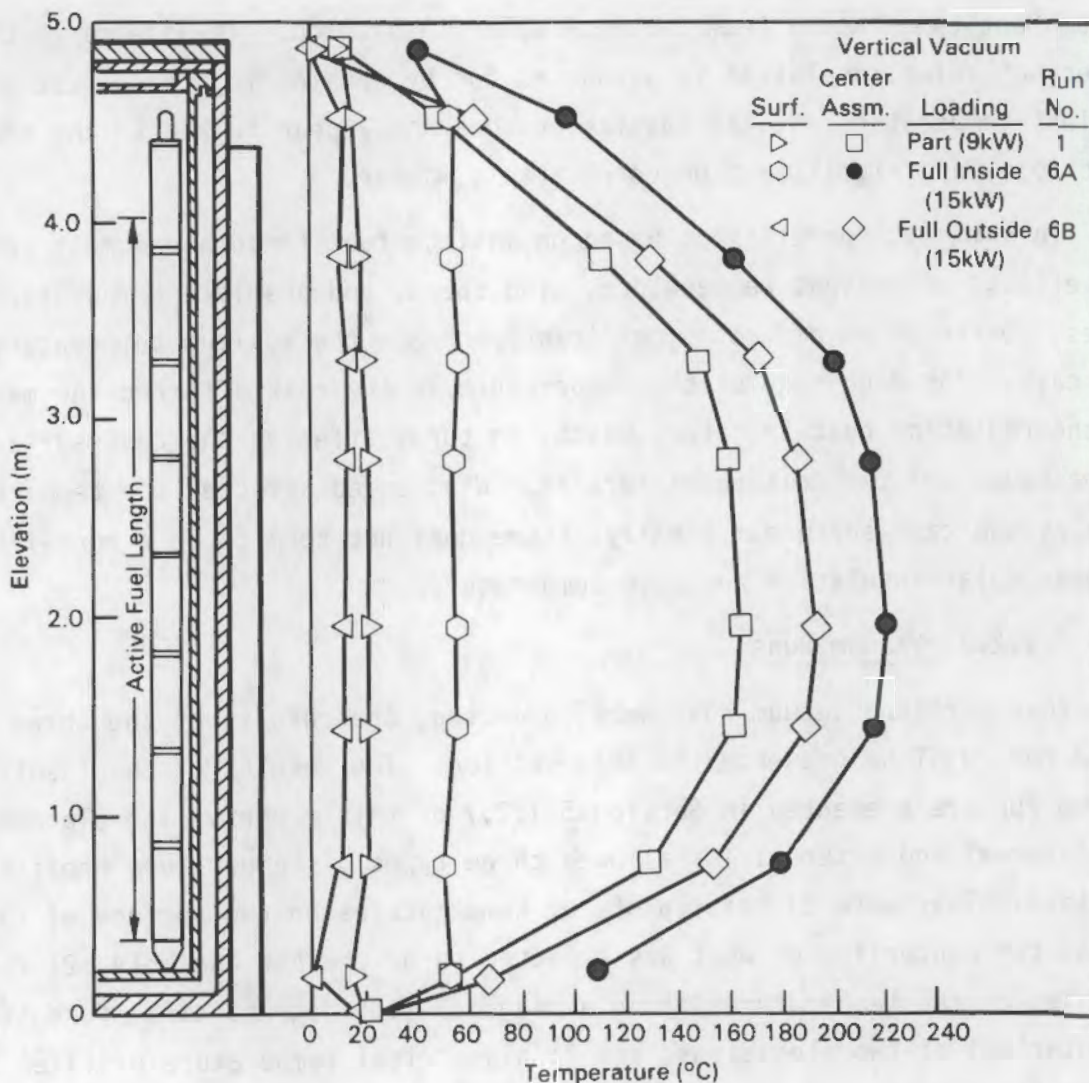


FIGURE 5.6. Axial Fuel and Surface Temperature Profiles for Vertical Vacuum Runs

If the average surface temperature is subtracted from the fuel temperatures, the results shown in Figure 5.7 are obtained. A comparison of Figures 5.6 and 5.7 shows the effect of thermal radiation in the cask. The profiles in Figure 5.6 show that the absolute temperature of the fuel in run 6A is greater than for run 6B. When referenced to the surface temperature (Figure 5.7), the positions of the axial profiles representing 6A and 6B are switched. Figure 5.7 shows that run 6A has a smaller difference between the surface temperature of the cask and the fuel temperature than does run 6B.



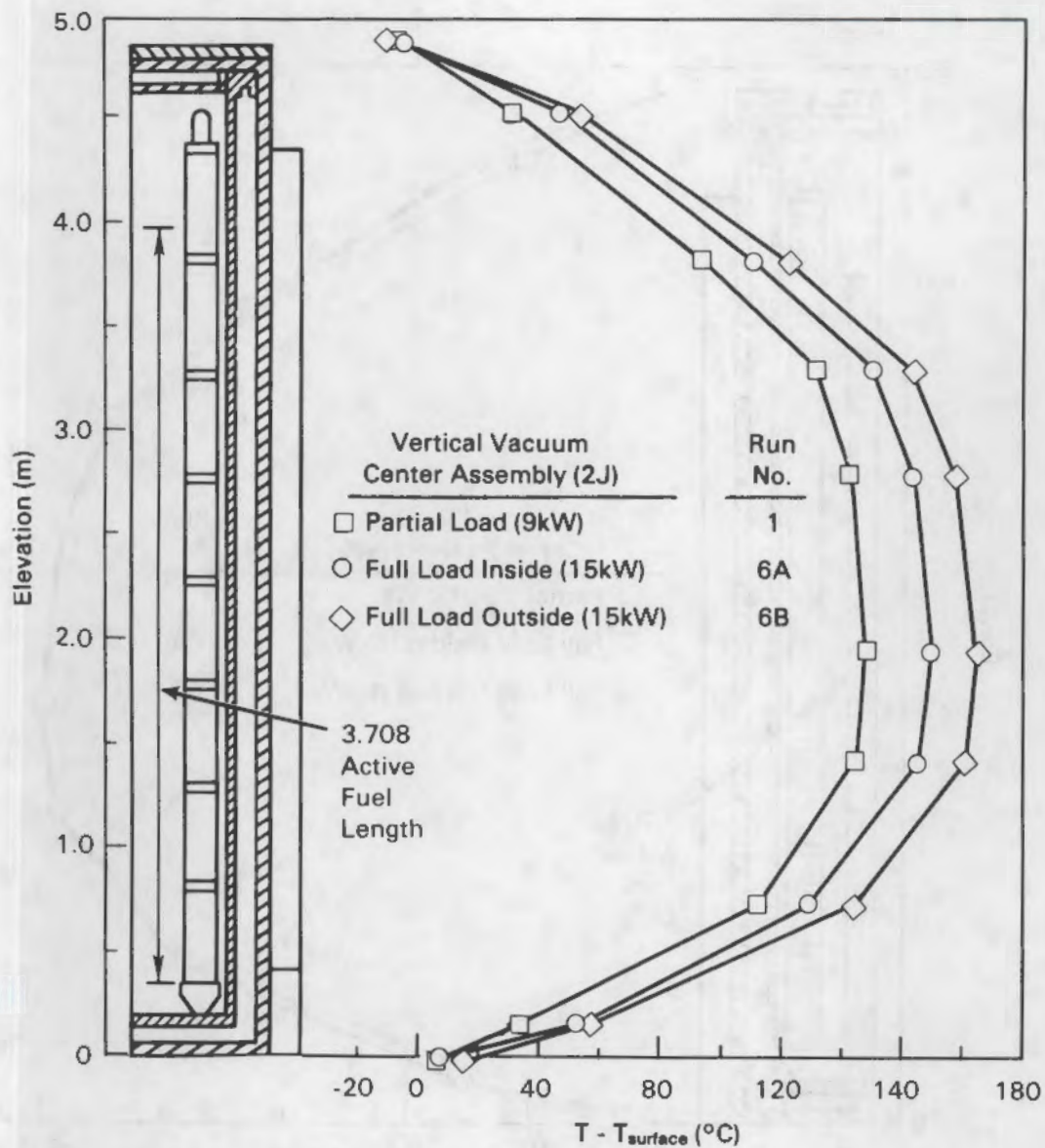
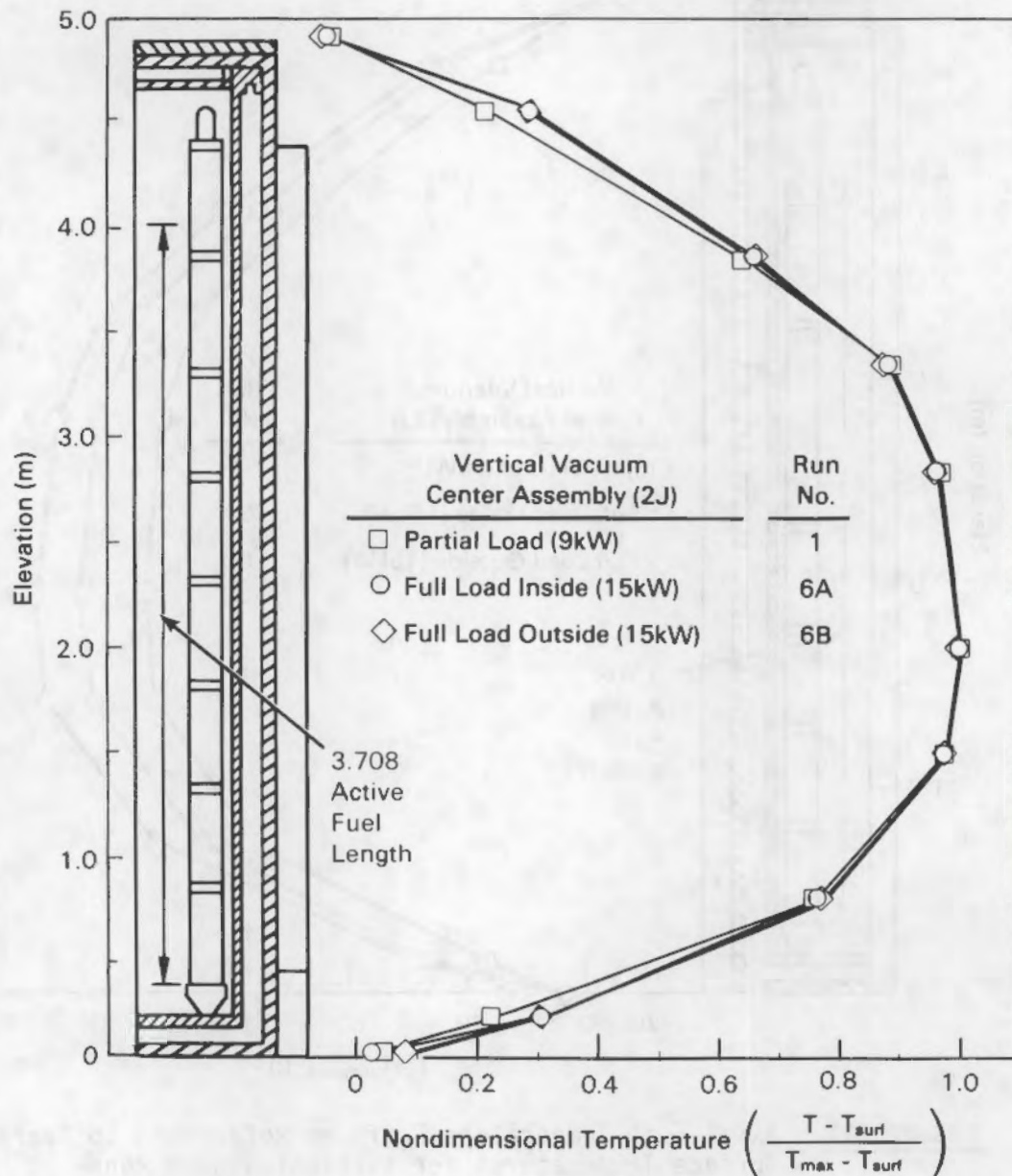


FIGURE 5.7. Axial Fuel Temperature Profiles Referenced to Average Surface Temperatures for Vertical Vacuum Runs

This smaller temperature difference between the surface and fuel in 6A is attributed to increased radiation heat transfer in the cask.

The similarities between the curves shown in Figures 5.6 and 5.7 can be seen by replotting the curves using a nondimensional temperature as shown in Figure 5.8. The nondimensional temperature used is referenced to the surface temperature and to the maximum fuel temperature. Except for small differences



**FIGURE 5.8.** Normalized Axial Fuel Temperature Profiles for Vertical Vacuum Runs

in the end effects between the partial and full loads, all three vacuum runs can be represented by a single axial profile.

Radial temperature profiles were obtained from data taken at two elevations in the cask, 1.45 and 3.33 m. The profiles shown in Figure 5.9 represent



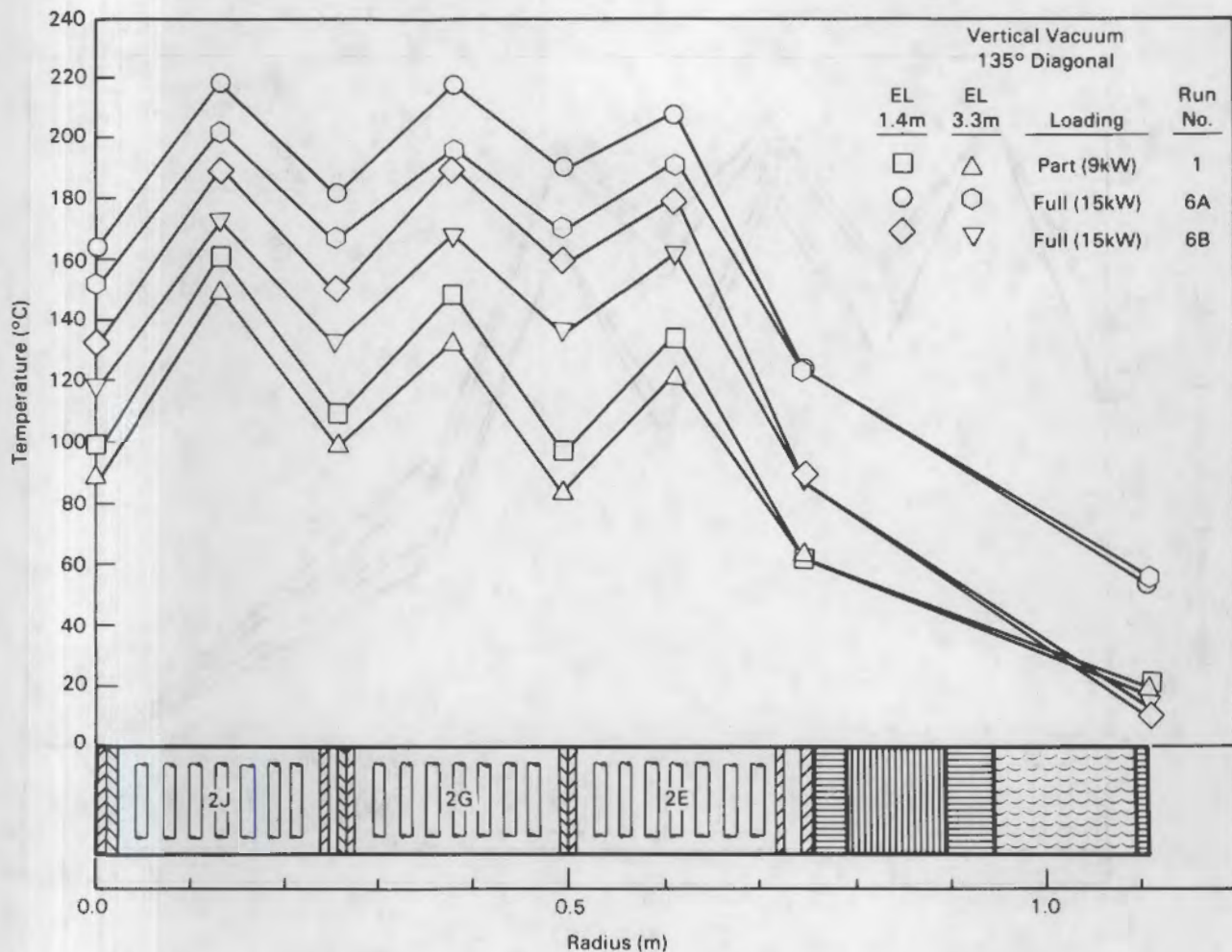


FIGURE 5.9. Radial Temperature Profiles for Vertical Vacuum Runs

data taken along the diagonal at 135 degrees. The data were taken at the center of the fuel assemblies and between fuel tubes in the basket. The data points have been connected by straight lines to make it convenient to visualize the profiles from a single run and at a particular elevation. The straight lines between the points do not represent the temperature profiles between the points, and temperature magnitudes are the only information that can be gained from Figure 5.9.

Plotting the information in Figure 5.9 as nondimensional temperatures shown in Figure 5.10 makes it easier to discuss the differences between loadings and the effect of radiation. These curves show the effect of radiation at different elevations. The temperatures at the 1.45-m elevation are higher than



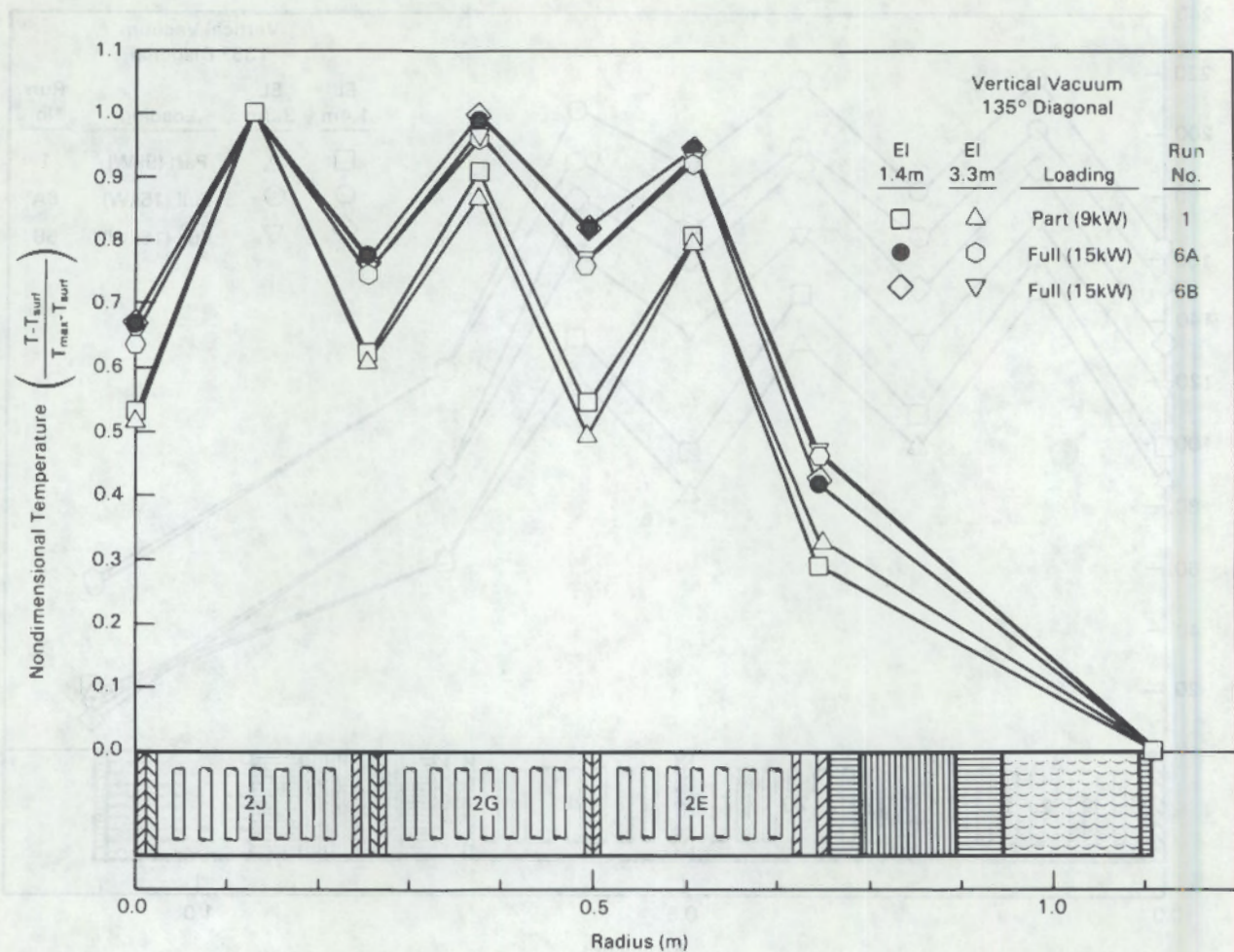


FIGURE 5.10. Normalized Radial Temperature Profiles for Vertical Vacuum Runs

temperatures at the 3.33-m elevation. Differences between fuel and basket temperatures are less where temperatures are greatest, showing that more radiation heat transfer is taking place. The fuel temperatures are about the same, showing the temperature-homogenizing effect of radiation. The temperatures for the partial load are less than for the full load as would be expected due to lower heat generation rates resulting from empty fuel tubes in the outer parts of the basket. The data shown in Figure 5.10 could be approximated by two curves, one for the partial load and one for the full load.

Figure 5.11 shows the diametrical data obtained in the cask during the vacuum runs. The inset on Figure 5.11 shows the temperature measurement



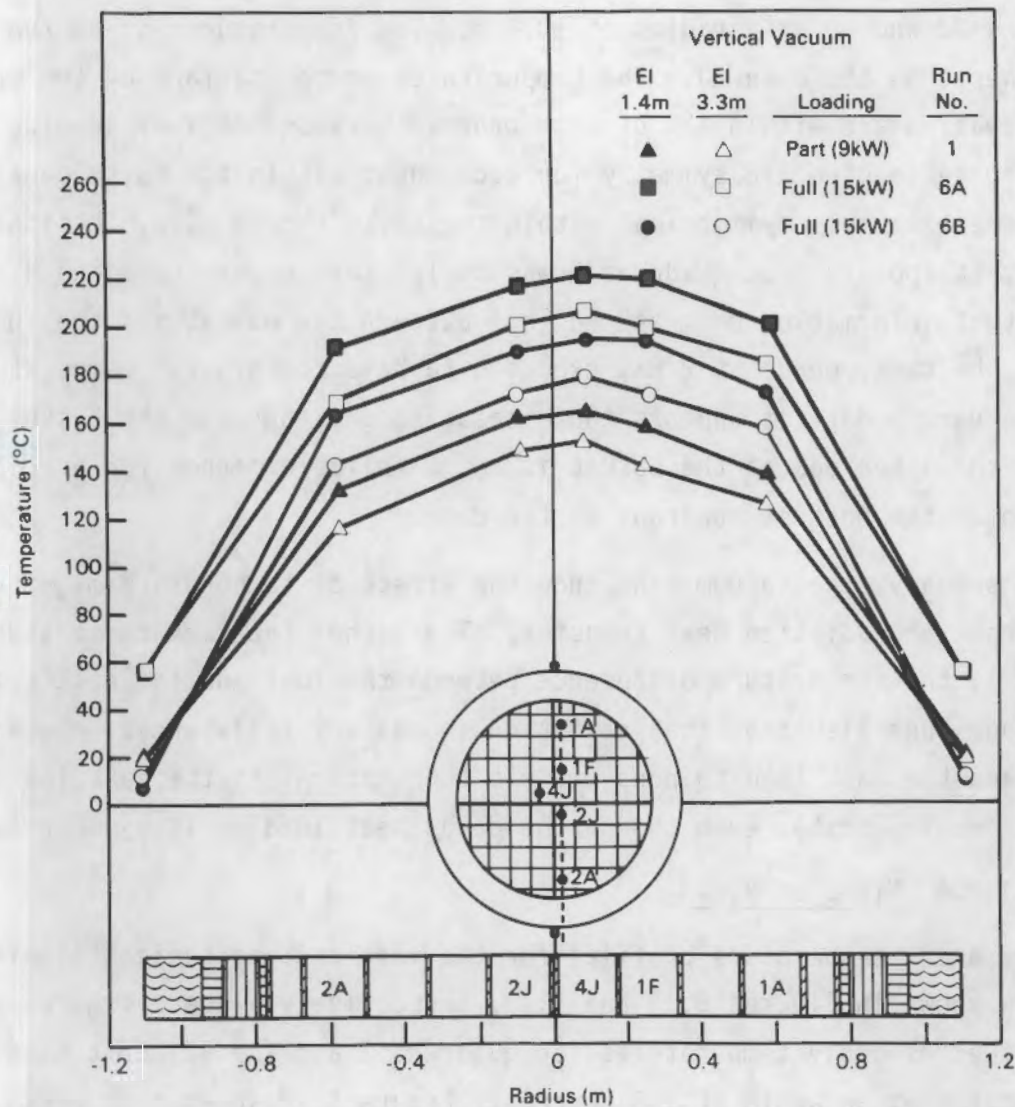


FIGURE 5.11. Diametrical Fuel Temperature Profiles for Vertical Vacuum Runs

locations and that temperatures were obtained in three quadrants in the cask. This gives two pairs of internal TCs (1A and 2A, 4J and 2J) and one pair of external TCs (0 and 180 degrees) at each measurement elevation that can be used to assess the symmetry of the temperatures in the cask. The symmetry of the temperatures in quadrants 1 and 2 can be assessed from the data points in basket locations 1A and 2A at a radius of  $\pm 0.6$  m. The temperatures in 1A are approximately  $10^{\circ}\text{C}$  higher than those for 2A. Similarly, the symmetry between quadrants 2 and 4 can be assessed from the temperatures in the center basket



locations 2J and 4J at a radius of  $\pm 0.1$  m. The temperatures in 4J run about  $4^{\circ}\text{C}$  higher than those in 2J. The temperatures on the surface of the cask at this elevation are within  $1^{\circ}\text{C}$  of each other. Because the fuel loading pattern was designed to give 1/8 symmetry for decay heat within the cask, decay heat rates were extremely symmetrical within the cask (Figure 3.13, Section 3). However, it appears that quadrant 2 was cooler than quadrants 1 and 4. From the pretest information on measured gaps between the basket and the inside surface of the cask, quadrant 2 was expected to have the highest temperatures. From the vacuum data it appears that measuring gaps between the basket and the cask at the upper end of the basket is not a reliable method for predicting the location of the hottest quadrant in the cask.

In summary, the vacuum runs show the effect of temperature magnitudes in the cask on radiation heat transfer. The higher the cask temperature, the smaller is the temperature difference between the fuel and the cask's surface. The vacuum runs also show that variation in contact resistances between the basket and the cask lead to nonsymmetric temperatures in the cask (as great as  $10^{\circ}\text{C}$  for the test), even though the decay heat loading is symmetric.

#### 5.1.2.4 Nitrogen Runs

The axial temperature profiles for the vertical and horizontal nitrogen runs are shown in Figures 5.12 and 5.13, respectively. These figures show the center fuel assembly temperatures for quadrant 2 and the adjacent cask surface temperatures at an angle of 135 degrees. Figure 5.12 shows that peak clad temperatures occurred in the upper portion of the cask for the vertical nitrogen run. This peak is about 1.3 m above the peak observed for the vacuum run. The change in the position of the peak temperature is due to convection. Internal and external convection cause a small surface temperature gradient that increases with elevation.

Run 8 shown in Figure 5.12 was performed to show the effect of fuel assembly location in the basket on the temperature profiles. Prior to run 7 the cask had been in the horizontal orientation, which shifted all the fuel assemblies containing TCs toward the quadrant 2 and 3 side of the cask. Just prior to run 8, the cask was again rotated to a horizontal position so that



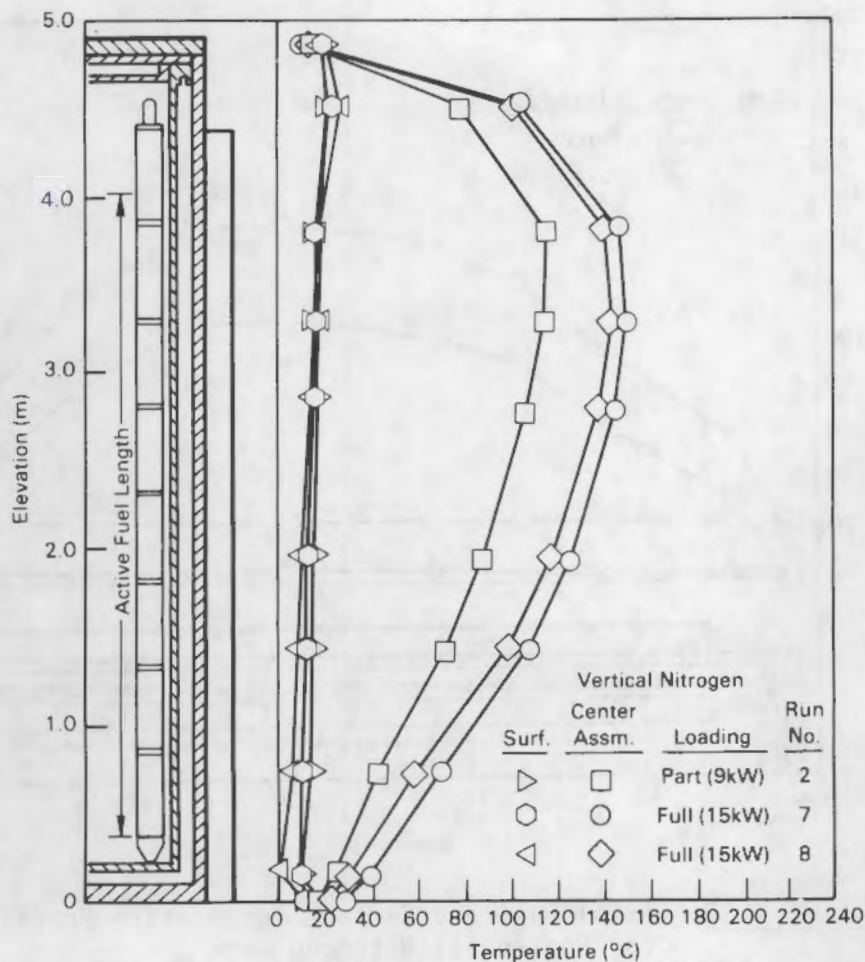


FIGURE 5.12. Axial Fuel and Surface Temperature Profiles for Vertical Nitrogen Runs

quadrants 1 and 4 were at the bottom of the cask. This caused fuel assemblies to shift to the opposite side of the basket fuel tubes. The small temperature difference seen between runs 7 and 8 reflects the insignificant effect of reorientation of the fuel assemblies in the basket.

Figure 5.13 shows the axial temperature profiles for the cask in the horizontal orientation. The dashed portion of the curve for run 9 is an estimate of the temperature in this region because there was a temporary loss of a TC output at an elevation of 2.8 m. It is apparent from Figure 5.13 that peak

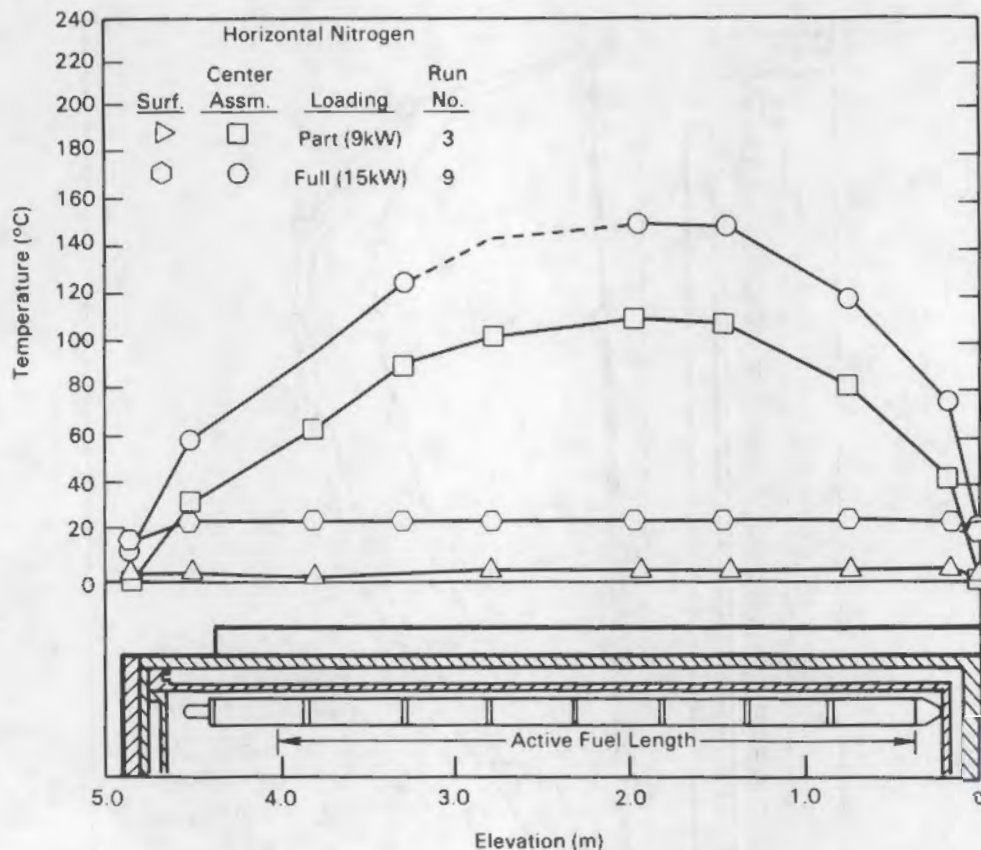
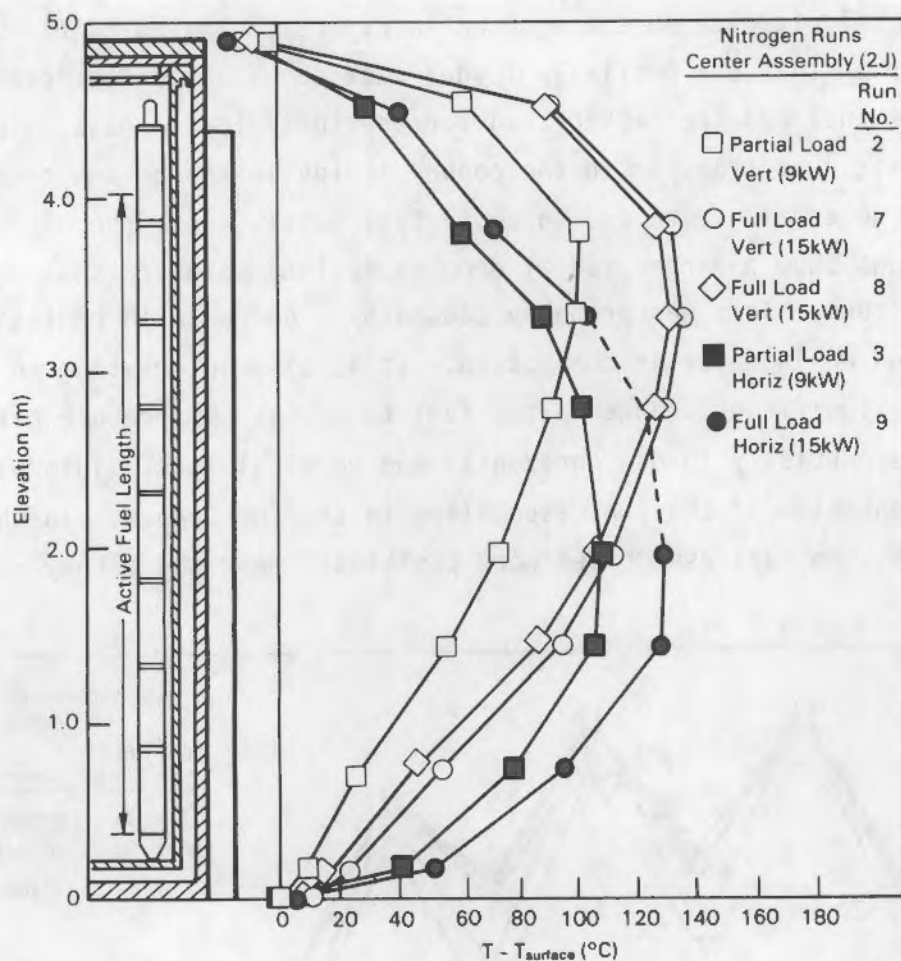


FIGURE 5.13. Axial Fuel and Surface Temperature Profiles for Horizontal Nitrogen Runs

cladding temperatures were located in the lower portion of the cask about 2 m from the bottom end of the cask during the horizontal nitrogen run, and there is no pronounced surface temperature gradient for the horizontal runs as was observed for the vertical runs. The peak temperature occurs at the same axial position as was observed for the vacuum runs, indicating the absence of convection; however, the magnitude of the peak is about 40 to 50°C less.

In Figure 5.14, the fuel assembly axial temperature profiles of Figures 5.12 and 5.13 have been replotted as differences between fuel temperatures and average surface temperatures of the cask. Figure 5.14 shows that peak cladding temperatures for nitrogen runs are only weakly dependent on cask orientation. Convection in the vertical runs results in peak temperatures shifting to the upper portion of the cask as previously discussed, but very





**FIGURE 5.14.** Axial Fuel temperature Profiles Referenced to Average Surface Temperatures for Vertical and Horizontal Nitrogen Runs

little change in temperature magnitudes are seen. It will become apparent as the radial plots are presented and compared that the contact resistance between the basket and the cask decreases for the lower quadrants 2 and 3 when the cask is horizontal. This, in turn, reduces the temperatures in instrumented quadrant 2. However, the decrease in contact resistance in the horizontal runs does not compensate for the increased convection in a vertical orientation. The net effect is that no significant change in the peak temperature results due to cask orientation, and only the location of the peak temperature is changed.

Normalized plots of the radial temperature profiles for the vertical and horizontal nitrogen runs are shown in Figures 5.15 and 5.16. The curves are similar in that the partially loaded cask shows larger temperature drops between the fuel and the basket than for the fully loaded cask. The reason for this is lower heat transfer in the copper strips in the basket coupled with a lower heat generation rate due to empty fuel tubes. Both the horizontal and vertical runs show a larger radial drop in fuel temperature than was seen in the vacuum runs. This was probably caused by a decrease in radiation heat transfer and an increase in convection. It is also interesting to note that there is a significant change in the fuel to basket temperature difference between the partially loaded horizontal and vertical runs. This was caused by a reorientation of the fuel assemblies in the fuel tubes. In the vertical orientation, the fuel assemblies were positioned near where they were at the

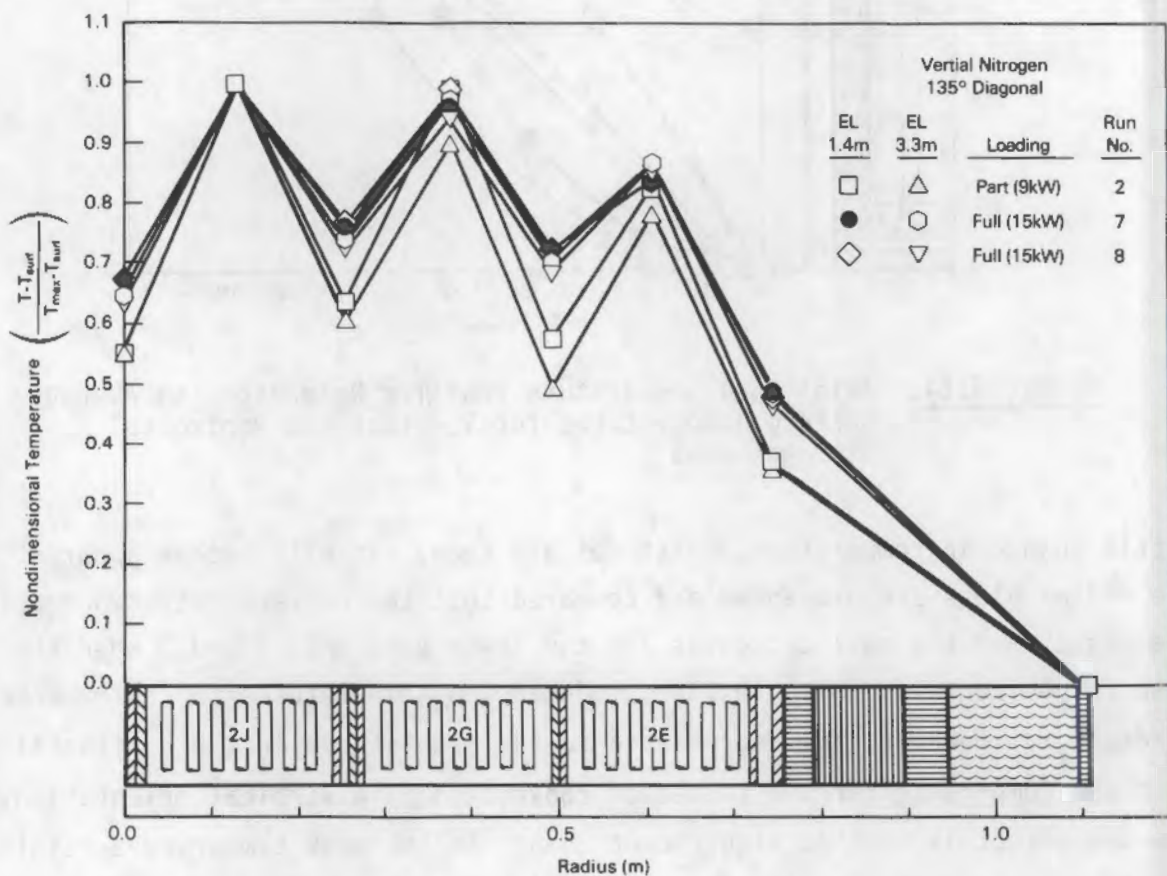


**FIGURE 5.15.** Normalized Radial Temperature Profiles for Vertical Nitrogen Runs



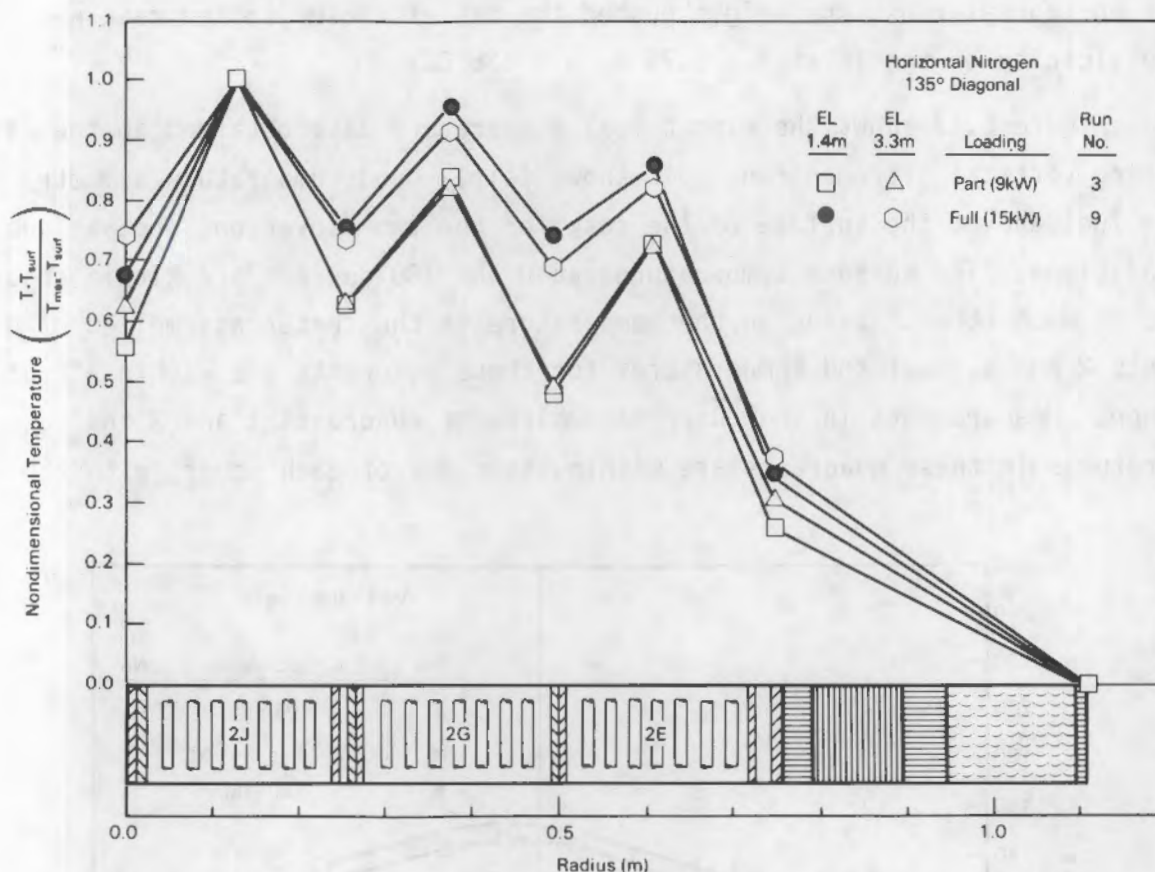


FIGURE 5.16. Normalized Radial Temperature Profiles for Horizontal Nitrogen Runs

time of loading, somewhat concentric with respect to the fuel tube. In the horizontal orientation, they were shifted to one side of the fuel tube. Hence, the decrease in the fuel-to-basket temperature difference is a result of the better contact between the fuel and the basket fuel tubes in the horizontal orientation.

A major difference between the radial temperature profiles for the vertical and the horizontal nitrogen runs is the temperature drop between the surface of the cask and the TC in the outer part of the basket ( $R = 0.75$  m). In horizontal runs this temperature drop is much less than in vertical runs. The reason for this is a decrease in the contact resistance between the basket and the inside wall of the cask caused by the weight of the basket and fuel. In

the horizontal runs, the weight pushed the basket closer to the cask wall in the vicinity of the TC at  $R = 0.75$  m,  $\theta = 135^\circ$ .

Figure 5.17 shows the diametrical temperature data obtained in the cask during vertical nitrogen runs. It shows fairly good temperature symmetry in the fuel and at the surface of the cask for the two elevations and various run conditions. The surface temperatures at 0 and 180 degrees are within about  $2^\circ\text{C}$  of each other. Based on the temperature in the center assemblies of quadrants 2 and 4, fuel rod temperatures for these quadrants are within  $1^\circ\text{C}$  of each other. Measurements in the outer assemblies of quadrants 1 and 2 indicate temperatures in these quadrants are within about  $8^\circ\text{C}$  of each other, with the

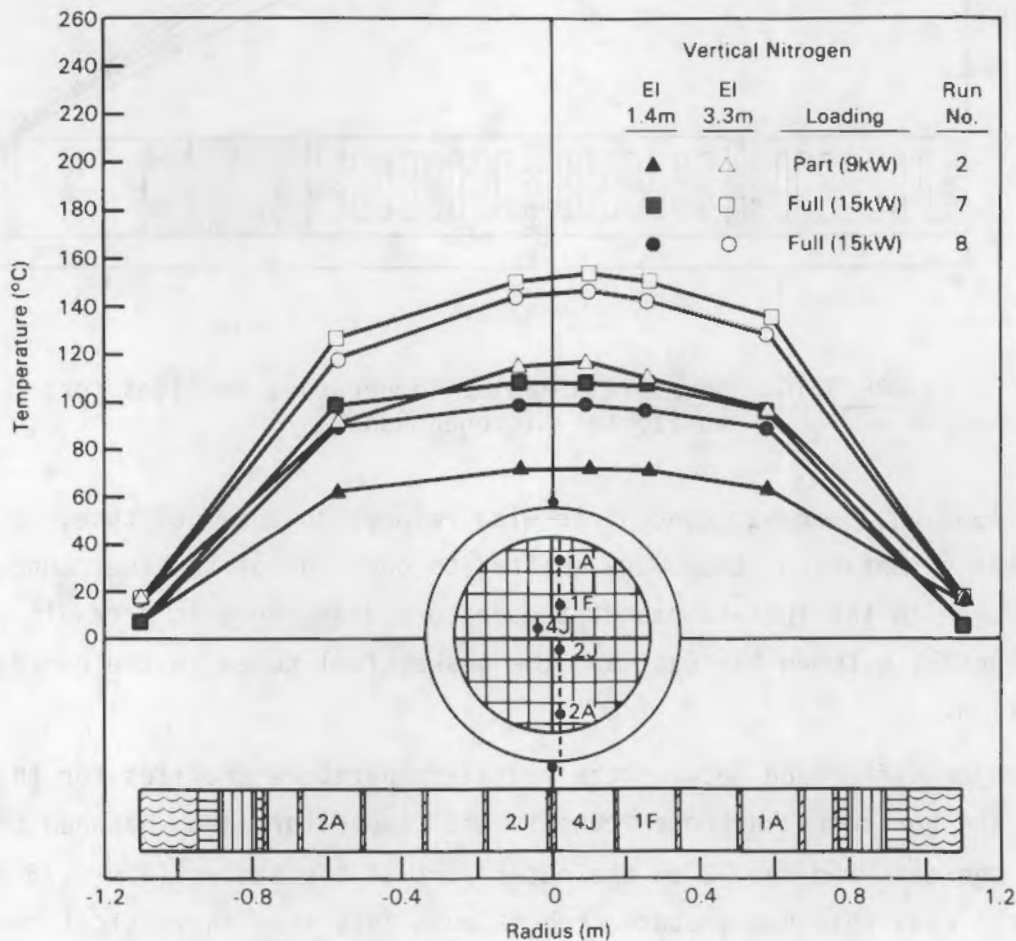


FIGURE 5.17. Diametrical Fuel Temperature Profiles for Vertical Nitrogen Runs



temperatures in quadrant 1 being the highest. The profiles at the lower elevation (1.45 m) are more symmetric than those at the upper elevation (3.33 m).

Figure 5.18 shows the diametrical temperature data obtained during horizontal runs. It shows significantly higher temperatures in quadrants 1 and 4 than did the vertical runs. The differences between temperatures in the outer assemblies of quadrants 1 and 2 range between 22°C and 37°C for the horizontal orientation compared to a maximum of 12°C for the vertical runs. Likewise, the temperatures in quadrant 4 are higher than those in quadrant 2 for horizontal runs. In the vertical runs, quadrant 2 and 4 temperatures were no more than

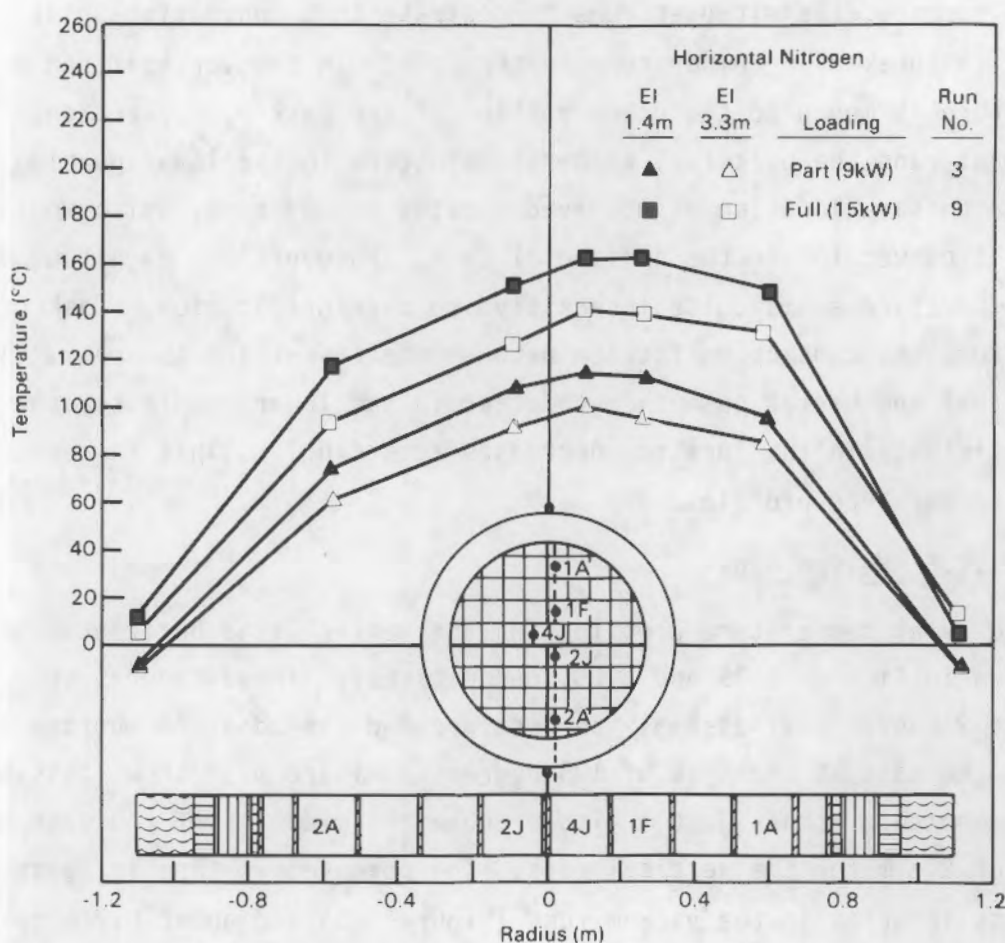


FIGURE 5.18. Diametrical Fuel Temperature Profiles for Horizontal Nitrogen Runs



3°C apart based on the temperatures measured in the center assembly. In the horizontal runs, quadrant 2 and 4 temperatures differ by 6 to 14°C, with quadrant 4 temperatures being the hottest. The increased temperature differences between quadrants 1 and 4 and quadrant 2 are probably due to a decrease in the contact resistance between the basket and the cask in lower quadrants 2 and 3 and an increase in the contact resistance in upper quadrants 1 and 4. A change in contact resistance could be caused by the effect of the weight of the basket and fuel in the horizontal orientation. Whatever the cause, the temperatures in quadrants 1 and 4 are significantly higher than those in quadrant 2 in a horizontal orientation.

In summary, the nitrogen runs demonstrate that convection shifts the location of the peak clad temperature in the cask. In the vertical run the peak temperature is moved to the upper portion of the cask by convection. In the horizontal runs the peak fuel temperature occurs in the lower portion of the cask at the same location as observed for the vacuum runs, which would indicate a lack of convection in the horizontal cask. However, the magnitude of the peak temperature seems quite insensitive to cask orientation. Cask orientation does affect the contact resistance between the basket and the cask. The weight of the fuel and basket push them together in the lower quadrants, and the contact resistance in the location decreases accordingly. This is seen in the radial temperature profiles.

#### 5.1.2.5 Helium Runs

The axial temperature profiles for the vertical and horizontal helium runs are shown in Figures 5.19 and 5.20, respectively. These figures show both the quadrant 2 center fuel assembly temperature and the adjacent surface temperature of the cask at an angle of 135 degrees. Figure 5.19 shows that the peak fuel temperature occurs just a little above the midpoint of the cask at an elevation of 2.8 m for the vertical runs. The peak temperature is about 0.8 m above its location in the vacuum runs (Figure 5.6) and about 0.7 m below its location in the nitrogen runs (Figure 5.7), indicating that some convection existed in the helium backfill gas. Runs 11B and 11A show a small increase in surface temperature with elevation, which could be caused by natural convection on the outside of the cask. These two runs had very low wind velocities, less



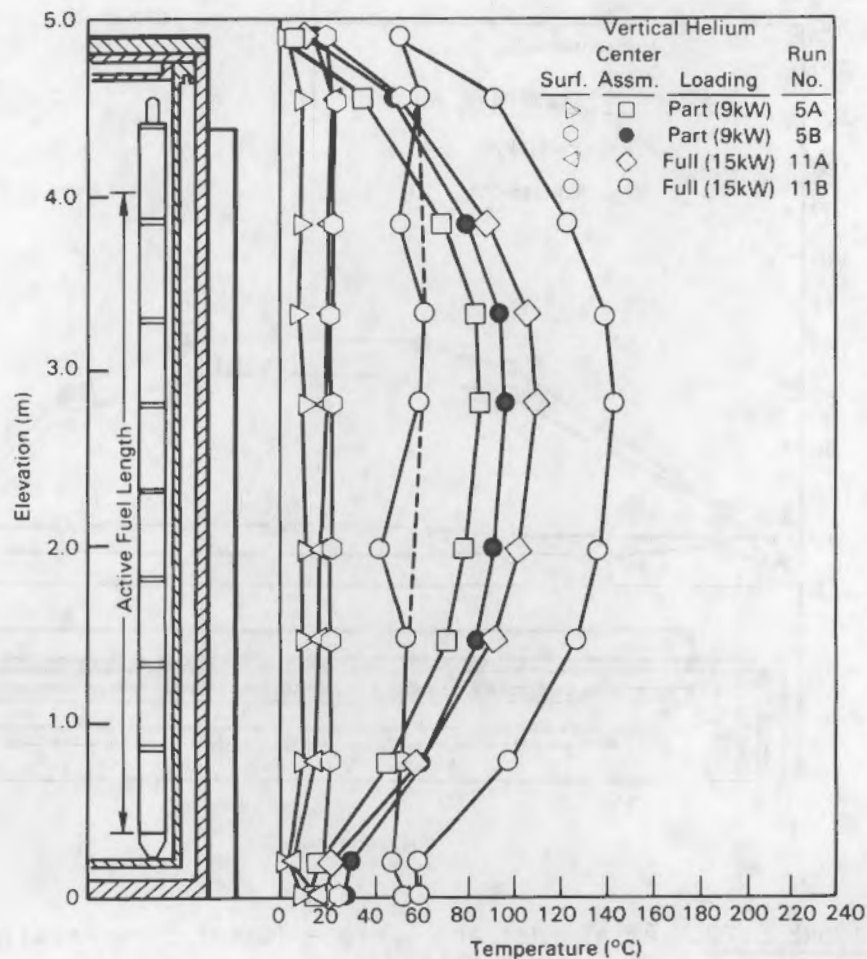


FIGURE 5.19. Axial Fuel and Surface Temperature Profiles for Vertical Helium Runs

than 1 m/s, compared to runs 5A and 5B, which had velocities greater than 3 m/s. Two of the points in the surface temperature profile for run 11B appear low compared to the rest of the points. This could have been caused by softening of the paint at elevated cask surface temperatures, which resulted in poor contact between the TCs and the surface. The dashed line is a better representation of the actual surface temperature of the cask for run 11B.

Axial temperature profiles for the horizontal helium runs are shown in Figure 5.20. Peak fuel temperatures are below the midpoint of the cask at an

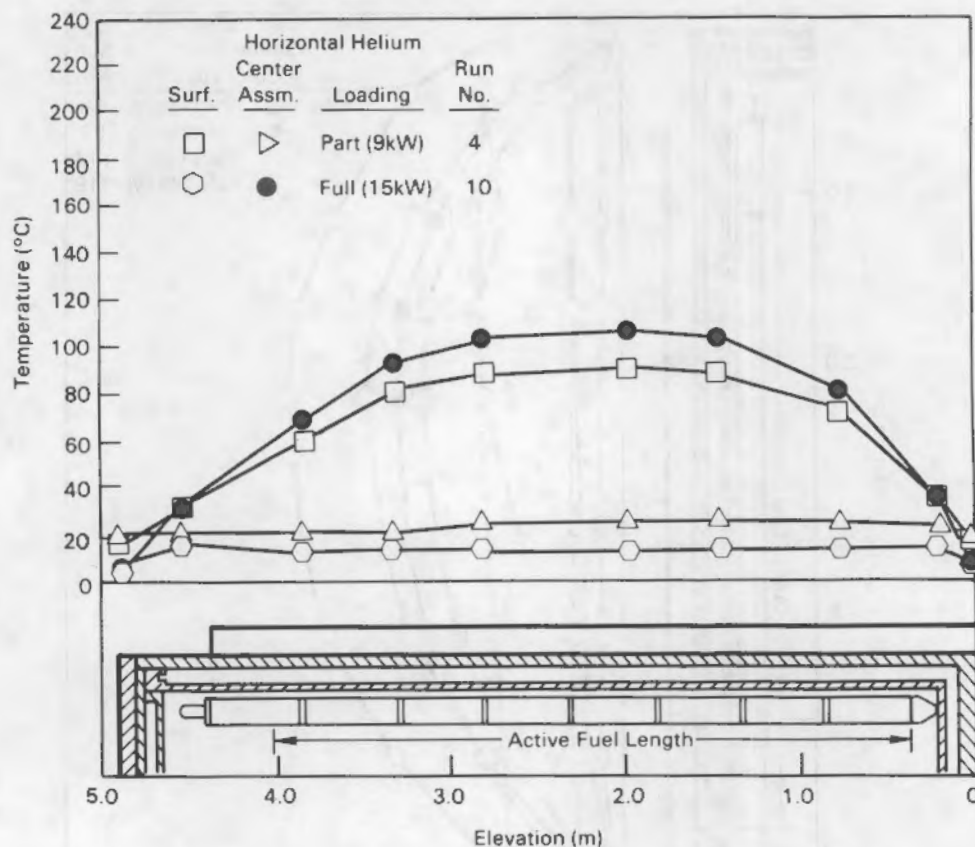


FIGURE 5.20. Axial Fuel and Surface Temperature Profiles for Horizontal Helium Runs

axial location 2 m from the bottom of the cask, the same location observed for vertical vacuum and horizontal nitrogen. This again indicates the lack of convection in helium horizontal runs.

A comparison between the vertical and horizontal axial temperature profiles can be made by examining Figure 5.21. The temperatures in Figure 5.21 are referenced to average surface temperatures. The effect of cask orientation is not as pronounced for helium as it was for nitrogen. However, the effect of convection is still apparent and shifts the peak temperature toward the upper portion of a vertical cask. The peak temperatures are about the same, irrespective of cask orientation.

Figure 5.21 also shows a small radiation effect for runs 5A, 5B, 11A, and 11B. From Figure 5.21 it is apparent that the difference between the surface



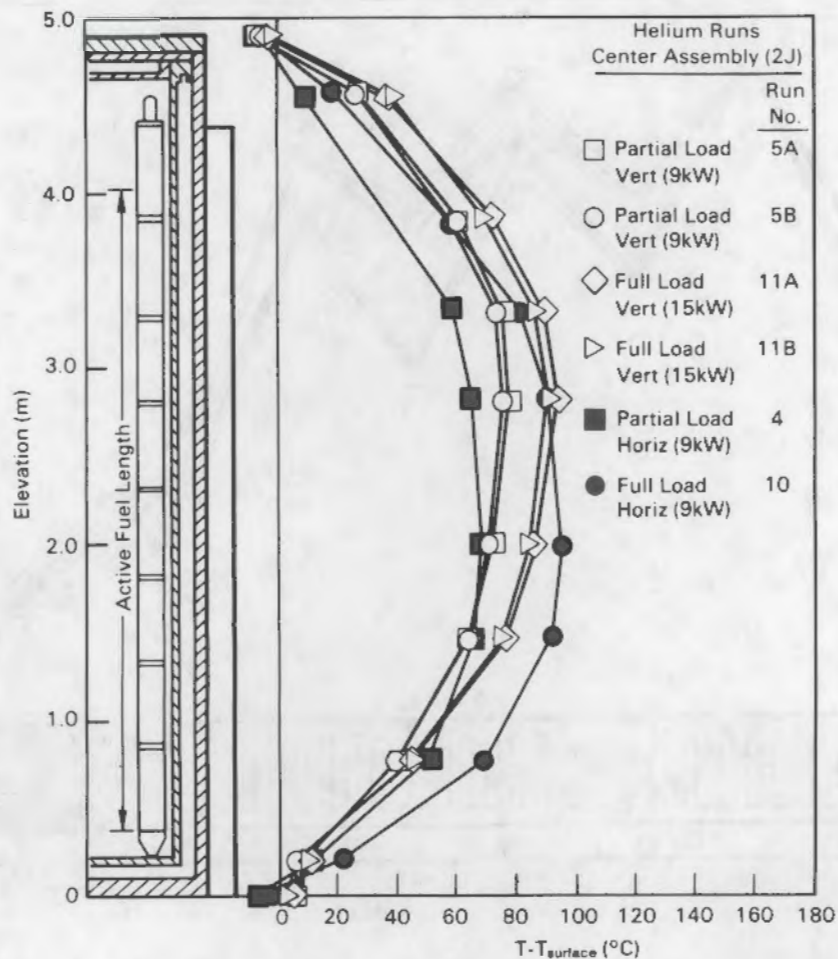


FIGURE 5.21. Axial Fuel Temperature Profiles Referenced to Average Surface Temperatures for Vertical and Horizontal Helium Runs

and the fuel is greater for runs 5A and 11A than for runs 5B and 11B, respectively. However, Figure 5.19 shows that the fuel temperatures for runs 5B and 11B are higher than the fuel temperatures for runs 5A and 11A, respectively. Therefore, the smaller temperature difference between the fuel and the cask surface can be attributed to the increased radiation heat transfer in the cask due to the higher absolute temperatures in the cask.

Normalized plots of the radial temperature profiles for the vertical and horizontal helium runs are shown in Figures 5.22 and 5.23. The curves are similar in that the partially loaded cask shows larger temperature drops between the fuel and basket than for the fully loaded cask. The reason for

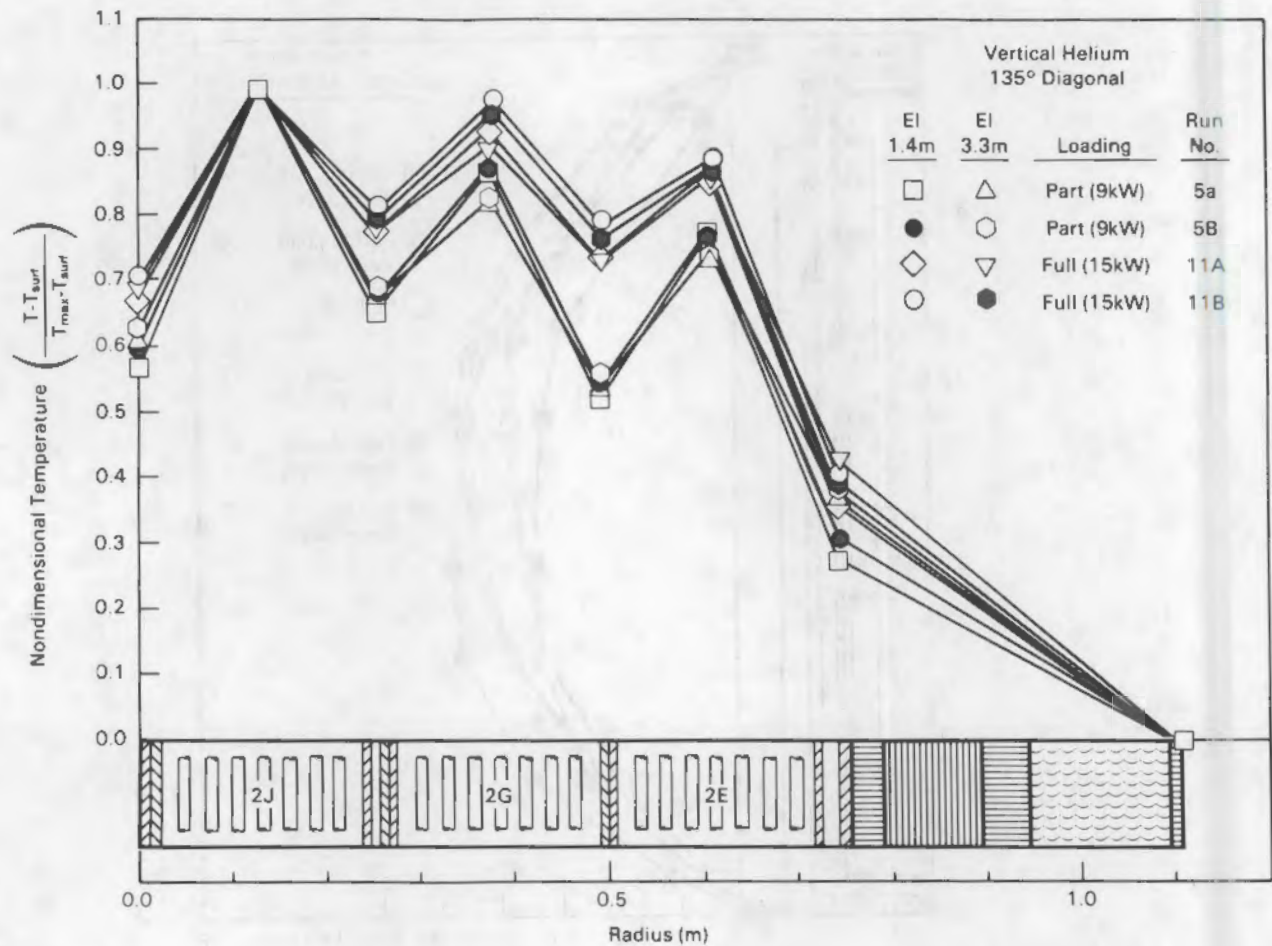


FIGURE 5.22. Normalized Radial Temperature Profiles for Vertical Helium Runs

this is the lower heat transfer in the copper strips in the basket coupled with a lower heat generation rate due to the empty basket fuel tubes. The profiles also show less temperature drop between the fuel and basket than was seen for the vacuum or nitrogen runs. This is due to the increased conduction in helium.

A major difference between the radial temperature profiles for the vertical and horizontal helium runs is the temperature drop between the surface of the cask and the thermocouple in the outer part of the basket ( $R = 0.75$  m,  $\theta = 135^\circ$ ). In the horizontal runs this temperature drop is much less than in the vertical runs. The reason for this is a decrease in the contact resistance between the basket and the inside wall of the cask caused by the weight of the



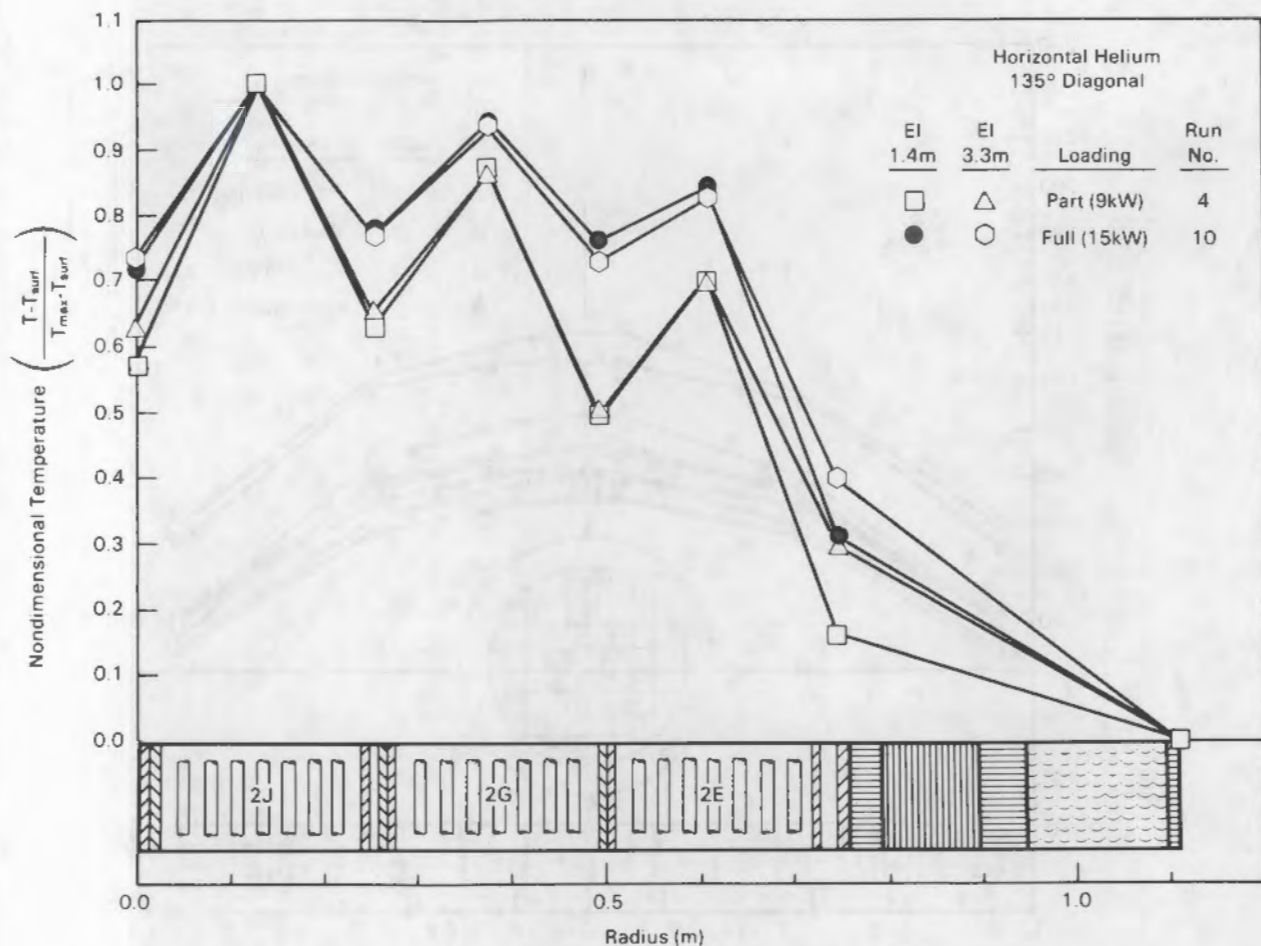


FIGURE 5.23. Normalized Radial Temperature Profiles for Horizontal Helium Runs

basket and fuel. In the horizontal run, the weight pushed the basket closer to the cask wall in the vicinity of the TC at  $R = 0.75$  m,  $\theta = 135^\circ$ .

Figure 5.24 shows the diametrical temperature data obtained in the cask during the vertical helium runs. It shows fairly good temperature symmetry in the fuel and at the surface of the cask for the two elevations and various run conditions. The surface temperatures at 0 and 180 degrees are the same. Based on the temperature in the center assemblies of quadrants 2 and 4, fuel rod temperatures for these quadrants are within  $1^\circ\text{C}$  of each other. Temperatures in the outer assemblies of quadrants 1 and 2 indicate that temperatures in these quadrants are within about  $5^\circ\text{C}$  of each other, with the temperatures in

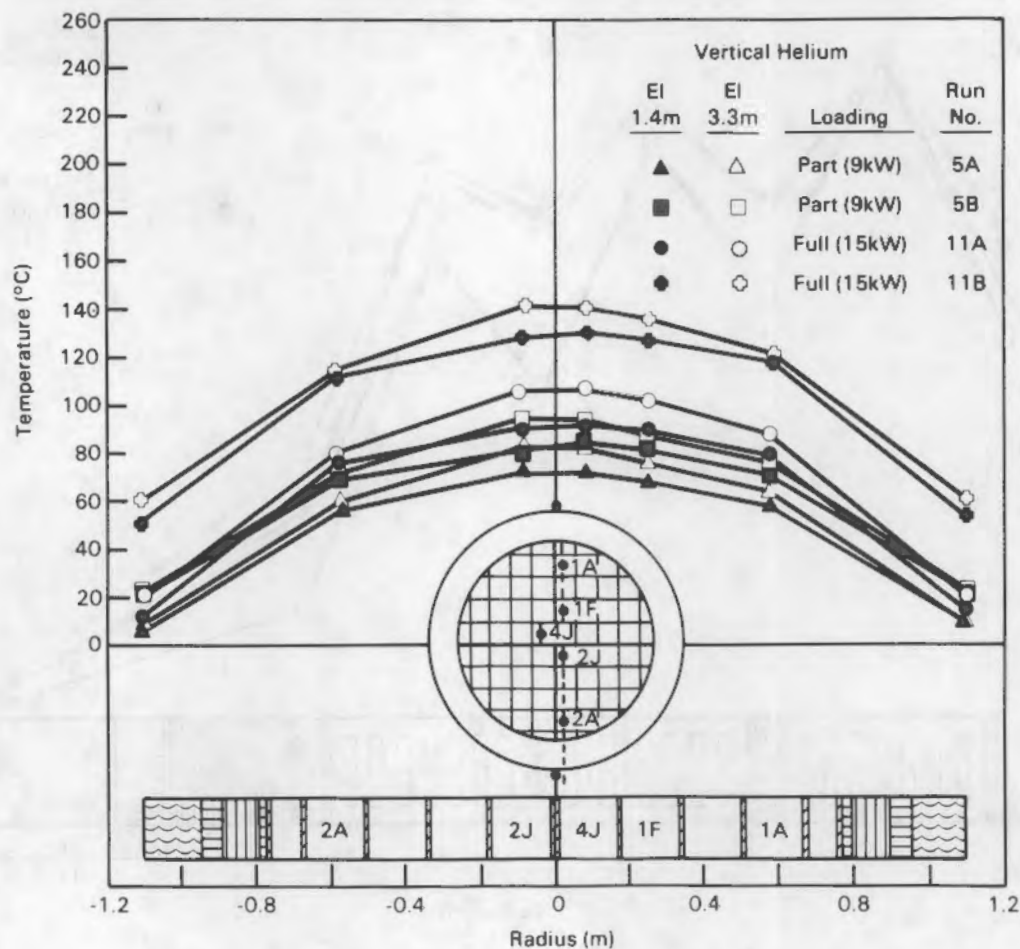


FIGURE 5.24. Diametrical Fuel Temperature Profiles for Vertical Helium Runs

quadrant 1 being the highest. The profiles at the lower elevation (1.45 m) are more symmetric than those at the upper elevation (3.33 m).

Figure 5.25 shows the diametrical temperature data obtained during the horizontal runs. It shows significantly higher temperatures in quadrants 1 and 4 than did the vertical runs. The differences between temperatures in the outer assemblies of quadrants 1 and 2 range between 12°C and 20°C for the horizontal orientation, compared to a maximum of 9°C for all of the vertical runs. Likewise, the temperatures in quadrant 4 are higher than those in quadrant 2. In the vertical runs, quadrant 2 and 4 temperatures were no more than 3°C apart.



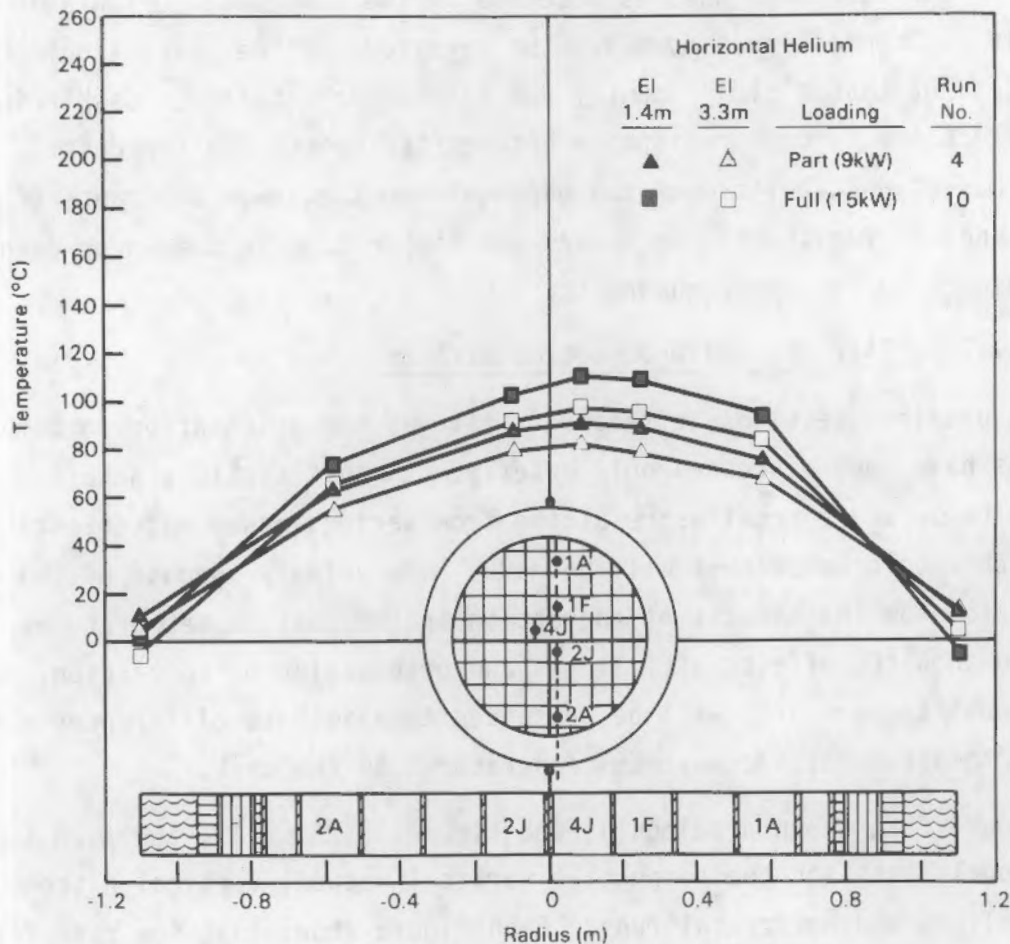


FIGURE 5.25. Diametrical Fuel Temperature Profiles for Horizontal Helium Runs

based on the temperature measured in the center assembly. In the horizontal runs, quadrant 2 and 4 temperatures differ by 3°C and 7°C, with quadrant 4 temperatures being the hottest.

Again, it is felt that the temperature asymmetry in the cask is caused by contact resistances between the fuel, basket, and cask. Greater asymmetry is observed in the horizontal runs due to the effect of basket and fuel weight on the contact resistances between the cask and lower quadrants of the basket.

In summary, the vertical helium runs show the effect of convection. The magnitude of the effect is not as great as was observed in nitrogen. However, convection in the vertical orientation does move the peak fuel temperature



upward in the cask over what is observed in the horizontal orientation where there is not convection. However, the magnitude of the peak cladding temperature does not change significantly due to cask orientation. Cask orientation does affect the contact resistance between the basket and the cask. The weight of the basket and fuel closes the gaps between the lower quadrants of the basket and the fuel, which decreases the temperature in the lower quadrants with respect to the upper quadrants.

#### 5.1.2.6 Fill Gas and Orientation Effects

In previous sections, effects of fill gas and orientation on temperature profiles have been discussed only briefly. In this section, detailed comparisons of temperature profiles resulting from various gases and orientations used during the performance test will be made. The primary purpose of the comparisons is to show the effects of convection in the cask on temperatures. In order to show the effects of fill gas and orientation on convection, non-dimensional temperatures will be presented to eliminate differences due to ambient temperatures and maximum temperatures in the cask.

Figure 5.8, shown previously, and Figures 5.26, 5.27, and 5.28 show non-dimensional plots for the respective vertical vacuum, vertical nitrogen, vertical helium, and horizontal runs. Each figure shows that the runs for the same orientation and fill gas are similar. If an average curve is generated for each of the nondimensional plots, Figure 5.29 results, which shows a single curve for each orientation/fill gas combination. The horizontal runs have been shown as a single curve because the differences due to different gases are small. The horizontal and vertical vacuum profiles agree closely with one another and also with the measured axial gamma curve of Figure 4.7 in Section 4, which supports the conclusion that there is insignificant convection in horizontal or vacuum runs. Convection in the vertical runs shifts peak temperatures upward in the cask. Peak temperatures in helium are 0.8 m above those in vacuum, and peak temperatures in nitrogen are 0.5 m above those in helium. The shift from the peak temperature location in vacuum is more pronounced for nitrogen than for helium, due to greater temperature differences (density differences) in nitrogen that increase buoyancy forces and result in higher natural convection velocities.



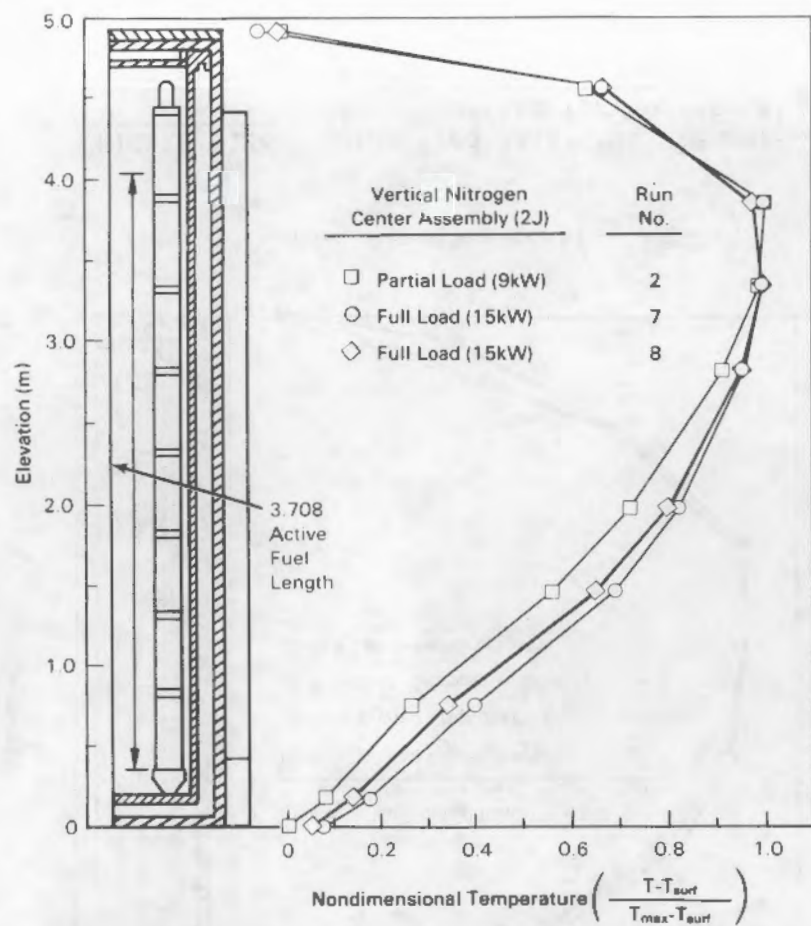


FIGURE 5.26. Normalized Axial Fuel Temperature Profiles for Vertical Nitrogen Runs

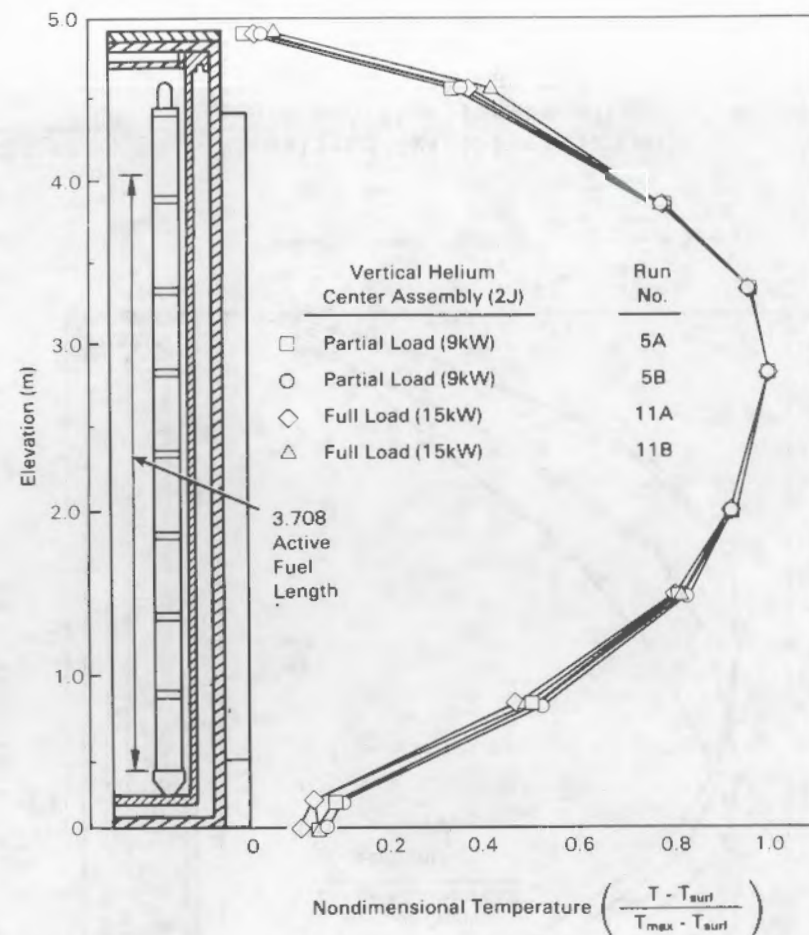


FIGURE 5.27. Normalized Axial Fuel Temperature Profiles for Vertical Helium Runs

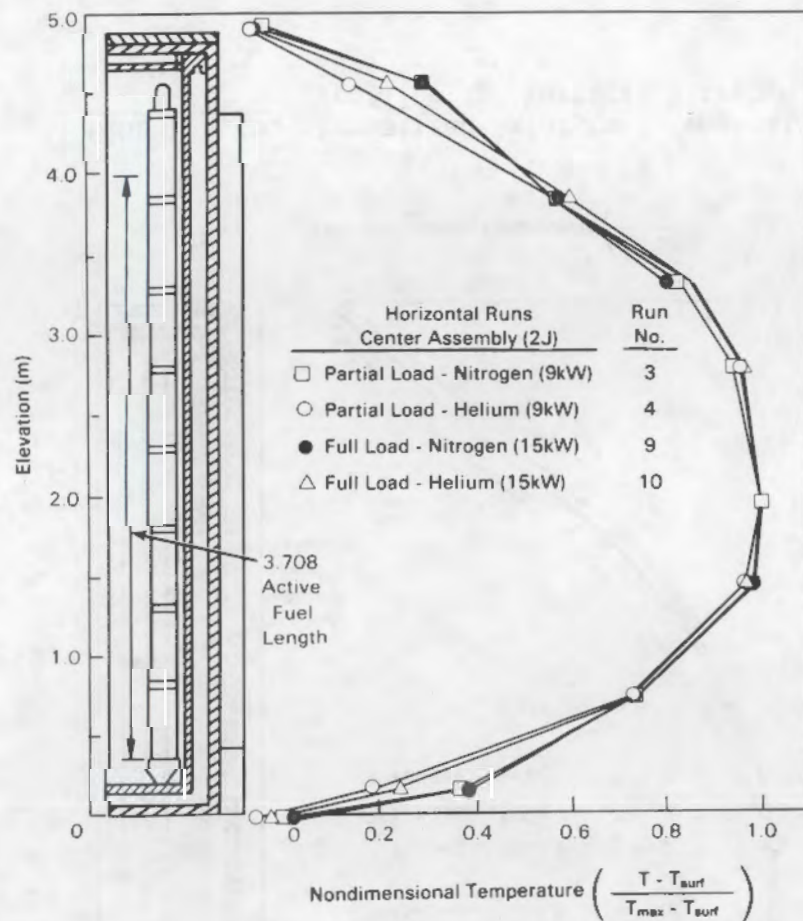


FIGURE 5.28. Normalized Axial Fuel Temperature Profiles for Horizontal Nitrogen and Helium Runs

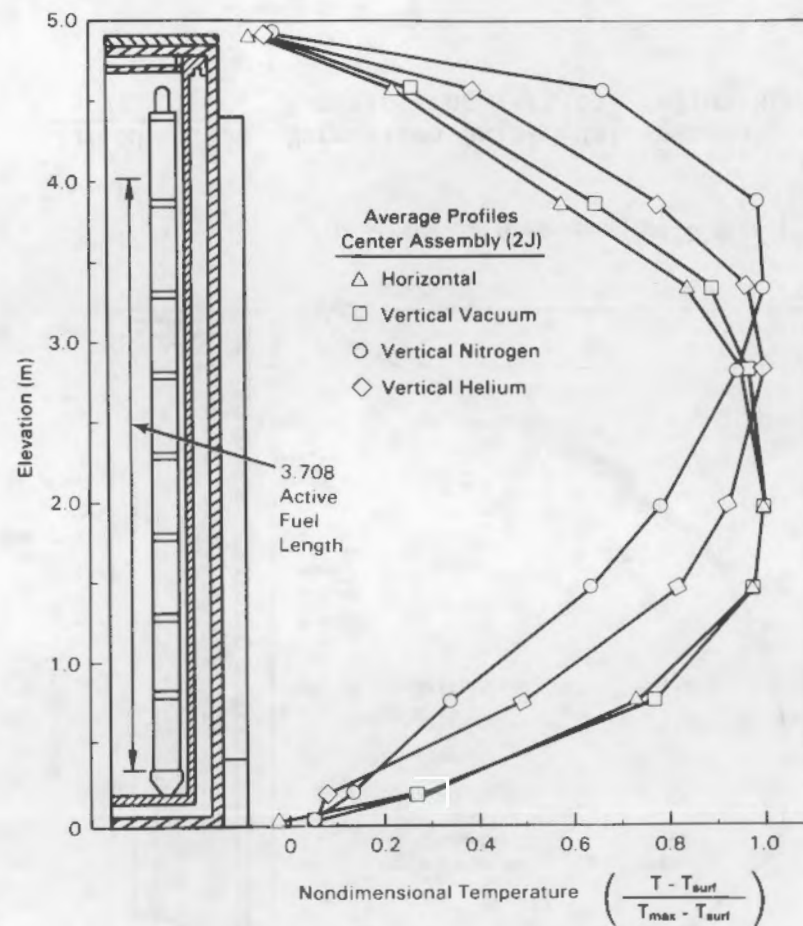


FIGURE 5.29. Normalized Axial Fuel Temperature Profiles for Showing Effects of Fill Gas and Cask Orientation



The averaged radial profiles for the three gases are shown in Figures 5.30 and 5.31, representing the normalized averages for the partial and full load, respectively. Both figures show that the higher thermal conductivity of helium resulted in lower fuel-to-basket temperature differences when compared to the other backfills. Both figures also show an almost linear decrease in the fuel temperature with radius for the vacuum runs. The nitrogen runs show a greater decrease in temperature between the outer and middle assembly than between the center and middle assembly for both loadings. Comparisons of the figures show that the fuel-to-basket temperature differences for the partial loads were greater than for the full loads. A comparison also shows a more rapid decrease in temperatures with radius for the partial load than for the full load.

Part of the differences between the full load and the partial load may be the result of the load pattern. In the partial load there are empty fuel tubes in the outer portions of the basket. These open fuel tubes affect the convective flow patterns in the basket. The lack of fuel in these fuel tubes also decreases the total heat load that must be transferred. The interplay among flow patterns, heat loads, and absolute temperatures in the cask determines the dominant and secondary modes of heat transfer in the cask that cause the temperature profiles seen in Figures 5.30 and 5.31. The radial data collected during the performance test is too limited to determine the cause and effect relationships for the radial data beyond what has been discussed.

In summary, the effects of fill gas on the thermal performance of the cask were apparent. The increased convection in a vertical cask filled with nitrogen shifted the peak cladding temperature near the top of the cask. The location of peak cladding temperatures for the vertical helium runs fell about midway between the peaks observed for vertical nitrogen and vertical vacuum. The vertical vacuum runs and the horizontal runs peak cladding temperatures occur at an axial location corresponding to the peak in the axial decay heat profile, which indicates an absence of convection for these runs.

#### 5.1.2.7 Insulated Runs

The original test plan called for 11 test runs to be conducted in the hottest part of the summer. The 11 runs discussed up to this point were conducted outside with ambient temperatures ranging from  $-16^{\circ}\text{C}$  to  $+14^{\circ}\text{C}$ . These

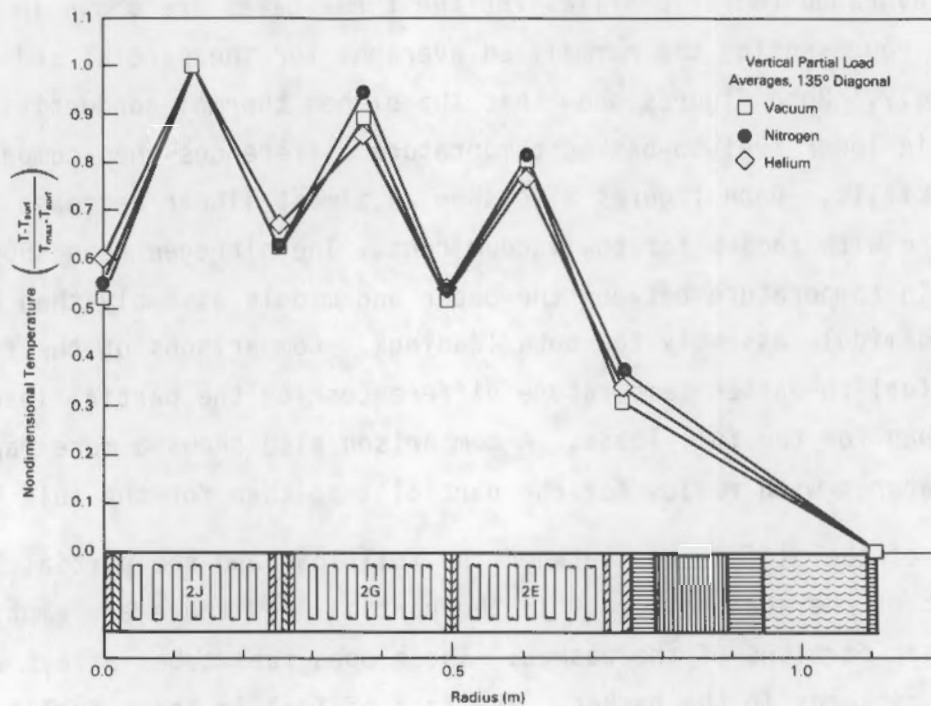


FIGURE 5.30. Partial Load, Normalized Radial Fuel Temperature Profiles Showing Effects of Fill Gas and Cask Orientation

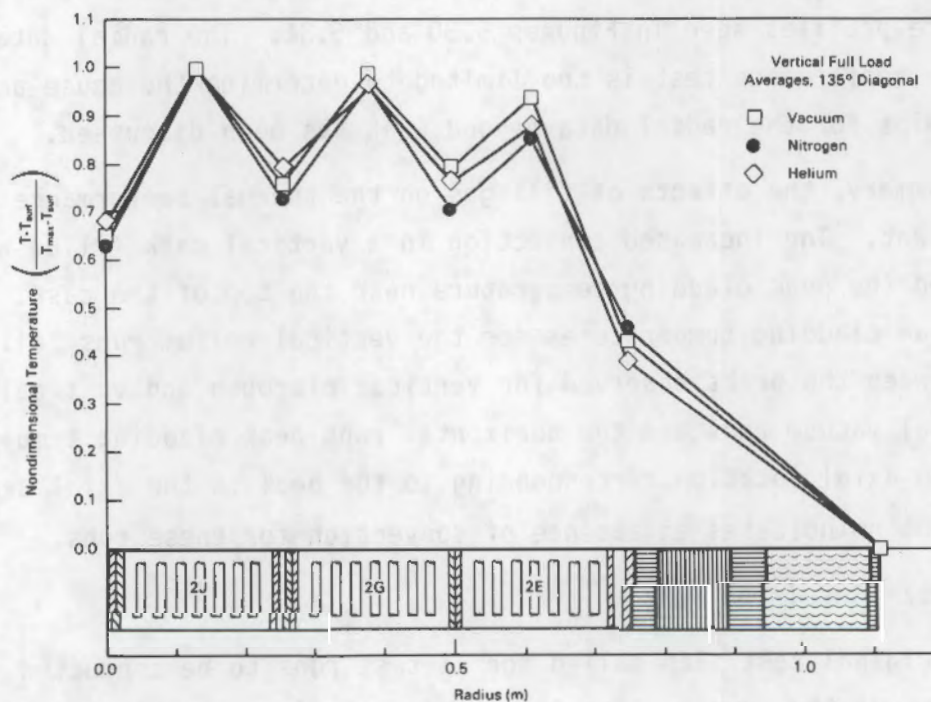


FIGURE 5.31. Full Load, Normalized Radial Fuel Temperature Profiles Showing Effects of Fill Gas and Cask Orientation



runs were augmented with a few duplicate runs conducted inside the CRA or cask service facility with ambient temperatures near 22°C and no wind. None of these runs produced cask surface temperatures typical of those anticipated in the summer. To get higher temperatures, three insulated runs were added to the test matrix near the conclusion of the testing. In these runs, the neutron shield was wrapped with about 5 mm (0.25 in.) of insulating paper. The remainder of the cask was as it was in the uninsulated runs; i.e., the area above the neutron shield including the lid was not insulated, and the bottom of the cask sat on the rail car like it did in the uninsulated runs. This resulted in peak neutron shield surface temperatures of about 110°C. This is about 60°C hotter than any of the previous runs.

The insulated runs were performed for the vertical orientation only, but with all three backfills. The results are plotted in Figure 5.32. These axial profiles show the same trends that were shown in Figure 5.29. The vacuum run had the highest peak temperature, 241°C, with the peak temperature occurring in the lower part of the cask. The peak temperature with nitrogen was 30°C lower than with vacuum, and occurred in the upper portion of the cask. The peak temperature in helium was lower than in either vacuum or nitrogen, and its location was between that observed for the nitrogen and vacuum runs.

The ambient temperature for the insulated runs was between 20 and 24°C. Figure 5.32 shows that the surface temperature of the lid and the upper portion of the cask was between 60 and 80°C. Hence, the temperature drop from the exposed cask surface to the ambient was greater than 40°C. This is twice the temperature drop found in the uninsulated runs, which indicates that a greater portion of heat is being transferred out the ends of the cask in the insulated runs than in the noninsulated runs, as would be expected. Also, the increased radiation in the cask due to higher absolute temperatures causes the temperature drop between the fuel and the neutron shield to be less in the insulated runs than was observed in the noninsulated runs.

The radial temperature profiles and symmetry information were not significantly different from those obtained for the noninsulated runs.

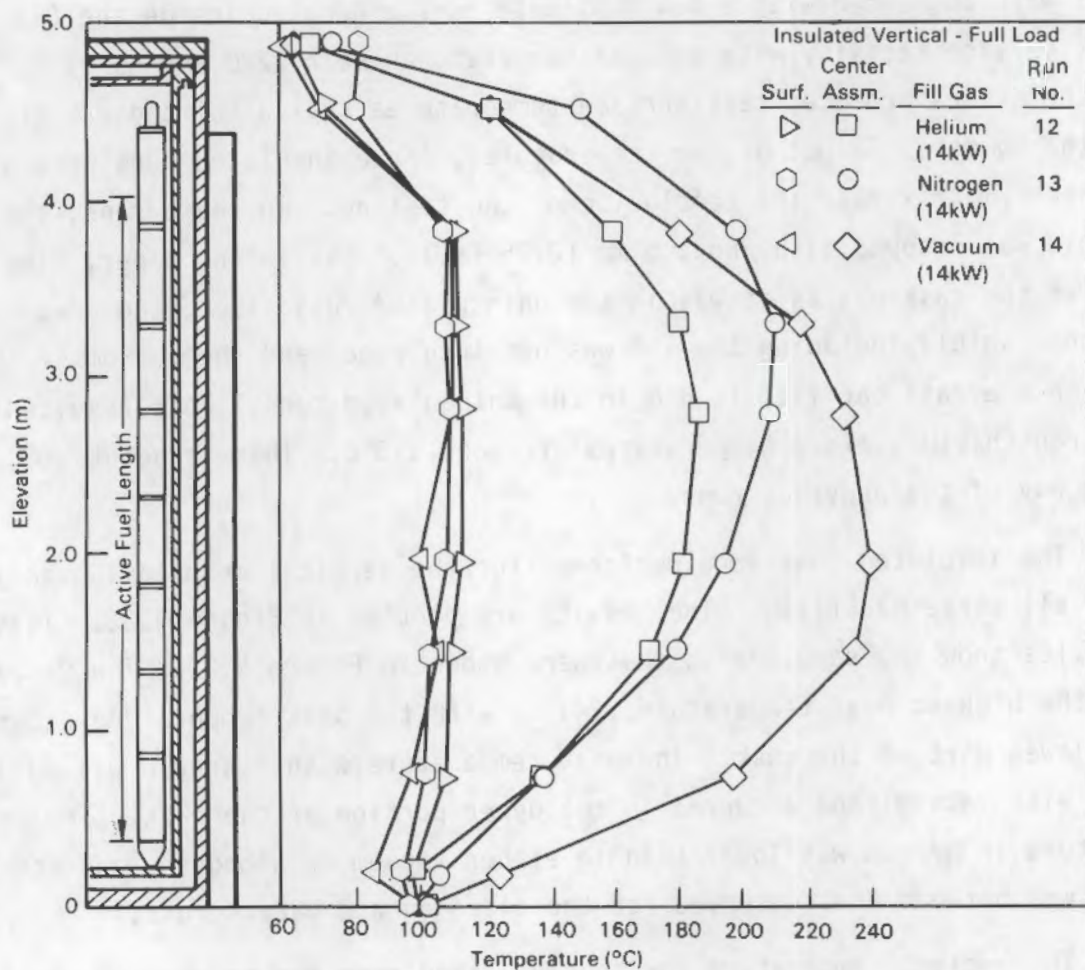


FIGURE 5.32. Axial Fuel and Surface Temperature Profiles for Insulated Vertical Runs

In summary, the temperature profiles in the insulated runs were quite similar to the temperature profiles observed for the noninsulated runs. Differences between the insulated and noninsulated runs reflect a greater amount of heat being transferred out the ends of the cask and increased radiation heat transfer for the insulated runs.

#### 5.1.2.8 Surface Temperatures

This section will present circumferential temperature profiles taken at three elevations on the surface of the cask. The axial surface temperature profiles were presented in the preceding sections of this report and will not be repeated here.



Figure 5.33 shows circumferential temperature profiles on the surface of the cask. Two of the profiles represent surface temperatures on the outer surface of the neutron shield, one for the horizontal orientation and the other for the vertical orientation. The remaining curve represents surface temperatures above the neutron shield. It is typical of the performance for both cask orientations. The horizontal circumferential profile of the neutron shield shows a significant decrease in temperature at 0 and 180 degrees. The low temperature at 0 degrees may be caused by convective currents in the liquid neutron shield or by an air bubble in the top of the neutron shield. The low temperature at 180 degrees is probably caused by convective currents in the liquid neutron shield. The low temperatures at 0 and 180 degrees do not appear in the vertical runs.

Standard deviations for differences between data from individual runs and representative average curves shown in Figure 5.33 were generally better than

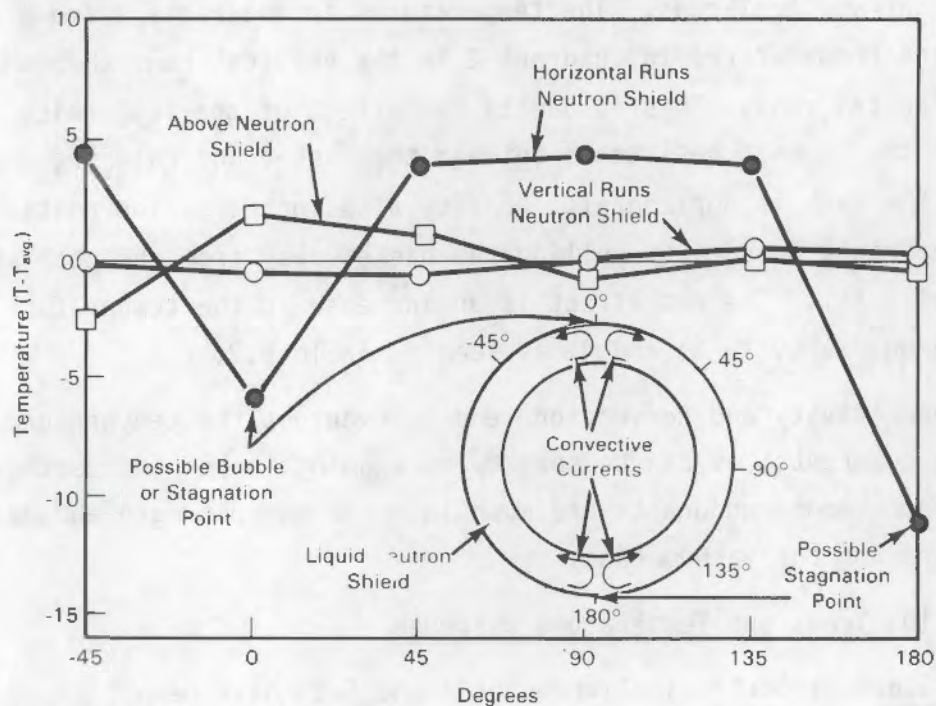


FIGURE 5.33. Circumferential Cask Surface Temperature Profiles



2°C, with the maximum deviation of any data point from the average curve being less than 6°C. Deviations of data from average curves are caused by a combination of wind, sun, and quality of TC attachment.

#### 5.1.2.9 Summary of Temperature Symmetry

Symmetry of the temperatures in the cask has been discussed in conjunction with Figures 5.11, 5.17, 5.18, 5.24, and 5.25. The information contained in those figures is summarized in Table 5.2. The average value shown in Table 5.2 was obtained by taking the difference between symmetric locations in the cask and then averaging these differences for all runs and elevations (two elevations) for which data was available. The standard deviation gives an indication of the spread in the data. Table 5.2 shows that there is good surface temperature symmetry for the vertical and horizontal runs. The average difference between temperatures at 0 and 180 degrees is about  $\pm 1^\circ\text{C}$ . The symmetry data for the internal temperatures shows a marked difference between the horizontal and the vertical runs. The temperatures in quadrants 1 and 4 are much closer to the temperatures in quadrant 2 in the vertical runs than they are in the horizontal runs. This is due to the effect of gravity, which causes a decrease in the contact resistance between the basket and cask for quadrants 2 and 3 when the cask is horizontal. Gravity also increases the contact resistance in quadrants 1 and 4 by pulling the basket away from the cask when the cask is horizontal. The net effect is an increase in the temperature differences among quadrants 1, 2, and 4, as seen in Table 5.2.

Gas conductivity and convection tend to even out the temperature differences among quadrants, as can be seen by an examination of the vertical runs. The differences among quadrants are much less for the nitrogen and helium runs than they are for the vacuum runs.

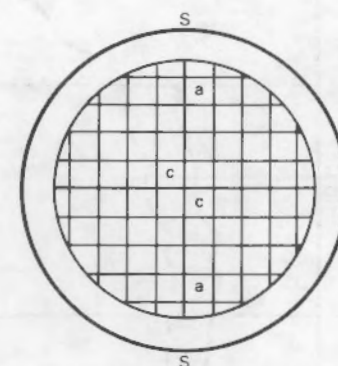
#### 5.1.2.10 Transient Temperature Response

Temperature histories in Figures 5.34 and 5.35 have been included to show the transient response of the cask. The duration of each run condition is not included in its entirety; only that portion showing the majority of the temperature transient is presented. Consequently, the time scale should not be used to determine elapsed time from the start of testing. The breaks in the curves



TABLE 5.2. Symmetry of Temperature Measurements

Run Condition	Surface Temp Difference, °C <sup>(a)</sup>		Outer Fuel Temp Difference, °C <sup>(b)</sup>		Inner Fuel Temp Difference, °C <sup>(c)</sup>	
	Average	Standard Deviation	Average	Standard Deviation	Average	Standard Deviation
Vacuum-Vertical	1	±2	10	±4	5	±2
Nitrogen						
Vertical	-1	±4	4	±4	1	±2
Horizontal	1	±6	29	±6	10	±3
Helium						
Vertical	0	±3	5	±2	1	±1
Horizontal	2	±6	17	±4	4	±2



- (a) Surface temperature differences were determined from measurements at 0 degrees minus measurements at 180 degrees (location 's').
- (b) Outer fuel temperature differences were determined from measurements in quadrant 1 minus those in quadrant 2 (location 'a').
- (c) Inner fuel temperature differences were determined from measurements in quadrant 4 minus those in quadrant 2 (location 'c').

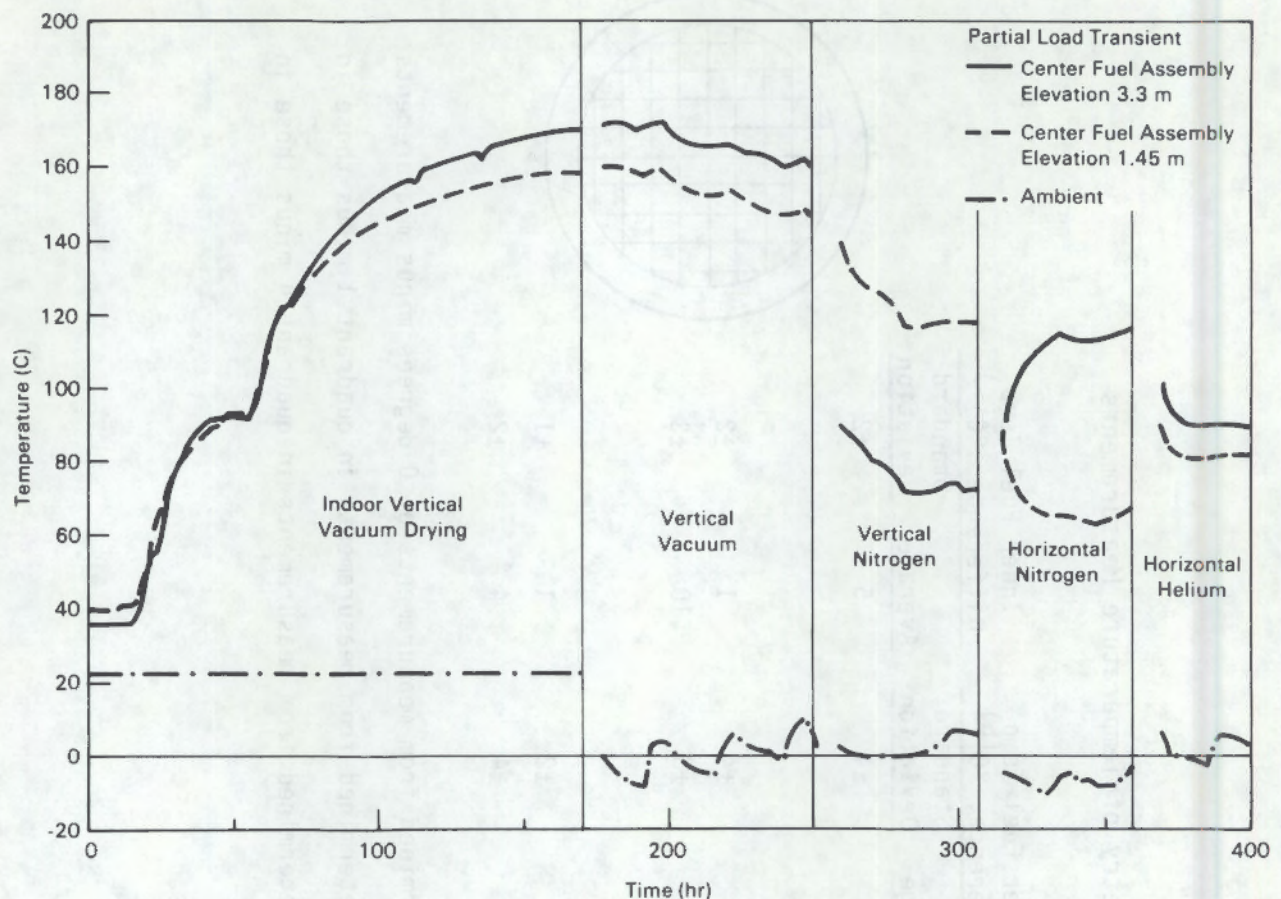


FIGURE 5.34. Partial Load Fuel and Ambient Temperature Transients

have been positioned near the point when steady state was achieved. The length of the gap (no curve) represents the time required to disconnect the data acquisition system (DAS), move the cask, change gases if required, return the cask to the test station, and reattach instrument leads to the DAS.

Figure 5.34 shows the response during the partial load, and Figure 5.35 shows the response during the full load. Three temperatures are shown: the ambient temperature and two temperatures taken at different elevations in a center fuel assembly. The elevations of these temperature measurements are indicated on the respective figures. The two internal temperature measurements allow an evaluation of how quickly the temperatures in the cask adjust to different orientations. Figures 5.34 and 5.35 show it takes about a week for the cask to come up to temperature, during the vacuum-drying process, and



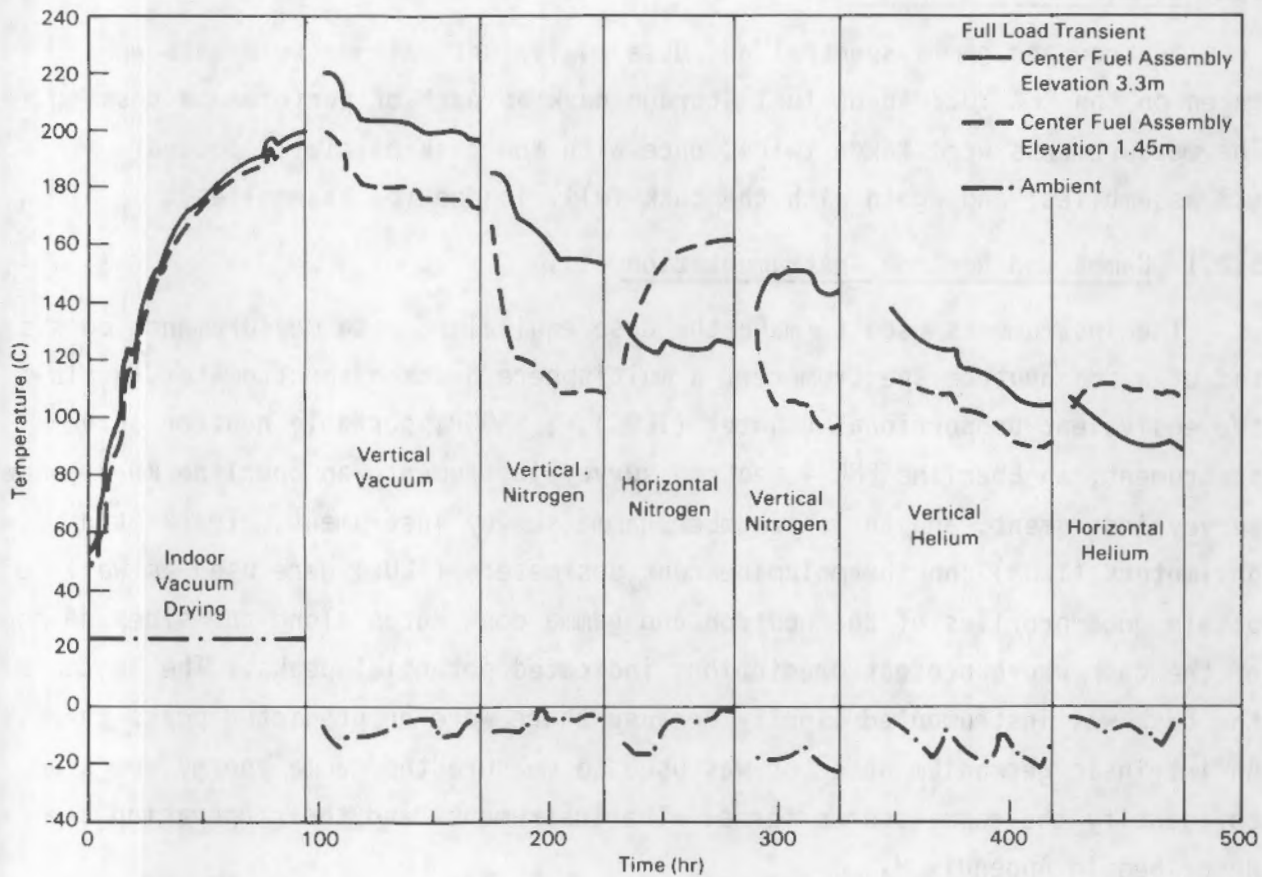


FIGURE 5.35. Full Load Fuel and Ambient Temperature Transients

then about 2 days to adjust to changes in cask orientation or fill gas. Both illustrations show a rapid adjustment of internal temperature profile in the cask when the cask is rotated from a vertical to a horizontal orientation. This is most apparent when the cask filled with nitrogen is rotated. Remember, the peak temperature is in the upper portion of the cask in a vertical nitrogen run and in the lower portion of the cask in a horizontal run. Thus, the elevation with the higher temperature after the cask has been rotated is reversed in Figures 5.34 and 5.35.



## 5.2 SHIELDING PERFORMANCE

Neutron and gamma spectral and dose equivalent rate measurements were taken on the REA 2023 spent fuel storage cask as part of performance testing. The measurements were taken twice, once with the cask partially loaded (28 assemblies) and again with the cask fully loaded (52 assemblies).

### 5.2.1 Gamma and Neutron Instrumentation

The instruments used to make the dose equivalent rate measurements consisted of a  $^3\text{He}$  neutron spectrometer, a multisphere neutron spectrometer, a tissue equivalent proportional counter (TEPC), a SNOOPY portable neutron survey instrument, an Eberline PNR-4 neutron survey instrument, an Eberline RO-3 gamma survey instrument, and an ion chamber gamma survey instrument. Track etch dosimeters (TEDs) and thermoluminescent dosimeters (TLDs) were used as well to obtain good profiles of the neutron and gamma dose rates along the side and top of the cask where pretest predictions indicated potential peaks. The bottom of the cask was instrumented lightly because there were no predicted peaks there. An intrinsic germanium detector was used to measure the gamma energy spectrum to identify the gamma source terms. The instruments and their operation are described in Appendix H.

### 5.2.2 Shielding Data

Both neutron and gamma radiation measurements were made at the surface of the cask. The radiation measurements were divided into two types: energy spectrum and radiation profile measurements. The radiation profile measurements were made with TLDs, TEDs, and hand-held instruments. These dosimeters/instruments were calibrated against standard sources whose energy spectra were different from the spectrum of the radiation leaving the cask. Because dose rates obtained with these dosimeters/instruments are dependent on the energy spectrum, spectrum measurements were made to determine the appropriate calibration factors. Had the spectrum measurements been less time- and cost-intensive, they could have been performed at each measurement location. However, due to time and cost considerations they were limited to four locations: the center of the lid, the center of the bottom, the side of the cask at a 90-degree angle and an elevation of 150 cm with respect to the bottom of the



cask, and the top of the neutron shield at a 90-degree angle. Radiation profiles obtained with the TLDs, TEDs, and hand-held instruments included those for the four spectrum locations plus several additional points along the side, top, and bottom of the cask.

#### 5.2.2.1 Energy Spectrum Measurements

The measured neutron dose rate data obtained from the spectrometers are presented in Tables 5.3 and 5.4 for the partial and full loads, respectively. Survey instrument measurements have also been included for comparison. The  $^3\text{He}$  spectrometer, TEPC, and the multisphere spectrometer (M/S) results are within 5% to 20% of each other, which is very good for measuring neutron dose equivalent rates. The PRM, SNOOPY, and PRN-4 survey instrument results are higher than the  $^3\text{He}$ , TEPC, and multisphere readings, which is typical because of the over-response to low-energy neutrons. The survey instruments are energy-dependent and were calibrated in a hard spectrum, which causes them to over-respond in a softer spectrum. Except for the side of the cask, the TED measurements are of about the same magnitude as the spectrometer results. On the side of the cask, the TED reading corresponds better with the reading from the pocket rem meter (PRM), an experimental instrument still in the developmental stage. The PRM seemed to perform adequately in most cases, but it seemed to give erroneous readings when it was left out in the cold for an extended period of time. Comparison of values in Tables 5.3 and 5.4 shows that the neutron dose is a little less for the full load than for the partial load. This is caused by self-shielding of the fuel and placement of colder fuel near the wall of the cask during the full load. There has also been some fuel decay between the two measurements.

A comparison of the gamma dose rate measurements can be made from the information contained in Table 5.5. An intrinsic germanium spectrometer was used to determine the gamma spectrum. The gamma spectrometer does not give a dose rate reading, but can identify major radionuclides present and does quantify the spectrum. The energy spectrum, along with individual energy response of an instrument, can then be used to correct dose rate measurements if required.

TABLE 5.3. Partial Load Reference Neutron Dose Rate Measurements

Location	He-3(a)	Dose Rate, mrem/hr				
		Spectrum-Based		Hand-Held		
		TEPC(b)	M/S(c)	PNL PRM(d)	SNOOPY	GE PRN-4(e)
Top of cask-CL						
at contact	17.0		17.3	16.4	20	35
at 1 meter			6.92	5.93	7.5	
Bottom of cask-CL						
at contact	39.0	41.8	34.3	49.0	50	55
at 1 meter		15.0	15.3	14.6	18	
Side of cask-90° (150 centimeters elevation)						
at contact	1.22	1.50	1.33	1.92	1.7	1.8
Top of neutron shield 90°						
at contact	8.14		11.8	12		

(a) Helium-3 neutron spectrometer.  
 (b) Tissue equivalent proportional counter.  
 (c) Multisphere neutron spectrometer.  
 (d) Pocket rem meter.  
 (e) Eberline PRN-4 used by GE.

Measurements were taken at the four locations identified previously, except that the reading at an elevation of 150 cm was taken on the backside of the cask (270 rather than 90 degrees). The major radionuclides identified were  $^{60}\text{Co}$  and  $^{144}\text{Ce/Pr}$  at the top and bottom of the cask and  $^{144}\text{Ce/Pr}$ ,  $^{154}\text{Eu}$ ,  $^{134}\text{Cs}$ ,  $^{137}\text{Cs}$ ,  $^{106}\text{Ru/Rh}$ , and  $^{60}\text{Co}$  at the side. The dominance of  $^{60}\text{Co}$  at the top and



TABLE 5.4. Full Load Reference Neutron Dose Rate Measurements

Location	He-3(a)	Dose Rate, rem/hr					
		Spectrum-Based		TED(d)	Hand-Held		
					PNL		GE
		TEPC(b)	M/S(c)		PRM(e)	SNOOPY	PRN-4(f)
Top of cask-CL							
at contact	13.7	13.1	12.2	12.6	16.9	19 (16)(g)	30
at 1 meter		4.33	5.2		6.65	6.5 (5.2)	
Bottom of cask-CL							
at contact	32.9	44.0	32.2	32.8	60.6	60 (47)	50
at 1 meter		11.8	11.2		19.8	18 (15)	
Side of cask-90° (el. = 150 cm)							
at contact	1.84	1.46	1.51	3.44	3.40	2.0 (1.5)	2.3
at 1 meter		0.87	0.97		2.30	1.4 (1.1)	
at top of neutron shield (contact)	11.3	8.9		9.3	17.8	13.5 (11)	

(a) Helium-3 neutron spectrometer.

(b) Tissue equivalent proportional counter.

(c) Multisphere neutron spectrometer.

(d) Track etch dosimeter.

(e) Pocket rem meter.

(f) Eberline PRN-4.

(g) The dose rate as converted from counts/second from a scaler attached to the SNOOPY using  $1.44 \times 10^{-4}$  mrem/count from  $^{252}\text{Cf}$  calibration run.

bottom is due to the activated stainless steel, which is heavily concentrated at the ends of the assemblies. The primary contributor at the side is  $^{144}\text{Ce/Pr}$ , a fission product present in spent fuel.

The gamma spectra did not vary between the partial loading and the full loading. Based on the measured energy spectrum, the TLD measurements do not require a calibration factor to correct for the difference between measured



TABLE 5.5. Reference Gamma Dose Rate Measurements (mR/hr)

Location	Partial Load			Full Load		
	TLD(a)	PNL Cutie Pie <sup>(b)</sup>	GE RO-3(c)	TLD(a)	PNL Cutie Pie <sup>(b)</sup>	GE RO-3(c)
Top of cask-CL	26.8 ± 0.8	28	30	28.6 ± 1.3	33	28
Bottom of cask-CL	68.6 ± 2	75	76	69.7 ± 1.4	62	66
Side of cask-90° (el. = 150 cm)	8.5 ± 0.1	8.4	10	13.6 ± 1.0	15	11

(a) Thermoluminescent dosimeter.

(b) Eberline RO-3B used by Pacific Northwest Laboratory.

(c) Eberline RO-3 used by General Electric.

and dosimeter/instrument calibration energy spectrum. It should also be noted that measurements made with the survey instruments are quite close to the TLD-measured values.

#### 5.2.2.2 Radiation Profile Measurements

Thermoluminescent dosimeters and TEDs were used to obtain gamma and neutron dose rate profiles at the cask surface. The measurements give a relative indication of gamma and neutron dose rates and agree favorably with those obtained with the spectral instruments at the top center and bottom center of the cask and at the top of the neutron shield. The profiles obtained are shown in Figures 5.36 through 5.39. Each figure shows partial and full load gamma profiles and full load neutron profile. Track etch dosimeters were not used during the partial load radiation measurements; thus, except for a few survey measurements, partial load neutron dose rates were not obtained.

Figure 5.36 shows axial profiles along the side of the cask. The full load profile was taken at an angle of 26.5 degrees and the part load profile was taken at 45 degrees. Spikes in the radiation profiles at both ends of the neutron shield are shown. The gamma profiles show another, more pronounced, peak corresponding to the end of the lead shielding at the top of the cask. The peak dose rate on the side was 42 mrem/hr, with the average dose being 18 mrem/hr for a full load.



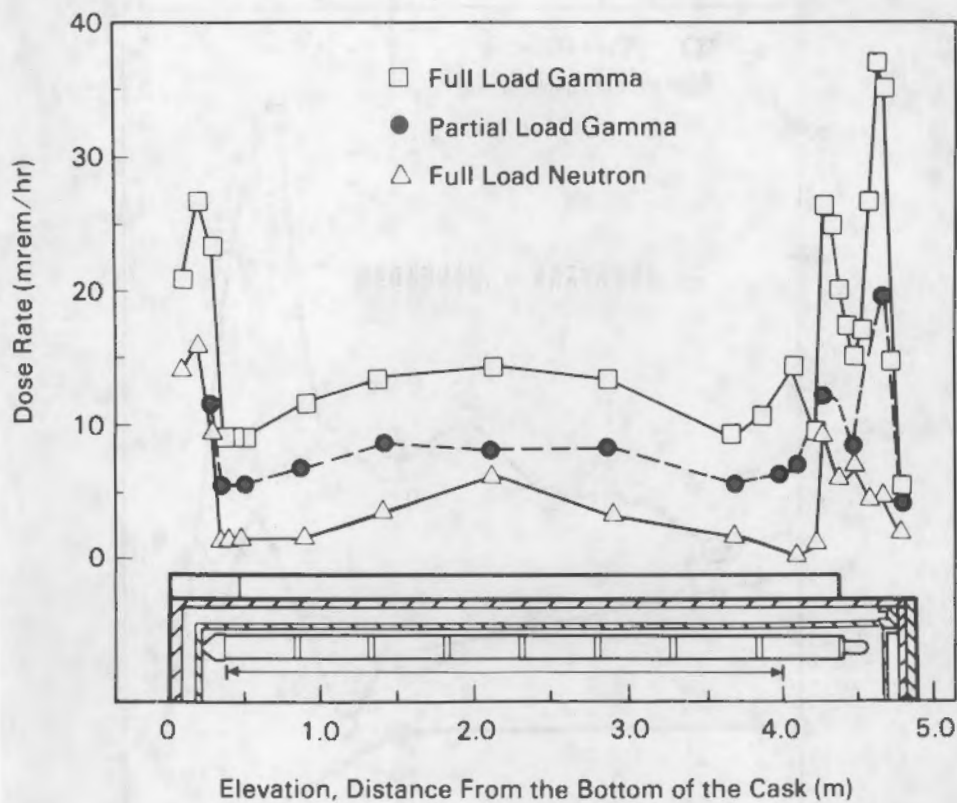
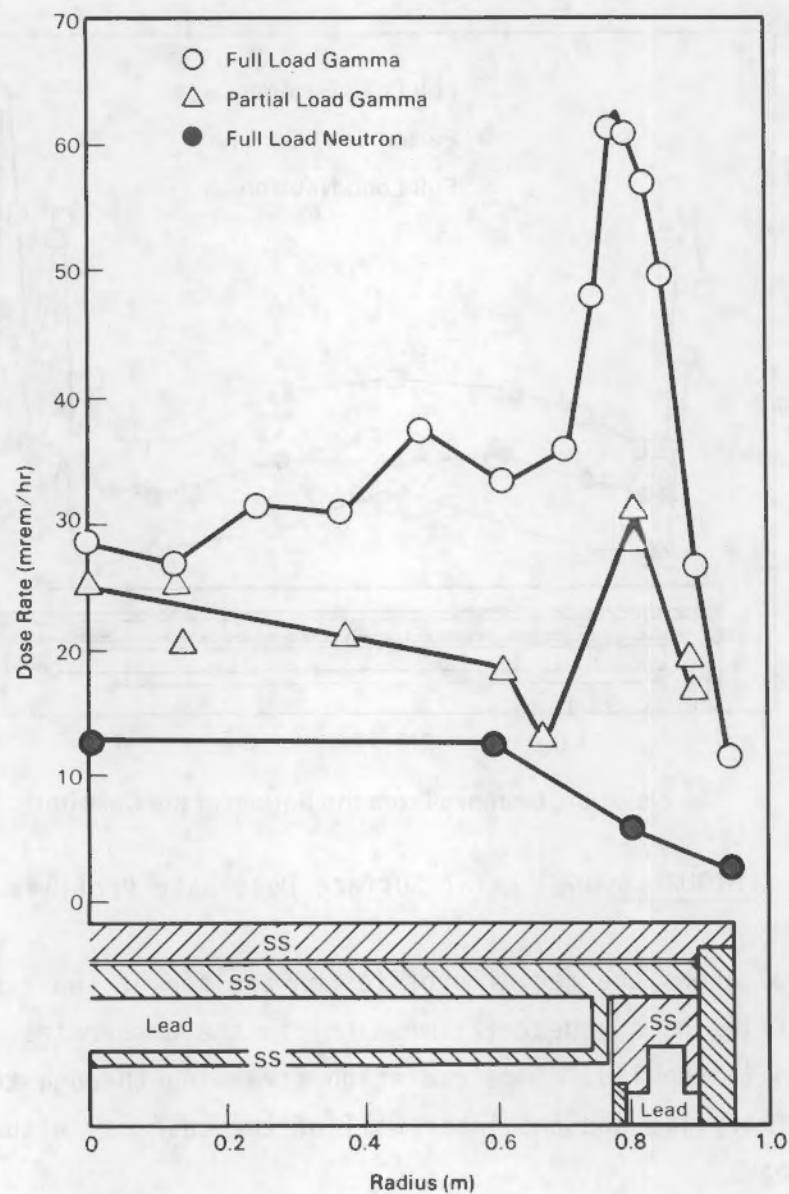


FIGURE 5.36. Axial Surface Dose Rate Profiles

Figure 5.37 shows the radial profiles on the top of the cask. The full load gamma profile shows a peak (71 mrem/hr) in the dose rates in the vicinity of the lead gap in the lid. Some radiation streaming through the small gap between the primary lid and the inner wall of the cask may also contribute to the observed peak.

Figure 5.38 shows the radial profile along the bottom of the cask taken on a 45-degree diagonal. It has a full load peak dose rate of about 100 mrem/hr located in the center of the bottom. The profile does not include an anomaly that was observed. The anomaly in the radiation shield was located in an area near 270 degrees and a radius of 0.5 m. It had a full load radiation dose rate measured with hand-held instruments of 145 mrem/hr gamma and 50 mrem/hr neutron. This was the maximum dose observed at any location on the cask.



**FIGURE 5.37.** Surface Dose Rate Profiles on Cask Lid

Figure 5.39 shows a circumferential profile at the surface of the neutron shield at an elevation of 223 cm. This profile shows that the peak dose occurs around 26.5 degrees for the full load. There is an observed change in the relationship between the dose rate at 26.5 degrees compared to the dose rate measurements at 0 and 45 degrees between the partial and full load. The



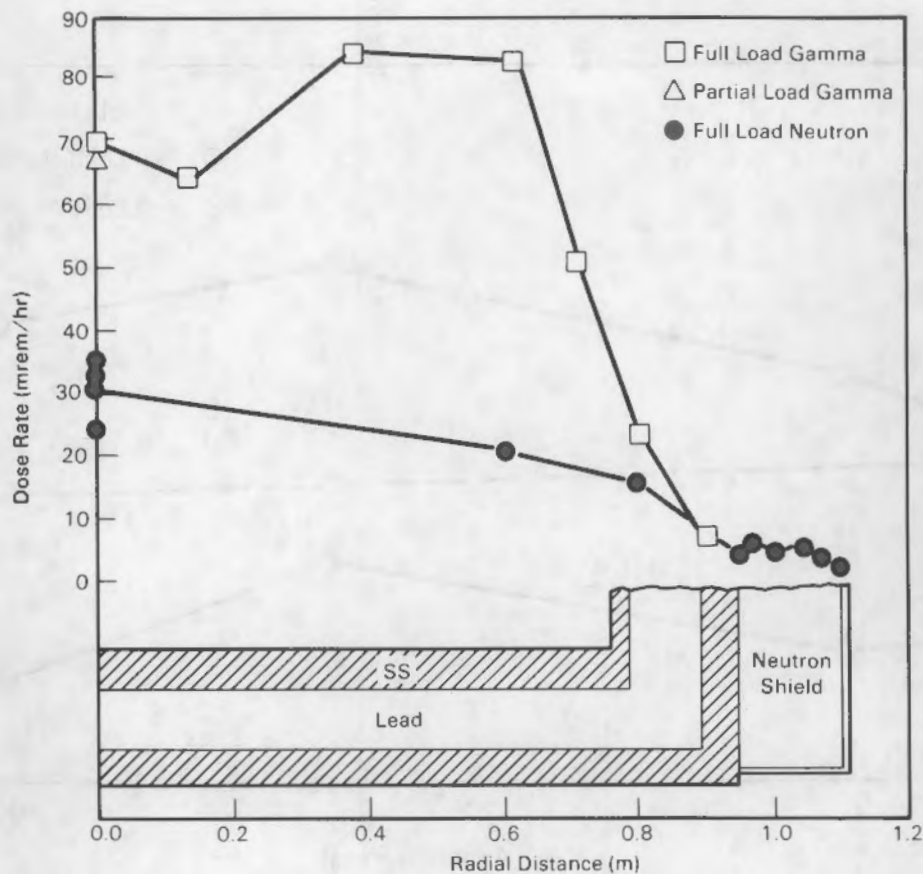


FIGURE 5.38. Surface Dose Rate Profiles on Cask Bottom

increase in the dose rate at 26.5 degrees for the full load was caused by the addition of a fuel assembly in this vicinity during full loading (see the fuel loading pattern in Section 3).

Portable hand-held instruments were also used by PNL and GE-MO to survey the surface of the cask. The results of these measurements for the side of the cask are shown in Figures 5.40 through 5.42. The PNL survey measurements were performed primarily to show a correspondence between measurements conducted with a Cutie Pie and SNOOPY and the more precise TLD and TED measurements that have already been presented. The measurements were taken at only a limited number of points as shown in Figure 5.40. In general, the gamma measurements made with the Cutie Pie are about the same as those made with TLDs. The neutron measurements made with the SNOOPY are about twice those made with the TEDs.

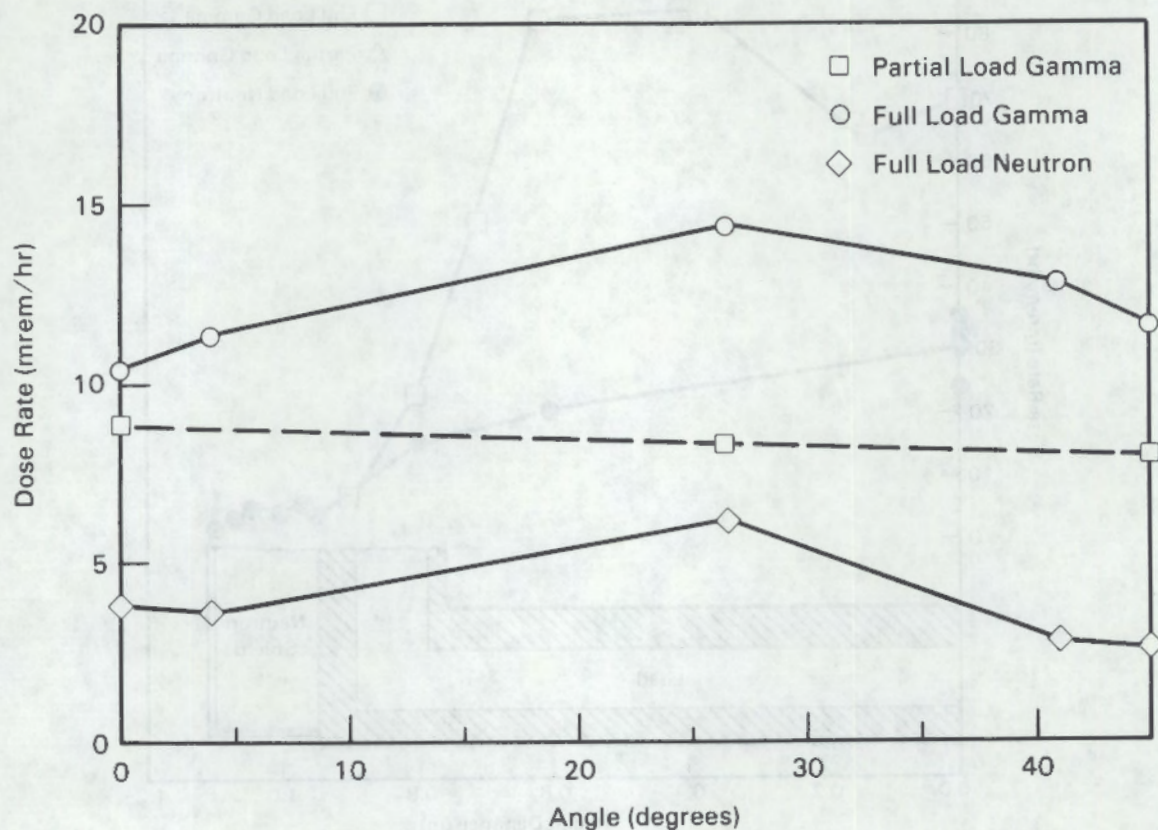


FIGURE 5.39. Circumferential Surface Dose Rate Profiles at 2.23-m Elevation

The GE-MO staff conducted a reasonably detailed survey of the cask, because they needed the information to limit personnel exposure and to ensure compliance with licensing requirements. For the GE-MO survey the cask surface was subdivided into a grid consisting of nine elevations and eight circumferential sectors (45 degrees apart) along the side and with two radii and eight sectors on the top and bottom. The surveys were done for both the partial and the full loads. The difference between the partial and full load radiation readings from the GE-MO survey is not as large as was observed from the TLD data and PNL survey. Due to the quantity of data collected by GE-MO and the similarity between the various measurements, only selected profiles for the full load measurements will be presented here. The rest of the data is contained in Appendix H.



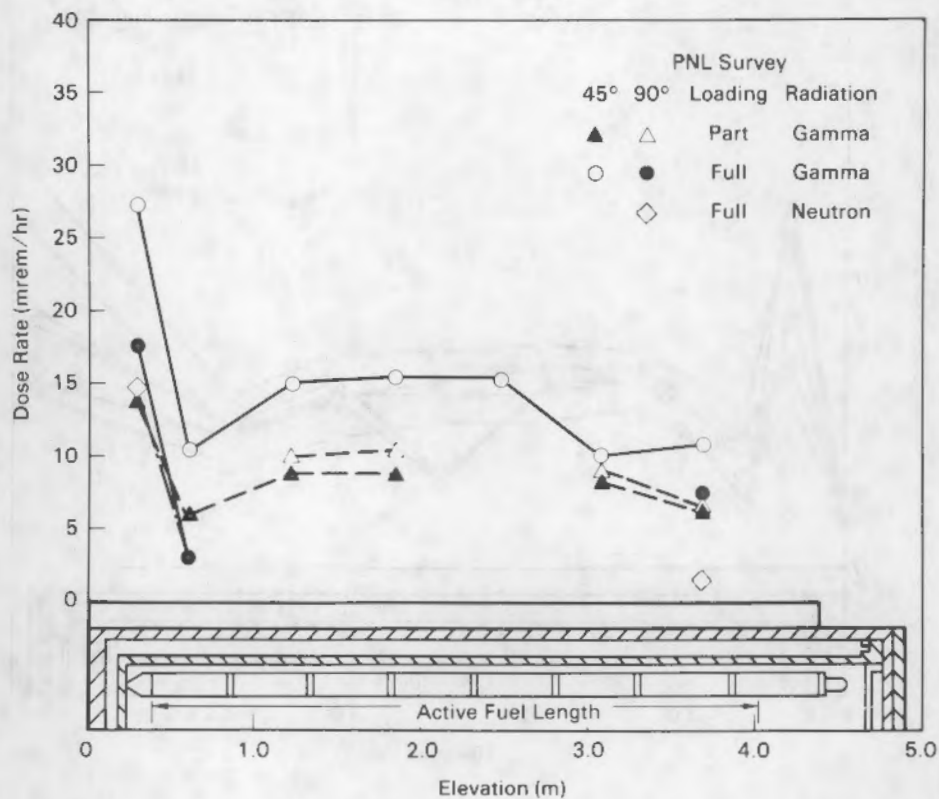


FIGURE 5.40. PNL Survey Instrument Axial Radiation Profile on Side of Cask

The GE-MO gamma surveys were performed with an Eberline R0-3 and are shown in Figure 5.41. These results compare quite favorably with those obtained with the TLDs along the side of the cask. If corrected for angular dependence as was shown in Figure 5.39, they become conservatively high by about 30%. There is an interesting dip at an elevation of 2.5 m in the 90- and 270-degree profiles. This dip is caused by the trunnions. A corresponding increase in the neutron dose is seen in this same location (Figure 5.42). This phenomenon is caused by the trunnions, which increase the amount of stainless steel in this location, thereby decreasing the gamma dose rate. The stainless steel displaces some of the neutron shield, which increases the neutron dose. The large scatter in the gamma dose measurements at the upper end is probably due to positioning errors in the measurements. It should be remembered that the primary purpose of these measurements was to control personnel exposure, not to show the performance of the cask.

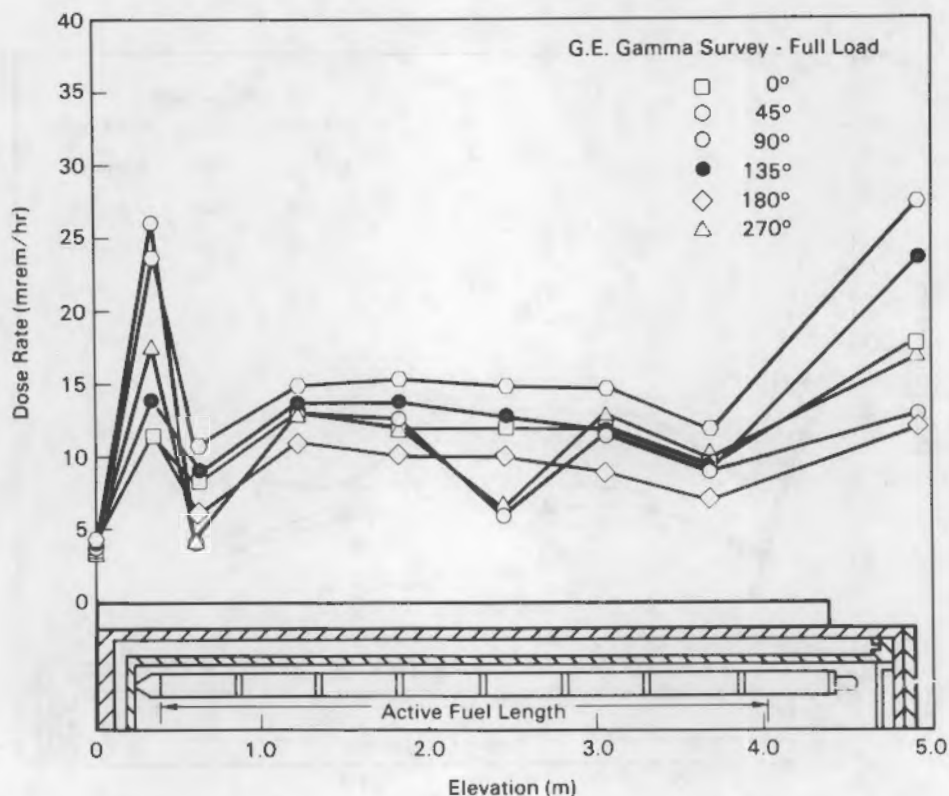


FIGURE 5.41. Full Load GE-MO Survey Instrument Axial Gamma Radiation Profile on Side of Cask

The GE-MO neutron survey measurements are shown in Figure 5.42. They were performed with an Eberline PNR-4 and show about twice the magnitude of the measurements made with the TEDs. At the upper end of the cask the measured peak is more than twice the value measured with the TEDs. This could be caused by positioning of the instrument with respect to the cask (Cosack 1981).

The GE-MO surveys on the top and bottom of the cask showed good agreement between the TLD and gamma survey measurement results. However, for the neutron measurements, the survey measurement results were about twice those obtained with the TEDs and spectrum instruments.

Additional radiation data is contained in Appendix H. Data in Figures 5.36 through 5.42 is included.

In summary, the average surface dose rate on the primary lid of the cask was ~50 mrem/hr (40 mrem/hr gamma and 10 mrem/hr neutron) with a peak of



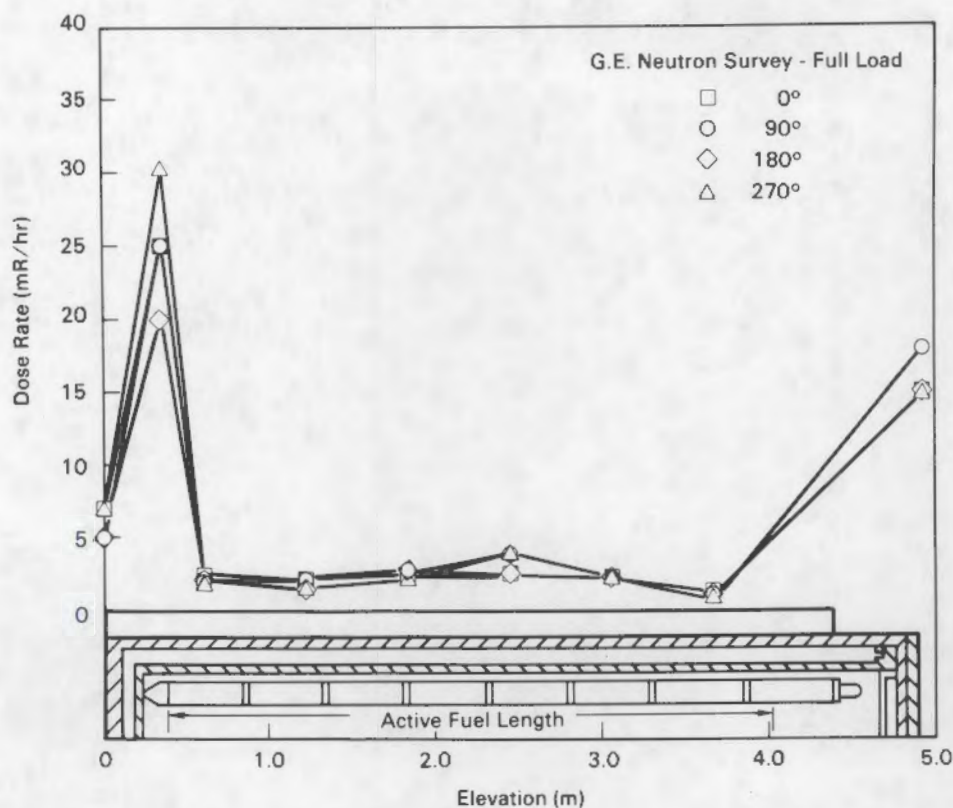


**FIGURE 5.42.** Full Load GE-MO Survey Instrument Axial Neutron Radiation Profile on Side of Cask

~80 mrem/hr (70 mrem/hr gamma and 10 mrem/hr neutron) in the vicinity of the parting plane of the lid. The average surface dose rate on the side of the cask was ~20 mrem/hr (15 mrem/hr gamma and 5 mrem/hr neutron) with peaks of ~40 mrem/hr (35 mrem/hr gamma and 5 mrem/hr neutron) near the ends where the neutron and/or gamma shield ended. The dose rate profile on the bottom of the cask was quite flat, with an average value of ~110 mrem/hr (85 gamma, 25 neutron). There appears to be an anomaly in the gamma shield in a very localized area, which was also identified during post-fabrication quality assurance verification activities. With minor shielding modifications, total surface dose rates of <50 mrem/hr can be attained.

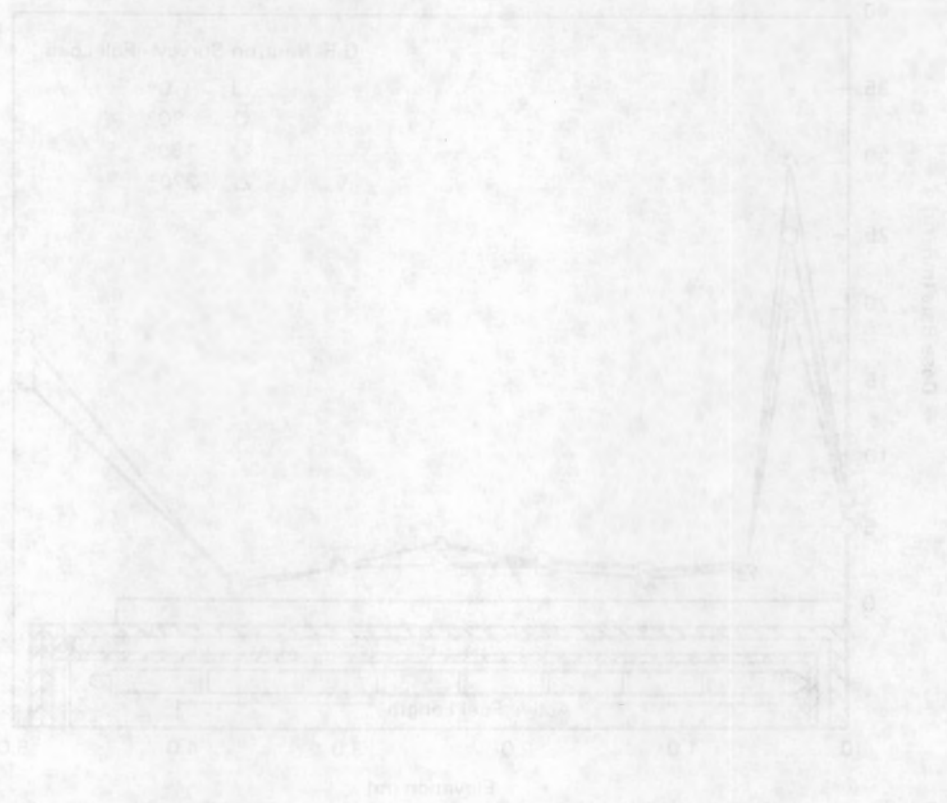


FIGURE 2-45. Radiation profiles on side of tank.

The radiation profiles on the side of the tank were measured at two elevations, 1.5 m and 0.5 m. The average surface dose rate on the side of the tank was 4.50 mrem/hr (1.5 mrem/hr) and 3.50 mrem/hr (1.5 mrem/hr) near the end where the radiation level was highest. The dose rate profile on the bottom of the tank was also measured, with an average value of 4.10 mrem/hr (1.5 mrem/hr). There appears to be no anomaly in the gamma shield in a very localized area, which was also identified during past radiation quality assurance work. The radiation level is 1.5 mrem/hr (0.5 mrem/hr) on the side of the tank.



## REFERENCES

- Cosack, M., and H. Lesiecke. 1981. "Dependence of the Response of Eight Neutron Dose Equivalent Survey Meters with Regard to the Energy Direction of Incident Neutrons." Presented to the Fourth Symposium on Neutron Dosimetry, June 1-5, 1981, Neuherberg, Germany.
- Einzig, R. E., et al. 1982. "High Temperature Postirradiation Materials Performance of Spent Pressurized Water Reactor Fuel Rods Under Dry Storage Conditions." Nuclear Technology. 57:65-80.
- Johnson, A. B., Jr., and E. R. Gilbert. 1983. Technical Basis for Storage of Zircaloy-Clad Spent Fuel in Inert Gases. PNL-4835, Pacific Northwest Laboratory, Richland, Washington.
- Judson, B. F., H. R. Strickler, J. W. Doman, K. J. Egger and Y. J. Lee. 1982. In-Plant Test Measurements for Spent Fuel Storage at Morris Operation: Volume III - Fuel Bundle Heat Generation Rates. NEDG-24922-3, General Electric, San Jose, California.
- McKinnon, M. A., J. W. Doman, C. M. Heeb and J. M. Creer. 1985. Decay Heat Measurements and Predictions of BWR Spent Fuel. NP-4269, Electric Power Research Institute, Palo Alto, California.
- Halbig, J. K., and J. C. Caine. 1985. ION-1 Technical Manual. LA-10433-M, Los Alamos National Laboratory, Los Alamos, New Mexico.
- Ridihalgh, Eggers & Associates (REA). 1983. Topical Report for the REA 2023 Dry Storage Cask for BWR Fuel. Docket No. M-33, U.S. Nuclear Regulatory Commission, Washington, D.C.
- Wiles, L. E., N. J. Lombardo, C. M. Heeb, U. P. Jenquin, J. M. Creer, C. L. Wheeler and R. A. McCann. 1986. BWR Spent Fuel Storage Cask Performance Test: Volume II - Pre- and Post-Test Decay Heat, Heat Transfer, and Shielding Analyses. PNL-5777 Vol. II, Pacific Northwest Laboratory, Richland, Washington.

1. Chen, K. H. and H. H. Hsu. 1987. "Dependence of the Response of Cyclic  
 Torsionally Reinforced Concrete Beams with Rectangular Cross-Section  
 to Torsion." *Journal of Bridge Engineering*, Vol. 2, No. 1, pp. 1-12.  
 2. Chen, K. H. and H. H. Hsu. 1987. "Dependence of the Response of Cyclic  
 Torsionally Reinforced Concrete Beams with Rectangular Cross-Section  
 to Torsion." *Journal of Bridge Engineering*, Vol. 2, No. 1, pp. 1-12.  
 3. Chen, K. H. and H. H. Hsu. 1987. "Dependence of the Response of Cyclic  
 Torsionally Reinforced Concrete Beams with Rectangular Cross-Section  
 to Torsion." *Journal of Bridge Engineering*, Vol. 2, No. 1, pp. 1-12.  
 4. Chen, K. H. and H. H. Hsu. 1987. "Dependence of the Response of Cyclic  
 Torsionally Reinforced Concrete Beams with Rectangular Cross-Section  
 to Torsion." *Journal of Bridge Engineering*, Vol. 2, No. 1, pp. 1-12.  
 5. Chen, K. H. and H. H. Hsu. 1987. "Dependence of the Response of Cyclic  
 Torsionally Reinforced Concrete Beams with Rectangular Cross-Section  
 to Torsion." *Journal of Bridge Engineering*, Vol. 2, No. 1, pp. 1-12.  
 6. Chen, K. H. and H. H. Hsu. 1987. "Dependence of the Response of Cyclic  
 Torsionally Reinforced Concrete Beams with Rectangular Cross-Section  
 to Torsion." *Journal of Bridge Engineering*, Vol. 2, No. 1, pp. 1-12.  
 7. Chen, K. H. and H. H. Hsu. 1987. "Dependence of the Response of Cyclic  
 Torsionally Reinforced Concrete Beams with Rectangular Cross-Section  
 to Torsion." *Journal of Bridge Engineering*, Vol. 2, No. 1, pp. 1-12.  
 8. Chen, K. H. and H. H. Hsu. 1987. "Dependence of the Response of Cyclic  
 Torsionally Reinforced Concrete Beams with Rectangular Cross-Section  
 to Torsion." *Journal of Bridge Engineering*, Vol. 2, No. 1, pp. 1-12.  
 9. Chen, K. H. and H. H. Hsu. 1987. "Dependence of the Response of Cyclic  
 Torsionally Reinforced Concrete Beams with Rectangular Cross-Section  
 to Torsion." *Journal of Bridge Engineering*, Vol. 2, No. 1, pp. 1-12.  
 10. Chen, K. H. and H. H. Hsu. 1987. "Dependence of the Response of Cyclic  
 Torsionally Reinforced Concrete Beams with Rectangular Cross-Section  
 to Torsion." *Journal of Bridge Engineering*, Vol. 2, No. 1, pp. 1-12.



APPENDIX A

INSTRUMENTATION AND DATA ACQUISITION SYSTEM

## APPENDIX A

### INSTRUMENTATION AND DATA ACQUISITION SYSTEM

This appendix describes the data acquisition system used in conjunction with the cask tests. The thermocouple attachment devices used inside the cask and on its external surface, as well as the pressure transmitters used to monitor cask internal pressure, are described. The weather station used to monitor the ambient conditions when the cask was located at its outside test station is also discussed.

#### DATA ACQUISITION SYSTEM

The data acquisition system for the REA cask consists of four major pieces of equipment:

- Kaye Digistrip III datalogger
- Kaye RAMP/Scanner
- Columbia 300D data cassette recorder
- miscellaneous connectors and connecting cables for remote data acquisition.

A schematic layout of the data acquisition system is shown in Figure A.1.

The data acquisition system was designed primarily around the Kaye Instruments Digistrip III, which was an in-house piece of equipment at GE-MO. The Digistrip has the capability to transmit data to an external device such as a computer or data cassette recorder. A Columbia 300D data cassette recorder was used in conjunction with the Digistrip III to produce magnetic tape as well as hard copy output for each test. A separate tape was used for each run in the test program.

The Digistrip was configured to accept 16 direct analog inputs and 64 inputs from a remote multiplexing unit known as a RAMP/Scanner (also manufactured by Kaye Instruments). Because most of the inputs to the data



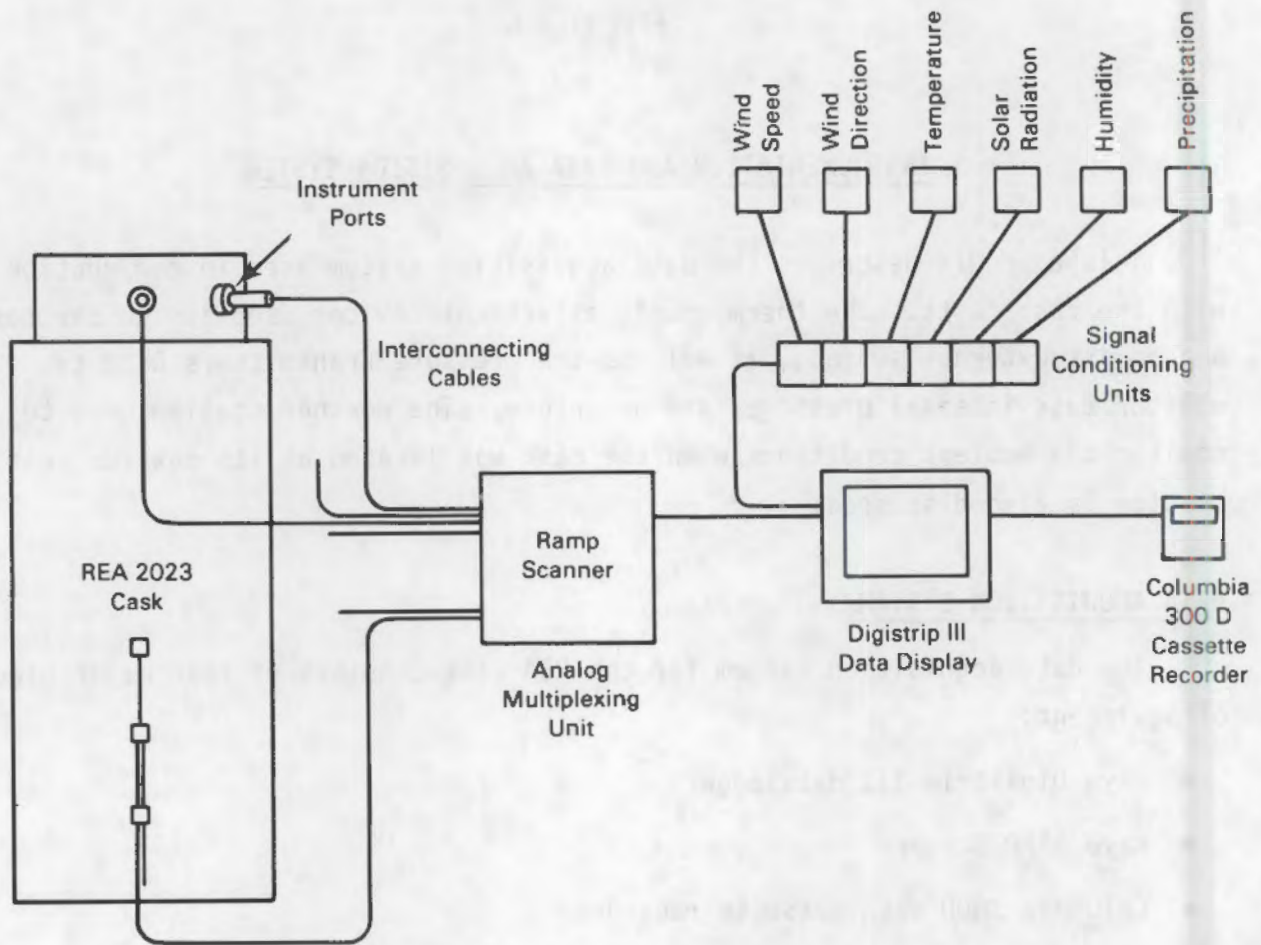


FIGURE A.1. REA Cask Data Acquisition System

acquisition system were Type K thermocouples, the RAMP/Scanner was the most efficient way to handle these inputs. The six interconnecting thermocouple cables terminated at the RAMP/Scanner. The scanner provided onboard cold junction reference and linearization of the Type K thermocouples.

The two pressure transducers and the six inputs from the weather station were directly connected to the Digistrip. Linearization and conversion of these inputs to engineering units was done by programmable functions within the Digistrip.

The data acquisition system was housed in a maintenance building adjacent to the test area. An area about 10 ft x 10 ft was required to accommodate the

equipment. The data acquisition area was isolated from the remainder of the building by enclosing it with plastic sheeting from ceiling to floor. Figure A.2 shows the equipment.

All temperature, pressure, and meteorological readings to the data acquisition system were logged on an hourly basis. The temperature readings were instantaneous values at the time of the data scan; the pressure and meteorological readings were 1-hour averages. Because the system was designed for remote data acquisition, it required a minimum of attention. The cask test area and the data acquisition area were checked only once per 8-hour shift. Checks included an inspection of the cask and interconnecting cables and inspection of the Digistrip to ensure that it was printing correctly and that there was sufficient paper. No problems were encountered with the RAMP/Scanner, Digistrip, or the data cassette recorder. Recording of data to

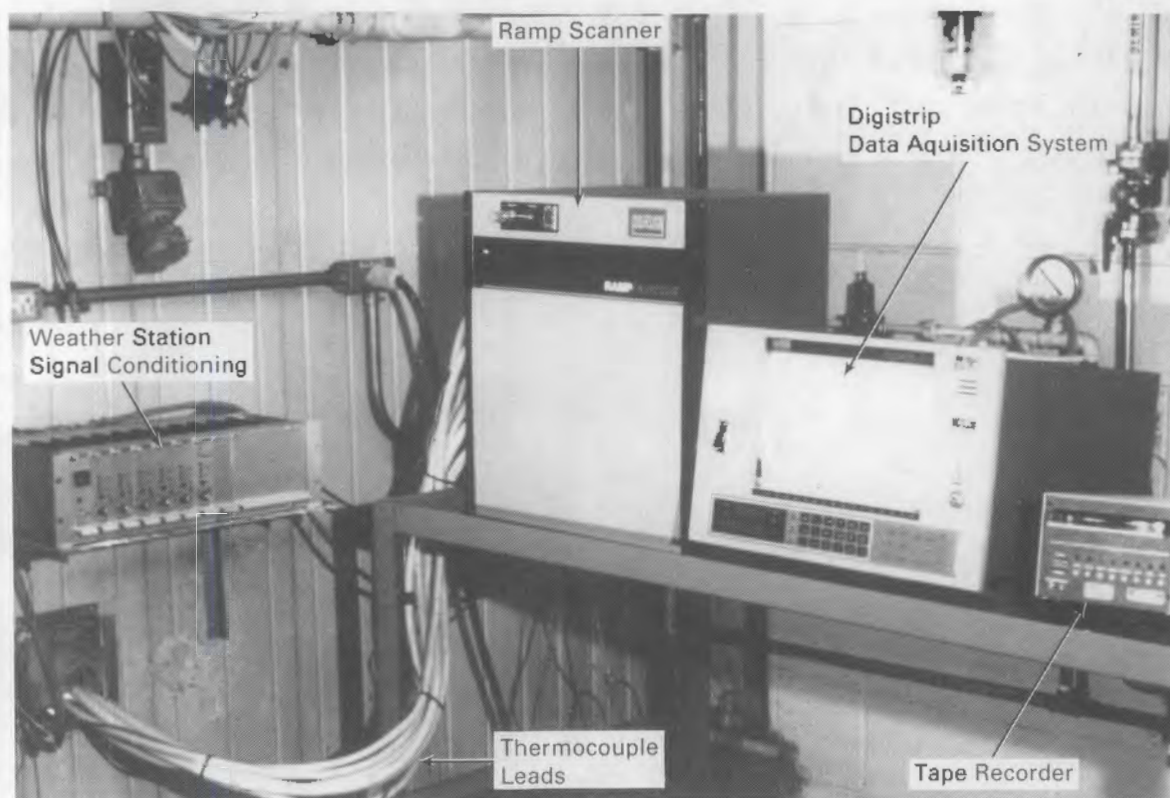


FIGURE A.2. Data Acquisition System



magnetic cassette generally was error-free (with a few minor exceptions) and greatly reduced data analysis time by avoiding manual re-entry of data.

#### THERMOCOUPLE ATTACHMENT DEVICES

Both internal and external thermocouple attachment devices are described in this section.

##### Internal

Twelve internal Type K thermocouples were located on the basket of the REA cask. Four of these thermocouples were attached to the bottom of the basket by REA during the installation of the basket. The method of attachment is shown in Figure A.3. The remaining eight thermocouples were placed between the slots of the basket in the small gaps formed between the copper plates and the Boral tubes. The exact location and elevation of each thermocouple were given in Section 5.

A unique feature of the REA cask characterization test program was the Thermocouple Attachment Device (TAD) used to measure the surface temperature of the center rod of a 7x7 fuel assembly. Figure A.4 shows a schematic of a TAD

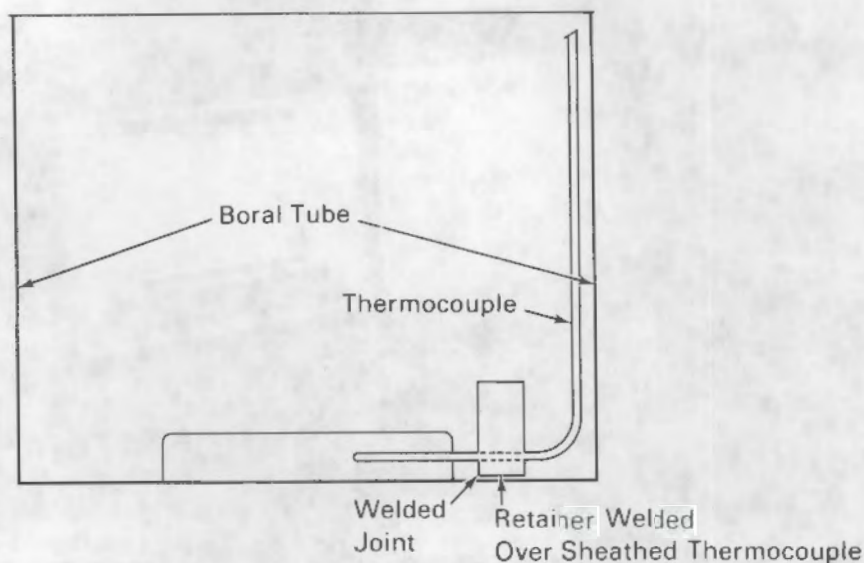


FIGURE A.3. Method Used to Attach Thermocouples to Basket Bottom

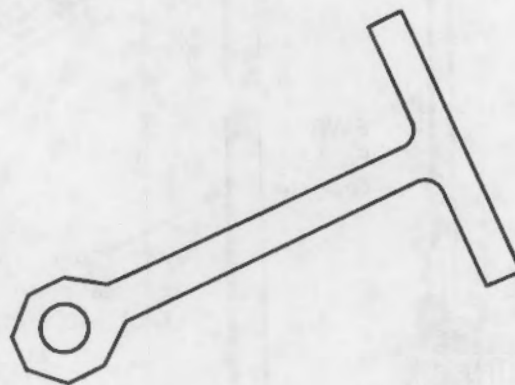
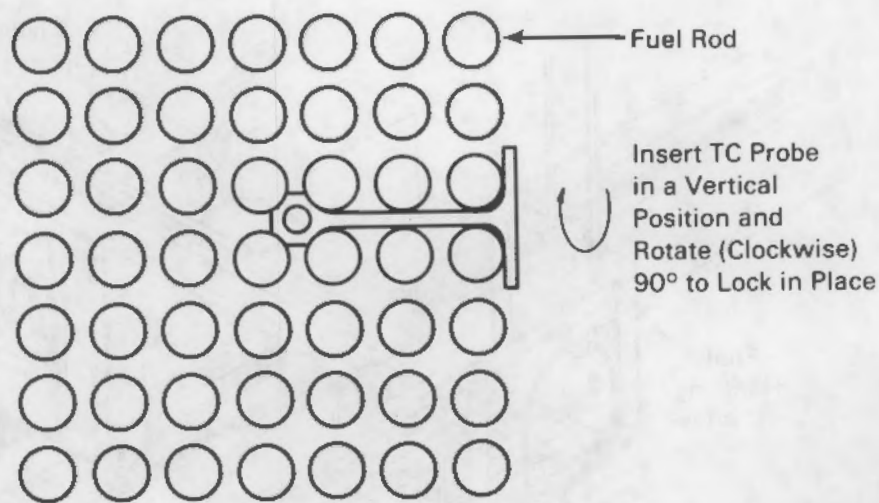


FIGURE A.4. Thermocouple Attachment Device for Inserting Thermocouples into Fuel Assemblies

installed in a 7x7 BWR fuel bundle. Seven fuel bundles were instrumented with TADs. The TAD installation was done in conjunction with the first incremental loading.

All fuel instrumentation was done underwater in the GE-MO unloading basin. A special TAD installation tool (referred to as a TAD-pole) was designed, fabricated, and used to install the TAD-mounted thermocouples. The TAD-pole was basically a 40-ft-long manipulator, with a "master" end located above water and a "slave" end located underwater, as shown in Figure A.5. The TAD-pole was



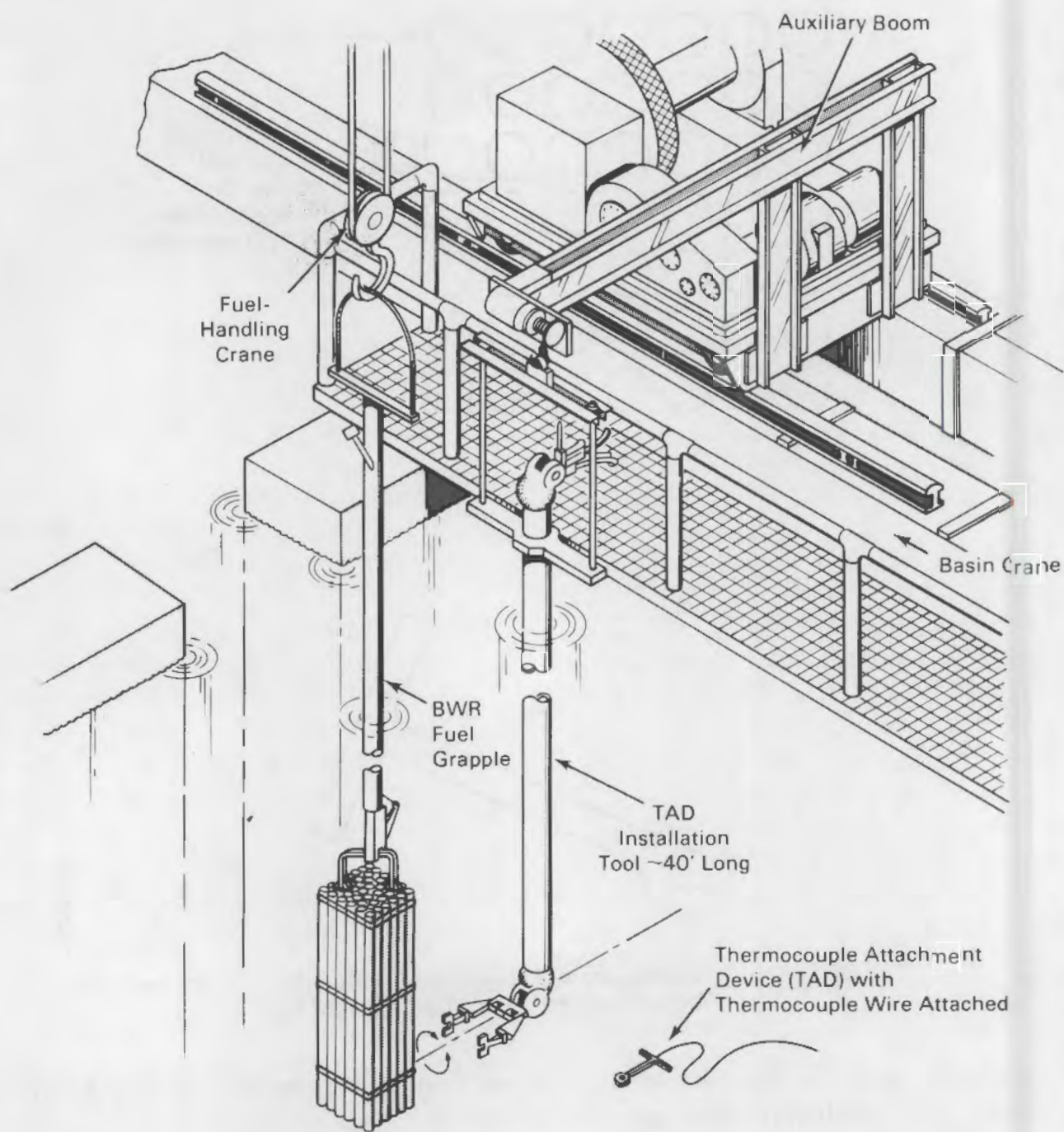


FIGURE A.5. View Showing TAD Installation Tool Attached to Basin Crane

used to pick up the TAD from a vertical position ("T" bar handle pointed up), rotate it to a horizontal position, insert it into a BWR fuel bundle, and rotate it 90 degrees to lock it in place. Figure A.6 shows the fingers of the TAD-pole grasping one of the TADs. Figure A.7 shows the installation of a TAD into a "dummy" fuel bundle.

An underwater TV camera was used to provide visual assistance during the TAD handling. The fuel grapple and TAD-pole were indexed to help install the TADs at specified elevations. The TADs had to be held in a specific orientation in order to be picked up with the TAD-pole. Several variations of the TAD-holder were tried before the one shown in Figure A.8 was finally selected. The TAD-holders were spring-mounted so that they would have some give if the TAD-pole was lowered too far and hit them. The exact location of each TAD-holder was carefully selected so that the TAD at the lowest elevation could be

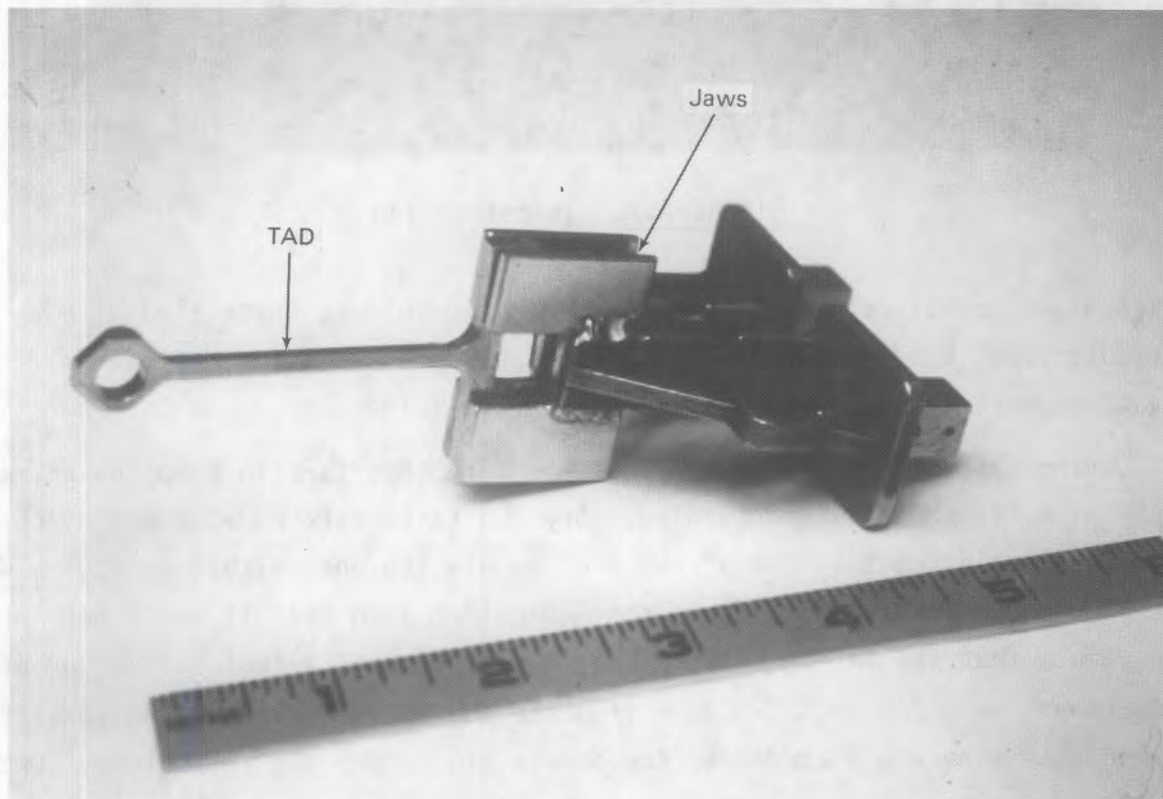


FIGURE A.6. TAD in Jaws



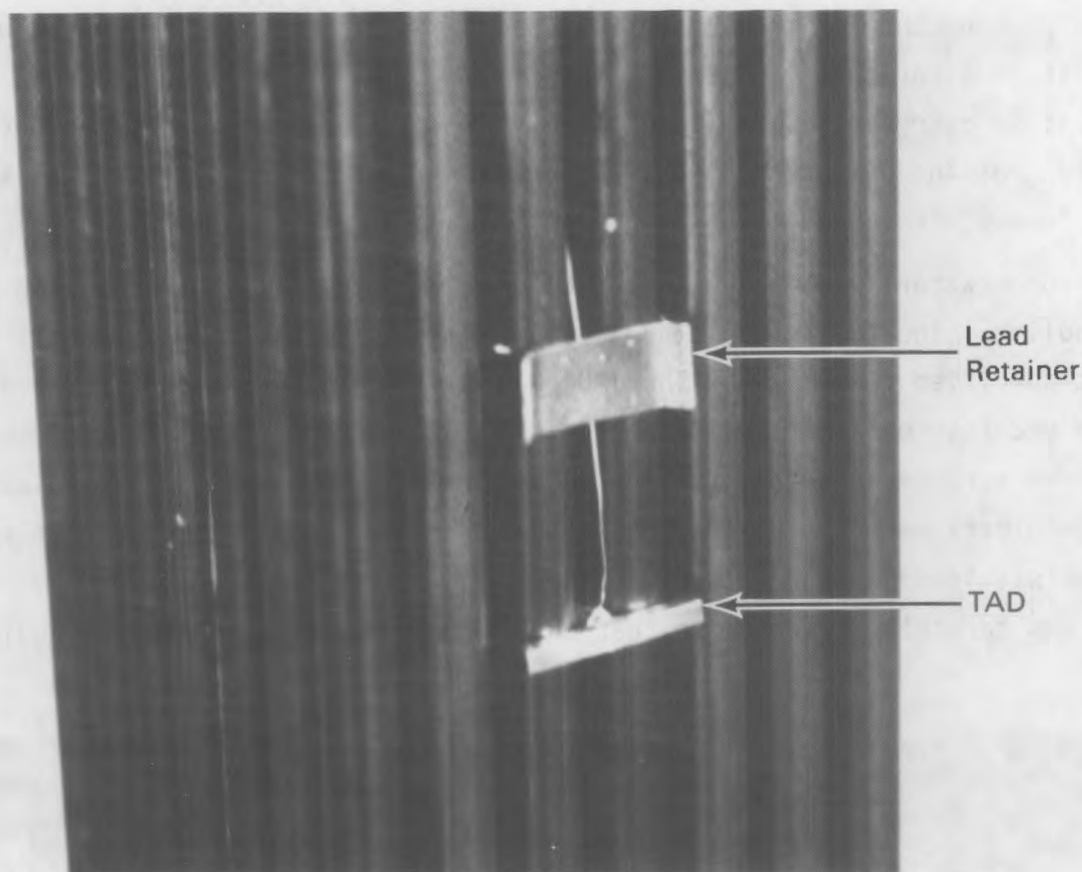


FIGURE A.7. Installed TAD

obtained and installed first. Each group of TAD-holders associated with a particular fuel bundle was color-coded to ease underwater identification. Elevations were also clearly marked on each TAD-holder.

During installation of the TADs it was very important to keep the thermocouple wires from becoming entangled. Dry run tests were made on the decontamination pad using the "dummy" BWR fuel bundle, to ensure that each wire was routed from the instrument port to the TAD-holder such that it would not interfere with either the TAD-holders or the installation of a fuel bundle, or prevent removal of a TAD or TAD-holder from the top of the basket. The "extra" thermocouple wire was placed down the bundle slot under the TAD-holder. Once the TAD was picked up by the TAD-pole, the TAD-holder was removed with a magnet. The TAD was then inserted into the correct fuel bundle at the correct elevation. Once inserted, the TADs proved to be sufficiently secure that they

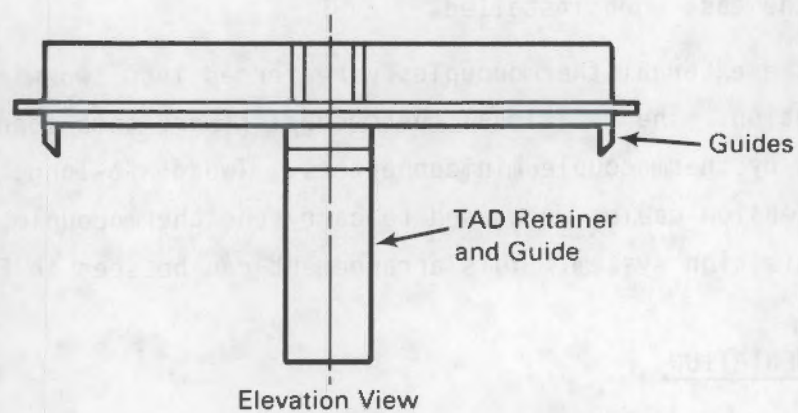
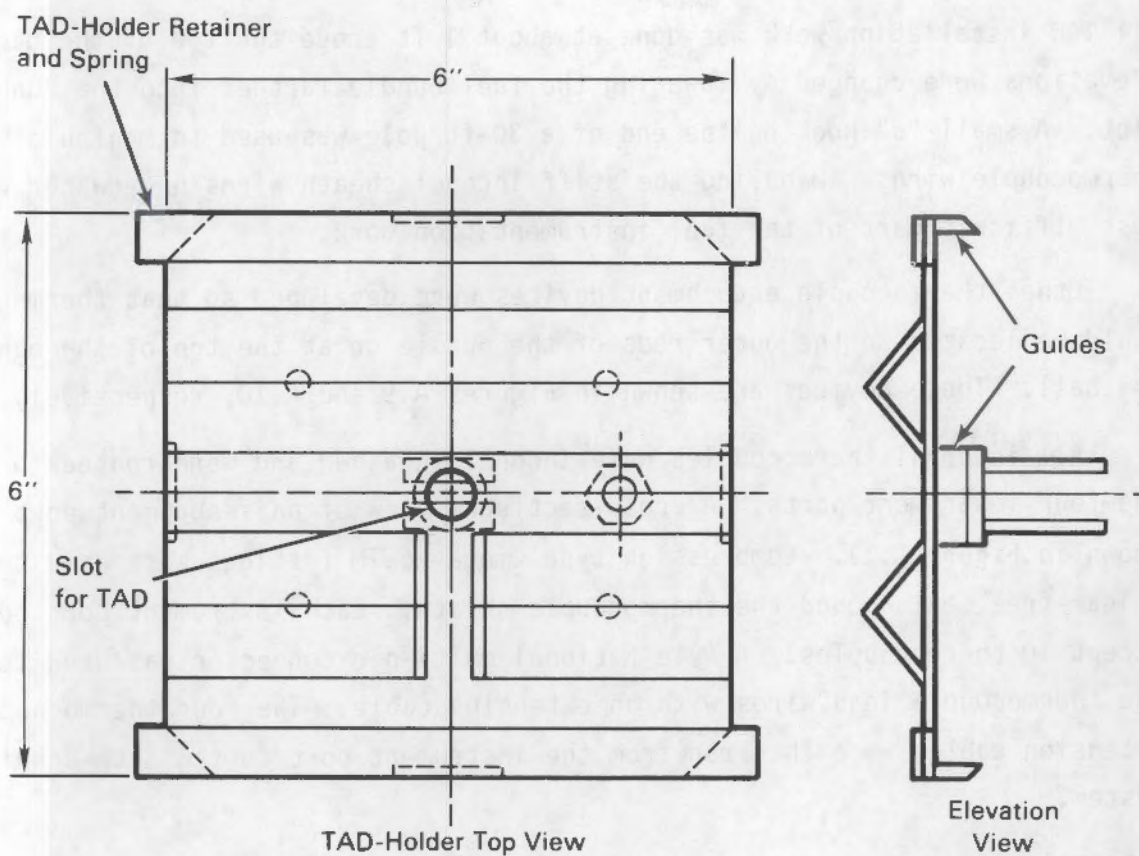


FIGURE A.8. TAD-Holder



All TAD installation work was done at about 1 ft above the top of the basket. Elevations were changed by lowering the fuel bundle farther into the bundle slot. A small "J" hook on the end of a 30-ft pole was used to manipulate the thermocouple wires. Handling the stiff Inconel sheath wires underwater was the most difficult part of the fuel instrumentation work.

Other thermocouple attachment devices were developed so that thermocouples could be located on the outer rods of the bundle or at the top of the bundle on the bail. These devices are shown in Figures A.9 and A.10, respectively.

All internal thermocouples were Inconel-sheathed and were routed to one of the four instrument ports. A cross-sectional view of an instrument port is shown in Figure A.11. Compression type Omega-Lok<sup>TM</sup> fittings were used to form a leak-free seal around the thermocouple sheath. Each instrument port could accept 10 thermocouples. A Pyle-National multi-pin connector was used to mate the thermocouple lead wires with an extension cable. The four thermocouple extension cables were then run from the instrument port to the data acquisition system.

#### External

A total of 32 thermocouples were placed on the surface of the cask using the mounting blocks shown in Figure A.12. The mounting blocks were fastened to the cask with epoxy. These blocks had setscrews so that the thermocouple wires could be easily removed when desired, yet would remain in tight contact with the surface of the cask when installed.

Leads for the external thermocouples were formed into two wiring harnesses to ease installation. The individual thermocouples were then connected to the extension cables by thermocouple miniconnectors. Two 65-ft-long, 20-pair thermocouple extension cables were used to carry the thermocouple information to the data acquisition system. This arrangement can be seen in Figure A.13.

#### PRESSURE INSTRUMENTATION

Two pressure transducers with a range of 0 to 50 psia were mounted on the REA cask. These transducers were located within the instrument ports and were connected to the data lead wires (separate from the thermocouple lead wires).

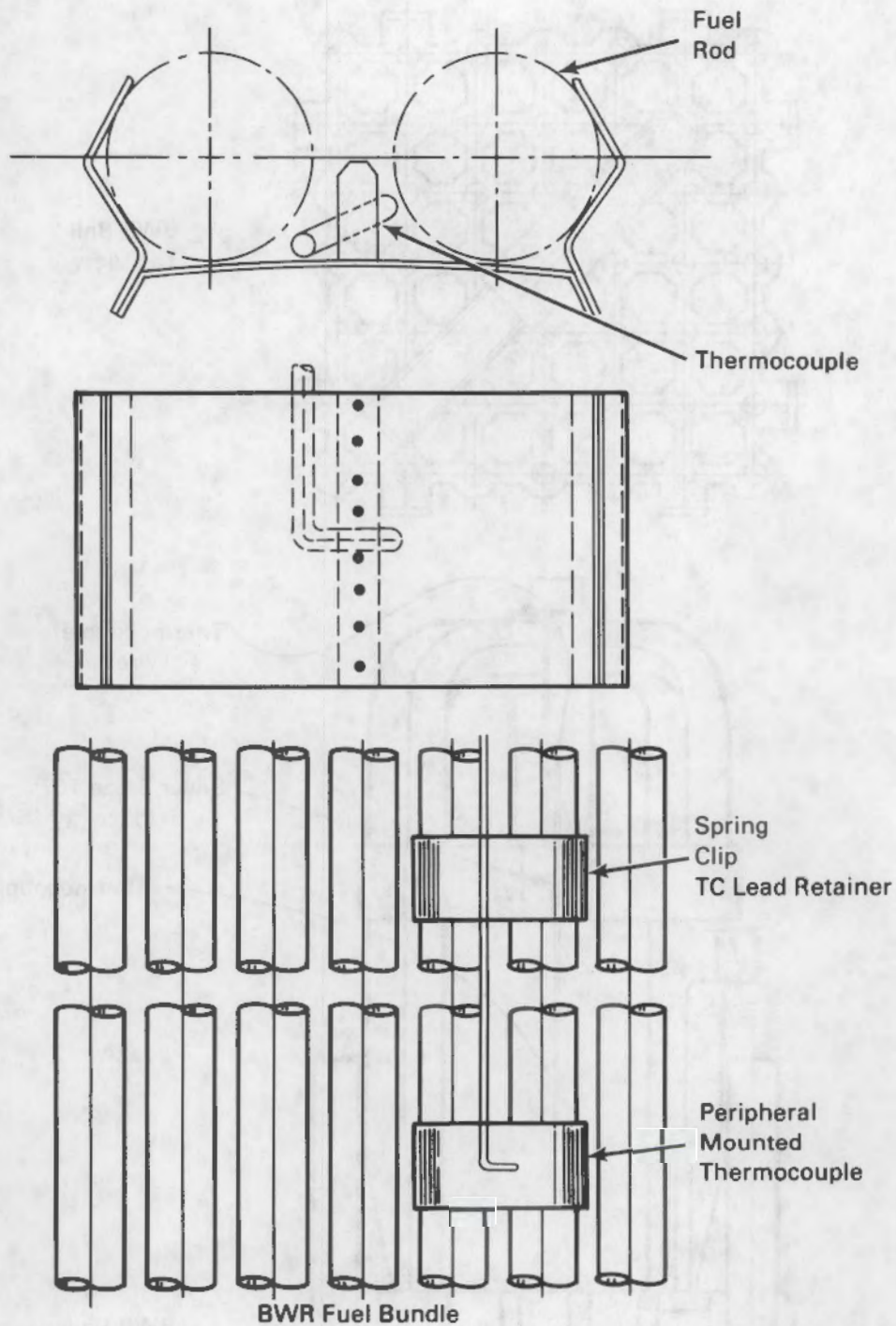
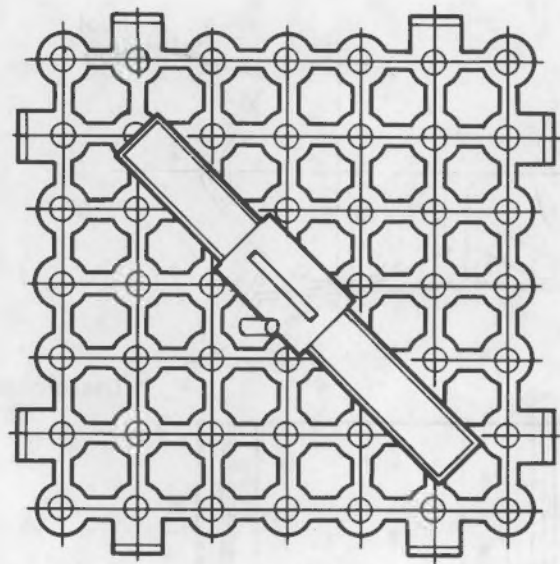
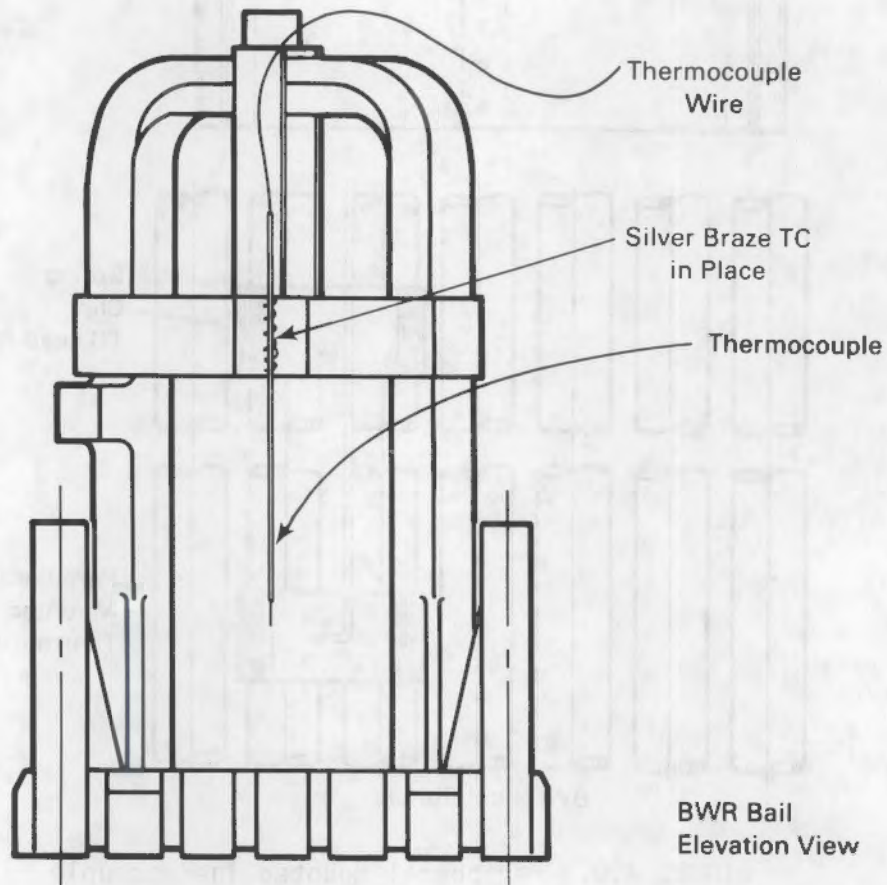


FIGURE A.9. Peripheral Mounted Thermocouple





BWR Bail  
Top View



BWR Bail  
Elevation View

FIGURE A.10. Bail-Mounted Thermocouple

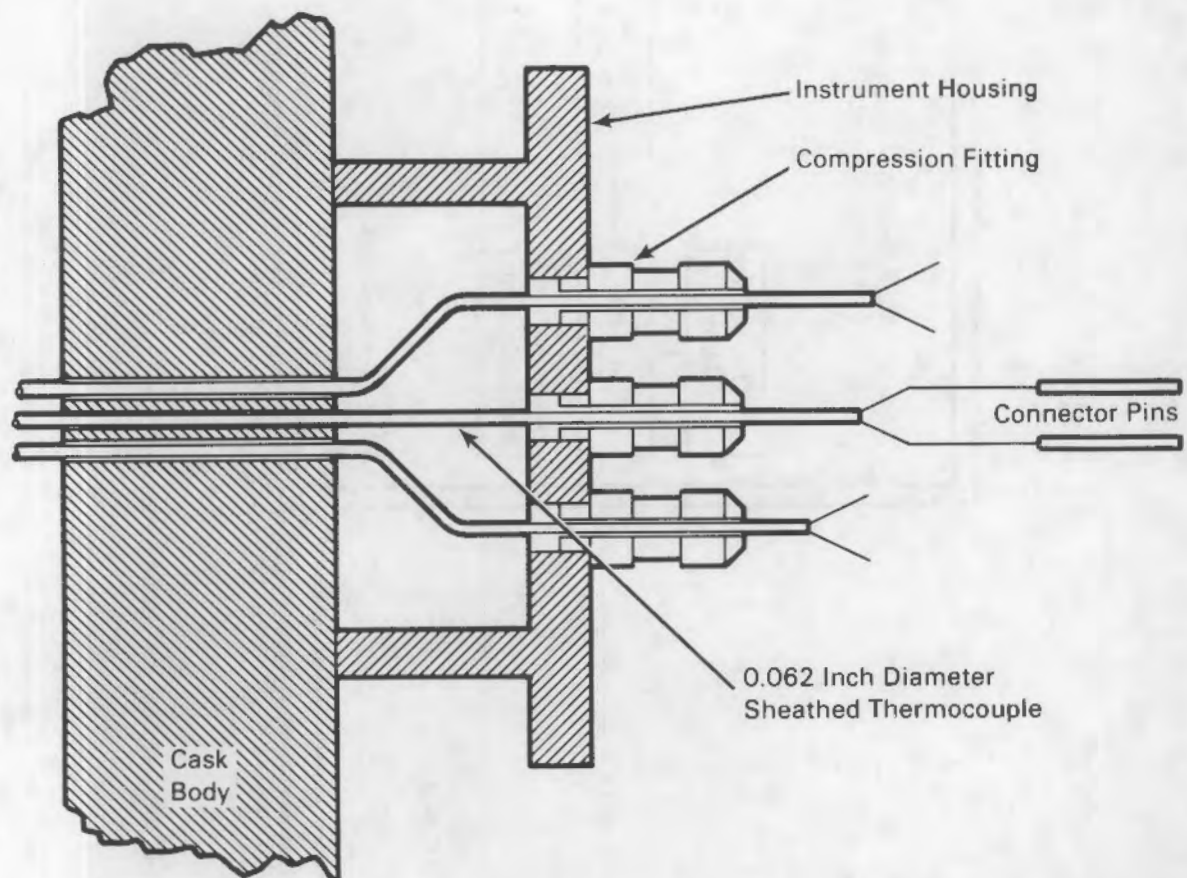


FIGURE A.11. Thermocouple Termination Details

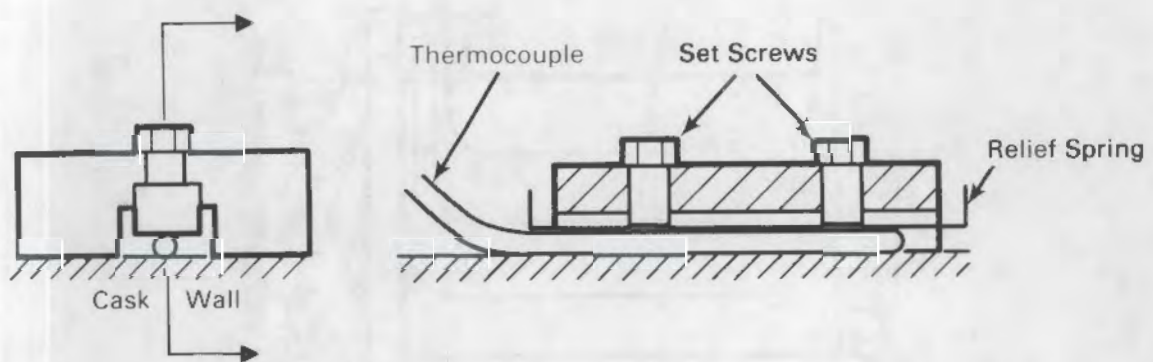


FIGURE A.12. External Thermocouple Mounting Block



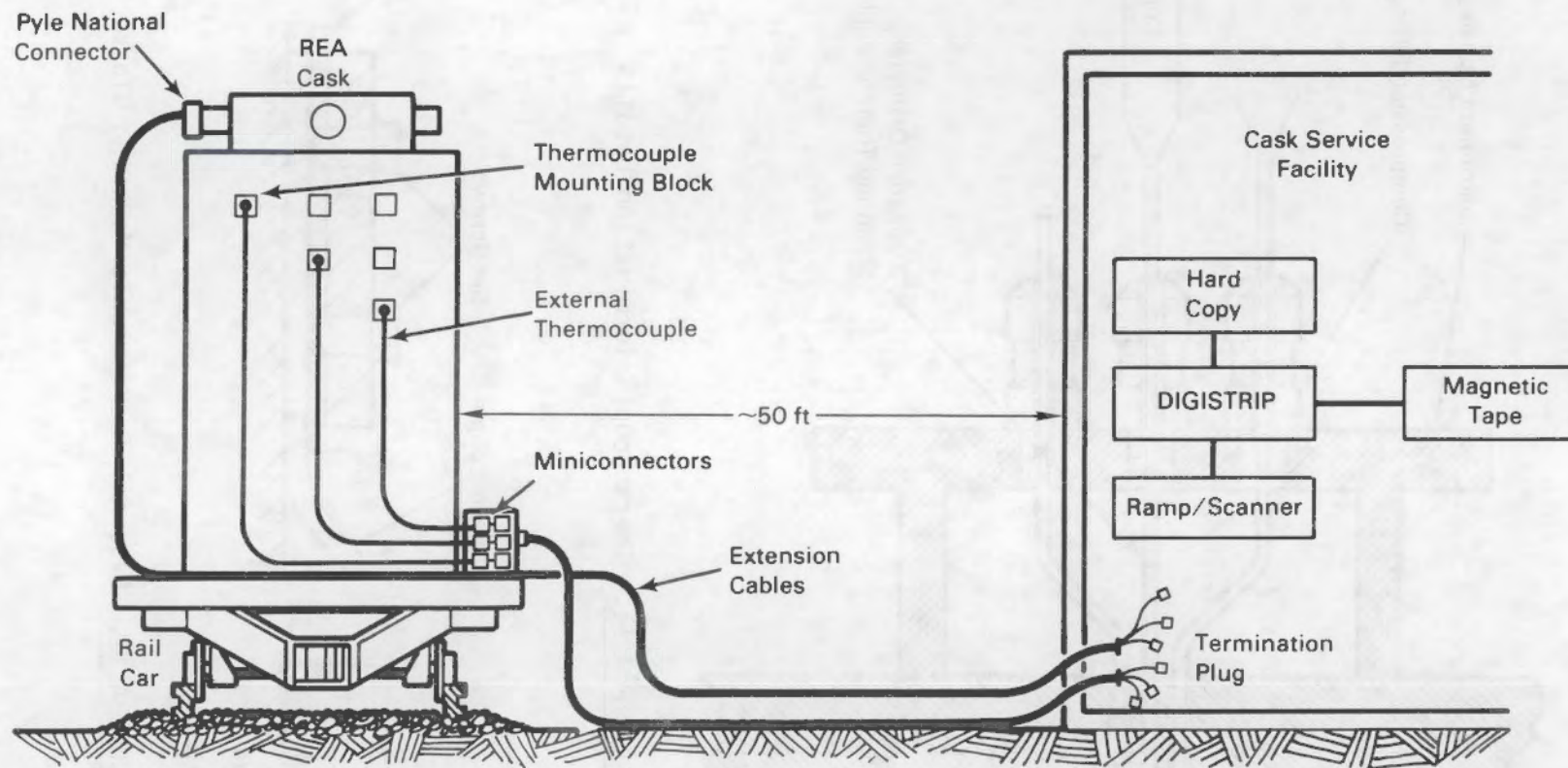


FIGURE A.13. Data Acquisition System External Hardware

The confined space within the instrument ports necessitated using miniaturized pressure transmitters. A Kulite<sup>(a)</sup> HEM-375-50 unit was supplied with the cask. The temperature sensitivity of the Kulite pressure transmitter made it difficult to determine if pressure changes inside the cask were due to changes in internal pressure or to changes in temperature. A Sensotec<sup>(b)</sup> Model A-105 transducer with temperature sensitivity specification an order of magnitude less than the Kulite unit was installed on the cask as a backup. The Kulite transducer failed midway through the test program. The Sensotec worked throughout the test program.

#### WEATHER STATION

The weather station, manufactured by Qualimetrics, Inc.,<sup>(c)</sup> monitored the following parameters:

- wind speed
- wind direction
- ambient temperature
- solar radiation
- humidity
- precipitation.

The individual sensing units were located at the test station site near the fence. The tripod and associated sensing equipment can be seen in Figure A.14. A multiconductor cable brought the analog signals indoors to a bank of six signal conditioning units. These signal conditioning units converted the analog inputs to proportional 0- to 5-V dc outputs. These outputs were then connected to the Digistrip and converted to the appropriate engineering units for display and data logging.

During the test program the weather station malfunctioned as follows:

- The rain gauge tripping bucket sensing relay failed.
- The humidity sensor failed.

---

(a) Kulite Semiconductor Products, Inc., Ridgefield, New Jersey.

(b) Sensotec, Inc., Columbus, Ohio.

(c) Qualimetrics, Inc., Weather Measure Division, North Highlands, California.



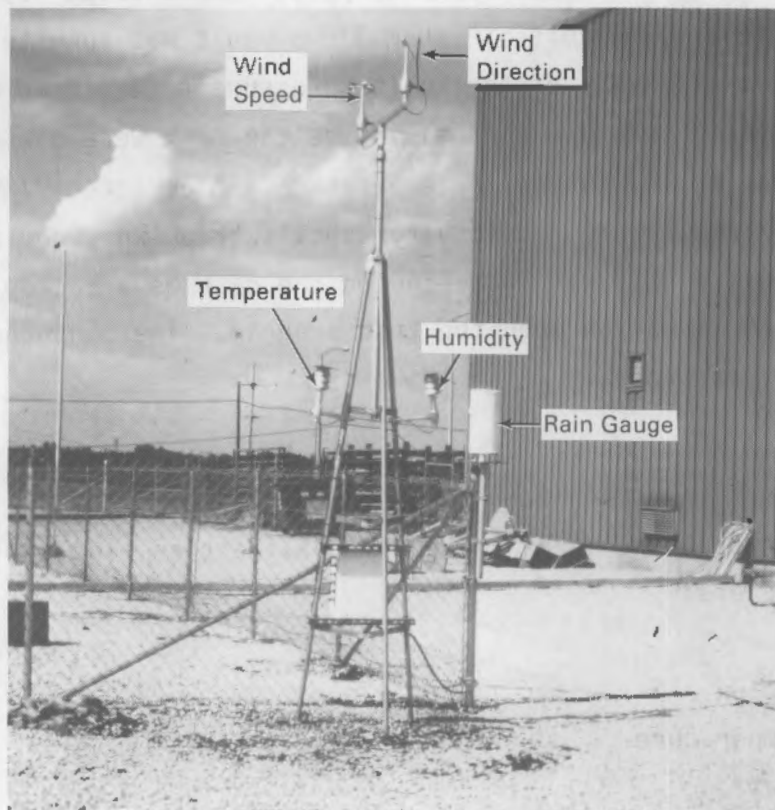


FIGURE A.14. Weather Station

- The wind speed signal conditioning unit failed.
- The solar radiation signal conditioning unit failed.

Of these failures, all except the wind speed signal conditioning unit were promptly discovered and repaired. The latter problem was not promptly discovered because the unit gave a reading but would not properly handle wind velocities above 17 mph. Backup wind speed data from GE-MO's meteorological contractor (Murry and Trettel, Inc.) was obtained to verify any questionable wind speed data. It was found that wind speeds during the testing program were not high enough to require making any correction to data obtained with the weather station.

APPENDIX B

VACUUM DRYING/GAS SAMPLING SYSTEM



## APPENDIX B

### VACUUM DRYING/GAS SAMPLING SYSTEM

The system used to vacuum-dry the cask and to sample the gases during cask performance testing is described in this appendix.

#### VACUUM DRYING

The REA cask was vacuum-dried to remove residual water from the inside cavity of the cask, from between the O-ring seals on the primary head, and from between the primary and secondary closure heads. It was never clear if the area between the two O-rings was properly dried, because the silicone grease used to hold the O-rings in place often flowed into and plugged the 1/8-in. vent in the primary head used for vacuum drying. The silicone grease also bridged the gap between the two O-rings, preventing complete evacuation of the entire annular space between the O-rings. The area between the two closure heads could not be vacuum-dried because a leak-free seal could not be formed between the outer head and the cask. The seal was to be formed by a seal welding. As discussed in Section 3, the seal welding was not used in the cask tests. Thus, vacuum drying as employed at GE-MO applies to only cask cavity drying.

The primary component of the vacuum drying system was the vacuum pump. A Stokes Model 148-H microvac pump was used. An oil separator was also procured for the discharge of the pump, to reduce oil carry-over. The discharge of the oil separator was routed to the facility off-gas header for final filtering, monitoring, and disposal to the atmosphere via a 300-ft-high stack. Figure B.1 shows the vacuum drying/gas sampling piping used in conjunction with the REA cask program. The equipment was located within the basin area with 2-in.-diameter flex hoses used to connect to the cask. All vacuum drying was done on the decontamination pad in conjunction with outgoing cask preparations; however, gas changes and sampling were usually done while the cask was in the CRA. The 2-in. hoses were fitted with quick connect adapters.

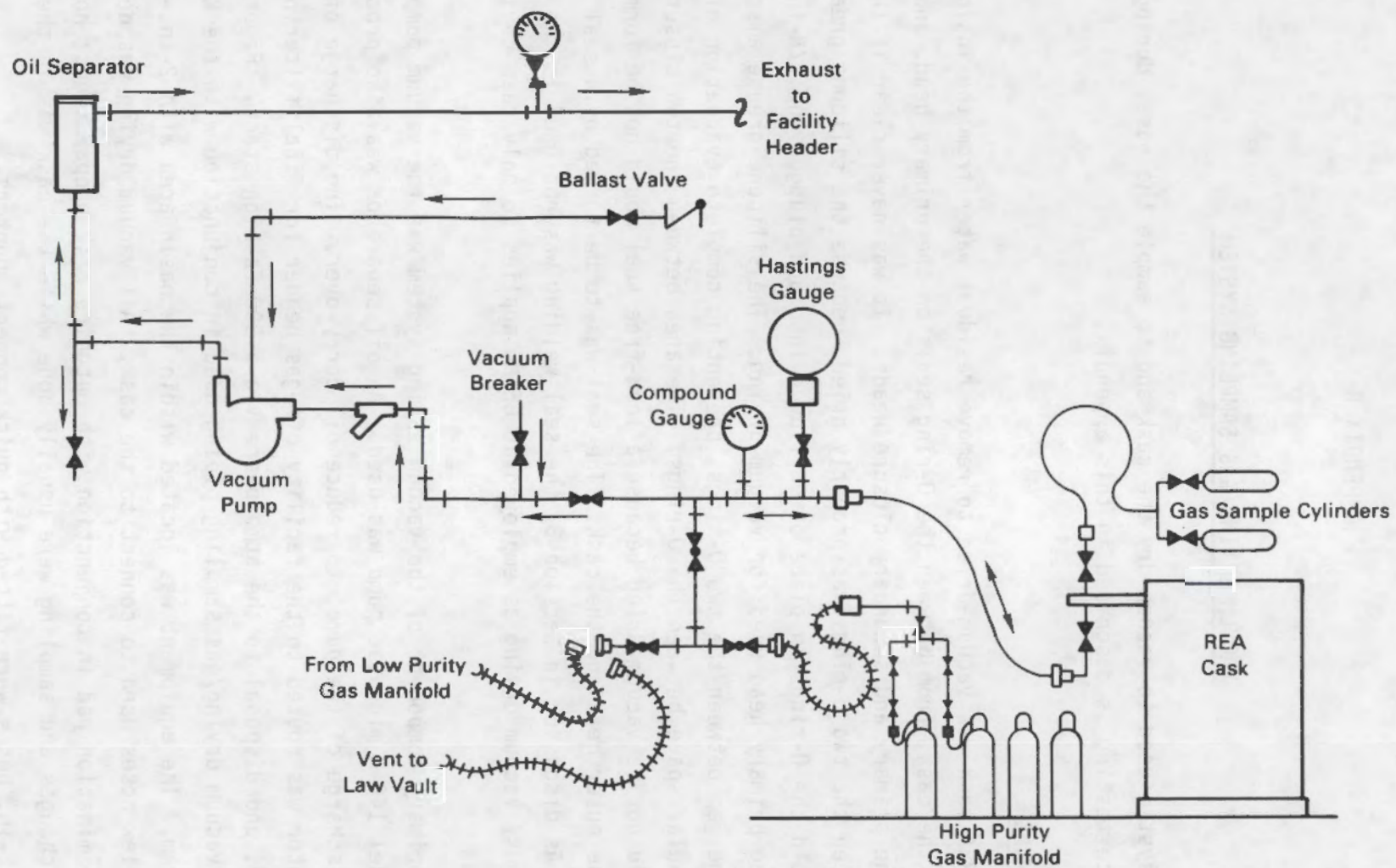


FIGURE B.1. Vacuum Drying/Gas Sampling System



A Hastings vacuum gauge, model VT-series, was used to indicate pressures during vacuum drying. The gauge was capable of 0.1 mm Hg low-range resolution. The Hastings gauge was valved out until the pressure in the system was below 26 mm Hg. A compound vacuum/pressure gauge was used to indicate pressure above 30 mm Hg.

Because of the very low pressures being monitored, and because of the 6-hour duration of the test, any small leaks in the manifold, connecting hoses, or fittings could not be tolerated. Therefore, the system was thoroughly leak-checked with helium before vacuum drying was attempted. After the cask was successfully leak-checked, the basin water remaining in the cask was then displaced by pressurizing the cask with helium. After the water was displaced, the cask was purged with helium for 2 hours to help remove any residual water.

The vacuum system was then valved in, and the cask evacuated to 30 mm Hg. The cask pressure was observed, and if it increased to over 35 mm Hg in a 1-hour period, successive evacuations were run until it held below 35 mm Hg.

Once this criterion was met, the cask was evacuated to 2 mm Hg. The rate of pressure decrease at 7 mm Hg pressure was observed for the possible formation of ice. Repressurization to 10 mm Hg and re-evacuation were done whenever any hesitancy in the rate of pressure decrease at 7 mm Hg was noted.

After the cask was evacuated to 2 mm Hg, the vacuum pump was valved out and the cask internal pressure was monitored for 6 hours. Any pressure increase over the 6-hour period was interpreted as residual water vapor in the cask or as a leak. However, no leaks were evident during vacuum drying. The re-evacuation and 6-hour pressure monitoring were repeated until there was no further increase in pressure over a 6-hour period.

The results of the vacuum drying for the first and second incremental loadings of the REA cask are shown in Table B.1. The first loading required five iterations of the 6-hour pressure monitoring procedure, and eleven iterations for the second loading. One-and-a-half days were required to complete vacuum drying for the first loading; slightly more than 3 days were required for the second loading.

TABLE B.1. Vacuum Drying Experience with the REA 2023 Cask

	Cycle	Initial Pressure, mm Hg	Final Pressure, mm Hg <sup>(a)</sup>
<u>First Loading</u>	1	2	<20
	2	2	7
	3	2	5
	4	3	2.5
	5	1	1
<u>Second Loading</u>	1	2	11
	2	0.85	Not Recorded
	3	1.7	8.5
	4	1.7	8.0
	5	1.2	4.25
	6	0.85	3.5
	7	0.85	2.5
	8	0.48	1.75
	9	0.5	1.1
	10	0.2	1.0
	11	0.2	0.93

(a) The final pressure reading was taken 6 hours after the initial pressure reading.

#### GAS SAMPLING

A special high-purity gas manifold was provided for the REA cask program to preclude mixing of commercial grade gases normally used at GE-MO with the high-purity gases used for filling the cask. The manifold was equipped with a log so that traceable records could be maintained for each cavity filling. High-purity helium (99.995%) and pre-purified nitrogen (99.998%) were supplied from a local vendor. Certificated analysis for each batch of gas supplied was provided, along with trace analysis for oxygen.

All fillings of the cask involved an initial filling with the designated gas followed by an evacuation to <2 mm Hg, followed by a second filling with the designated gas. Duplicate samples were obtained at the conclusion of the second filling of each designated cover gas run. This sample was used as the control sample. Immediately before the cask was evacuated or the gases were



changed, another sample was taken. The differences between the control sample and this final sample were used to evaluate what had happened in the cask.

Section 3 of this report describes the procedure used for gas sampling. Section 4 of the report discusses the results of the gas sampling.

changes, another sample was taken. The difference between the control sample and this (real) sample was used to evaluate what had happened in the cell. Section 3 of this report describes the procedure used for gas sampling. Section 4 of the report discusses the results of the gas sampling.



APPENDIX C

CASK DECONTAMINATION

## APPENDIX C

### CASK DECONTAMINATION

Tests were run at GE-MO to assess the ease of decontaminating the REA cask. These tests involved taking smear surveys of the cask when it was delivered to the test storage area (outgoing survey) and when it was returned to the basin area (incoming survey). The outgoing and incoming surveys were performed for both the partial and full loading of the cask.

#### SURFACE

The cask was sectioned into 96 areas that would allow for identification of each smear. These areas are mapped in Figures C.1 and C.2. Each area on the side of the cask was approximately 2 ft x 3 ft. Smaller areas were marked off on the top and bottom of the cask and around the outer head closure area. Surveys were made by wiping a 100-cm<sup>2</sup> area from each designated area of the cask with a paper planchet. The smear results for the partial and full load are given in Table C.1.

The outgoing and incoming smear surveys were compared to assess the leaching of radioactive contamination from the cask's surface. As can be seen in Table C.1, the results of the incoming surveys were very similar to those of the outgoing surveys. This indicates that the cask surface exhibited very little tendency to leach (or hold) radioactive contamination. The time increment between incoming and outgoing smear surveys was 45 days for the first loading and 91 days for the second loading.

Decontamination times for the REA cask after the first and second loadings were not excessive, and generally required three to four 8-hour shifts to complete. The final decontamination of the cask was the most time-intensive due to insulation sticking to the paint. This made the surface fuzzy, and it had to be hand-scraped with razor blades to remove the fuzz.



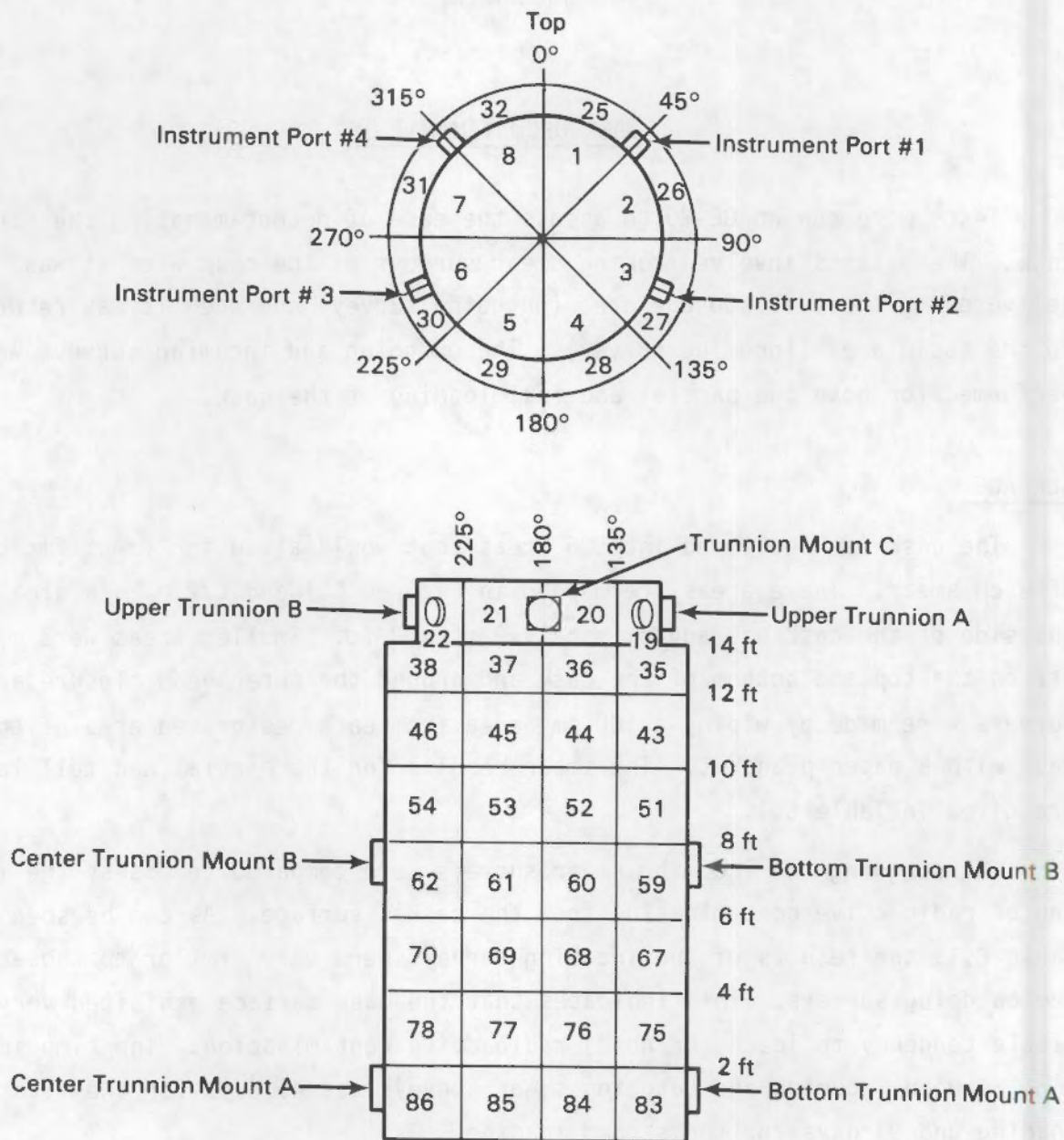


**FIGURE C.1.** REA Cask - Top and South Side Maps

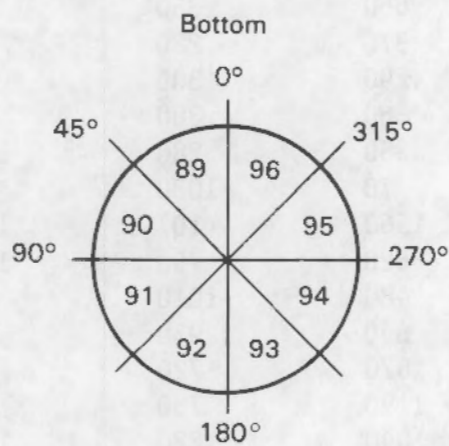
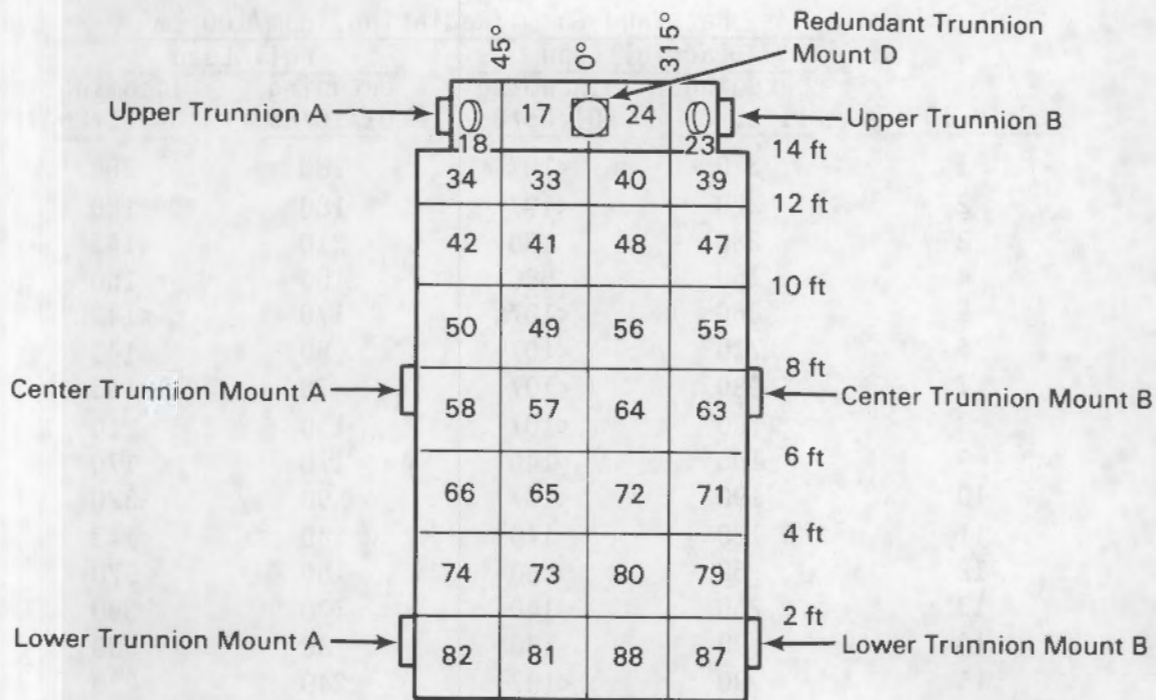


FIGURE C.2. REA Cask - Bottom and North Side Maps



TABLE C.1. REA Cask Smearable Contamination Survey Results

Grid ID	Beta and Gamma Radiation, dpm/100 cm <sup>2</sup>			
	Partial Load		Full Load	
	Outgoing 11/19/84	Incoming 01/03/85	Outgoing 01/10/85	Incoming 04/11/85
1	310	<107	180	200
2	220	<107	180	180
3	230	120	210	<143
4	150	880	100	150
5	860	<107	170	<143
6	710	<107	50	<143
7	980	<107	70	<143
8	180	<107	150	210
9	100	140	170	170
10	190	<107	90	320
11	120	140	140	<143
12	60	80	150	570
13	250	140	170	390
14	90	180	80	530
15	90	<107	240	230
16	130	120	390	<143
17	310	400	1090	1520
18	660	360	1360	3810
19	370	280	430	580
20	290	300	480	1000
21	860	300	540	720
22	350	280	1970	300
23	70	1030	490	560
24	1560	<107	1030	800
25	520	790	1070	1120
26	480	1010	860	1270
27	590	930	670	790
28	1070	720	870	1170
29	1190	730	400	700
30	1040	1220	1630	2140
31	640	450	1880	5650
32	420	560	1750	1030
33	220	370	1120	600
34	70	260	1030	210
35	90	160	1000	320
36	290	230	860	240
37	130	230	520	<143
38	300	290	650	310
39	420	460	1820	490

TABLE C.1. (contd)

Grid ID	Beta and Gamma Radiation, dpm/100 cm <sup>2</sup>			
	Partial Load		Full Load	
	Outgoing 11/19/84	Incoming 01/03/85	Outgoing 01/10/85	Incoming 04/11/85
40	930	200	1520	220
41	450	400	680	600
42	1000	620	360	440
43	390	540	920	190
44	590	380	1250	150
45	510	560	740	<143
46	370	320	610	300
47	1270	520	1450	470
48	240	360	740	400
49	490	710	1270	320
50	1040	280	1220	320
51	1610	510	780	240
52	390	530	690	260
53	250	160	330	160
54	200	170	540	<143
55	430	330	980	480
56	1280	190	1470	210
57	250	300	930	<143
58	470	550	1580	370
59	1240	620	870	290
60	470	200	1290	<143
61	280	160	800	<143
62	440	420	530	510
63	620	500	1120	180
64	550	980	1440	220
65	1890	250	500	320
66	540	460	1260	250
67	590	560	890	680
68	1090	400	240	370
69	530	280	200	370
70	620	530	640	<143
71	490	800	1130	<143
72	410	390	1000	200
73	820	300	460	630
74	510	430	1150	800
75	670	1060	1680	<143
76	370	230	630	<143
77	440	250	670	190
78	620	470	640	490



TABLE C.1. (contd)

Grid ID	Beta and Gamma Radiation, dpm/100 cm <sup>2</sup>			
	Partial Load		Full Load	
	Outgoing 11/19/84	Incoming 01/03/85	Outgoing 01/10/85	Incoming 04/11/85
79	940	370	770	<143
80	290	260	560	<143
81	910	1100	1140	310
82	880	420	980	310
83	1810	320	700	380
84	530	170	690	310
85	670	170	220	430
86	470	240	490	410
87	500	320	1270	380
88	1330	170	1460	380
89	280	300	680	<143
90	80	<107	1780	310
91	60	240	1156	<143
92	210	160	210	170
93	290	180	1560	300
94	130	200	1570	580
95	150	150	1800	240
96	80	410	610	<143

Instrument  
Port #

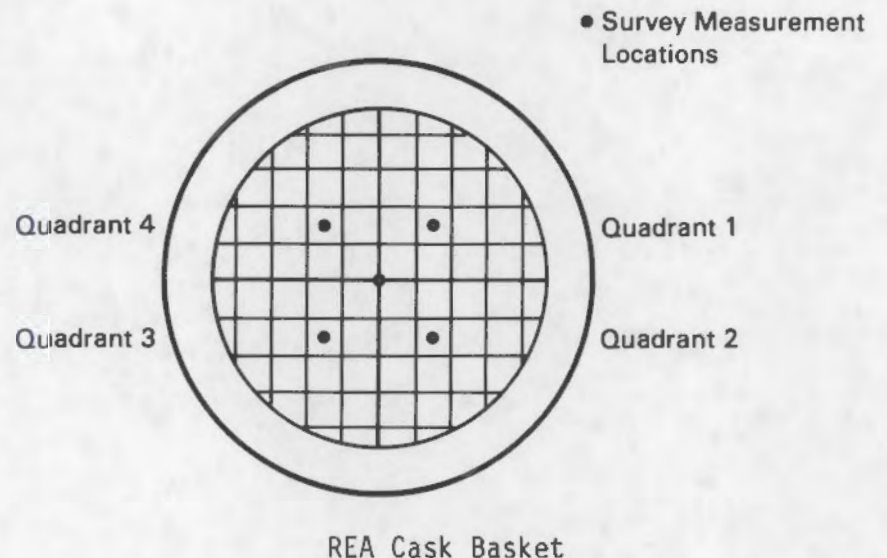
1	710
2	1860
3	2130
4	160

Trunnions

Upper	A	2080	1850	1930	2290
	B	540	280	1470	3250
	C	630	2020	960	2490
	D	1640	540	870	210
Center	A	280	370	330	350
	B	490	450	380	430
Lower	A	110	260	1750	1180
	B	1030	210	1950	750

## INTERIOR

The cask's potential to retain radioactive material within the cavity was assessed. Dose rate measurements were taken above the cask cavity before fuel was loaded into the cask and upon termination of the test program after all the fuel was removed. The post-test radiation readings were taken after the cask was returned to the decontamination pad and the water was drained out. The cavity was not rinsed or flushed. Figure C.3 shows where the radiation readings were taken and also lists the pretest and post-test readings. Post-test dose rates ranged from 25 mrem/hr to 50 mrem/hr at the top of the cask. No dose rate measurements were taken below the top of the cask basket.



<u>Survey Location</u>	<u>Initial Survey, mrem/hr 9/25/84<sup>(a)</sup></u>	<u>Final Survey, mrem/hr 4/18/85</u>
Center	0.9	40
Quadrant 1	0.8	41
Quadrant 2	0.7	37
Quadrant 3	0.7	27.5
Quadrant 4	0.7	45

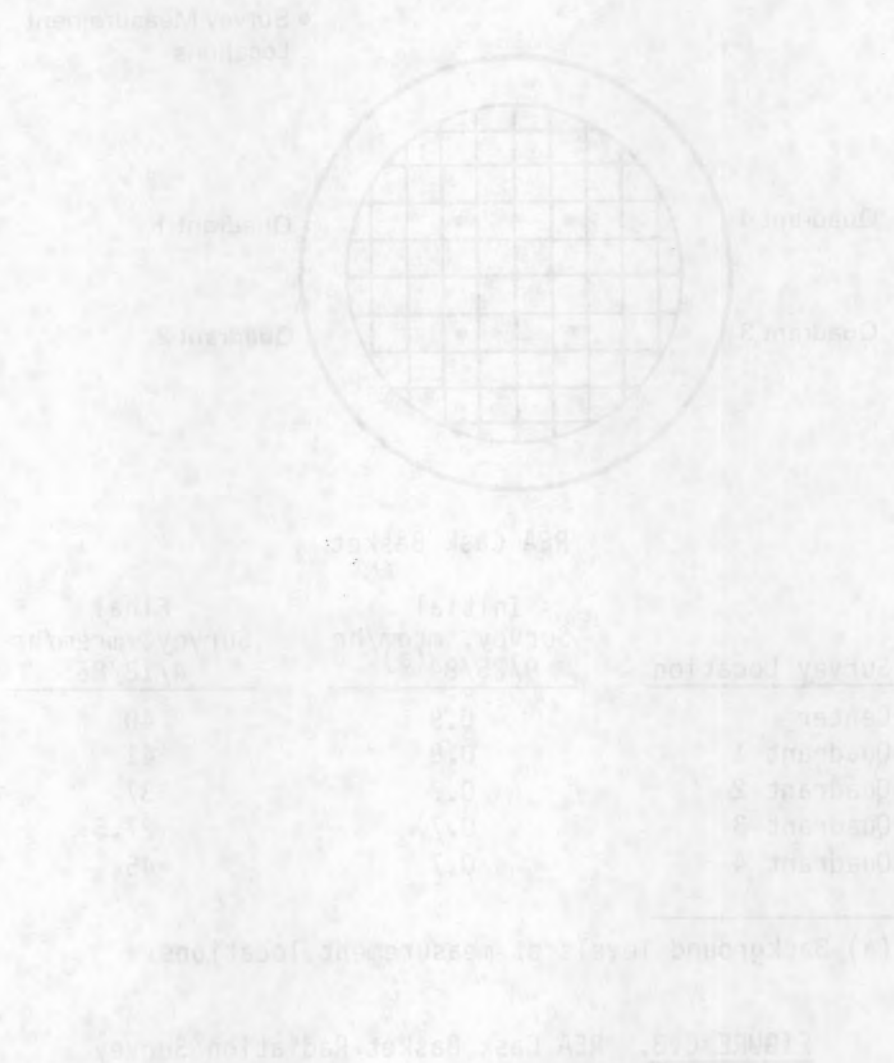
(a) Background levels at measurement locations.

FIGURE C.3. REA Cask Basket Radiation Survey



An attempt was made to obtain crud samples from the inside of the REA cask. However, the cask contained very little observable crud. Instead, smears were taken of the reddish film present at some locations on the inside surface of the bundle slots. The smear papers were included among samples sent to LLNL for analysis.

When the last 2 in. of water were pumped from the cask cavity, the water was filtered by passing it through a cloth filter. Again, very little observable material was obtained, even though the cloth filter read upward of 25 mrem/hr. Small specks of dirt or other hard material were obtained and were included in the samples. The cloth filter was cut up and pieces of it were included among samples sent to LLNL.



APPENDIX D

DECAY HEAT MEASUREMENTS



## APPENDIX D

### DECAY HEAT MEASUREMENTS

This appendix contains the calorimetry data for the Cooper spent fuel assemblies used during the cask performance tests. It includes the October 1984 calorimeter calibration and the correction factor that must be used with that calibration to correct the measured data for gamma energy losses and differences between the specific heat of the calorimeter in the calibration configuration and in the spent fuel decay heat measurement configuration. The calibration data is presented first, followed by the correction factors and the data.

#### CALORIMETER CALIBRATION

All calorimeter data reported in this document are referenced to an October 1984 calibration of the calorimeter. Calibration of the calorimeter was performed by putting a known amount of energy into the calorimeter and observing the increase in internal water temperature with time. The slope of the temperature curve at the moment when the difference between the internal calorimeter temperature and the external basin water temperature reached 1°F was correlated to the heater input. This slope versus power curve was used to determine the decay heat output of a fuel assembly.

The energy was input to the calorimeter by means of an electrical resistance heater. The heater consists of 60 ft of resistive stainless steel sheath heating tape wound around a 4-in. pipe 14.5 ft long. The pipe is open at both ends and fills with water during submergence in the basin. It is suspended from the underside of the head by four bolts.

The power delivered to the calibration heater was controlled by a variable power transformer and measured by a precision wattmeter. The datalogger continuously monitored the signal and printed out average power at 15-min. intervals. The datalogger power printouts were then averaged over a 5-hour interval



to arrive at the "actual" power delivered to the calorimeter. This power was then corrected for the power lost (3.36%) in the heater leads external to the calorimeter.

The steps used to calibrate the calorimeter were performed as follows:

1. The vessel was purged to remove hot water.
2. The vessel was allowed to equilibrate with the surrounding basin water.
3. A delta T across the calorimeter of  $0.0 \pm 0.1^\circ\text{F}$  was maintained for 1 hour.
4. The electric heater was energized to the proper wattage.
5. The head/heater was lowered into place.
6. The head was torqued down and leak-checked.
7. Automatic data acquisition was initiated when the datalogger showed a temperature difference of  $1.0^\circ\text{F}$  between the interior vessel surface and outside skin.

Additional care was exercised to maintain the unloading pit water at a constant temperature during the runs. Each calibration run lasted 5 hours from the time the datalogger was put into automatic operation.

Calibration runs were obtained at 0, 50, 100, 200, 300, 400, and 500 W. A repeat run was made at 200 W. The temperature-versus-time curves for these calibration runs were shown in Figure D.1. The technique used to convert from the calibration curves shown in Figure D.1 to heat output in watts was as follows: 1) a polynomial equation of the form  $y = ax^2 + bx + c$  was determined for each heat-up curve, 2) the slope of each line at  $t = 0$  was calculated, and 3) the relationship between "slope value" and power was determined. This relationship forms the calibration curve as shown in Figure D.2. The relationship is linear with a correlation coefficient of 0.9996 determined from linear regression analysis of the data. The calibration equation is  $Q = 372.5445x - 85.9749$  where  $x$  is the slope value at time zero and  $Q$  is the heat generation rate. Table D.1 lists the slope values, index of determination values, and percentage differences for all of the October 1984 calibration runs. As can be



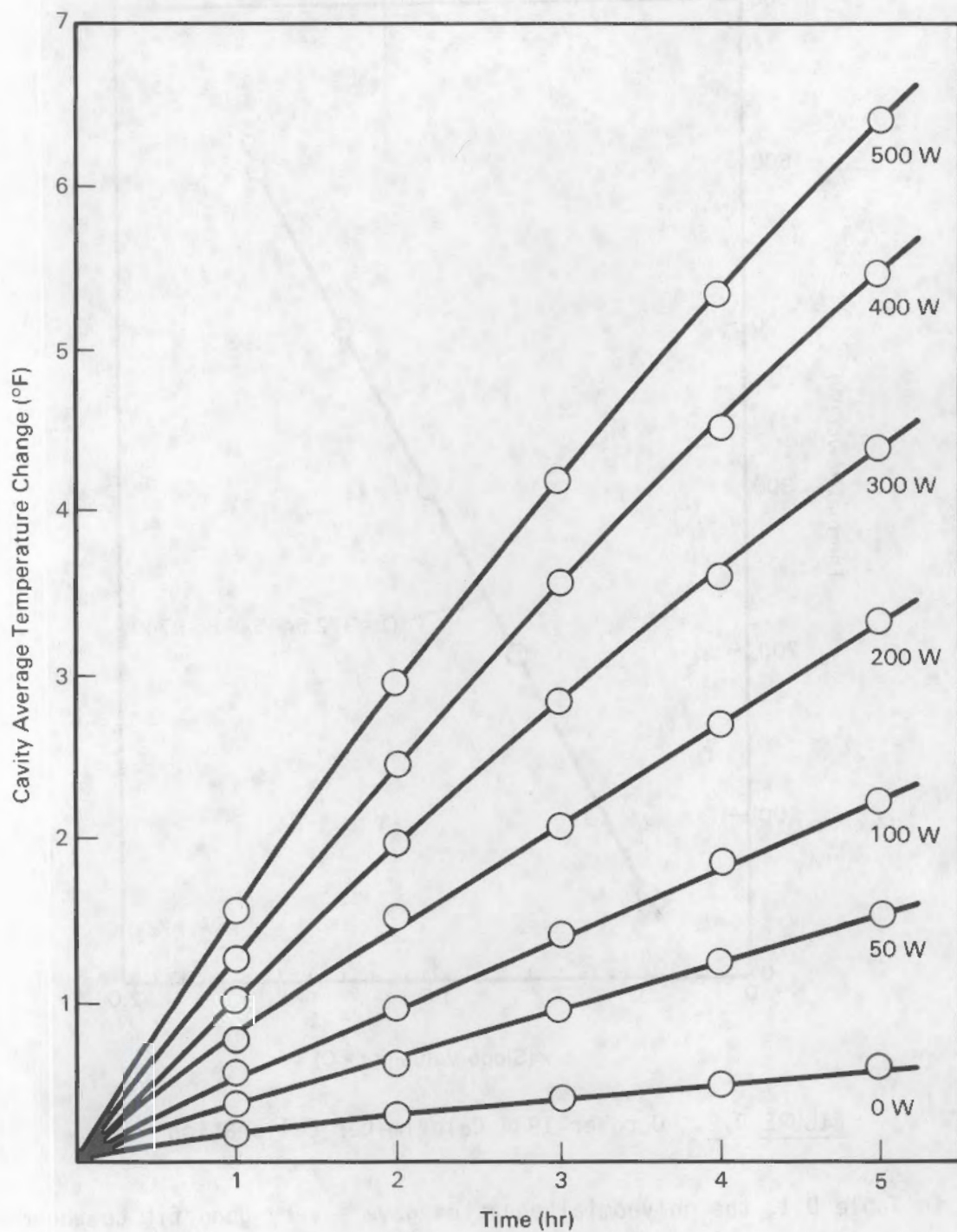
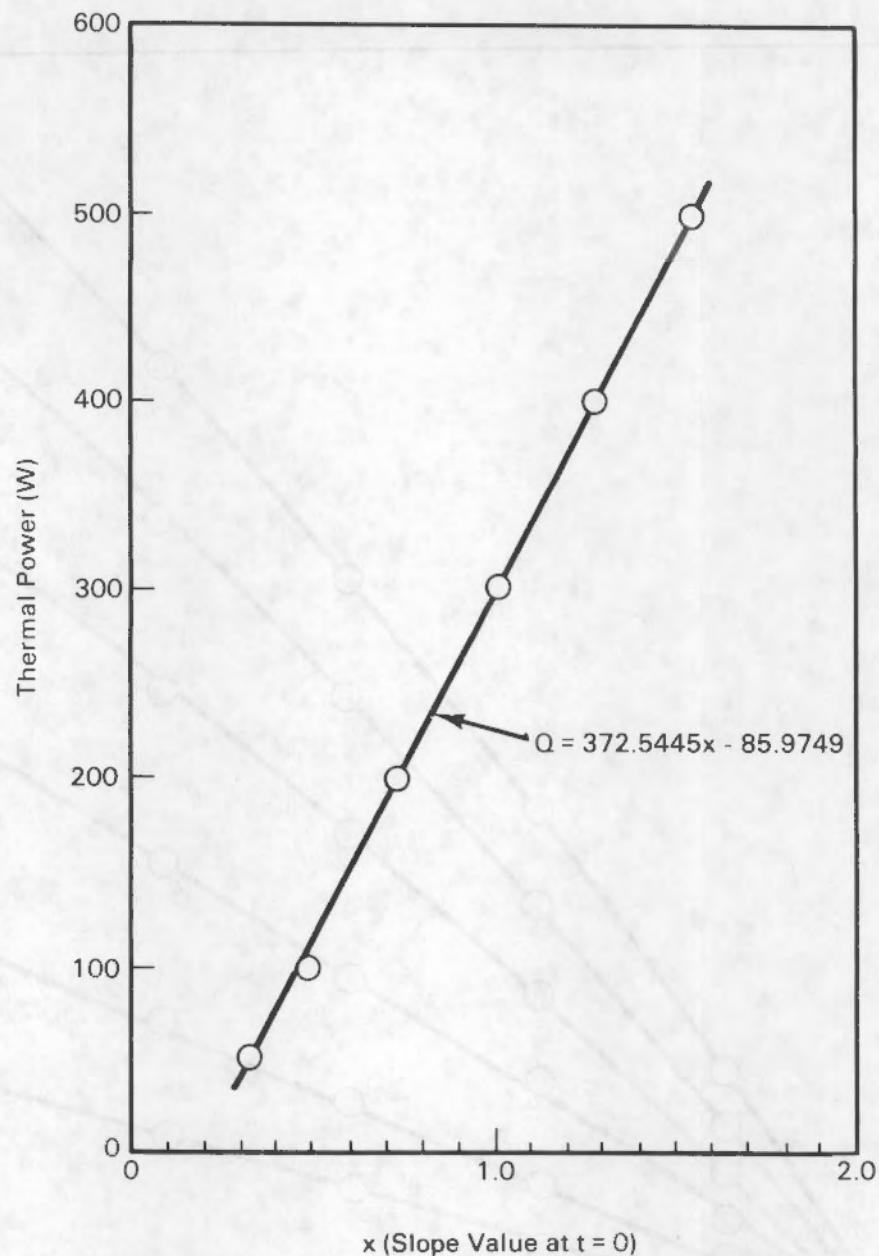


FIGURE D.1. October 1984 Calorimeter Calibration Heat-Up Curves



**FIGURE D.2.** October 1984 Calorimeter Calibration Curve

seen in Table D.1, the polynomial equation gave a very good fit to the data above 50 W (index of determination values generally greater than 0.9999). The repeatability of the calibrations at 200 W was better than 0.2%. Previous calibrations show that the repeatability of data is better at higher power outputs than at lower power outputs.



TABLE D.1. October 1984 Calorimeter Calibration Data

Calibration Run Date	Design Power, W	Measured Power, W <sup>(a)</sup>	Slope Value	Index of Determination	Curve Fit, W <sup>(b)</sup>	Percentage Difference <sup>(c)</sup>
10/13/84	200	199.6	0.765893	0.999998	199.4	-0.1
10/13/84	400	398.9	1.291536	0.999999	395.1	-1.0
10/14/84	300	298.8	1.028286	0.999993	297.1	-0.6
10/14/84	100	99.7	0.522143	0.999984	108.5	+8.8
10/15/84	50	49.2	0.352357	0.99996	45.3	-7.9
10/15/84	200	199.7	0.758893	0.999995	199.4	-0.2
10/16/84	500	492.6	1.562893	0.999997	496.3	+0.7
10/16/84	0	0.0	0.156464	0.99959	-27.7	

(a) Actual watts are 5-hour averages, corrected for power loss in lines to calibration heater.

(b) Calibration curve determined from linear regression of all slope values excluding the zero run. Power = 372.5445 (slope value) - 85.9749; correlation coefficient = 0.9996.

(c) Percentage difference =  $\frac{(\text{Curve Fit Value}) - (\text{Measured Value})}{(\text{Measured Value})} \times 100$

To calculate the decay heat of a spent fuel assembly, two corrections have to be made to the thermal value determined from the calibration curve. First, a correction must be made for the difference in heat capacity between the calorimeter with an electric heater and the calorimeter with a fuel assembly. The second correction involves compensating for the gamma energy that escapes from the calorimeter. The amount of gamma energy escaping from the vessel was measured with the three gamma sensors located on the outside of the calorimeter and one inside the calorimeter. In total, twelve radiation readings were taken for each fuel assembly. These readings were averaged and multiplied by a conversion factor to calculate the number of watts lost from the calorimeter due to gamma radiation. The average of the twelve readings is included as part of the calorimeter data. The methodology used in determining the conversion factor was originated in 1981 during initial calorimetry work for the DOE (Judson et al. 1982), and then modified based upon measurement of the actual amount of absorption that occurred in the outer wall of the calorimeter. The specifics relating to the development of these correction factors follow.

#### DETERMINATION OF HEAT CAPACITY CORRECTION FACTOR

##### I. Calibration Runs

- A. Volume of water in calorimeter = 133.4 gal measured heater attached.  
Weight of water =  $(144.5)(8.3 \text{ lb/gal}) = 1107.2 \text{ lb}$
- B. Weight of pipe holding calibration heater = 151 lb
- C. Heat capacity of system  
 $(1107.2 \text{ lb})(1.0 \text{ Btu/lb}^\circ\text{F}) = 1107.2 \text{ Btu/}^\circ\text{F}$   
 $(151 \text{ lb})(0.11 \text{ Btu/lb}^\circ\text{F}) = \frac{16.6 \text{ Btu/}^\circ\text{F}}{1123.8 \text{ Btu/}^\circ\text{F}}$

##### II. BWR - Dresden Fuel Element

- A. Volume of water in calorimeter  
 BWR fuel assembly displaces 8.08 gal  
 $(8.08 \text{ gal})(8.3 \text{ lb/gal}) = 67.1 \text{ lb}$



$$\begin{array}{r} \text{Thus, } 1107.2 \\ - 67.1 \\ \hline \end{array}$$

1040.1 lb in calorimeter

B. From published information

$$\text{UO}_2 = 398.8 \text{ lb (197 kg U/bundle)}$$

$$\text{Weight of hardware} = 216.8 \text{ lb}$$

C. Heat capacity of system

During fuel runs, the calibration heater was removed; therefore, the volume of water would be increased slightly.

$$151 \text{ lb as steel} = 18.2 \text{ lb as water (equal volumes)}$$

$$1040.1 \text{ lb}$$

$$+ 18.2 \text{ lb}$$

$$\hline 1058.3 \text{ lb}$$

$$(1058.3 \text{ lb})(1.0 \text{ Btu/}^\circ\text{F}) = 1058.3 \text{ Btu/}^\circ\text{F}$$

$$(398.8 \text{ lb})(0.06 \text{ Btu/}^\circ\text{F}) = 23.9 \text{ Btu/}^\circ\text{F}$$

$$(216.8 \text{ lb})(0.11 \text{ Btu/}^\circ\text{F}) = 23.8 \text{ Btu/}^\circ\text{F}$$

$$\hline 1106.0 \text{ Btu/}^\circ\text{F}$$

$$\frac{1123.8 - 1106.0}{1123.8} = 0.0158$$

$$\text{Correction factor} = 1 - 0.0158 = 0.9842$$

The correction factor is used to reduce the measured thermal output ("Slope" watts) to correct for bias between heat capacity of system during calibration and actual fuel assembly runs.

$$\text{Thus: (Measured watts)}(0.9842) = \text{corrected watts.}$$

#### CORRECTION FOR GAMMA HEAT LOST FROM THE CALORIMETER VESSEL

Because the walls of the calorimeter are not thick, some radiation passes through and does not contribute to the temperature rise within the calorimeter. It is essentially "lost" and, if not compensated for, will result in a negative bias in the calorimetric determination of the thermal output of the fuel.

In this analysis the following bases and assumptions apply:

1. Gamma energy absorbed in the inner steel shell of the calorimeter is transferred as heat to the water in the calorimeter.

2. Gamma energy absorbed by the foam insulation is insignificant and is ignored.
3. Gamma energy absorbed in the outer steel shell of the calorimeter is transferred to the basin water.
4. From dose rate measurements made by ion chambers mounted on both sides of the outer shell, the attenuation factor due to the steel shell was determined to be 2.16.

The average energy of the gamma radiation traversing the outer shell may be calculated from the attenuation coefficient using the expression

$$\frac{I}{I_0} = e^{-\mu x}$$

where  $I$  = intensity of the transmitted radiation  
 $I_0$  = intensity of the incident radiation  
 $x$  = surface density of the absorber =  $\text{g/cm}^2$   
 $\mu$  = mass attenuation coefficient -  $\text{cm}^2/\text{g}$ .

The wall thickness is 0.375 in. (0.953 cm) and the surface density (0.953 cm) is multiplied by the shell's density ( $7.86 \text{ g/cm}^3$ ) or  $7.49 \text{ g/cm}^2$ .

$$\mu = \frac{1}{x} \ln \frac{I_0}{I} \quad \text{or} \quad \mu = \frac{1}{7.49} \ln 2.16 = 0.1028$$

A mass attenuation coefficient of 0.1028 for iron corresponds to a gamma energy of 0.345 MeV (U.S. HEW 1970, p. 138).

At an energy of 0.345 MeV, 1 R/hr is equivalent to an energy fluence rate of  $5.25 \times 10^5 \text{ MeV/cm}^2$  (U.S. HEW 1970, p. 132).

Because 1 W is equal to  $6.24 \times 10^{12} \text{ MeV/sec}$ ,

$$1 \text{ R/hr} = \frac{5.25 \times 10^5 \text{ MeV}}{\text{cm}^2 \text{ sec}} \times \frac{1 \text{ watt sec}}{6.24 \times 10^{12} \text{ MeV}} = \frac{8.41 \times 10^{-8} \text{ watt}}{\text{cm}^2}$$



The calorimeter vessel is 15 ft long and 22 in. in diameter. Its surface area at the inner surface of the outer shell is  $3.1416 \times 21.25 \text{ in.} \times 180 \text{ in.} + 2 (3.1416)(21.25/2)^2 = 12,795 \text{ in.}^2 = 82,550 \text{ cm}^2$ .

For an outer surface dose rate of 1 R/hr the inner surface dose rate is 2.16 R/hr. Hence, the gamma energy lost from the calorimeter for an outer surface dose rate of 1 R/hr is

$$2.16 \text{ R/hr} \frac{82,550 \text{ cm}^2 \times 8.41 \times 10^{-8} \text{ watt}}{\text{cm}^2 \text{ R/hr}} = 0.01499 \text{ watts}$$

$$\text{correction factor} = \frac{0.01499 \text{ watts}}{1 \text{ R/hr gamma at outer surface}}$$

#### REFERENCES

U.S. Department of Health, Education and Welfare. 1970. Radiological Health Handbook. Revised Ed., U.S. Government Printing Office, Washington, D.C.

Judson, B. F., H. R. Strickler, J. W. Doman, K. J. Eger and Y. J. Lee. 1982. In-Plant Test Measurement of Spent Fuel Storage at Morris Operation: Volume 3 - Fuel Bundle Heat Generation Rates. NEDG-24922-3, General Electric Company, San Jose, California.

Bundle ID	CZ147	
Date/Time Bundle Loaded	11-04-84	08:22
Date/Time Bundle Removed	11-04-84	15:00

<u>t</u>	<u>Delta T<sub>c</sub></u>	<u>Delta T<sub>v</sub></u>	<u>T<sub>pit</sub></u>	<u>Pump Power, W</u>
0	0.00	1.00	77.39	253.0
1	0.89	1.84	77.41	252.3
2	1.72	2.60	77.42	251.7
3	2.49	3.33	77.43	251.6
4	3.20	3.99	77.46	251.6
5	3.88	4.63	77.47	251.4

"b" Coefficient	0.9108931
Index of Determination	0.999985
Slope Watts	253.3733
Corrected Slope Watts (0.9842)	249.37
Ave. Corrected Radiation Value	1818.8 R/hr
Gamma Watts (0.01499)	27.3
Total Thermal Output	276.7

Bundle ID	CZ148	
Date/Time Bundle Loaded	10-23-84	17:04
Date/Time Bundle Removed	10-23-84	23:30

<u>t</u>	<u>Delta T<sub>c</sub></u>	<u>Delta T<sub>v</sub></u>	<u>T<sub>pit</sub></u>	<u>Pump Power, W</u>
0	0.00	1.02	76.00	--
1	0.88	1.84	76.01	2.56
2	1.70	2.62	76.03	2.51
3	2.48	3.34	76.05	2.50
4	3.19	4.03	76.06	2.49
5	3.86	4.67	76.08	2.46

"b" Coefficient	0.9047501
Index of Determination	0.999995
Slope Watts	251.1
Corrected Slope Watts (0.9842)	247.1
Ave. Corrected Radiation Value	1740 R/hr
Gamma Watts (0.01499)	26.4
Total Thermal Output	273.5



Bundle ID	CZ182	
Date/Time Bundle Loaded	9-27-84	20:24
Date/Time Bundle Removed	9-28-84	03:20

t	Delta $T_c$	Delta $T_v$	$T_{pit}$	Pump Power, W
0	0.00	1.01	80.76	--
1	1.05	1.99	80.76	--
2	2.02	2.95	80.77	--
3	2.93	3.81	80.78	--
4	3.77	4.61	80.78	--
5	4.55	5.33	80.79	--

"b" Coefficient	1.0761071
Index of Determination	0.999997
Slope Watts	314.92288
Corrected Slope Watts (0.9842)	309.9471
Ave. Corrected Radiation Value	2184.4 R/hr
Gamma Watts (0.01499)	32.7
Total Thermal Output	342.6

Bundle ID	CZ195	
Date/Time Bundle Loaded	10-29-84	18:14
Date/Time Bundle Removed	10-30-84	01:30

t	Delta $T_c$	Delta $T_v$	$T_{pit}$	Pump Power, W
0	0.00	1.00	78.73	252.1
1	0.84	1.83	78.75	252.2
2	1.61	2.58	78.76	252.2
3	2.32	3.30	78.78	251.8
4	2.99	3.94	78.79	251.5
5	3.61	4.55	78.81	251.3

"b" Coefficient	0.8542
Index of Determination	0.999982
Slope Watts	232.25
Corrected Slope Watts (0.9842)	228.6
Ave. Corrected Radiation Value	1796.5 R/hr
Gamma Watts (0.01499)	26.9
Total Thermal Output	255.5

Bundle ID	CZ205	
Date/Time Bundle Loaded	9-24-84	06:30
Date/Time Bundle Removed	9-24-84	13:30

t	Delta $T_c$	Delta $T_v$	$T_{pit}$	Pump Power, W
0	0.00	0.98	79.81	--
1	1.01	1.96	79.82	--
2	1.93	2.88	79.82	--
3	2.80	3.75	79.84	--
4	3.62	4.54	79.84	--
5	4.37	5.26	79.85	--

"b" Coefficient	1.0246429
Index of Determination	0.999986
Slope Watts	295.75
Corrected Slope Watts (0.9842)	291.07
Ave. Corrected Radiation Value	2196.3 R/hr
Gamma Watts (0.01499)	32.9
Total Thermal Output	324

Bundle ID	CZ205	
Date/Time Bundle Loaded	10-04-84	19:57
Date/Time Bundle Removed	10-05-84	03:00

t	Delta $T_c$	Delta $T_v$	$T_{pit}$	Pump Power, W
0	0.00	1.00	77.16	--
1	1.12	2.05	77.19	--
2	2.11	3.02	77.23	--
3	3.05	3.93	77.26	--
4	3.91	4.75	77.28	--
5	4.71	5.53	77.31	--

"b" Coefficient	1.1281429
Index of Determination	0.999961
Slope Watts	334.3
Corrected Slope Watts (0.9842)	329.02
Ave. Corrected Radiation Value	2167.6 R/hr
Gamma Watts (0.01499)	32.5
Total Thermal Output	361.5



Bundle ID	CZ205	
Date/Time Bundle Loaded	10-08-84	15:08
Date/Time Bundle Removed	10-08-84	21:10

<u>t</u>	<u>Delta T<sub>c</sub></u>	<u>Delta T<sub>v</sub></u>	<u>T<sub>pit</sub></u>	<u>Pump Power, W</u>
0	0.00	1.00	76.70	--
1	1.05	2.02	76.72	--
2	2.04	2.99	76.74	--
3	2.95	3.87	76.75	--
4	3.81	4.70	76.78	--
5	4.60	5.47	76.80	--

"b" Coefficient	1.0822143
Index of Determination	0.999997
Slope Watts	317.198
Corrected Slope Watts (0.9842)	312.18
Ave. Corrected Radiation Value	2095 R/hr
Gamma Watts (0.01499)	31.3
Total Thermal Output	343.5

Bundle ID	CZ205	
Date/Time Bundle Loaded	10-09-84	10:42
Date/Time Bundle Removed	10-09-84	16:45

<u>t</u>	<u>Delta T<sub>c</sub></u>	<u>Delta T<sub>v</sub></u>	<u>T<sub>pit</sub></u>	<u>Pump Power, W</u>
0	0.00	1.00	76.91	--
1	1.08	2.07	76.93	--
2	2.08	3.00	76.95	--
3	3.02	3.90	76.96	--
4	3.90	4.74	76.98	--
5	4.70	5.49	77.00	--

"b" Coefficient	1.1078571
Index of Determination	0.999996
Slope Watts	326.75
Corrected Slope Watts (0.9842)	321.58
Ave. Corrected Radiation Value	2005 R/hr
Gamma Watts (0.01499)	31.3
Total Thermal Output	352.9

Bundle ID	CZ205	
Date/Time Bundle Loaded	10-22-84	20:54
Date/Time Bundle Removed	10-23-84	03:23

t	Delta T <sub>c</sub>	Delta T <sub>v</sub>	T <sub>pit</sub>	Pump Power, W
0	0.00	1.02	75.61	--
1	1.02	2.01	75.65	--
2	1.98	2.92	75.67	--
3	2.88	3.81	75.69	--
4	3.72	4.62	75.71	--
5	4.50	5.35	75.73	--

"b" Coefficient	1.0500000e 00
Index of Determination	1
Slope Watts	305.2
Corrected Slope Watts (0.9842)	300.4
Ave. Corrected Radiation Value	2095 R/hr
Gamma Watts (0.01499)	31.3
Total Thermal Output	331.7

Bundle ID	CZ205	
Date/Time Bundle Loaded	10-24-84	11:17
Date/Time Bundle Removed	10-24-84	17:19

t	Delta T <sub>c</sub>	Delta T <sub>v</sub>	T <sub>pit</sub>	Pump Power, W
0	0.00	1.01	76.34	2.56
1	1.04	2.00	76.37	2.50
2	2.01	2.93	76.40	2.50
3	2.91	3.79	76.43	2.57
4	3.74	4.60	76.46	2.64
5	4.52	5.33	76.47	2.68

"b" Coefficient	1.0689286
Index of Determination	0.999995
Slope Watts	312.2
Corrected Slope Watts (0.9842)	307.3
Ave. Corrected Radiation Value	2095 R/hr
Gamma Watts (0.01499)	31.3
Total Thermal Output	338.6



Bundle ID	CZ205	
Date/Time Bundle Loaded	10-29-84	09:24
Date/Time Bundle Removed	10-29-84	16:22

<u>t</u>	<u>Delta T<sub>c</sub></u>	<u>Delta T<sub>v</sub></u>	<u>T<sub>pit</sub></u>	<u>Pump Power, W</u>
0	0.00	1.01	78.59	253.0
1	1.01	2.00	78.61	252.4
2	1.94	2.92	78.61	252.3
3	2.83	3.78	78.64	251.8
4	3.63	4.58	78.65	251.3
5	4.38	5.30	78.68	250.9

"b" Coefficient	1.038214
Index of Determination	0.99999
Slope Watts	300.806
Corrected Slope Watts (0.9842)	296.0532
Ave. Corrected Radiation Value	2095 R/hr
Gamma Watts (0.01499)	31.3
Total Thermal Output	327.4

Bundle ID	CZ205	
Date/Time Bundle Loaded	11-02-84	12:02
Date/Time Bundle Removed	11-02-84	19:00

<u>t</u>	<u>Delta T<sub>c</sub></u>	<u>Delta T<sub>v</sub></u>	<u>T<sub>pit</sub></u>	<u>Pump Power, W</u>
0	0.00	1.01	77.63	--
1	0.98	1.99	77.63	--
2	1.87	2.88	77.64	--
3	2.70	3.67	77.65	--
4	3.46	4.44	77.65	--
5	4.17	5.13	77.65	--

"b" Coefficient	0.9989644
Index of Determination	0.999985
Slope Watts	286.1838
Corrected Slope Watts (0.9842)	281.6621
Ave. Corrected Radiation Value	2095 R/hr
Gamma Watts (0.01499)	31.3
Total Thermal Output	313.0

Bundle ID	CZ205	
Date/Time Bundle Loaded	11-05-84	14:32
Date/Time Bundle Removed	11-05-84	21:39

<u>t</u>	<u>Delta T<sub>c</sub></u>	<u>Delta T<sub>v</sub></u>	<u>T<sub>pit</sub></u>	<u>Pump Power, W</u>
0	0.00	1.02	78.04	254.9
1	0.96	1.98	78.04	253.5
2	1.86	2.87	78.05	252.9
3	2.70	3.71	78.07	252.8
4	3.47	4.49	78.08	253.0
5	4.18	5.20	78.09	253.1

"b" Coefficient	0.9943216
Index of Determination	0.999999
Slope Watts	284.4541
Corrected Slope Watts (0.9842)	279.9597
Ave. Corrected Radiation Value	2095 R/hr
Gamma Watts (0.01499)	31.3
Total Thermal Output	311.3

Bundle ID	CZ205	
Date/Time Bundle Loaded	12-05-84	19:21
Date/Time Bundle Removed	12-06-84	01:45

<u>t</u>	<u>Delta T<sub>c</sub></u>	<u>Delta T<sub>v</sub></u>	<u>T<sub>pit</sub></u>	<u>Pump Power, W</u>
0	0.00	1.01	81.31	251.1
1	0.97	1.96	81.34	250.4
2	1.86	2.84	81.35	249.8
3	2.70	3.65	81.34	249.3
4	3.46	4.41	81.35	249.1
5	4.15	5.10	81.38	249.1

"b" Coefficient	1.001714
Index of Determination	0.999995
Slope Watts	287.2081
Corrected Slope Watts (0.9842)	282.6702
Ave. Corrected Radiation Value	2091 R/hr
Gamma Watts (0.01499)	31.3
Total Thermal Output	314.0



Bundle ID	CZ205	
Date/Time Bundle Loaded	12-11-84	23:06
Date/Time Bundle Removed	12-12-84	05:25

<u>t</u>	<u>Delta T<sub>c</sub></u>	<u>Delta T<sub>v</sub></u>	<u>T<sub>pit</sub></u>	<u>Pump Power, W</u>
0	0.00	1.02	82.56	251.4
1	1.02	2.00	82.55	251.8
2	1.98	2.95	82.56	251.9
3	2.87	3.82	82.58	251.9
4	3.68	4.63	82.57	251.9
5	4.46	5.38	82.59	252.0

"b" Coefficient	1.051286
Index of Determination	0.999984
Slope Watts	305.6759
Corrected Slope Watts (0.9842)	300.8462
Ave. Corrected Radiation Value	2021.9 R/hr
Gamma Watts (0.01499)	30.3
Total Thermal Output	331.1

Bundle ID	CZ205	
Date/Time Bundle Loaded	12-21-84	19:09
Date/Time Bundle Removed	12-22-84	01:40

<u>t</u>	<u>Delta T<sub>c</sub></u>	<u>Delta T<sub>v</sub></u>	<u>T<sub>pit</sub></u>	<u>Pump Power, W</u>
0	0.00	1.01	81.59	251.3
1	0.99	1.94	81.62	251.5
2	1.88	2.81	81.63	251.8
3	2.68	3.60	81.65	251.4
4	3.42	4.30	81.66	251.3
5	4.09	4.93	81.67	251.4

"b" Coefficient	1.011857
Index of Determination	0.99997
Slope Watts	290.9869
Corrected Slope Watts (0.9842)	286.3893
Ave. Corrected Radiation Value	2052 R/hr
Gamma Watts (0.01499)	30.8
Total Thermal Output	317.2

Bundle ID	CZ205	
Date/Time Bundle Loaded	5-13-85	14:10
Date/Time Bundle Removed	5-14-85	01:31

<u>t</u>	<u>Delta T<sub>c</sub></u>	<u>Delta T<sub>v</sub></u>	<u>T<sub>pit</sub></u>	<u>Pump Power, W</u>
0	0.00	1.01	75.43	--
1	0.93	1.86	75.46	248.3
2	1.79	2.68	75.46	247.0
3	2.59	3.46	75.48	246.5
4	3.33	4.19	75.50	246.1
5	4.05	4.85	75.53	245.9

"b" Coefficient	0.94375
Index of Determination	0.999966
Slope Watts	265.61
Corrected Slope Watts (0.9842)	261.5
Ave. Corrected Radiation Value	1886 R/hr
Gamma Watts (0.01499)	28.3
Total Thermal Output	289.7

Bundle ID	CZ205	
Date/Time Bundle Loaded	5-28-85	04:45
Date/Time Bundle Removed	5-28-85	16:00

<u>t</u>	<u>Delta T<sub>c</sub></u>	<u>Delta T<sub>v</sub></u>	<u>T<sub>pit</sub></u>	<u>Pump Power, W</u>
0	0.00	1.00	73.09	--
1	0.99	1.95	73.12	251.84
2	1.88	2.81	73.15	251.39
3	2.70	3.57	73.19	250.94
4	3.46	4.28	73.21	250.66
5	4.19	4.96	73.25	250.55

"b" Coefficient	0.9962144
Index of Determination	0.999934
Slope Watts	285.1
Corrected Slope Watts (0.9842)	280.6
Ave. Corrected Radiation Value	1818 R/hr
Gamma Watts (0.01499)	27.3
Total Thermal Output	308.0



Bundle ID	CZ209	
Date/Time Bundle Loaded	10-28-84	14:55
Date/Time Bundle Removed	10-28-84	22:12

<u>t</u>	<u>Delta T<sub>c</sub></u>	<u>Delta T<sub>v</sub></u>	<u>T<sub>pit</sub></u>	<u>Pump Power, W</u>
0	0.00	1.03	78.22	252.1
1	0.89	1.90	78.28	251.8
2	1.73	2.69	78.26	251.7
3	2.50	3.44	78.31	251.4
4	3.23	4.16	78.32	251.4
5	3.88	4.76	78.32	251.4

"b" Coefficient	0.9233
Index of Determination	0.99991
Slope Watts	258.9901
Corrected Slope Watts (0.9842)	253.9139
Ave. Corrected Radiation Value	1707 R/hr
Gamma Watts (0.01499)	25.6
Total Thermal Output	279.5

Bundle ID	CZ211	
Date/Time Bundle Loaded	10-01-84	20:12
Date/Time Bundle Removed	10-01-84	03:10

<u>t</u>	<u>Delta T<sub>c</sub></u>	<u>Delta T<sub>v</sub></u>	<u>T<sub>pit</sub></u>	<u>Pump Power, W</u>
0	0.00	1.00	75.82	--
1	0.94	1.89	75.84	--
2	1.80	2.69	75.87	--
3	2.61	3.45	75.91	--
4	3.37	4.14	75.95	--
5	4.07	4.78	75.97	--

"b" Coefficient	0.95571429
Index of Determination	0.99999
Slope Watts	270.07
Corrected Slope Watts (0.9842)	265.8
Ave. Corrected Radiation Value	2015.4 R/hr
Gamma Watts (0.01499)	30.2
Total Thermal Output	296

Bundle ID	CZ211	
Date/Time Bundle Loaded	5-20-85	11:43
Date/Time Bundle Removed	5-20-85	21:48

<u>t</u>	<u>Delta T<sub>c</sub></u>	<u>Delta T<sub>v</sub></u>	<u>T<sub>pit</sub></u>	<u>Pump Power, W</u>
0	0.00	1.00	76.70	251.22
1	0.80	1.77	76.72	250.34
2	1.52	2.49	76.71	250.10
3	2.22	3.16	76.72	249.92
4	2.86	3.78	76.73	249.68
5	3.45	4.37	76.73	249.17

"b" Coefficient	0.81175
Index of Determination	0.999978
Slope Watts	216.4381
Corrected Slope Watts (0.9842)	213.0184
Ave. Corrected Radiation Value	1820.5 R/hr
Gamma Watts (0.01499)	27.3
Total Thermal Output	240.3

Bundle ID	CZ222	
Date/Time Bundle Loaded	11-04-84	17:10
Date/Time Bundle Removed	11-04-84	23:29

<u>t</u>	<u>Delta T<sub>c</sub></u>	<u>Delta T<sub>v</sub></u>	<u>T<sub>pit</sub></u>	<u>Pump Power, W</u>
0	0.00	1.00	77.53	251.0
1	1.07	2.03	77.54	251.8
2	2.08	2.96	77.57	252.1
3	3.02	3.89	77.59	252.4
4	3.87	4.68	77.60	252.2
5	4.66	5.45	77.62	251.9

"b" Coefficient	1.114714
Index of Determination	0.999994
Slope Watts	329.3057
Corrected Slope Watts (0.9842)	324.1026
Ave. Corrected Radiation Value	2107.1 R/hr
Gamma Watts (0.01499)	31.6
Total Thermal Output	355.7



Bundle ID	CZ225	
Date/Time Bundle Loaded	10-02-84	05:50
Date/Time Bundle Removed	10-02-84	14:16

<u>t</u>	<u>Delta T<sub>c</sub></u>	<u>Delta T<sub>v</sub></u>	<u>T<sub>pit</sub></u>	<u>Pump Power, W</u>
0	0.00	1.00	76.10	--
1	1.02	1.95	76.12	--
2	1.97	2.84	76.14	--
3	2.85	3.64	76.17	--
4	3.69	4.42	76.21	--
5	4.47	5.13	76.23	--

"b" Coefficient	1.039
Index of Determination	0.999989
Slope Watts	301.09
Corrected Slope Watts (0.9842)	296.34
Ave. Corrected Radiation Value	2069.65 R/hr
Gamma Watts (0.01499)	31.0
Total Thermal Output	327.3

Bundle ID	CZ234	
Date/Time Bundle Loaded	10-30-84	03:45
Date/Time Bundle Removed	10-30-84	10:30

<u>t</u>	<u>Delta T<sub>c</sub></u>	<u>Delta T<sub>v</sub></u>	<u>T<sub>pit</sub></u>	<u>Pump Power, W</u>
0	0.00	1.00	78.96	253.1
1	1.10	2.06	79.00	252.5
2	2.14	3.11	79.03	252.3
3	3.10	4.03	79.04	252.0
4	4.00	4.91	79.07	251.6
5	4.82	5.71	79.09	251.5

"b" Coefficient	1.139571
Index of Determination	0.999998
Slope Watts	338.566
Corrected Slope Watts (0.9842)	333.2167
Ave. Corrected Radiation Value	2222 R/hr
Gamma Watts (0.01499)	33.3
Total Thermal Output	366.5

Bundle ID	CZ246	
Date/Time Bundle Loaded	11-02-84	02:04
Date/Time Bundle Removed	11-02-84	08:45

<u>t</u>	<u>Delta T<sub>c</sub></u>	<u>Delta T<sub>v</sub></u>	<u>T<sub>pit</sub></u>	<u>Pump Power, W</u>
0	0.00	1.09	78.61	253.1
1	0.99	2.17	78.49	253.2
2	1.89	3.19	78.39	253.1
3	2.72	4.17	78.27	253.2
4	3.48	5.07	78.13	253.3
5	4.15	5.87	78.00	253.1

"b" Coefficient	1.022857
Index of Determination	0.999995
Slope Watts	295.0849
Corrected Slope Watts (0.9842)	290.4225
Ave. Corrected Radiation Value	2032.8 R/hr
Gamma Watts (0.01499)	30.5
Total Thermal Output	320.9

Bundle ID	CZ246	
Date/Time Bundle Loaded	11-05-84	02:55
Date/Time Bundle Removed	11-05-84	09:45

<u>t</u>	<u>Delta T<sub>c</sub></u>	<u>Delta T<sub>v</sub></u>	<u>T<sub>pit</sub></u>	<u>Pump Power, W</u>
0	0.00	1.01	77.75	251.7
1	1.05	2.03	77.76	253.0
2	2.02	2.98	77.79	253.3
3	2.91	3.86	77.82	253.1
4	3.73	4.63	77.83	253.1
5	4.49	5.31	77.87	253.6

"b" Coefficient	1.079607
Index of Determination	0.9999929
Slope Watts	316.2268
Corrected Slope Watts (0.9842)	311.2304
Ave. Corrected Radiation Value	2032 R/hr
Gamma Watts (0.01499)	30.5
Total Thermal Output	341.7



Bundle ID	CZ259	
Date/Time Bundle Loaded	10-29-84	00:40
Date/Time Bundle Removed	10-29-84	07:17

<u>t</u>	<u>Delta T<sub>c</sub></u>	<u>Delta T<sub>y</sub></u>	<u>T<sub>pit</sub></u>	<u>Pump Power, W</u>
0	0.00	1.00	78.48	249.5
1	0.82	1.80	78.50	249.6
2	1.57	2.51	78.48	249.5
3	2.28	3.23	78.52	249.4
4	2.94	3.97	78.52	249.4
5	3.55	4.46	78.52	249.5

"b" Coefficient	0.835035
Index of Determination	0.999992
Slope Watts	225.1131
Corrected Slope Watts (0.9842)	221.5563
Ave. Corrected Radiation Value	1739 R/hr
Gamma Watts (0.01499)	26.1
Total Thermal Output	247.7

Bundle ID	CZ259	
Date/Time Bundle Loaded	12-20-84	10:58
Date/Time Bundle Removed	12-20-84	17:28

<u>t</u>	<u>Delta T<sub>c</sub></u>	<u>Delta T<sub>y</sub></u>	<u>T<sub>pit</sub></u>	<u>Pump Power, W</u>
0	0.00	1.01	81.07	--
1	0.93	1.91	81.10	--
2	1.78	2.72	81.10	--
3	2.57	3.49	81.14	--
4	3.33	4.20	81.16	--
5	4.01	4.86	81.18	--

"b" Coefficient	0.9448929
Index of Determination	0.999978
Slope Watts	266.0397
Corrected Slope Watts (0.9842)	261.8363
Ave. Corrected Radiation Value	1781 R/hr
Gamma Watts (0.01499)	26.7
Total Thermal Output	288.5

Bundle ID	CZ259	
Date/Time Bundle Loaded	5-14-85	09:55
Date/Time Bundle Removed	5-14-85	17:27

<u>t</u>	<u>Delta T<sub>c</sub></u>	<u>Delta T<sub>v</sub></u>	<u>T<sub>pit</sub></u>	<u>Pump Power, W</u>
0	0.00	1.00	75.88	246.7
1	0.85	1.80	75.88	246.2
2	1.60	2.52	75.91	245.6
3	2.29	3.17	75.93	244.8
4	2.92	3.78	75.95	244.3
5	3.52	4.33	75.96	244

"b" Coefficient	0.8544644
Index of Determination	0.999918
Slope Watts	232.3511
Corrected Slope Watts (0.9842)	228.68
Ave. Corrected Radiation Value	1693 R/hr
Gamma Watts (0.01499)	25.4
Total Thermal Output	254.1

Bundle ID	CZ264	
Date/Time Bundle Loaded	10-23-84	08:09
Date/Time Bundle Removed	10-23-84	15:00

<u>t</u>	<u>Delta T<sub>c</sub></u>	<u>Delta T<sub>v</sub></u>	<u>T<sub>pit</sub></u>	<u>Pump Power, W</u>
0	0.00	1.01	75.84	--
1	0.87	1.82	75.86	--
2	1.66	2.54	75.88	--
3	2.41	3.26	75.90	--
4	3.10	3.90	75.92	--
5	3.75	4.50	75.94	--

"b" Coefficient	8.8221429e-01
Index of Determination	0.999983
Slope Watts	242.7
Corrected Slope Watts (0.9842)	238.8
Ave. Corrected Radiation Value	1669 R/hr
Gamma Watts (0.01499)	25.0
Total Thermal Output	263.8



Bundle ID	<u>CZ277</u>	
Date/Time Bundle Loaded	<u>10-27-84</u>	<u>19:42</u>
Date/Time Bundle Removed	<u>10-28-84</u>	<u>02:06</u>

<u>t</u>	<u>Delta T<sub>c</sub></u>	<u>Delta T<sub>v</sub></u>	<u>T<sub>pit</sub></u>	<u>Pump Power, W</u>
0	0.00	1.00	77.89	250.1
1	0.85	1.84	77.90	248.8
2	1.65	2.59	77.93	248.7
3	2.38	3.29	77.94	248.2
4	3.08	3.95	77.98	247.9
5	3.70	4.56	77.99	247.7

"b" Coefficient	0.8790
Index of Determination	0.999987
Slope Watts	241.5
Corrected Slope Watts (0.9842)	237.7
Ave. Corrected Radiation Value	1671 R/hr
Gamma Watts (0.01499)	25.0
Total Thermal Output	262.7

Bundle ID	<u>CZ277</u>	
Date/Time Bundle Loaded	<u>5-26-85</u>	<u>16:41</u>
Date/Time Bundle Removed	<u>5-26-85</u>	<u>23:48</u>

<u>t</u>	<u>Delta T<sub>c</sub></u>	<u>Delta T<sub>v</sub></u>	<u>T<sub>pit</sub></u>	<u>Pump Power, W</u>
0	0.00	1.01	72.79	--
1	0.82	1.79	72.82	242.06
2	1.56	2.51	72.84	242.22
3	2.26	3.17	72.86	242.30
4	2.93	3.78	72.88	242.34
5	3.54	4.37	72.89	242.57

"b" Coefficient	0.8253216
Index of Determination	0.999969
Slope Watts	221.5
Corrected Slope Watts (0.9842)	218.0
Ave. Corrected Radiation Value	1668 R/hr
Gamma Watts (0.01499)	25.0
Total Thermal Output	243

Bundle ID	CZ286	
Date/Time Bundle Loaded	12-06-84	09:22
Date/Time Bundle Removed	12-06-84	17:50

<u>t</u>	<u>Delta T<sub>c</sub></u>	<u>Delta T<sub>v</sub></u>	<u>T<sub>pit</sub></u>	<u>Pump Power, W</u>
0	0.00	1.00	81.50	252.7
1	0.88	1.90	81.50	253.2
2	1.70	2.73	81.48	253.3
3	2.44	3.52	81.53	253.2
4	3.13	4.24	81.51	253.0
5	3.77	4.88	81.59	252.8

"b" Coefficient	0.9061429
Index of Determination	0.999985
Slope Watts	251.6037
Corrected Slope Watts (0.9842)	247.6283
Ave. Corrected Radiation Value	2058 R/hr
Gamma Watts (0.01499)	30.8
Total Thermal Output	278.4

Bundle ID	CZ286	
Date/Time Bundle Loaded	5-28-85	19:43
Date/Time Bundle Removed	5-29-85	02:30

<u>t</u>	<u>Delta T<sub>c</sub></u>	<u>Delta T<sub>v</sub></u>	<u>T<sub>pit</sub></u>	<u>Pump Power, W</u>
0	0.00	1.02	73.52	247.86
1	0.92	1.91	73.56	248.11
2	1.76	2.71	73.58	248.20
3	2.53	3.44	73.61	247.97
4	3.27	4.15	73.64	248.06
5	3.95	4.79	73.66	248.25

"b" Coefficient	0.9305715
Index of Determination	0.999966
Slope Watts	260.7
Corrected Slope Watts (0.9842)	256.6
Ave. Corrected Radiation Value	1841 R/hr
Gamma Watts (0.01499)	27.6
Total Thermal Output	284.2



Bundle ID	CZ296	
Date/Time Bundle Loaded	11-03-84	00:39
Date/Time Bundle Removed	11-03-84	08:15

<u>t</u>	<u>Delta T<sub>c</sub></u>	<u>Delta T<sub>v</sub></u>	<u>T<sub>pit</sub></u>	<u>Pump Power, W</u>
0	0.00	1.00	77.57	253.4
1	0.83	1.89	77.52	252.9
2	1.59	2.70	77.48	252.7
3	2.30	3.46	77.43	252.7
4	2.95	4.14	77.40	252.8
5	3.55	4.78	77.36	252.9

"b" Coefficient	0.8511072
Index of Determination	0.999995
Slope Watts	231.1004
Corrected Slope Watts (0.9842)	227.449
Ave. Corrected Radiation Value	1955 R/hr
Gamma Watts (0.01499)	29.3
Total Thermal Output	256.7

Bundle ID	CZ296	
Date/Time Bundle Loaded	5-21-85	01:19
Date/Time Bundle Removed	5-21-85	08:00

<u>t</u>	<u>Delta T<sub>c</sub></u>	<u>Delta T<sub>v</sub></u>	<u>T<sub>pit</sub></u>	<u>Pump Power, W</u>
0	0.00	1.00	76.73	248.16
1	0.83	1.80	76.73	247.78
2	1.59	2.53	76.74	247.89
3	2.29	3.19	76.74	247.85
4	2.94	3.84	76.75	247.97
5	3.55	4.41	76.75	247.97

"b" Coefficient	0.8454999
Index of Determination	0.99998
Slope Watts	229.0114
Corrected Slope Watts (0.9842)	225.3931
Ave. Corrected Radiation Value	1770 R/hr
Gamma Watts (0.01499)	26.5
Total Thermal Output	251.9

Bundle ID	<u>CZ302</u>	
Date/Time Bundle Loaded	<u>10-24-84</u>	<u>02:41</u>
Date/Time Bundle Removed	<u>10-24-84</u>	<u>09:00</u>

<u>t</u>	<u>Delta T<sub>c</sub></u>	<u>Delta T<sub>v</sub></u>	<u>T<sub>pit</sub></u>	<u>Pump Power, W</u>
0	0.00	1.01	76.16	--
1	0.91	1.88	76.18	2.04
2	1.76	2.70	76.19	2.02
3	2.54	3.47	76.22	2.02
4	3.28	4.16	76.24	2.01
5	3.96	4.80	76.25	1.99

"b" Coefficient	0.9331071
Index of Determination	0.999993
Slope Watts	261.6
Corrected Slope Watts (0.9842)	257.5
Ave. Corrected Radiation Value	1873 R/hr
Gamma Watts (0.01499)	28.1
Total Thermal Output	285.6

Bundle ID	<u>CZ308</u>	
Date/Time Bundle Loaded	<u>11-01-84</u>	<u>16:42</u>
Date/Time Bundle Removed	<u>11-01-84</u>	<u>23:21</u>

<u>t</u>	<u>Delta T<sub>c</sub></u>	<u>Delta T<sub>v</sub></u>	<u>T<sub>pit</sub></u>	<u>Pump Power, W</u>
0	0.00	0.99	79.04	252.6
1	0.87	1.84	79.04	253.6
2	1.68	2.64	79.04	253.9
3	2.42	3.30	79.05	254.0
4	3.11	4.02	79.07	253.8
5	3.74	4.73	79.05	253.5

"b" Coefficient	0.8974288
Index of Determination	0.999997
Slope Watts	248.3573
Corrected Slope Watts (0.9842)	244.4332
Ave. Corrected Radiation Value	1685.3 R/hr
Gamma Watts (0.01499)	25.3
Total Thermal Output	269.7



Bundle ID	CZ311	
Date/Time Bundle Loaded	10-26-84	18:29
Date/Time Bundle Removed	10-26-84	00:50

<u>t</u>	<u>Delta T<sub>c</sub></u>	<u>Delta T<sub>v</sub></u>	<u>T<sub>pit</sub></u>	<u>Pump Power, W</u>
0	0.00	0.99	77.45	253.0
1	1.09	2.05	77.46	252.6
2	2.08	3.00	77.50	252.3
3	3.00	3.91	77.53	252.2
4	3.85	4.70	77.54	251.9
5	4.61	5.44	77.55	251.4

"b" Coefficient	1.11875
Index of Determination	0.9999929
Slope Watts	330.8093
Corrected Slope Watts (0.9842)	325.5325
Ave. Corrected Radiation Value	2090 R/hr
Gamma Watts (0.01499)	31.3
Total Thermal Output	356.9

Bundle ID	CZ315	
Date/Time Bundle Loaded	12-07-84	18:46
Date/Time Bundle Removed	12-08-84	01:15

<u>t</u>	<u>Delta T<sub>c</sub></u>	<u>Delta T<sub>v</sub></u>	<u>T<sub>pit</sub></u>	<u>Pump Power, W</u>
0	0.00	1.00	82.05	250.0
1	1.01	2.01	82.13	251.2
2	1.94	2.94	82.15	250.8
3	2.82	3.80	82.16	250.3
4	3.61	4.60	82.18	250.3
5	4.36	5.34	82.18	250.3

"b" Coefficient	1.036929
Index of Determination	0.999989
Slope Watts	300.3273
Corrected Slope Watts (0.9842)	295.5821
Ave. Corrected Radiation Value	2161 R/hr
Gamma Watts (0.01499)	32.4
Total Thermal Output	328

Bundle ID	CZ318	
Date/Time Bundle Loaded	12-07-84	08:20
Date/Time Bundle Removed	12-07-84	15:40

t	$\Delta T_c$	$\Delta T_v$	$T_{pit}$	Pump Power, W
0	0.00	1.00	81.85	250.8
1	0.88	1.89	81.88	250.4
2	1.71	2.74	81.89	250.8
3	2.49	3.52	81.91	250.9
4	3.21	4.22	81.93	250.7
5	3.88	4.90	81.96	250.5

"b" Coefficient	0.9093216
Index of Determination	0.999999
Slope Watts	252.7879
Corrected Slope Watts (0.9842)	248.7938
Ave. Corrected Radiation Value	1923 R/hr
Gamma Watts (0.01499)	28.8
Total Thermal Output	277.6

Bundle ID	CZ337	
Date/Time Bundle Loaded	11-01-84	01:05
Date/Time Bundle Removed	11-01-84	07:28

t	$\Delta T_c$	$\Delta T_v$	$T_{pit}$	Pump Power, W
0	0.00	1.01	79.96	250.6
1	1.07	2.05	79.98	250.2
2	2.03	3.02	80.01	249.8
3	2.97	3.93	80.04	249.8
4	3.82	4.78	80.06	249.8
5	4.58	5.53	80.07	249.5

"b" Coefficient	1.094536
Index of Determination	0.999962
Slope Watts	321.7885
Corrected Slope Watts (0.9842)	316.7042
Ave. Corrected Radiation Value	2070.6 R/hr
Gamma Watts (0.01499)	31.0
Total Thermal Output	347.7



Bundle ID	CZ337	
Date/Time Bundle Loaded	5-24-85	14:49
Date/Time Bundle Removed	5-24-85	21:54

t	Delta $T_c$	Delta $T_v$	$T_{pit}$	Pump Power, W
0	0.00	0.99	71.73	--
1	0.95	1.87	71.76	246.03
2	1.83	2.72	71.79	246.05
3	2.67	3.50	71.82	245.44
4	3.44	4.19	71.85	245.08
5	4.16	4.82	71.87	244.91

"b" Coefficient	0.9724158
Index of Determination	0.999995
Slope Watts	276.3
Corrected Slope Watts (0.9842)	271.9
Ave. Corrected Radiation Value	1901 R/hr
Gamma Watts (0.01499)	28.5
Total Thermal Output	300.4

Bundle ID	CZ342	
Date/Time Bundle Loaded	12-06-84	22:10
Date/Time Bundle Removed	12-07-84	05:30

t	Delta $T_c$	Delta $T_v$	$T_{pit}$	Pump Power, W
0	0.00	1.01	81.69	249.1
1	0.90	1.93	81.69	249.0
2	1.73	2.78	81.70	249.3
3	2.52	3.57	81.72	249.3
4	3.25	4.30	81.73	249.3
5	3.92	4.99	81.75	249.3

"b" Coefficient	0.9223931
Index of Determination	0.999995
Slope Watts	257.6575
Corrected Slope Watts (0.9842)	253.5866
Ave. Corrected Radiation Value	1770 R/hr
Gamma Watts (0.01499)	26.5
Total Thermal Output	280.1

Bundle ID	CZ342	
Date/Time Bundle Loaded	5-26-85	03:07
Date/Time Bundle Removed	5-26-85	09:52

<u>t</u>	<u>Delta T<sub>c</sub></u>	<u>Delta T<sub>v</sub></u>	<u>T<sub>pit</sub></u>	<u>Pump Power, W</u>
0	0.00	1.01	72.36	--
1	0.97	1.92	72.39	246.94
2	1.85	2.75	72.42	246.99
3	2.65	3.52	72.45	247.11
4	3.42	4.24	72.48	247.25
5	4.14	4.91	72.52	247.23

"b" Coefficient	0.9751788
Index of Determination	0.999936
Slope Watts	277.3
Corrected Slope Watts (0.9842)	272.9
Ave. Corrected Radiation Value	1805 R/hr
Gamma Watts (0.01499)	27.1
Total Thermal Output	300.0

Bundle ID	CZ346	
Date/Time Bundle Loaded	10-27-84	11:46
Date/Time Bundle Removed	10-27-84	17:51

<u>t</u>	<u>Delta T<sub>c</sub></u>	<u>Delta T<sub>v</sub></u>	<u>T<sub>pit</sub></u>	<u>Pump Power, W</u>
0	0.00	1.01	77.77	--
1	1.17	2.17	77.76	--
2	2.24	3.21	77.79	--
3	3.26	4.19	77.81	--
4	4.20	5.12	77.83	--
5	5.06	5.92	77.85	--

"b" Coefficient	1.196536
Index of Determination	0.999992
Slope Watts	359.788
Corrected Slope Watts (0.9842)	354.1033
Ave. Corrected Radiation Value	2309 R/hr
Gamma Watts (0.01499)	34.6
Total Thermal Output	388.7

Bundle ID	CZ348	
Date/Time Bundle Loaded	10-31-84	16:46
Date/Time Bundle Removed	10-31-84	23:28

<u>t</u>	<u>Delta T<sub>c</sub></u>	<u>Delta T<sub>v</sub></u>	<u>T<sub>pit</sub></u>	<u>Pump Power, W</u>
0	0.00	1.02	79.79	252.1
1	1.04	2.01	79.80	251.9
2	2.01	2.96	79.84	251.8
3	2.94	3.84	79.86	251.3
4	3.75	4.63	79.87	250.9
5	4.53	5.36	79.90	250.3

"b" Coefficient	1.079214
Index of Determination	0.999969
Slope Watts	316.0803
Corrected Slope Watts (0.9842)	311.0863
Ave. Corrected Radiation Value	2117 R/hr
Gamma Watts (0.01499)	31.7
Total Thermal Output	342.8

Bundle ID	CZ351	
Date/Time Bundle Loaded	12-09-84	22:21
Date/Time Bundle Removed	12-10-84	04:45

<u>t</u>	<u>Delta T<sub>c</sub></u>	<u>Delta T<sub>v</sub></u>	<u>T<sub>pit</sub></u>	<u>Pump Power, W</u>
0	0.00	1.00	82.58	249.5
1	0.99	1.97	82.60	250.4
2	1.90	2.87	82.59	250.6
3	2.75	3.75	82.59	250.6
4	3.54	4.53	82.58	250.5
5	4.29	5.25	82.60	250.7

"b" Coefficient	1.005714
Index of Determination	0.999982
Slope Watts	288.6983
Corrected Slope Watts (0.9842)	284.1369
Ave. Corrected Radiation Value	1978 R/hr
Gamma Watts (0.01499)	29.7
Total Thermal Output	313.8



Bundle ID	CZ355	
Date/Time Bundle Loaded	10-28-84	04:46
Date/Time Bundle Removed	10-28-84	11:05

<u>t</u>	<u>Delta T<sub>c</sub></u>	<u>Delta T<sub>v</sub></u>	<u>T<sub>pit</sub></u>	<u>Pump Power, W</u>
0	0.00	1.00	78.06	250.6
1	0.94	1.92	78.08	250.7
2	1.78	2.71	78.07	251.0
3	2.57	3.49	78.11	251.2
4	3.29	4.19	78.12	251.1
5	3.96	4.84	78.14	251.1

"b" Coefficient	0.9531073
Index of Determination	0.999974
Slope Watts	269.1
Corrected Slope Watts (0.9842)	264.8482
Ave. Corrected Radiation Value	1712 R/hr
Gamma Watts (0.01499)	25.7
Total Thermal Output	290.5

Bundle ID	CZ357	
Date/Time Bundle Loaded	12-08-84	04:50
Date/Time Bundle Removed	12-08-84	12:55

<u>t</u>	<u>Delta T<sub>c</sub></u>	<u>Delta T<sub>v</sub></u>	<u>T<sub>pit</sub></u>	<u>Pump Power, W</u>
0	0.00	1.00	82.29	249.4
1	0.98	1.98	82.34	249.1
2	1.87	2.85	82.35	249.1
3	2.65	3.65	82.35	249.0
4	3.35	4.34	82.39	249.2
5	3.99	4.96	82.40	249.3

"b" Coefficient	1.01572
Index of Determination	0.999965
Slope Watts	292.1846
Corrected Slope Watts (0.9842)	287.5681
Ave. Corrected Radiation Value	2184 r/hr
Gamma Watts (0.01499)	32.7
Total Thermal Output	320.3

Bundle ID	CZ369	
Date/Time Bundle Loaded	10-25-84	04:59
Date/Time Bundle Removed	10-25-84	11:26

<u>t</u>	<u>Delta T<sub>c</sub></u>	<u>Delta T<sub>v</sub></u>	<u>T<sub>pit</sub></u>	<u>Pump Power, W</u>
0	0.00	1.00	76.83	--
1	1.06	2.02	76.86	2.23
2	2.05	2.97	76.88	2.24
3	2.95	3.84	76.92	2.25
4	3.78	4.64	76.94	2.29
5	4.54	5.36	76.97	2.34

"b" Coefficient	1.098500
Index of Determination	0.999997
Slope Watts	323.3
Corrected Slope Watts (0.9842)	318.2
Ave. Corrected Radiation Value	1966 R/hr
Gamma Watts (0.01499)	29.5
Total Thermal Output	347.7

Bundle ID	CZ370	
Date/Time Bundle Loaded	9-28-84	05:45
Date/Time Bundle Removed	9-28-84	13:10

<u>t</u>	<u>Delta T<sub>c</sub></u>	<u>Delta T<sub>v</sub></u>	<u>T<sub>pit</sub></u>	<u>Pump Power, W</u>
0	0.00	0.99	80.82	--
1	0.91	1.85	80.83	--
2	1.76	2.66	80.83	--
3	2.56	3.43	80.85	--
4	3.31	4.15	80.88	--
5	3.99	4.79	80.89	--

"b" Coefficient	0.93696427
Index of Determination	0.999996
Slope Watts	263.08
Corrected Slope Watts (0.9842)	258.92
Ave. Corrected Radiation Value	1951 R/hr
Gamma Watts (0.01499)	29.2
Total Thermal Output	288.1

Bundle ID	CZ372	
Date/Time Bundle Loaded	9-26-84	23:22
Date/Time Bundle Removed	9-27-84	07:55

<u>t</u>	<u>Delta T<sub>c</sub></u>	<u>Delta T<sub>v</sub></u>	<u>T<sub>pit</sub></u>	<u>Pump Power, W</u>
0	0.00	1.00	80.53	--
1	0.92	1.90	80.57	--
2	1.77	2.74	80.61	--
3	2.55	3.53	80.64	--
4	3.29	4.26	80.66	--
5	3.98	4.94	80.67	--

"b" Coefficient	0.93596428
Index of Determination	0.99998
Slope Watts	262.7
Corrected Slope Watts (0.9842)	258.56
Ave. Corrected Radiation Value	2017.4 R/hr
Gamma Watts (0.01499)	30.2
Total Thermal Output	288.8

Bundle ID	CZ379	
Date/Time Bundle Loaded	11-03-84	21:14
Date/Time Bundle Removed	11-04-84	

<u>t</u>	<u>Delta T<sub>c</sub></u>	<u>Delta T<sub>v</sub></u>	<u>T<sub>pit</sub></u>	<u>Pump Power, W</u>
0	0.00	0.99	77.33	--
1	0.92	1.89	77.33	--
2	1.78	2.71	77.34	--
3	2.59	3.49	77.34	--
4	3.34	4.22	77.35	--
5	4.05	4.87	77.36	--

"b" Coefficient	0.9421786
Index of Determination	0.999996
Slope Watts	265.0286
Corrected Slope Watts (0.9842)	260.8411
Ave. Corrected Radiation Value	1772.5 R/hr
Gamma Watts (0.01499)	26.6
Total Thermal Output	287.4



Bundle ID	CZ398	
Date/Time Bundle Loaded	10-27-84	02:51
Date/Time Bundle Removed	10-27-84	

<u>t</u>	<u>Delta T<sub>c</sub></u>	<u>Delta T<sub>v</sub></u>	<u>T<sub>pit</sub></u>	<u>Pump Power, W</u>
0	0.00	1.01	77.60	--
1	1.13	2.13	77.62	--
2	2.17	3.13	77.63	--
3	3.15	4.10	77.66	--
4	4.06	4.96	77.67	--
5	4.89	5.79	77.68	--

"b" Coefficient	1.158072
Index of Determination	0.999996
Slope Watts	345.4584
Corrected Slope Watts (0.9842)	340.00D2
Ave. Corrected Radiation Value	2138 R/hr
Gamma Watts (0.01499)	32
Total Thermal Output	372

Bundle ID	CZ415	
Date/Time Bundle Loaded	9-26-84	05:39
Date/Time Bundle Removed	9-26-84	12:50

<u>t</u>	<u>Delta T<sub>c</sub></u>	<u>Delta T<sub>v</sub></u>	<u>T<sub>pit</sub></u>	<u>Pump Power, W</u>
0	0.00	0.99	79.95	--
1	0.91	1.87	79.97	--
2	1.75	2.42	79.99	--
3	2.51	3.08	80.00	--
4	3.21	3.82	80.01	--
5	3.86	4.45	80.05	--

"b" Coefficient	0.93635713
Index of Determination	0.999984
Slope Watts	262.85
Corrected Slope Watts (0.9842)	258.7
Ave. Corrected Radiation Value	2039.47 R/hr
Gamma Watts (0.01499)	30.6
Total Thermal Output	289.3

Bundle ID	CZ416	
Date/Time Bundle Loaded	10-31-84	07:01
Date/Time Bundle Removed	10-31-84	13:15

t	Delta $T_c$	Delta $T_v$	$T_{pit}$	Pump Power, W
0	0.00	1.00	79.58	251.5
1	0.99	1.95	79.60	252.3
2	1.92	2.86	79.62	252.9
3	2.77	3.69	79.65	253.2
4	3.57	4.45	79.66	253.3
5	4.29	5.14	79.68	253.2

"b" Coefficient	1.02525
Index of Determination	0.999996
Slope Watts	295.9763
Corrected Slope Watts (0.9842)	291.2999
Ave. Corrected Radiation Value	1902.6 R/hr
Gamma Watts (0.01499)	28.5
Total Thermal Output	319.8

Bundle ID	CZ429	
Date/Time Bundle Loaded	10-26-84	07:39
Date/Time Bundle Removed	10-26-84	13:30

t	Delta $T_c$	Delta $T_v$	$T_{pit}$	Pump Power, W
0	0.00	1.00	77.23	--
1	1.15	2.13	77.26	2.51
2	2.23	3.19	77.26	2.50
3	3.26	4.17	77.30	2.50
4	4.21	5.12	77.31	2.54
5	5.09	5.95	77.33	2.57

"b" Coefficient	1.185822
Index of Determination	0.999996
Slope Watts	355.7966
Corrected Slope Watts (0.9842)	350.175
Ave. Corrected Radiation Value	2363 R/hr
Gamma Watts (0.01499)	35.4
Total Thermal Output	385.6

Bundle ID	CZ430	
Date/Time Bundle Loaded	10-30-84	22:39
Date/Time Bundle Removed	10-30-84	04:58

t	$\Delta T_c$	$\Delta T_v$	$T_{pit}$	Pump Power, W
0	0.00	1.00	79.42	251.6
1	1.08	2.06	79.43	251.3
2	2.08	3.01	79.46	251.7
3	3.00	3.91	79.49	251.7
4	3.85	4.73	79.50	251.6
5	4.64	5.49	79.52	251.4

"b" Coefficient	1.109608
Index of Determination	0.999994
Slope Watts	327.4035
Corrected Slope Watts (0.9842)	322.2305
Ave. Corrected Radiation Value	2075.7 R/hr
Gamma Watts (0.01499)	31.1
Total Thermal Output	353.3

Bundle ID	CZ433	
Date/Time Bundle Loaded	9-25-84	20:42
Date/Time Bundle Removed	9-26-85	03:35

t	$\Delta T_c$	$\Delta T_v$	$T_{pit}$	Pump Power, W
0	0.00	1.02	79.94	--
1	0.91	1.93	79.93	--
2	1.76	2.77	79.93	--
3	2.54	3.56	79.92	--
4	3.27	4.28	79.92	--
5	3.95	4.96	79.92	--

"b" Coefficient	D.93439287
Index of Determination	0.999993
Slope Watts	262.128
Corrected Slope Watts (0.9842)	257.98
Ave. Corrected Radiation Value	1959 R/hr
Gamma Watts (0.01499)	29.4
Total Thermal Output	287.4



Bundle ID	CZ433	
Date/Time Bundle Loaded	5-21-85	10:38
Date/Time Bundle Removed	5-21-85	17:35

<u>t</u>	<u>Delta T<sub>c</sub></u>	<u>Delta T<sub>v</sub></u>	<u>I<sub>pit</sub></u>	<u>Pump Power, W</u>
0	0.00	0.98	76.79	249.69
1	0.84	1.76	76.80	249.69
2	1.62	2.47	76.81	249.25
3	2.34	3.15	76.82	248.99
4	3.03	3.78	76.83	248.84
5	3.65	4.36	76.85	248.63

"b" Coefficient	0.8600715
Index of Determination	0.999989
Slope Watts	234.44
Corrected Slope Watts (0.9842)	230.7
Ave. Corrected Radiation Value	1735.2 R/hr
Gamma Watts (0.01499)	26.0
Total Thermal Output	256.7

Bundle ID	CZ460	
Date/Time Bundle Loaded	12-09-84	12:48
Date/Time Bundle Removed	12-09-84	19:20

<u>t</u>	<u>Delta T<sub>c</sub></u>	<u>Delta T<sub>v</sub></u>	<u>I<sub>pit</sub></u>	<u>Pump Power, W</u>
0	0.00	1.00	82.63	250.2
1	0.97	1.99	82.61	249.5
2	1.89	2.88	82.61	249.3
3	2.73	3.72	82.61	249.0
4	3.52	4.51	82.61	249.0
5	4.25	5.23	82.60	248.9

"b" Coefficient	1.003286
Index of Determination	0.999995
Slope Watts	287.7938
Corrected Slope Watts (0.9842)	283.2466
Ave. Corrected Radiation Value	2023 R/hr
Gamma Watts (0.01499)	30.3
Total Thermal Output	313.5

Bundle ID	CZ466	
Date/Time Bundle Loaded	9-28-84	75:00
Date/Time Bundle Removed	9-28-84	21:55

<u>t</u>	<u>Delta T<sub>c</sub></u>	<u>Delta T<sub>v</sub></u>	<u>T<sub>pit</sub></u>	<u>Pump Power, W</u>
0	0.00	1.00	80.96	--
1	0.94	1.92	80.99	--
2	1.84	2.77	81.00	--
3	2.64	3.56	81.02	--
4	3.41	4.29	81.04	--
5	4.11	4.96	81.06	--

"b" Coefficient	0.9752857
Index of Determination	0.999978
Slope Watts	277.36
Corrected Slope Watts (0.9842)	272.98
Ave. Corrected Radiation Value	1939.37 R/hr
Gamma Watts (0.01499)	29.1
Total Thermal Output	302.1

Bundle ID	CZ468	
Date/Time Bundle Loaded	12-11-84	16:11
Date/Time Bundle Removed	12-11-84	23:01

<u>t</u>	<u>Delta T<sub>c</sub></u>	<u>Delta T<sub>v</sub></u>	<u>T<sub>pit</sub></u>	<u>Pump Power, W</u>
0	0.00	1.02	82.56	248.7
1	1.01	2.00	82.58	248.3
2	1.94	2.93	82.58	249.0
3	2.82	3.80	82.58	249.5
4	3.63	4.59	82.58	250.1
5	4.39	5.35	82.59	250.4

"b" Coefficient	1.033072
Index of Determination	0.999995
Slope Watts	298.9
Corrected Slope Watts (0.9842)	294.2
Ave. Corrected Radiation Value	2074.4 R/hr
Gamma Watts (0.01499)	31.1
Total Thermal Output	325.3

Bundle ID	CZ472	
Date/Time Bundle Loaded	9-26-84	15:03
Date/Time Bundle Removed	9-26-84	21:56

<u>t</u>	<u>Delta T<sub>c</sub></u>	<u>Delta T<sub>y</sub></u>	<u>T<sub>pit</sub></u>	<u>Pump Power, W</u>
0	0.00	1.00	80.16	--
1	1.00	2.00	80.19	--
2	1.93	2.91	80.20	--
3	2.79	3.77	80.23	--
4	3.59	4.56	80.27	--
5	4.33	5.28	80.33	--

"b" Coefficient	1.0276428
Index of Determination	0.999997
Slope Watts	296.86777
Corrected Slope Watts (0.9842)	292.17726
Ave. Corrected Radiation Value	2187 R/hr
Gamma Watts (0.01499)	32.8
Total Thermal Output	325

Bundle ID	CZ473	
Date/Time Bundle Loaded	12-10-84	07:11
Date/Time Bundle Removed	12-10-84	14:05

<u>t</u>	<u>Delta T<sub>c</sub></u>	<u>Delta T<sub>y</sub></u>	<u>T<sub>pit</sub></u>	<u>Pump Power, W</u>
0	0.00	1.00	82.57	250.6
1	0.93	1.94	82.57	250.8
2	1.80	2.78	82.58	251.0
3	2.60	3.59	82.57	251.3
4	3.36	4.33	82.57	251.5
5	4.06	5.03	82.57	251.6

"b" Coefficient	0.9531074
Index of Determination	0.9999929
Slope Watts	269.1
Corrected Slope Watts (0.9842)	264.8483
Ave. Corrected Radiation Value	1895 R/hr
Gamma Watts (0.01499)	28.4
Total Thermal Output	293.2



Bundle ID	CZ498	
Date/Time Bundle Loaded	10-24-84	20:17
Date/Time Bundle Removed	12-25-84	02:50

<u>t</u>	<u>Delta T<sub>c</sub></u>	<u>Delta T<sub>v</sub></u>	<u>T<sub>pit</sub></u>	<u>Pump Power, W</u>
0	0.00	1.02	76.62	2.38
1	1.10	2.08	76.63	2.57
2	2.11	3.06	76.67	2.50
3	3.06	3.97	76.67	2.40
4	3.95	4.84	76.72	2.33
5	4.75	5.61	76.74	2.29

"b" Coefficient	1.1267857
Index of Determination	0.999992
Slope Watts	333.8
Corrected Slope Watts (0.9842)	328.5
Ave. Corrected Radiation Value	2065 R/hr
Gamma Watts (0.01499)	30.9
Total Thermal Output	359.4

Bundle ID	CZ508	
Date/Time Bundle Loaded	12-09-84	03:55
Date/Time Bundle Removed	12-09-84	10:46

<u>t</u>	<u>Delta T<sub>c</sub></u>	<u>Delta T<sub>v</sub></u>	<u>T<sub>pit</sub></u>	<u>Pump Power, W</u>
0	0.00	0.99	82.57	250.2
1	0.98	1.96	82.59	249.9
2	1.87	2.83	82.58	249.8
3	2.72	3.65	82.59	249.9
4	3.50	4.42	82.58	249.8
5	4.23	5.12	82.59	249.6

"b" Coefficient	0.9954644
Index of Determination	0.999987
Slope Watts	284.8799
Corrected Slope Watts (0.9842)	280.3788
Ave. Corrected Radiation Value	1977 R/hr
Gamma Watts (0.01499)	29.6
Total Thermal Output	310

Bundle ID	CZ515	
Date/Time Bundle Loaded	9-25-84	11:41
Date/Time Bundle Removed	9-25-84	19:14

<u>t</u>	<u>Delta T<sub>c</sub></u>	<u>Delta T<sub>v</sub></u>	<u>T<sub>pit</sub></u>	<u>Pump Power, W</u>
0	0.00	1.01	79.98	--
1	0.92	1.92	79.97	--
2	1.79	2.77	79.97	--
3	2.58	3.47	79.97	--
4	3.33	4.32	79.96	--
5	4.01	5.00	79.96	--

"b" Coefficient	0.9520001
Index of Determination	0.999993
Slope Watts	268.688
Corrected Slope Watts (0.9842)	264.44
Ave. Corrected Radiation Value	1973.8 R/hr
Gamma Watts (0.01499)	29.6
Total Thermal Output	294

Bundle ID	CZ515	
Date/Time Bundle Loaded	10-25-84	22:03
Date/Time Bundle Removed	10-26-84	04:44

<u>t</u>	<u>Delta T<sub>c</sub></u>	<u>Delta T<sub>v</sub></u>	<u>T<sub>pit</sub></u>	<u>Pump Power, W</u>
0	0.00	1.01	77.20	--
1	0.93	1.95	77.21	2.33
2	1.80	2.82	77.20	2.32
3	2.61	3.64	77.20	2.31
4	3.38	4.38	77.19	2.29
5	4.07	5.09	77.18	2.27

"b" Coefficient	0.9574286
Index of Determination	0.999992
Slope Watts	270.7
Corrected Slope Watts (0.9842)	266.4
Ave. Corrected Radiation Value	1974 R/hr
Gamma Watts (0.01499)	29.6
Total Thermal Output	296

Bundle ID	CZ526	
Date/Time Bundle Loaded	10-01-84	11:40
Date/Time Bundle Removed	10-01-84	18:25

<u>t</u>	<u>Delta T<sub>c</sub></u>	<u>Delta T<sub>v</sub></u>	<u>T<sub>pit</sub></u>	<u>Pump Power, W</u>
0	0.00	1.00	75.47	--
1	1.16	2.15	75.60	--
2	2.26	3.19	75.63	--
3	3.27	4.16	75.66	--
4	4.21	5.06	75.68	--
5	5.07	5.89	75.71	--

"b" Coefficient	1.2056428
Index of Determination	0.999997
Slope Watts	363.18
Corrected Slope Watts (0.9842)	357.44
Ave. Corrected Radiation Value	2530.97 R/hr
Gamma Watts (0.01499)	37.9
Total Thermal Output	395.3

Bundle ID	CZ526	
Date/Time Bundle Loaded	5-21-85	22:51
Date/Time Bundle Removed	5-21-85	05:45

<u>t</u>	<u>Delta T<sub>c</sub></u>	<u>Delta T<sub>v</sub></u>	<u>T<sub>pit</sub></u>	<u>Pump Power, W</u>
0	0.00	1.02	76.93	247.71
1	1.02	1.97	76.94	247.69
2	1.93	2.86	76.96	247.82
3	2.78	3.67	76.97	248.00
4	3.58	4.42	77.00	248.16
5	4.33	5.13	77.02	248.22

"b" Coefficient	1.02210
Index of Determination	0.999947
Slope Watts	294.8
Corrected Slope Watts (0.9842)	290.1
Ave. Corrected Radiation Value	2112.3 R/hr
Gamma Watts (0.01499)	31.7
Total Thermal Output	321.8



Bundle ID	CZ528	
Date/Time Bundle Loaded	10-25-84	13:01
Date/Time Bundle Removed	10-25-84	19:13

t	Delta $T_c$	Delta $T_v$	$T_{pit}$	Pump Power, W
0	0.00	1.00	77.03	--
1	0.95	1.90	77.06	2.39
2	1.81	2.75	77.09	2.42
3	2.65	3.52	77.10	2.45
4	3.40	4.28	77.14	2.45
5	4.11	4.93	77.17	2.44

"b" Coefficient	0.9675715
Index of Determination	0.9999749
Slope Watts	274.5
Corrected Slope Watts (0.9842)	270.2
Ave. Corrected Radiation Value	1831 R/hr
Gamma Watts (0.01499)	27.4
Total Thermal Output	297.6

Bundle ID	CZ531	
Date/Time Bundle Loaded	10-30-84	13:06
Date/Time Bundle Removed	10-30-84	19:24

t	Delta $T_c$	Delta $T_v$	$T_{pit}$	Pump Power, W
0	0.00	1.03	79.20	254.0
1	1.08	2.05	79.21	253.0
2	2.05	3.04	79.25	253.0
3	2.99	3.92	79.26	252.9
4	3.83	4.76	79.31	252.5
5	4.63	5.52	79.33	252.5

"b" Coefficient	1.095429
Index of Determination	0.999971
Slope Watts	322.1211
Corrected Slope Watts (0.9842)	317.0316
Ave. Corrected Radiation Value	2016.8 R/hr
Gamma Watts (0.01499)	30.2
Total Thermal Output	347.2

Bundle ID	CZ536	
Date/Time Bundle Loaded	9-27-84	10:47
Date/Time Bundle Removed	9-27-84	17:18

t	Delta T <sub>c</sub>	Delta T <sub>v</sub>	T <sub>pit</sub>	Pump Power, W
0	0.00	1.01	80.71	--
1	0.94	1.88	80.71	--
2	1.80	2.72	80.72	--
3	2.61	3.51	80.73	--
4	3.36	4.22	80.73	--
5	4.07	4.88	80.73	--

"b" Coefficient	0.95396429
Index of Determination	0.999984
Slope Watts	269.41922
Corrected Slope Watts (0.9842)	265.16239
Ave. Corrected Radiation Value	2006.1 R/hr
Gamma Watts (0.01499)	30.0
Total Thermal Output	295.2

Bundle ID	CZ542	
Date/Time Bundle Loaded	12-08-84	15:10
Date/Time Bundle Removed	12-08-84	22:05

t	Delta T <sub>c</sub>	Delta T <sub>v</sub>	T <sub>pit</sub>	Pump Power, W
0	0.00	1.00	82.49	248.8
1	0.96	1.94	82.49	248.2
2	1.86	2.83	82.49	248.2
3	2.71	3.67	82.51	248.3
4	3.48	4.42	82.51	248.4
5	4.19	5.11	82.53	248.4

"b" Coefficient	0.9968931
Index of Determination	0.9999929
Slope Watts	285.4121
Corrected Slope Watts (0.9842)	280.9026
Ave. Corrected Radiation Value	2071 R/hr
Gamma Watts (0.01499)	31
Total Thermal Output	311.9

Bundle ID	CZ545	
Date/Time Bundle Loaded	12-11-84	01:20
Date/Time Bundle Removed	12-11-84	07:40

<u>t</u>	<u>Delta T<sub>c</sub></u>	<u>Delta T<sub>y</sub></u>	<u>T<sub>pit</sub></u>	<u>Pump Power, W</u>
0	0.00	1.02	82.61	249.5
1	0.93	1.93	82.61	248.8
2	1.80	2.80	82.59	248.5
3	2.63	3.59	82.62	248.5
4	3.37	4.36	82.61	248.4
5	4.08	5.04	82.61	248.2

"b" Coefficient	0.9603573
Index of Determination	0.999984
Slope Watts	271.8
Corrected Slope Watts (0.9842)	267.5
Ave. Corrected Radiation Value	1845 R/hr
Gamma Watts (0.01499)	27.7
Total Thermal Output	295.2



APPENDIX E

AXIAL RADIATION PROFILES

## APPENDIX E

### AXIAL RADIATION PROFILES

Gamma and neutron axial profile readings were taken on each of the fuel bundles subjected to calorimetry. The Los Alamos National Laboratory (LANL) portable spent-fuel detector known as the ION-1/fork measurement system was used at GE-MO to make the radiation readings. LANL's involvement was voluntary and benefitted them through data access and the opportunity to test and demonstrate their equipment in actual field conditions.

This appendix describes the LANL measurement system and presents the data obtained with it during the cask performance test efforts.

#### ION-1/FORK DETECTOR

Basically, the LANL ION-1 measurement system consists of underwater sensors and above-water electronics that measure and display the radiation reading. Hard copy output of the data was obtained via a portable Epson computer.

The underwater unit is shown in Figure E.1. It consists of two fork "tines" through which a BWR fuel bundle will pass. The opening between the two tines is about 1/2 in. larger than a typical 7x7 BWR fuel bundle. The tines are made of polyethylene and can be sized to fit the different bundles to be run through the detector. Each tine contains two fission chambers and one ion chamber. One of the fission chambers is cadmium-covered, and the other is not.

The fork is suspended in the GE-MO unloading basin by a 2-1/2 in.-diameter stainless steel pipe. The fork is located on the east wall of the basin and is not movable. A pre-amplifier is located at the top of the support column. When a fuel bundle is to be measured, it is grappled from the fuel storage basket and moved into the forks of the detector. The grapple is indexed (relative to the north handrail of the basin crane) so that the bottom of the fuel bundle will be at the exact center of the tines when the reference mark on the

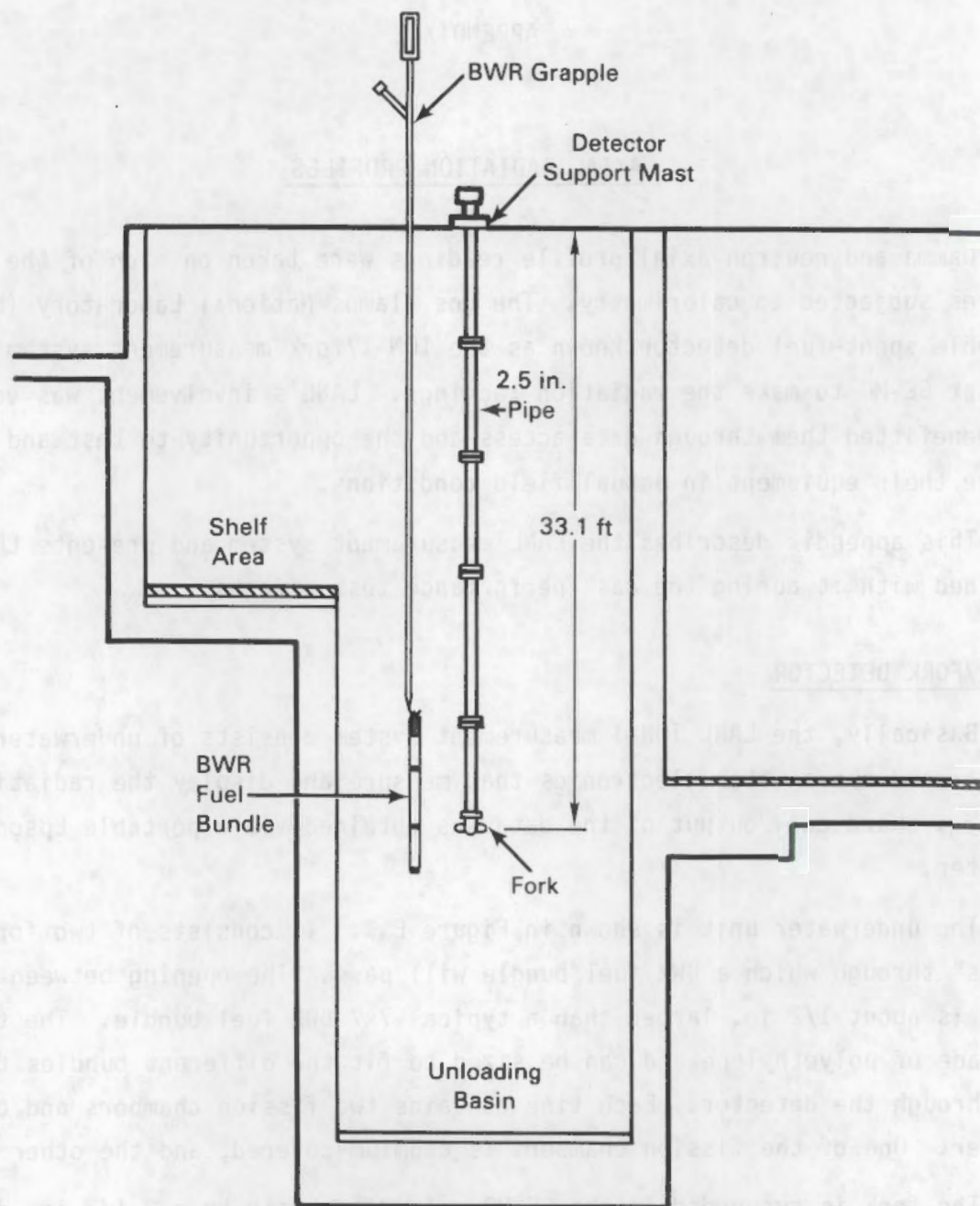


**FIGURE E.1.** View Showing Los Alamos Fork Measurement System Detector Installed in Morris Basin



grapple reads "0" elevation. Then the fuel bundle is lowered through the forks of the detector until the desired elevation is reached.

The ION-1 electronics instrument was located approximately 8 ft from the edge of the fuel unloading basin. This unit is shown in Figure E.2. The device was fairly easy to operate because of its self-prompting display. Various count times were examined; however, for most of the measurements taken at GE-MO, a count time of 10 seconds was allowed at each measurement position. The ION-1 was connected to a small portable Epson computer, which provided magnetic tape interface capability and hard copy of the data.



FIGURE E.2. Electronics Instrument for ION-1 System

Fuel bundles were run through the ION-1 detector in conjunction with unloading the fuel from the IF-300 shipping cask. Actual time to do a profile varied because the number of points measured varied from bundle to bundle. About 6 minutes of data-taking and 15 minutes of fuel-handling were required for a seven-point scan.

The axial positions for fuel assembly measurements are shown in Figure E.3. The data for the scan points common to all assemblies are listed in Tables E.1 and E.2. Additional measurements were taken on fuel assembly CZ528 to determine the influence of fuel assembly spacers on the radiation profile. This data, plotted in Figure E.4, shows a dip in the gamma and neutron profiles at the spacer locations.

#### CALIBRATION INFORMATION

Neutron measurements were made with the ION-1/fork detector system against a  $^{252}\text{Cf}$  source of known strength. Using the  $^{252}\text{Cf}$  source in water, efficiency factors of  $2.68 \times 10^{-5}$  and  $5.2 \times 10^{-5}$  were determined for the cadmium-covered detectors and bare detectors, respectively. Between the time of the pretest neutron calibration and measurement and the post-test measurement, the electronics were changed. This resulted in the post-test neutron count ratio being about one-half the pretest values.

The ion chambers used at GE-MO were measured with a  $^{60}\text{Co}$  source that was used to calibrate survey instruments at Los Alamos. The measurements were performed in air. Comparisons were made of the response of the ion chambers both outside and inside of the polyethylene forks used at Morris. The following linear response coefficients were determined for the two ion chambers:

- right arm - 68.9 R/hr per ION-1 reading
- left arm - 70.71 R/hr per ION-1 reading.



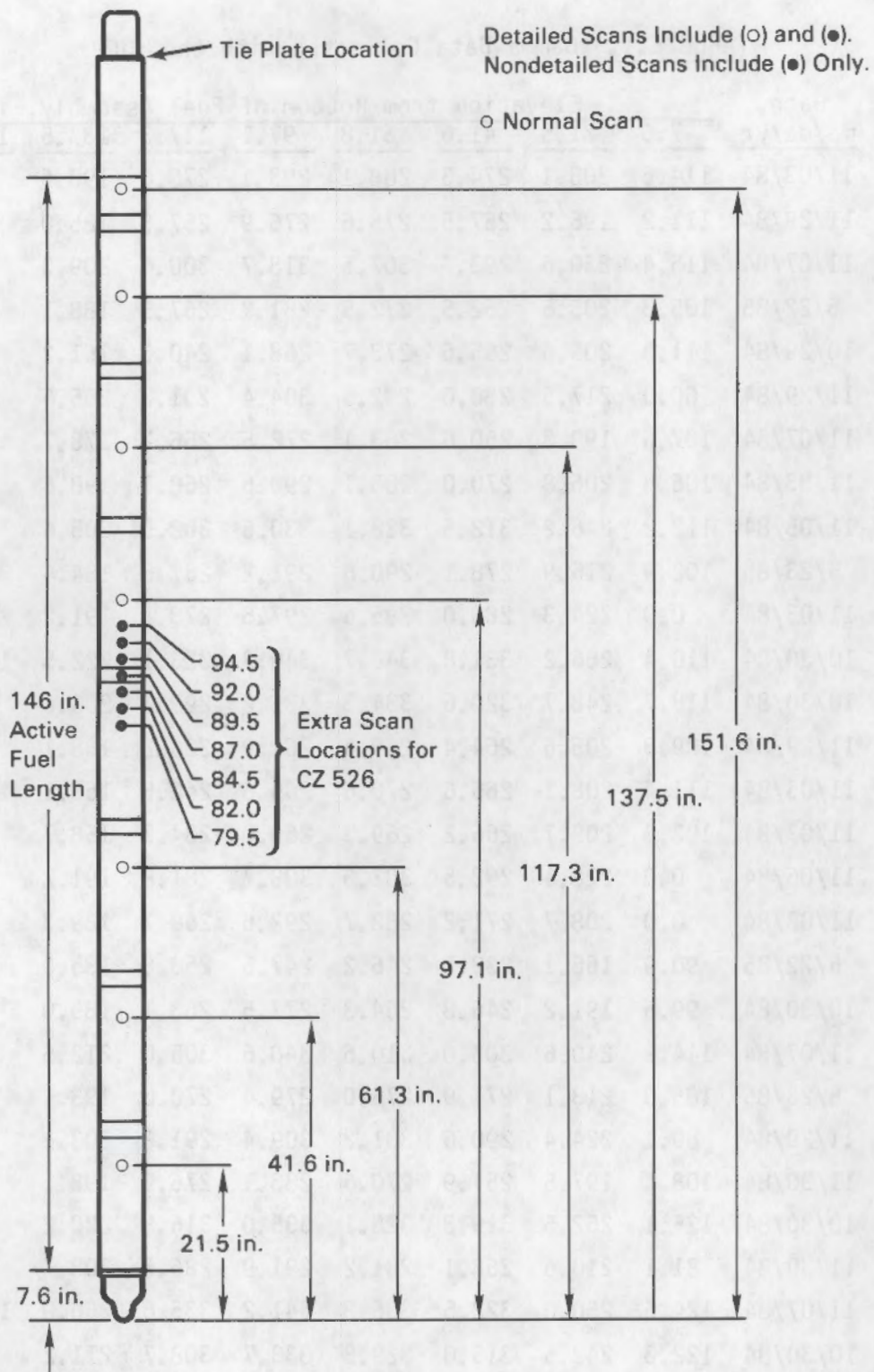


**FIGURE E.3.** Gamma/Neutron Scan Locations



TABLE E.1. Gamma Data Collected with the ION-1

Assembly	Date, mo/da/yr	Elevation from Bottom of Fuel Assembly, in.								
		7.6	21.5	41.6	61.8	97.1	117.3	137.5	151.6	169.5
CZ147	11/03/84	114.6	208.1	274.3	288.1	293.1	270.6	190.6	90.1	23.0
CZ148	11/29/84	111.2	196.2	257.5	275.6	276.9	257.5	185.0	87.2	23.0
CZ182	11/07/84	115.4	230.6	293.7	307.5	318.7	300.6	209.3	93.4	21.2
CZ182	5/22/85	105.3	205.6	262.5	272.5	281.8	267.5	188.1	86.5	19.9
CZ195	10/29/84	111.3	205.6	265.6	273.7	268.1	240.6	161.2	72.7	12.1
CZ205	11/29/84	60.0	217.5	280.0	292.5	304.4	291.2	205.6	95.3	20.9
CZ209	11/07/84	107.6	199.3	250.6	263.1	272.5	256.2	178.7	84.8	21.3
CZ211	11/03/84	106.8	206.8	270.0	288.1	290.6	268.1	190.6	88.9	22.6
CZ222	11/05/84	113.2	246.2	312.5	328.1	330.6	302.5	205.6	94.6	0.0
CZ222	5/23/85	102.9	216.9	278.1	290.6	291.2	267.5	184.4	86.4	20.7
CZ225	11/03/84	0.0	224.3	280.0	295.6	297.5	278.1	191.2	91.2	22.4
CZ239	10/30/84	110.4	256.2	331.8	348.7	349.3	323.1	222.5	100.7	15.1
CZ246	10/30/84	118.7	248.7	320.6	334.3	331.2	299.3	200.0	90.4	22.1
CZ259	11/29/84	109.5	205.6	264.4	269.4	261.9	236.2	158.1	74.5	13.4
CZ264	11/05/84	111.4	208.1	265.6	270.6	265.6	242.5	163.1	76.4	12.4
CZ277	11/07/84	102.9	208.7	266.2	269.3	260.0	234.3	158.7	74.7	13.3
CZ286	11/06/84	0.0	228.1	292.5	302.5	308.7	281.8	191.2	86.5	21.1
CZ296	11/03/84	0.0	208.7	271.2	288.7	292.5	268.7	189.3	90.9	26.5
CZ302	5/22/85	90.9	168.1	232.5	246.2	247.5	250.6	185.0	88.1	12.8
CZ308	10/30/84	99.5	191.2	246.8	264.3	277.5	263.1	185.0	85.9	18.7
CZ311	11/07/84	114.9	240.6	305.0	310.6	340.6	305.0	212.5	97.8	21.4
CZ311	5/23/85	105.0	213.1	271.9	275.0	279.4	270.6	193.1	88.6	20.7
CZ315	11/29/84	89.1	224.4	290.6	301.2	309.4	291.2	203.1	88.9	21.2
CZ318	11/30/84	108.4	197.5	251.9	270.6	283.1	276.2	198.1	91.5	16.9
CZ337	10/30/84	125.1	252.5	319.3	328.1	335.0	316.8	220.2	98.1	20.1
CZ342	11/30/84	81.1	210.6	268.1	281.2	291.9	286.2	208.7	94.7	21.9
CZ346	11/07/84	124.6	250.0	322.5	336.8	341.2	335.6	260.0	117.4	15.2
CZ348	10/30/84	122.3	242.5	315.0	329.3	333.7	308.7	211.2	92.2	12.4
CZ351	11/30/84	114.8	219.4	272.5	278.7	295.0	283.3	196.9	91.9	20.2
CZ351	5/22/85	107.5	198.1	247.5	253.7	268.1	259.3	183.7	86.9	20.3
CZ355	11/07/84	106.3	192.4	246.2	260.6	271.8	254.9	176.2	80.1	17.9

TABLE E.1. (contd)

Assembly	Date, mo/da/yr	Elevation from Bottom of Fuel Assembly, in.								
		7.6	21.5	41.6	61.8	97.1	117.3	137.5	151.6	169.5
CZ357	11/30/84	106.2	233.1	295.6	305.6	311.2	301.2	211.2	95.0	21.4
CZ369	11/03/84	0.0	220.6	293.1	307.5	315.0	301.8	213.7	100.3	24.0
CZ370	11/07/84	76.4	193.1	268.1	282.5	290.6	273.7	193.1	88.7	12.6
CZ372	11/07/84	95.7	195.0	263.1	285.0	292.5	287.5	213.1	98.6	13.9
CZ379	11/03/84	110.9	200.6	253.1	262.5	268.1	267.5	207.5	99.8	17.2
CZ398	11/07/84	125.9	242.5	306.8	323.7	335.6	329.3	238.7	107.8	22.8
CZ415	11/07/84	91.3	202.5	276.2	293.7	304.3	294.3	212.5	101.5	15.1
CZ416	10/30/84	120.1	216.2	276.8	295.0	310.0	297.5	211.8	97.3	21.4
CZ429	11/07/84	127.1	265.6	337.5	349.3	357.5	336.2	234.3	104.5	13.8
CZ430	10/30/84	105.1	248.7	317.5	335.0	328.1	308.7	213.1	92.5	13.1
CZ433	11/08/84	73.6	201.2	266.9	282.5	289.4	277.5	197.5	90.1	21.0
CZ460	11/30/84	117.3	225.0	278.1	280.6	290.6	279.4	193.7	90.3	13.1
CZ466	11/30/84	112.5	192.5	242.5	259.4	295.0	266.2	193.7	89.5	12.8
CZ468	11/30/84	113.3	230.6	297.5	301.2	301.9	280.6	188.1	83.6	10.7
CZ468	5/22/85	105.4	208.7	271.2	275.0	273.1	255.6	176.2	79.5	11.7
CZ472	11/30/84	115.4	231.2	297.5	300.0	296.2	280.6	198.7	88.0	11.0
CZ473	11/30/84	97.8	194.4	245.0	262.5	278.7	271.9	193.7	89.2	20.7
CZ498	11/03/84	95.6	246.2	313.7	323.1	328.7	310.0	212.5	95.7	13.0
CZ498	5/22/85	83.7	213.7	276.2	285.6	288.1	272.5	192.5	91.5	13.8
CZ508	11/30/84	88.4	215.6	271.2	280.6	293.7	281.9	198.7	95.1	14.3
CZ515	11/08/84	91.2	196.9	267.5	280.0	288.1	273.7	191.9	92.6	14.2
CZ526	5/23/85	97.3	220.6	286.9	298.7	302.5	303.7	236.2	117.5	25.5
CZ528	11/03/84	58.6	200.6	266.2	284.3	295.6	286.2	209.9	102.3	24.2
CZ531	10/30/84	68.6	243.7	307.5	320.0	321.8	322.5	243.7	116.2	16.0
CZ531	5/22/85	58.0	213.7	274.3	277.5	282.5	281.8	216.2	106.2	16.8
CZ536	11/07/84	53.9	191.2	263.7	285.6	298.7	288.1	207.5	98.7	25.8
CZ542	11/30/84	115.9	205.6	263.7	280.0	301.2	291.2	201.2	90.0	23.0
CZ545	11/30/84	111.8	210.6	262.5	270.6	275.6	255.0	171.9	82.8	11.1

TABLE E.2. Neutron Data Collected with the ION-1

Assembly	Date, mo/da/yr	Elevation from Bottom of Fuel Assembly, in.								
		7.6	21.5	41.6	61.8	97.1	117.3	137.5	151.6	169.5
CZ147	11/03/84	4.3	70.2	150.0	161.3	175.0	144.3	55.0	4.1	0.0
CZ148	11/27/84	3.0	60.9	124.0	144.8	164.2	125.9	50.5	2.7	1.0
CZ182	11/07/84	5.1	90.7	190.3	194.0	246.2	208.7	72.2	4.8	0.0
CZ182	5/22/85	2.7	45.4	93.0	102.5	116.7	99.4	33.5	3.0	0.0
CZ195	10/29/84	4.9	67.3	152.7	157.0	142.0	107.2	34.4	2.2	0.0
CZ205	11/29/84	5.6	75.6	169.7	183.3	214.6	207.9	75.2	5.2	0.0
CZ209	11/07/84	3.8	73.7	150.3	170.6	182.3	149.4	49.1	3.5	0.0
CZ211	11/03/84	3.4	70.4	152.1	184.4	180.5	147.5	57.3	3.3	0.0
CZ222	11/05/84	6.7	109.4	225.4	241.9	233.5	193.0	93.6	4.2	0.0
CZ222	5/23/85	3.1	47.7	108.0	122.1	120.2	63.3	31.3	2.3	0.0
CZ225	11/03/84	0.0	95.1	191.2	205.9	202.0	164.0	59.5	5.2	0.0
CZ239	10/30/84	7.5	111.6	231.0	260.7	251.7	196.4	65.0	5.2	0.0
CZ246	10/30/84	8.0	114.3	235.7	269.3	251.0	186.5	59.4	5.2	0.0
CZ259	11/29/84	5.2	69.9	151.2	165.0	139.7	103.3	31.8	2.3	0.0
CZ264	11/05/84	4.1	73.3	150.3	150.8	146.4	109.7	37.0	3.5	0.0
CZ277	11/07/84	4.2	66.5	147.6	143.1	127.3	95.9	31.8	1.8	0.0
CZ286	11/06/84	0.0	103.3	213.0	220.5	223.9	165.4	55.7	3.7	0.0
CZ296	11/03/84	0.0	65.1	140.4	162.4	175.0	143.9	51.8	4.0	0.0
CZ302	11/05/84	0.5	57.0	164.4	196.4	243.0	245.7	102.9	3.8	0.0
CZ302	5/22/85	1.7	26.9	79.9	102.7	119.2	125.2	55.7	4.8	0.0
CZ308	10/30/84	4.8	62.9	147.3	163.1	177.1	153.1	58.7	4.6	0.0
CZ311	11/07/84	6.6	105.5	223.5	223.1	239.5	229.7	93.4	6.2	0.0
CZ311	5/23/85	2.3	49.5	110.7	111.6	119.7	114.0	45.2	2.5	0.0
CZ315	11/29/84	4.4	85.1	187.9	219.8	246.4	214.8	77.1	5.0	0.1
CZ318	11/30/84	3.8	63.3	152.0	184.9	232.1	221.2	87.1	6.5	0.0
CZ337	10/30/84	5.5	112.2	220.9	229.8	253.7	215.7	78.8	4.9	0.0
CZ342	11/30/84	4.8	77.2	169.5	191.8	226.7	221.0	100.1	7.3	0.0
CZ346	11/07/84	6.1	102.7	226.0	242.6	264.5	271.3	149.1	11.5	0.0
CZ348	10/30/84	5.7	104.9	236.2	260.5	284.2	223.8	8.8	7.4	0.0
CZ351	5/22/85	2.7	43.0	92.3	94.8	114.9	102.1	42.5	3.0	0.0
CZ351	11/30/84	5.8	92.6	181.2	182.1	232.6	207.2	74.1	6.7	0.0



TABLE E.2. (contd)

Assembly	Date, mo/da/yr	Elevation from Bottom of Fuel Assembly, in.								
		7.6	21.5	41.6	61.8	97.1	117.3	137.5	151.6	169.5
CZ355	11/07/84	4.5	65.7	152.2	173.5	186.8	156.3	57.4	3.7	0.0
CZ357	11/30/84	4.9	101.8	216.6	222.4	250.1	250.3	95.3	6.5	0.0
CZ369	11/03/84	0.0	79.8	175.6	204.0	256.5	231.2	89.7	6.6	0.0
CZ370	11/07/84	3.4	68.7	178.1	207.3	238.5	218.4	91.6	7.1	0.0
CZ372	11/07/84	4.2	62.7	170.9	214.9	248.9	251.7	122.8	8.7	0.0
CZ379	11/03/84	5.2	69.8	155.9	164.1	183.7	197.8	97.6	9.0	0.0
CZ398	11/07/84	4.9	93.9	200.0	235.7	260.8	262.3	111.4	9.4	0.0
CZ415	11/07/84	3.7	65.5	187.3	219.6	270.2	254.7	110.6	8.3	0.0
CZ416	10/30/84	3.9	80.7	180.3	209.2	253.4	245.3	94.3	7.4	0.1
CZ429	11/07/84	8.1	123.7	245.8	287.6	295.1	251.0	93.7	8.9	0.0
CZ430	10/30/84	8.0	116.6	241.3	246.0	265.2	233.7	80.2	6.7	0.0
CZ433	11/08/84	3.5	67.1	182.3	212.3	236.5	236.5	93.1	8.1	0.0
CZ460	11/30/84	4.6	104.3	205.8	196.5	215.1	188.5	70.7	6.4	0.0
CZ466	11/30/84	4.8	69.3	150.2	173.6	203.4	198.8	82.7	6.5	0.0
CZ468	11/30/84	5.3	100.4	224.4	202.3	203.2	180.6	59.5	3.5	0.0
CZ468	5/22/85	1.7	47.6	113.3	107.1	106.8	98.9	32.8	2.0	0.0
CZ472	11/30/84	6.8	103.2	208.5	210.6	210.2	183.7	75.3	5.3	0.0
CZ473	11/30/84	4.6	69.7	141.3	173.8	226.2	217.6	84.7	5.2	0.1
CZ498	11/03/84	5.8	113.4	231.3	224.9	244.7	217.0	75.2	5.0	0.1
CZ498	5/22/85	2.9	51.7	110.7	109.3	119.9	106.0	37.7	3.4	0.0
CZ508	11/30/84	5.4	86.1	177.0	197.5	222.6	207.4	76.8	5.8	0.0
CZ515	11/08/84	3.8	69.5	184.1	212.5	260.6	242.8	95.0	5.9	0.0
CZ526	5/23/85	2.4	50.1	116.0	120.3	137.0	146.5	82.6	5.8	0.0
CZ528	11/03/84	3.9	71.4	173.4	209.9	247.2	249.2	117.5	8.7	0.0
CZ531	10/30/84	5.3	110.0	209.7	227.4	240.4	261.7	136.0	9.8	0.2
CZ531	5/22/85	2.0	47.6	103.4	101.7	122.3	128.0	68.0	6.0	0.0
CZ536	11/07/84	3.8	64.0	175.2	209.8	263.1	253.1	112.2	8.0	0.0
CZ542	11/30/84	4.7	80.0	170.1	187.6	242.4	227.4	78.2	4.3	0.0
CZ545	11/30/84	6.1	91.2	180.6	206.0	214.5	164.9	57.9	3.6	0.0

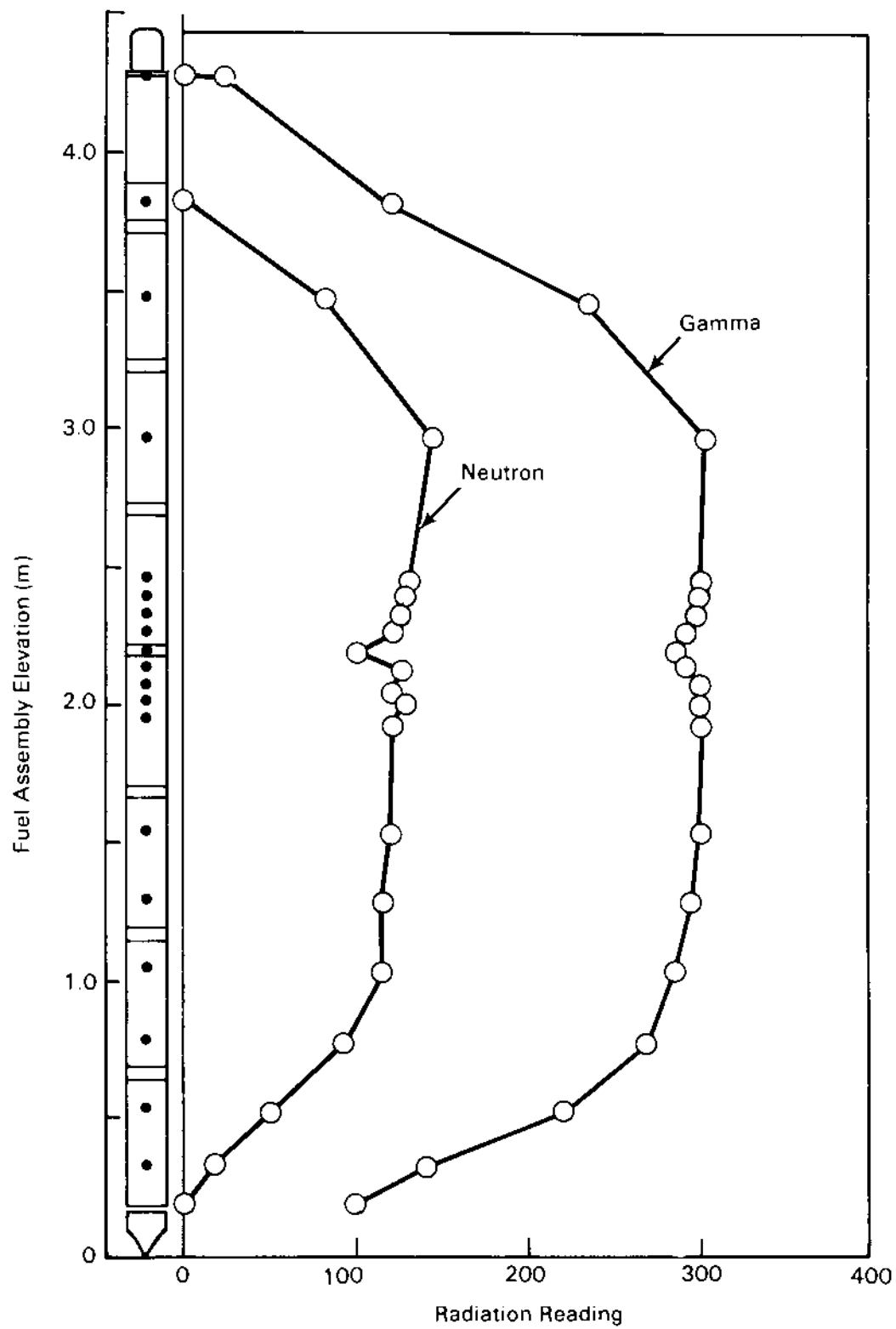


FIGURE E.4. Influence of Fuel Assembly Spacers on Radiation Profile

APPENDIX F

IN-BASIN SIPPING RESULTS



## APPENDIX F

### IN-BASIN SIPPING RESULTS

The detailed sipping data for the fuel bundles used in the performance test are given in this appendix. Background levels of  $^{137}\text{Cs}$  and  $^{60}\text{Co}$  in the basin are given, as are pool temperature and date of examination. Some of the tables include analyses of CZ205 before and after the sipping of fuel bundles from a given basket. Bundle CZ205 was used as a calibration check. Occasionally the date of examination, pool temperature, background concentration, or other parameter changed; such changes are reported as required. Concentrations given in the tables are the differences between the measured value and the basin levels. All these values are expressed as Ci/ml and should be multiplied by  $10^{-5}$ .

TABLE F.1. Sipping Tests For Cooper Fuel  
Pre-Characterization, Basket B-85

Date Tested		: September 19, 1984			
Basin Water Temperature		: 29.5°C			
Basin Sample $^{137}\text{Cs}$ Concentration:		5.77 x 10 <sup>-5</sup> $\mu\text{Ci/ml}$			
Basin Sample $^{60}\text{Co}$ Concentration :		1.22 x 10 <sup>-4</sup> $\mu\text{Ci/ml}$			
Bask. Pos.	Bundle No.	$^{137}\text{Cs}$ Concen.	Delta $^{137}\text{Cs}$	$^{60}\text{Co}$ Concen.	Delta $^{60}\text{Co}$
	CZ205	5.99	+0.22	59.1	+ 46.9
A	CZ302	6.34	+0.57	26.8	+ 14.6
B	CZ259	6.50	+0.73	61.2	+ 49.0
C	CZ264	5.92	+0.15	11.5	- 0.7
D	CZ331	6.29	+0.52	6.0	- 6.2
E	CZ205	5.13	-0.64	121.0	+108.8
F	CZ102	5.20	-0.57	6.64	- 5.56
G	CZ286	5.01	-0.76	8.76	- 3.44
H	CZ148	4.74	-1.03	4.94	- 7.26
I	CZ195	5.68	-0.09	35.4	+ 23.2

TABLE F.2. Sipping Tests For Cooper Fuel  
Pre-Characterization, Basket B-86

Date Tested		: September 17, 1984			
Basin Water Temperature		: 29.2°C			
Basin Sample $^{137}\text{Cs}$ Concentration:		5.42 x 10 <sup>-5</sup> $\mu\text{Ci/ml}$			
Basin Sample $^{60}\text{Co}$ Concentration :		3.79 x 10 <sup>-5</sup> $\mu\text{Ci/ml}$			
Bask. Pos.	Bundle No.	$^{137}\text{Cs}$ Concen.	Delta $^{137}\text{Cs}$	$^{60}\text{Co}$ Concen.	Delta $^{60}\text{Co}$
	CZ205	5.53	+0.11	14.5	+ 10.71
A	CZ296	7.03	+1.61	10.9	+ 7.11
B	CZ225	8.48	+3.06	21.9	+ 18.11
C	CZ526	5.43	+0.01	13.6	+ 9.81
D	CZ379	10.3	+4.88	65.5	+ 61.71
E	CZ147	10.1	+4.68	31.6	+ 27.81
F	CZ369	7.07	+1.65	42.5	+ 38.71
G	CZ528	5.74	+0.32	55.4	+ 51.61
H	CZ498	6.86	+1.44	67.1	+ 63.31
I	CZ211	5.82	+0.40	63.7	+ 60.11

TABLE F.3. Sipping Tests For Cooper Fuel  
Pre-Characterization, Basket B-88

Date Tested		: September 18, 1984			
Basin Water Temperature		: 29.5°C			
Basin Sample $^{137}\text{Cs}$ Concentration:		6.15 x 10 <sup>-5</sup> $\mu\text{Ci/ml}$			
Basin Sample $^{60}\text{Co}$ Concentration :		2.89 x 10 <sup>-5</sup> $\mu\text{Ci/ml}$			
Bask.	Bundle	$^{137}\text{Cs}$	Delta	$^{60}\text{Co}$	Delta
Pos.	No.	Concen.	$^{137}\text{Cs}$	Concen.	$^{60}\text{Co}$
	CZ205	5.70	-0.45	18.3	- 10.6
A	CZ239	4.81	-1.34	5.04	- 23.86
B	CZ531	5.08	-1.07	8.87	- 20.03
C	CZ430	5.01	-1.14	12.4	- 16.5
D	CZ416	5.51	-0.64	7.64	- 21.26
E	CZ34B	5.10	-1.05	8.13	- 20.77
F	CZ337	5.16	-0.99	8.77	- 20.13
G	CZ308	6.08	-0.07	18.6	- 10.30
H	CZ246	13.3	+7.15	235.	+206.1
I	CZ222	8.12	+1.95	81.2	+ 52.3

TABLE F.4. Sipping Tests For Cooper Fuel  
Pre-Characterization, Basket B-90

Date Tested		: September 20, 1984			
Basin Water Temperature		: 29.1°C			
Basin Sample $^{137}\text{Cs}$ Concentration:		4.14 x 10 <sup>-5</sup> $\mu\text{Ci/ml}$			
Basin Sample $^{60}\text{Co}$ Concentration :		8.11 x 10 <sup>-5</sup> $\mu\text{Ci/ml}$			
Bask.	Bundle	$^{137}\text{Cs}$	Delta	$^{60}\text{Co}$	Delta
Pos.	No.	Concen.	$^{137}\text{Cs}$	Concen.	$^{60}\text{Co}$
	CZ205	5.28	+1.14	26.9	+ 18.8
A	CZ342	7.45	+3.31	34.	+ 25.9
B	CZ318	10.3	+6.16	163.	+154.9
C	CZ315	10.6	-3.08	111.	+102.9
D	CZ182	8.77	+4.63	54.5	+ 46.4
E	CZ370	5.31	+1.17	7.49	- 0.6
F	CZ357	4.97	+0.83	8.85	+ 0.75
G	CZ542	5.28	+1.14	7.20	- 0.9
H	CZ508	5.78	+1.64	9.40	+ 1.3
I	CZ466	4.70	+0.56	8.62	+ 0.52
Basin Sample $^{137}\text{Cs}$ Concentration:		4.73 x 10 <sup>-5</sup> $\mu\text{Ci/ml}$			
Basin Sample $^{60}\text{Co}$ Concentration :		4.32 x 10 <sup>-4</sup> $\mu\text{Ci/ml}$			
	CZ205	4.73	-0.45	43.2	- 24.4



TABLE F.5. Sipping Tests For Cooper Fuel  
Pre-Characterization, Basket B-91

Date Tested	:	September 21, 1984			
Basin Water Temperature	:	28.9°C			
Basin Sample <sup>137</sup> Cs Concentration:	:	4.10 x 10 <sup>-5</sup> μCi/ml			
Basin Sample <sup>60</sup> Co Concentration :	:	1.25 x 10 <sup>-4</sup> μCi/ml			
Bask.	Bundle	<sup>137</sup> Cs	Delta	<sup>60</sup> Co	Delta
<u>Pos.</u>	<u>No.</u>	<u>Concen.</u>	<u><sup>137</sup>Cs</u>	<u>Concen.</u>	<u><sup>60</sup>Co</u>
	CZ205	8.42	+ 4.32	15.0	+ 12.5
A	CZ460	8.21	+ 4.11	40.9	+ 28.4
B	CZ351	8.28	+ 4.18	80.2	+ 67.7
C	CZ415	6.24	+ 2.14	57.8	+ 45.3
D	CZ473	6.95	+ 2.85	59.3	+ 46.8
E	CZ472	6.03	+ 1.93	48.3	+ 35.8
F	CZ468	1.38	- 2.72	12.0	- 0.5
G	CZ545	9.70	+ 5.60	11.3	- 1.2
H	CZ372	13.4	+ 9.3	21.3	+ 8.8
I	CZ536	17.6	+13.5	9.74	- 2.76
	Back-ground	4.43	+ 0.33	88.3	+ 75.8

TABLE F.6. Sipping Tests For Cooper Fuel  
Pre-Characterization, Basket B-92

Date Tested	:	See below				
Basin Water Temperature	:	Not Available				
Basin Sample <sup>137</sup> Cs Concentration:	:	4.43 x 10 <sup>-5</sup> μCi/ml				
Basin Sample <sup>60</sup> Co Concentration :	:	8.83 x 10 <sup>-4</sup> μCi/ml				
Bask.	Bundle	<sup>137</sup> Cs	Delta	<sup>60</sup> Co	Delta	
Pos.	No.	Concen.	<sup>137</sup> Cs	Concen.	<sup>60</sup> Co	
	CZ205	092284	4.48	+ 0.05	51.6	- 36.7
A	CZ515	092184	9.52	+ 5.09	80.6	- 7.7
I	CZ433	092184	8.78	+ 4.35	150.	+ 61.7

TABLE F.7. Sipping Tests For Cooper Fuel  
Pre-Characterization, Basket B-93

Date Tested		: September 18, 1984			
Basin Water Temperature		: 29.2°C			
Basin Sample $^{137}\text{Cs}$ Concentration:		$5.18 \times 10^{-5} \mu\text{Ci/ml}$			
Basin Sample $^{60}\text{Co}$ Concentration :		$4.15 \times 10^{-5} \mu\text{Ci/ml}$			
Bask. Pos.	Bundle No.	$^{137}\text{Cs}$ Concen.	Delta $^{137}\text{Cs}$	$^{60}\text{Co}$ Concen.	Delta $^{60}\text{Co}$
	CZ205	5.43	+ 0.25	28.1	+ 23.9
A	CZ429	5.05	- 0.13	10.1	+ 5.95
B	CZ311	5.01	- 0.17	7.55	+ 3.40
C	CZ398	5.99	+ 0.81	20.1	+ 15.95
E	CZ346	10.3	+ 5.12	117.	+172.8
G	CZ277	8.27	+ 3.09	78.0	+ 73.85
H	CZ355	5.41	+ 0.23	11.9	+ 7.75
I	CZ209	6.00	+ 0.82	53.2	+ 49.1

TABLE F.8. Sipping Tests For Cooper Fuel  
Post-Characterization, Basket B-85

Date Tested		: May 2, 1985			
Basin Water Temperature		: 25.5°C			
Basin Sample $^{137}\text{Cs}$ Concentration:		$8.70 \times 10^{-5} \mu\text{Ci/ml}$			
Basin Sample $^{60}\text{Co}$ Concentration :		$6.51 \times 10^{-5} \mu\text{Ci/ml}$			
Bask. Pos.	Bundle No.	$^{137}\text{Cs}$ Concen.	Delta $^{137}\text{Cs}$	$^{60}\text{Co}$ Concen.	Delta $^{60}\text{Co}$
	CZ205	9.69	+ 0.99	23.2	+ 16.69
A	CZ302	11.9	+ 3.2	29.1	+ 22.59
B	CZ259	10.9	+ 2.2	33.1	+ 26.59
Date Tested		: May 3, 1985			
Basin Water Temperature		: 26.1°C			
Basin Sample $^{137}\text{Cs}$ Concentration:		$7.64 \times 10^{-5} \mu\text{Ci/ml}$			
Basin Sample $^{60}\text{Co}$ Concentration :		$3.28 \times 10^{-5} \mu\text{Ci/ml}$			
Bask. Pos.	Bundle No.	$^{137}\text{Cs}$ Concen.	Delta $^{137}\text{Cs}$	$^{60}\text{Co}$ Concen.	Delta $^{60}\text{Co}$
C	CZ264	8.45	+ 0.81	11.6	+ 8.32
D	CZ331	13.2	+ 5.56	33.7	+ 30.42
F	CZ102	12.3	+ 4.66	25.3	+ 22.02
G	CZ2B6	8.97	+ 1.33	18.0	+ 14.72
H	CZ148	9.02	+ 1.38	18.2	+ 17.92
I	CZ195	10.4	+ 2.76	29.3	+ 26.02

TABLE F.9. Sipping Tests For Cooper Fuel  
Post-Characterization, Basket B-86

Date Tested		: May 4, 1985			
Basin Water Temperature		: 27.5°C			
Basin Sample <sup>137</sup> Cs Concentration:		8.79 x 10 <sup>-5</sup> μCi/ml			
Basin Sample <sup>60</sup> Co Concentration :		3.37 x 10 <sup>-5</sup> μCi/ml			
<u>Bask.</u> <u>Pos.</u>	<u>Bundle</u> <u>No.</u>	<sup>137</sup> Cs <u>Concen.</u>	Delta <sup>137</sup> Cs	<sup>60</sup> Co <u>Concen.</u>	Delta <sup>60</sup> Co
	CZ205	9.20	+ 0.41	24.3	+ 20.93
A	CZ296	11.9	+ 3.11	15.3	+ 11.93
B	CZ225	9.34	+ 0.55	13.2	+ 9.83
D	CZ379	6.34	- 2.45	12.8	+ 9.43
E	CZ147	6.10	- 2.69	4.68	+ 1.28
F	CZ369	6.37	- 2.42	6.34	+ 2.97
H	CZ498	4.47	- 4.32	5.70	+ 2.33
I	CZ211	10.4	+ 1.61	21.6	+ 18.23

TABLE F.10. Sipping Tests For Cooper Fuel  
Post-Characterization, Basket B-88

Date Tested		: May 5, 1985			
Basin Water Temperature		: 28°C			
Basin Sample <sup>137</sup> Cs Concentration:		8.92 x 10 <sup>-5</sup> μCi/ml			
Basin Sample <sup>60</sup> Co Concentration :		3.47 x 10 <sup>-5</sup> μCi/ml			
<u>Bask.</u> <u>Pos.</u>	<u>Bundle</u> <u>No.</u>	<sup>137</sup> Cs <u>Concen.</u>	Delta <sup>137</sup> Cs	<sup>60</sup> Co <u>Concen.</u>	Delta <sup>60</sup> Co
	CZ205	7.40	- 1.52	8.72	+ 5.25
A	CZ239	9.89	+ 0.97	9.05	+ 5.58
B	CZ531	8.27	- 0.65	6.57	+ 3.10
C	CZ416	8.93	+ 0.01	6.68	+ 3.21
E	CZ348	9.09	+ 0.17	8.91	+ 5.44
G	CZ308	7.92	- 1.00	6.51	+ 3.04
H	CZ430	10.2	+ 1.28	11.3	+ 7.83
I	CZ337	9.14	+ 0.22	7.89	+ 4.42



TABLE F.11. Sipping Tests For Cooper Fuel  
Post-Characterization, Basket B-90

Date Tested		: May 6, 1985			
Basin Water Temperature		: 27.1°C			
Basin Sample <sup>137</sup> Cs Concentration:		6.61 x 10 <sup>-5</sup> μCi/ml			
Basin Sample <sup>60</sup> Co Concentration :		2.80 x 10 <sup>-5</sup> μCi/ml			
Bask. Pos.	Bundle No.	<sup>137</sup> Cs Concen.	Delta <sup>137</sup> Cs	<sup>60</sup> Co Concen.	Delta <sup>60</sup> Co
	CZ205	8.34	+ 1.73	13.7	+ 10.9
A	CZ342	10.4	+ 3.79	24.1	+ 21.3
B	CZ318	11.6	+ 4.99	16.6	+ 13.8
C	CZ315	10.1	+ 3.49	13.8	+ 11.0
D	CZ182	10.7	+ 4.09	23.1	+ 20.3
F	CZ357	8.54	+ 1.93	13.7	+ 10.9
G	CZ542	9.88	+ 3.27	15.4	+ 12.6
H	CZ508	10.2	+ 3.59	12.8	+ 10.0
I	CZ466	8.66	+ 2.05	11.6	+ 8.8

TABLE F.12. Sipping Tests For Cooper Fuel  
Post-Characterization, Basket B-91

Date Tested		: May 6, 1985			
Basin Water Temperature		: 26.0°C			
Basin Sample <sup>137</sup> Cs Concentration:		6.88 x 10 <sup>-5</sup> μCi/ml			
Basin Sample <sup>60</sup> Co Concentration :		3.62 x 10 <sup>-5</sup> μCi/ml			
Bask. Pos.	Bundle No.	<sup>137</sup> Cs Concen.	Delta <sup>137</sup> Cs	<sup>60</sup> Co Concen.	Delta <sup>60</sup> Co
	CZ205	6.37	- 0.51	6.52	+ 2.9
A	CZ460	5.94	- 0.94	7.72	+ 4.1
B	CZ351	6.00	- 0.88	8.11	+ 4.49
Date Tested		: May 7, 1985			
Basin Water Temperature		: 26.0°C			
Basin Sample <sup>137</sup> Cs Concentration:		8.00 x 10 <sup>-5</sup> μCi/ml			
Basin Sample <sup>60</sup> Co Concentration :		3.47 x 10 <sup>-5</sup> μCi/ml			
Bask. Pos.	Bundle No.	<sup>137</sup> Cs Concen.	Delta <sup>137</sup> Cs	<sup>60</sup> Co Concen.	Delta <sup>60</sup> Co
C	CZ415	5.57	- 3.43	6.37	+ 2.9
D	CZ473	9.39	+ 1.39	11.1	+ 7.63
E	CZ472	8.49	+ 0.49	8.14	+ 4.67
F	CZ468	9.73	+ 1.73	10.5	+ 7.03
G	CZ545	11.1	+ 3.1	12.7	+ 9.23
H	CZ372	11.1	+ 3.1	13.1	+ 9.63

TABLE F.13. Sipping Tests For Cooper Fuel  
Post-Characterization, Basket B-92

Date Tested	:	May 7, 1985			
Basin Water Temperature	:	26.5°C			
Basin Sample <sup>137</sup> Cs Concentration:	:	8.00 x 10 <sup>-5</sup> μCi/ml			
Basin Sample <sup>60</sup> Co Concentration :	:	3.47 x 10 <sup>-5</sup> μCi/ml			
Bask.	Bundle	<sup>137</sup> Cs	Delta	<sup>60</sup> Co	Delta
<u>Pos.</u>	<u>No.</u>	<u>Concen.</u>	<u><sup>137</sup>Cs</u>	<u>Concen.</u>	<u><sup>60</sup>Co</u>
	CZ205	8.33	+ 0.33	10.0	+ 7.53
A	CZ515	11.8	+ 3.80	20.2	+ 16.73
B	CZ370	10.9	+ 2.90	12.9	+ 9.43
C	CZ526	7.77	- 0.23	5.71	+ 2.24
D	CZ536	8.18	+ 0.18	8.01	+ 4.54
E	CZ222	7.90	- 0.10	6.72	+ 3.25
F	CZ346	8.34	+ 0.34	10.7	+ 7.23

Date Tested	:	May 8, 1985			
Basin Water Fuel Temperature	:	26.5°C			
Basin Sample <sup>137</sup> Cs Concentration:	:	8.00 x 10 <sup>-5</sup> μCi/ml			
Basin Sample <sup>60</sup> Co Concentration :	:	3.47 x 10 <sup>-5</sup> μCi/ml			
Bask.	Bundle	<sup>137</sup> Cs	Delta	<sup>60</sup> Co	Delta
<u>Pos.</u>	<u>No.</u>	<u>Concen.</u>	<sup>137</sup> Cs	<u>Concen.</u>	<sup>60</sup> Co
F	CZ346	7.55	- 0.45	7.22	+ 3.75
G	CZ528	8.01	+ 0.01	5.62	+ 2.15
H	CZ246	7.83	- 0.17	6.55	+ 3.08
I	CZ433	8.98	+ 0.98	3.98	+ 0.51

TABLE F.14. Sipping Tests For Cooper Fuel  
Post-Characterization, Basket B-93

Date Tested	:	May 8, 1985			
Basin Water Temperature	:	27.5°C			
Basin Sample $^{137}\text{Cs}$ Concentration:	:	$8.79 \times 10^{-5} \mu\text{Ci/ml}$			
Basin Sample $^{60}\text{Co}$ Concentration :	:	$3.47 \times 10^{-5} \mu\text{Ci/ml}$			
Bask.	Bundle	$^{137}\text{Cs}$	Delta	$^{60}\text{Co}$	Delta
<u>Pos.</u>	<u>No.</u>	<u>Concen.</u>	$^{137}\text{Cs}$	<u>Concen.</u>	$^{60}\text{Co}$
	CZ205	8.51	- 0.28	8.88	+ 5.41
A	CZ429	10.8	+ 2.01	16.3	+ 12.83
B	CZ311	9.88	+ 1.09	18.9	+ 15.43
C	CZ209	10.0	+ 1.21	15.3	+ 11.83
G	CZ277	11.2	+ 2.41	15.0	+ 11.53
H	CZ355	12.1	+ 3.31	25.2	+ 21.73
I	CZ398	13.0	+ 4.21	15.6	+ 11.13

APPENDIX G

CASK TEMPERATURE PERFORMANCE DATA

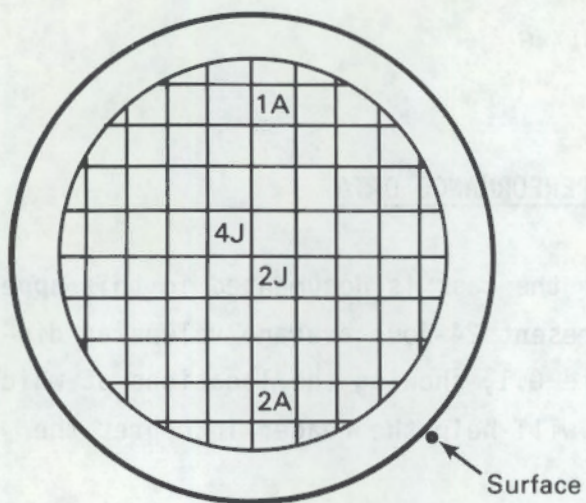


## APPENDIX G

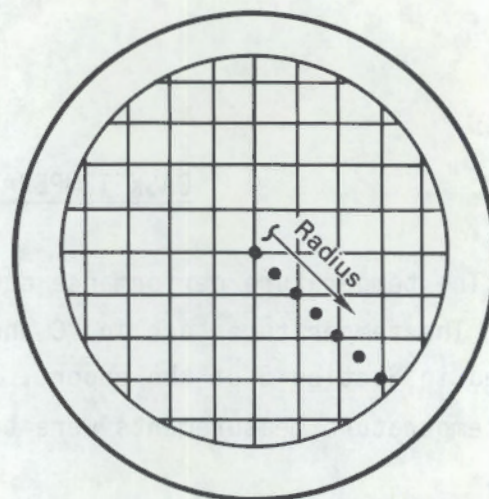
### CASK TEMPERATURE PERFORMANCE DATA

The temperature performance data for the cask is documented in this appendix. The temperatures are in °C and represent 24-hour average values as discussed in Section 5 of the report. Figure G.1, showing the locations at which the temperature measurements were taken, will help the reader interpret the data.

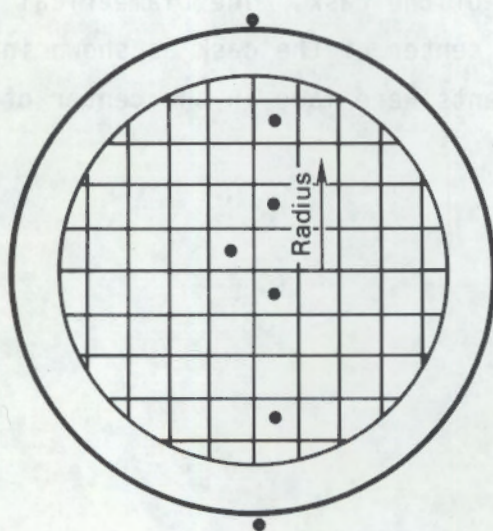
Both English and metric units have been used in the tables. All elevations and radii are in meters. The positions under Radial and Diametrical profiles are in inches. EL.50 represents a cross section of the cask 1.45 m (50 in.) above the bottom. Likewise, EL.123 and EL.169 are plane 3.3 m (123 in.) and 4.3 m (169 in.) above the bottom of the cask. The Diametrical radius and Radial radius are referenced to the center of the cask as shown in Figure G.1. All internal temperature measurements were made in the center of fuel assemblies or in basket slots.



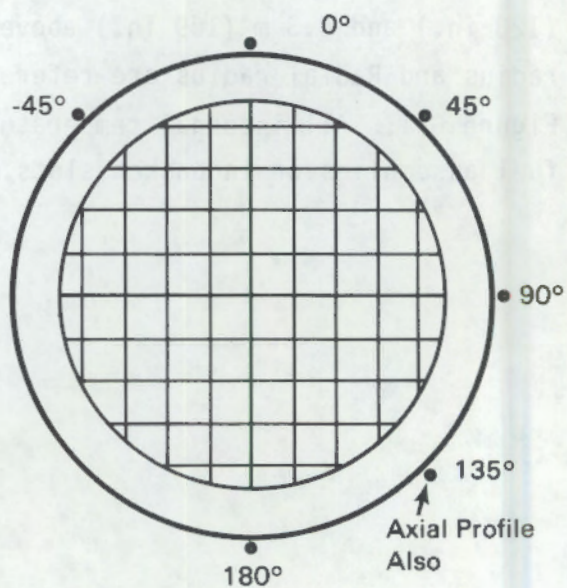
a. Axial Temperature Measurement Locations



b. Radial Temperature Measurement Locations



c. Diametrical Temperature Measurement Locations



d. Surface Temperature Measurement Locations

FIGURE G.1. Key to Temperature Measurement Locations

TABLE G.1. Vertical Vacuum Run

GENERAL RUN CONDITIONS			
Run No.	1	Date:	Nov 25, 1984
Loading	Partial	Temp.	6.7 C
Wind Sp.	5 MPH	Solar	85 W/m <sup>2</sup>
Cask P	4 mm Hg	Power	9 KW

AXIAL PROFILE DATA				
ELEV (M)	-----Basket Locations-----			
	2J	4J SURFACE	1A	2A
4.9	10.7	11.5		
4.5	48.6	16.1	43.4	43.0
3.8	111.6	18.4		
3.3	149.4	154.4	126.8	116.9
2.8	161.2	21.3		
2.0	165.7	21.3	143.6	135.5
1.4	162.6	166.4	138.8	132.6
0.7	129.9	19.9		
0.2	50.8	13.4	46.9	47.0
0.0	24.1	18.9		

RADIAL PROFILES			DIAMETRICAL PROFILES		
RADIUS (M)	---Position--		RADIUS (M)	---Position--	
	EL.50	EL.123		EL.50	EL.123
0.00	95.2	86.1	1.11	20.3	19.1
0.13	162.6	149.9	0.58	138.8	126.8
0.25	108.3	98.8	0.25	159.6	142.7
0.38	149.8	133.4	0.09	166.4	154.4
0.49	97.1	83.6	-0.09	162.6	149.4
0.61	135.3	123.6	-0.58	132.6	116.9
0.75	61.3	61.4	-1.11	17.0	19.0
1.11	20.0	18.0	AMB.	6.7	6.7

SURFACE TEMPERATURE PROFILE			
ANGLE	-----Position-----		
	EL.50	EL.123	EL.169
-45	17.1	19.2	19.5
0	17.0	19.1	20.5
45	15.2	18.7	19.0
90	20.1	18.3	17.3
135	20.0	18.0	16.1
180	20.3	19.1	14.5



TABLE G.2. Vertical Nitrogen Run

GENERAL RUN CONDITIONS					
Run No.	2	Date:	Dec 1, 1984		
Loading	Partial	Temp.	1 C		
Wind Sp.	3 MPH	Solar	84 W/m <sup>2</sup>		
Cask P	20.4 psia	Power	8.9 KW		

AXIAL PROFILE DATA					
ELEV (M)	-----Basket Locations-----				
	2J	4J	SURFACE	1A	2A
4.9	13.5		22.5		
4.5	79.1		20.9	74.3	77.1
3.8	116.0		15.1		
3.3	114.9	116.8	13.7	97.5	91.9
2.8	107.4		16.6		
2.0	88.0		14.7	77.0	73.9
1.4	71.5	71.9	13.5	63.4	62.5
0.7	41.7		12.5		
0.2	23.5		8.8	33.5	32.7
0.0	15.3		11.0		

RADIAL PROFILES			DIAMETRICAL PROFILES		
RADIUS (M)	---Position---		RADIUS (M)	---Position---	
	EL.50	EL.123		EL.50	EL.123
0.00	45.5	69.6	1.11	13.5	13.6
0.13	71.5	114.9	0.58	63.4	97.5
0.25	50.4	75.2	0.25	71.6	110.4
0.38	70.9	105.2	0.09	71.9	116.8
0.49	47.0	63.8	-0.09	71.5	114.9
0.61	62.3	93.5	-0.58	62.5	91.9
0.75	35.3	50.6	-1.11	8.2	14.7
1.11	13.5	13.7	AMB.	1.3	1.3

SURFACE TEMPERATURE PROFILE			
ANGLE	-----Position-----		
	EL.50	EL.123	EL.169
-45	8.1	14.0	19.9
0	8.2	13.6	21.1
45	6.7	13.5	21.0
90	13.1	13.9	21.4
135	13.5	13.7	20.9
180	13.5	14.7	18.6

TABLE G.3. Horizontal Nitrogen Run

GENERAL RUN CONDITIONS			
Run No.	3	Date:	Dec 6, 1984
Loading	Partial	Temp.	-10 C
Wind Sp.	8 MPH	Solar	94 W/m <sup>2</sup>
Cask P	20 psia	Power	8.9 KW

AXIAL PROFILE DATA					
ELEV	-----Basket Locations-----				
(M)	2J	4J	SURFACE	1A	2A
4.9	-4.0		1.5		
4.5	31.9		2.4	35.0	20.5
3.8	63.6		-0.5		
3.3	91.7	100.5	-0.6	85.3	60.7
2.8	103.6		3.1		
2.0	110.1		3.6	100.0	77.9
1.4	108.3	114.3	3.6	96.5	74.3
0.7	82.1		3.5		
0.2	42.3		4.2	50.3	29.8
0.0	0.3		1.1		

RADIAL PROFILES			DIAMETRICAL PROFILES		
RADIUS	---Position---		RADIUS	---Position---	
(M)	EL.50	EL.123	(M)	EL.50	EL.123
0.00	62.0	57.5	1.11	-7.1	-8.6
0.13	108.3	91.7	0.58	96.5	85.3
0.25	69.0	57.7	0.25	113.2	95.1
0.38	91.3	75.2	0.09	114.3	100.5
0.49	53.7	45.0	-0.09	108.3	91.7
0.61	79.8	67.2	-0.58	74.3	60.7
0.75	30.2	27.8	-1.11	-8.4	-11.3
1.11	3.6	-0.6	AMB.	-9.8	-9.8

SURFACE TEMPERATURE PROFILE			
-----Position-----			
ANGLE	EL.50	EL.123	EL.169
-45	-0.2	0.3	-3.7
0	-8.4	-8.6	2.2
45	-2.3	0.6	2.2
90	5.2	0.1	1.1
135	3.6	-0.6	2.4
180	-7.1	-11.3	3.5

TABLE G.4. Horizontal Helium Run

GENERAL RUN CONDITIONS					
Run No.	4	Date:	Dec 9, 1984		
Loading	Partial	Temp.	4.5 C		
Wind Sp.	3 MPH	Solar	87 W/m <sup>2</sup>		
Cask P	22 psia	Power	8.8 KW		

AXIAL PROFILE DATA					
ELEV	-----Basket Locations-----				
(M)	2J	4J	SURFACE	1A	2A
4.9	14.3		18.4		
4.5	29.6		19.0	30.2	24.0
3.8	59.6		19.0		
3.3	79.7	82.2	18.9	68.4	56.0
2.8	86.9		22.6		
2.0	89.9		23.4	78.7	64.4
1.4	87.5	90.4	23.5	75.9	62.4
0.7	70.8		23.7		
0.2	33.2		21.9	37.5	27.1
0.0	15.7		17.2		

RADIAL PROFILES			DIAMETRICAL PROFILES		
RADIUS	---Position---		RADIUS	---Position---	
(M)	EL.50	EL.123	(M)	EL.50	EL.123
0.00	60.0	57.1	1.11	10.5	12.1
0.13	87.5	79.7	0.58	75.9	68.4
0.25	63.8	58.5	0.25	88.7	78.2
0.38	79.3	71.4	0.09	90.4	82.2
0.49	55.2	49.4	-0.09	87.5	79.7
0.61	68.3	61.6	-0.58	62.4	56.0
0.75	33.6	36.9	-1.11	10.8	5.6
1.11	23.5	18.9	AM8.	4.5	4.5

SURFACE TEMPERATURE PROFILE			
	-----Position-----		
ANGLE	EL.50	EL.123	EL.169
-45	20.3	20.4	18.4
0	10.8	12.1	22.3
45	18.3	20.3	20.3
90	24.3	19.8	19.1
135	23.5	18.9	19.0
180	10.5	5.6	19.5



TABLE G.5. Vertical Helium Run

GENERAL RUN CONDITIONS			
Run No.	5A	Date:	Dec 19, 1984
Loading	Partial	Temp.	-3 C
Wind Sp.	8 MPH	Solar	21 W/m <sup>2</sup>
Cask P	21.5 psia	Power	8.8 KW

AXIAL PROFILE DATA				
ELEV	-----Basket Locations-----			
(M)	2J	4J SURFACE	1A	2A
4.9	-0.2	2.9		
4.5	34.3	8.6	29.6	27.8
3.8	68.6	7.6		
3.3	83.1	6.6	63.8	58.7
2.8	85.6	9.7		
2.0	79.2	9.3	64.3	60.0
1.4	71.4	8.5	58.0	55.7
0.7	46.4	8.2		
0.2	14.6	2.1	18.3	17.6
0.0	11.4	7.1		

RADIAL PROFILES			DIAMETRICAL PROFILES		
RADIUS	---Position---		RADIUS	---Position---	
(M)	EL.50	EL.123	(M)	EL.50	EL.123
0.00	43.9	53.8	1.11	8.3	7.5
0.13	71.4	83.1	0.58	58.0	63.8
0.25	49.6	58.1	0.25	68.4	76.0
0.38	63.5	69.9	0.09	71.6	82.9
0.49	41.5	48.7	-0.09	71.4	83.1
0.61	57.3	64.3	-0.58	55.7	58.7
0.75	26.2	35.2	-1.11	4.5	7.9
1.11	8.5	6.6	AMB.	-3.1	-3.1

SURFACE TEMPERATURE PROFILE			
-----Position-----			
ANGLE	EL.50	EL.123	EL.169
-45	4.0	7.5	3.2
0	4.5	7.5	10.6
45	2.9	7.6	9.9
90	9.5	7.8	9.6
135	8.5	6.6	8.6
180	8.3	7.9	4.5

TABLE G.6. Vertical Helium Run

GENERAL RUN CONDITIONS					
Run No.	5B	Date:	Dec 28, 1984		
Loading	Partial	Temp.	14 C		
Wind Sp.	14 MPH	Solar	16 W/m <sup>2</sup>		
Cask P	21.5 psia	Power	8.7 KW		

AXIAL PROFILE DATA					
ELEV (M)	-----Basket Locations-----				
	2J	4J	SURFACE	1A	2A
4.9	16.1		18.2		
4.5	48.0		21.9	43.2	40.9
3.8	79.3		21.6		
3.3	93.9	93.9	20.5	75.9	71.3
2.8	96.6		20.7		
2.0	91.1		20.5	76.8	73.3
1.4	84.1	84.4	20.1	71.2	68.9
0.7	60.5		20.2		
0.2	29.0		16.9	34.0	32.5
0.0	26.3		22.3		

RADIAL PROFILES			DIAMETRICAL PROFILES		
RADIUS (M)	---Position---		RADIUS (M)	---Position---	
	EL.50	EL.123		EL.50	EL.123
0.00	58.4	66.2	1.11	20.1	21.5
0.13	84.1	93.9	0.58	71.2	75.9
0.25	63.1	70.6	0.25	81.9	87.7
0.38	76.7	81.5	0.09	84.4	93.9
0.49	55.1	61.0	-0.09	81.5	93.9
0.61	70.2	75.8	-0.58	68.9	71.3
0.75	40.3	47.8	-1.11	19.4	22.1
1.11	20.1	20.9	AMB.	13.9	13.9

SURFACE TEMPERATURE PROFILE			
ANGLE	-----Position-----		
	EL.50	EL.123	EL.169
-45	19.8	21.9	18.9
0	19.4	21.5	23.6
45	18.4	21.5	23.6
90	20.9	22.0	23.2
135	20.1	20.9	21.9
180	20.1	22.1	20.5

TABLE G.7. Vertical Vacuum Run

GENERAL RUN CONDITIONS				
Run No.	6A	Date:	Jan 13, 1985	
Loading	Full	Temp.	24 C	
Wind Sp.	0	Solar	0	
Cask P	1 mm Hg	Power	15.2 KW	

AXIAL PROFILE DATA				
ELEV (M)	-----Basket Locations-----			
	2J	4J SURFACE	1A	2A
4.9		38.4		
4.5	98.4	54.6	91.6	91.7
3.8	162.6	54.2		
3.3	202.0	207.8	56.3	186.4
2.8	216.0	53.5		
2.0	222.0	54.7	209.2	195.5
1.4	217.9	222.7	54.4	202.4
0.7	181.0	49.3		192.6
0.2	104.4	52.0	98.7	97.7
0.0				

RADIAL PROFILES			DIAMETRICAL PROFILES		
RADIUS (M)	---Position---		RADIUS (M)	---Position---	
	EL.50	EL.123		EL.50	EL.123
0.00	164.1	150.9	1.11	54.5	56.8
0.13	217.9	202.2	0.58	202.4	186.4
0.25	181.1	165.9	0.25	221.6	201.2
0.38	217.5	196.4	0.09	222.7	207.8
0.49	189.0	168.8	-0.09	217.9	202.2
0.61	208.3	191.2	-0.58	192.6	171.7
0.75	122.4	123.7	-1.11	55.1	57.5
1.11	54.4	56.3	AMB.	24.3	24.3

SURFACE TEMPERATURE PROFILE			
ANGLE	-----Position-----		
	EL.50	EL.123	EL.169
-45	55.1	57.2	50.9
0	55.1	56.8	52.6
45	54.5	56.0	53.3
90	53.8	56.0	53.8
135	54.4	56.3	54.6
180	54.5	57.5	55.4



TABLE G.8. Vertical Vacuum Run

GENERAL RUN CONDITIONS					
Run No.	6B	Date:	Jan 19, 1985		
Loading	Full	Temp.	-10 C		
Wind Sp.	8 MPH	Solar	60 W/m <sup>2</sup>		
Cask P	4.4 mm Hg	Power	15.2 KW		

AXIAL PROFILE DATA					
ELEV (M)	-----Basket Locations-----				
	2J	4J	SURFACE	1A	2A
4.9	-2.0		-0.8		
4.5	62.0		11.2	54.0	54.1
3.8	131.8		9.9		
3.3	172.8	180.2	13.1	158.2	143.2
2.8	187.5		13.2		
2.0	194.6		10.9	181.0	168.2
1.4	190.7	196.2	10.5	174.2	164.7
0.7	153.6		9.7		
0.2	66.4		0.4	64.5	61.5
0.0	24.1		15.1		

RADIAL PROFILES			DIAMETRICAL PROFILES		
RADIUS (M)	---Position--		RADIUS (M)	---Position--	
	EL.50	EL.123		EL.50	EL.123
0.00	131.6	116.7	1.11	9.6	11.1
0.13	190.7	172.8	0.58	174.2	158.2
0.25	148.9	132.2	0.25	195.6	173.3
0.38	190.6	168.1	0.09	196.2	180.2
0.49	158.1	135.4	-0.09	190.7	172.8
0.61	180.9	162.3	-0.58	164.7	143.2
0.75	86.8	87.7	-1.11	7.4	13.1
1.11	10.5	13.1	AMB.	-9.8	-9.8

SURFACE TEMPERATURE PROFILE			
ANGLE	-----Position-----		
	EL.50	EL.123	EL.169
-45	9.3	12.3	6.7
0	7.4	11.1	9.7
45	9.2	11.9	11.4
90	7.8	11.5	10.4
135	10.5	13.1	11.2
180	9.6	13.1	13.5

TABLE G.9. Vertical Nitrogen Run

GENERAL RUN CONDITIONS			
Run No.	7	Date:	Jan 25, 1985
Loading	Full	Temp.	-4 C
Wind Sp.	7 MPH	Solar	43 W/m <sup>2</sup>
Cask P	20.5 psia	Power	15.1 KW

AXIAL PROFILE DATA				
ELEV	-----Basket Locations-----			
(M)	2J	4J SURFACE	1A	2A
4.9	7.7	20.4		
4.5	105.4	21.0	97.1	100.2
3.8	147.6	17.8		
3.3	150.9	151.1	17.3	136.3
2.8	145.8	15.3		
2.0	126.9	11.3	114.5	111.2
1.4	108.7	106.3	10.9	97.5
0.7	69.3	9.6		
0.2	38.7	7.5	64.3	60.1
0.0	25.4	16.7		

RADIAL PROFILES			DIAMETRICAL PROFILES		
RADIUS	---Position--		RADIUS	---Position--	
(M)	EL.50	EL.123	(M)	EL.50	EL.123
0.00	77.2	104.8	1.11	4.0	17.3
0.13	108.7	150.9	0.58	97.5	136.3
0.25	85.3	116.0	0.25	106.3	151.1
0.38	106.1	146.3	0.09	107.7	154.1
0.49	82.0	111.6	-0.09	108.7	150.9
0.61	93.7	133.9	-0.58	97.7	127.0
0.75	59.4	82.8	-1.11	9.2	16.7
1.11	10.9	17.3	AMB.	-3.9	-3.9

SURFACE TEMPERATURE PROFILE			
-----Position-----			
ANGLE	EL.50	EL.123	EL.169
-45	10.7	17.0	17.2
0	9.2	17.3	28.0
45	10.6	17.2	28.7
90	9.5	16.4	24.3
135	10.9	17.3	21.0
180	4.0	16.7	18.1

TABLE G.10. Vertical Nitrogen Run

GENERAL RUN CONDITIONS					
Run No.	8	Date:	Feb 3, 1985		
Loading	Full	Temp.	-16.5 C <sub>2</sub>		
Wind Sp.	3 MPH	Solar	143 W/m <sup>2</sup>		
Cask P	20.8 psia	Power	14.9 KW		

AXIAL PROFILE DATA					
ELEV	-----Basket Locations-----				
(M)	2J	4J	SURFACE	1A	2A
4.9	9.8		20.6		
4.5	100.5		26.2	93.6	93.1
3.8	141.3		16.7		
3.3	144.5	145.7	15.4	129.5	117.9
2.8	138.6		13.4		
2.0	118.2		8.1	107.7	102.1
1.4	98.8	98.4	7.5	89.6	89.5
0.7	58.0		5.0		
0.2	30.5		-1.2	55.9	51.1
0.0	19.7		11.2		

RADIAL PROFILES			DIAMETRICAL PROFILES		
RADIUS	---Position---		RADIUS	---Position---	
(M)	EL.50	EL.123	(M)	EL.50	EL.123
0.00	69.4	97.4	1.11	5.3	15.9
0.13	98.8	144.5	0.58	89.6	129.5
0.25	77.9	108.6	0.25	97.2	141.6
0.38	97.6	137.3	0.09	98.4	145.7
0.49	73.8	104.2	-0.09	98.8	144.5
0.61	86.6	127.9	-0.58	89.5	117.9
0.75	52.1	75.6	-1.11	5.5	15.6
1.11	7.5	15.4	AMB.	-16.5	-16.5

SURFACE TEMPERATURE PROFILE			
-----Position-----			
ANGLE	EL.50	EL.123	EL.169
-45	7.8	16.1	21.0
0	5.5	15.9	30.5
45	7.1	14.1	28.1
90	6.3	14.0	20.1
135	7.5	15.4	26.2
180	5.3	15.6	21.1



TABLE G.11. Horizontal Nitrogen Run

GENERAL RUN CONDITIONS			
Run No.	9	Date:	Jan 30, 1985
Loading	Full	Temp.	-3.9 C
Wind Sp.	4.5 MPH	Solar	47.5 W/m <sup>2</sup>
Cask P	20.8 psia	Power	15 KW

AXIAL PROFILE DATA					
ELEV (M)	-----Basket Locations-----				
	2J	4J	SURFACE	1A	2A
4.9	11.0		15.4		
4.5	59.8		24.7	66.8	45.7
3.8	95.7		23.9		
3.3	126.8	140.7	24.6	131.3	94.2
2.8			23.8		
2.0	152.4		22.8	156.4	94.7
1.4	150.8	161.8	23.9	150.3	117.0
0.7	119.2		25.0		
0.2	73.6		24.3	89.3	64.4
0.0	24.8		22.0		

RADIAL PROFILES			DIAMETRICAL PROFILES		
RADIUS (M)	---Position---		RADIUS (M)	---Position---	
	EL.50	EL.123		EL.50	EL.123
0.00	109.9	100.0	1.11	4.2	13.3
0.13	150.8	126.8	0.58	150.3	131.3
0.25	119.3	99.8	0.25	162.8	138.9
0.38	145.1	118.5	0.09	161.8	140.7
0.49	117.8	94.7	-0.09	150.8	126.8
0.61	132.6	108.8	-0.58	117.0	94.2
0.75	67.8	62.0	-1.11	11.8	4.3
1.11	23.9	24.6	AMB.	-3.9	-3.9

SURFACE TEMPERATURE PROFILE			
ANGLE	-----Position-----		
	EL.50	EL.123	EL.169
-45	26.5	26.4	22.4
0	11.8	13.3	27.6
45	25.8	24.6	25.5
90	23.7	24.3	22.0
135	23.9	24.6	24.7
180	4.2	4.3	26.1

TABLE G.12. Horizontal Helium Run

GENERAL RUN CONDITIONS					
Run No.	10	Date:	Feb 14, 1985		
Loading	Full	Temp.	-8 C		
Wind Sp.	9.4 MPH	Solar	127 W/m <sup>2</sup>		
Cask P	20.2 psia	Power	14.8 KW		

AXIAL PROFILE DATA					
ELEV	-----Basket Locations-----				
(M)	2J	4J	SURFACE	1A	2A
4.9	2.7		5.5		
4.5	30.2		14.5	31.0	22.0
3.8	67.6		10.2		
3.3	92.1	96.8	11.6	84.4	65.2
2.8	102.3		11.2		
2.0	106.0		10.1	99.9	77.6
1.4	102.8	110.2	11.5	95.5	74.5
0.7	80.4		11.6		
0.2	32.7		12.2	44.1	27.4
0.0	6.7		5.9		

RADIAL PROFILES			DIAMETRICAL PROFILES		
RADIUS	---Position---		RADIUS	---Position---	
(M)	EL.50	EL.123	(M)	EL.50	EL.123
0.00	77.0	70.7	1.11	-4.5	4.1
0.13	102.8	92.1	0.58	95.5	84.4
0.25	81.8	73.3	0.25	109.0	95.7
0.38	97.8	86.7	0.09	110.2	96.8
0.49	80.6	70.3	-0.09	102.8	92.1
0.61	88.4	78.1	-0.58	74.5	65.2
0.75	39.4	43.6	-1.11	2.7	-4.9
1.11	11.5	11.6	AMB.	-7.8	-7.8

SURFACE TEMPERATURE PROFILE			
	-----Position-----		
ANGLE	EL.50	EL.123	EL.169
-45	11.7	11.8	8.7
0	2.7	4.1	14.1
45	15.4	13.4	13.6
90	12.2	10.1	10.1
135	11.5	11.6	14.5
180	-4.5	-4.9	14.6

TABLE G.13. Vertical Helium Run

GENERAL RUN CONDITIONS					
Run No.	11A	Date:	Feb 5, 1985		
Loading	Full	Temp.	-14 C		
Wind Sp.	2 MPH	Solar	141 W/m <sup>2</sup>		
Cask P	20.4 psia	Power	14.9 KW		

AXIAL PROFILE DATA					
ELEV	-----Basket Locations-----				
(M)	2J	4J	SURFACE	1A	2A
4.9	8.8		12.7		
4.5	51.0		23.0	43.0	43.0
3.8	88.2		19.0		
3.3	105.9	106.3	18.9	88.4	80.0
2.8	109.8		18.8		
2.0	101.9		15.4	90.0	81.6
1.4	91.4	92.2	14.7	80.0	75.5
0.7	59.1		12.7		
0.2	19.7		2.6	31.8	29.1
0.0	17.1		13.0		

RADIAL PROFILES			DIAMETRICAL PROFILES		
RADIUS	---Position--		RADIUS	---Position--	
(M)	EL.50	EL.123	(M)	EL.50	EL.123
0.00	66.3	78.6	1.11	13.8	19.0
0.13	91.4	105.9	0.58	80.0	88.4
0.25	74.3	86.7	0.25	89.7	101.8
0.38	86.4	98.3	0.09	92.2	106.3
0.49	71.2	82.6	-0.09	91.4	105.9
0.61	81.6	94.4	-0.58	75.5	80.0
0.75	42.4	56.1	-1.11	11.5	19.0
1.11	14.7	18.9	AMB.	-14.3	-14.3

SURFACE TEMPERATURE PROFILE			
-----Position-----			
ANGLE	EL.50	EL.123	EL.169
-45	14.5	18.8	17.7
0	11.5	19.0	22.9
45	13.4	17.6	22.0
90	13.6	16.8	19.6
135	14.7	18.9	23.0
180	13.8	19.0	23.9



TABLE G.14. Vertical Helium Run

GENERAL RUN CONDITIONS					
Run No.	11B	Date:	Feb 8, 1985		
Loading	Full	Temp.	22 C		
Wind Sp.	0	Solar	0		
Cask P	22.3 psia	Power	14.6 KW		

AXIAL PROFILE DATA					
ELEV	-----Basket Locations-----				
(M)	2J	4J	SURFACE	1A	2A
4.9	49.6		50.5		
4.5	90.8		59.8	79.0	80.1
3.8	122.7		49.3		
3.3	139.4	140.7	60.9	123.4	114.6
2.8	143.2		58.5		
2.0	136.9		41.1	127.6	118.2
1.4	127.1	129.7	52.9	117.9	112.6
0.7	96.2		50.9		
0.2	57.2		45.4	67.8	65.2
0.0	57.7		52.7		

RADIAL PROFILES			DIAMETRICAL PROFILES		
RADIUS	---Position---		RADIUS	---Position---	
(M)	EL.50	EL.123	(M)	EL.50	EL.123
0.00	104.9	115.7	1.11	52.8	61.0
0.13	127.1	139.4	0.58	117.9	123.4
0.25	112.7	123.0	0.25	126.8	136.1
0.38	125.6	136.5	0.09	129.7	140.7
0.49	111.2	121.0	-0.09	127.1	139.4
0.61	119.1	129.3	-0.58	112.6	114.6
0.75	81.3	93.7	-1.11	50.5	60.3
1.11	52.9	60.9	AMB.	22.3	22.3

SURFACE TEMPERATURE PROFILE			
-----Position-----			
ANGLE	EL.50	EL.123	EL.169
-45	56.2	50.6	59.5
0	50.5	61.0	66.1
45	55.1	58.5	60.7
90	53.9	29.2	60.4
135	52.9	60.9	59.8
180	52.8	60.3	57.3

TABLE G.15. Insulated Vertical Helium Run

GENERAL RUN CONDITIONS				
Run No.	12	Date:	Mar 11, 1985	
Loading	Full	Temp.	20.2 C	
Wind Sp.	0	Solar	0	
Cask P	25.5 psia	Power	14.4 KW	

AXIAL PROFILE DATA				
ELEV (M)	-----Basket Locations-----			
	2J	4J SURFACE	1A	2A
4.9	67.9	66.2		
4.5	121.6	72.5	110.6	115.7
3.8	160.5	112.6		
3.3	179.6	177.8	111.7	153.2
2.8	185.1	114.3		
2.0	181.0	113.8	171.5	160.0
1.4	170.7	172.9	110.1	157.2
0.7	138.3	109.0		
0.2	97.9	98.7	107.9	106.7
0.0	99.6	100.0		

RADIAL PROFILES			DIAMETRICAL PROFILES		
RADIUS (M)	---Position---		RADIUS (M)	---Position---	
	EL.50	EL.123		EL.50	EL.123
0.00	148.7	129.6	1.11	112.3	111.3
0.13	170.7	179.6	0.58	161.4	161.0
0.25	159.6	165.0	0.25	167.8	172.9
0.38	169.1	175.8	0.09	172.9	177.8
0.49	158.4	161.6	-0.09	170.7	179.6
0.61	164.1	169.1	-0.58	157.2	153.2
0.75	131.3	136.9	-1.11	117.1	118.6
1.11	110.1	111.7	AMB.	20.2	20.2

SURFACE TEMPERATURE PROFILE			
ANGLE	-----Position-----		
	EL.50	EL.123	EL.169
-45	113.9	110.9	66.9
0	117.1	111.3	39.8
45	112.6	118.4	64.5
90	111.2	112.1	94.4
135	110.1	111.7	72.5
180	112.3	118.6	39.7

TABLE G.16. Insulated Vertical Nitrogen Run

GENERAL RUN CONDITIONS					
Run No.	13	Date:	Mar 13, 1985		
Loading	Full	Temp.	21.9 C		
Wind Sp.	0	Solar	0		
Cask P	21.6 psia	Power	14.4 KW		

AXIAL PROFILE DATA				
ELEV	-----Basket Locations-----			
(M)	2J	4J SURFACE	1A	2A
4.9	73.3	82.7		
4.5	146.3	81.0	139.9	145.7
3.8	195.6	109.1		
3.3	207.7	209.4	108.4	186.4
2.8	207.0	110.4		
2.0	193.2	109.0	178.7	172.4
1.4	177.1	175.7	103.8	162.2
0.7	136.8	102.6		
0.2	106.5	95.5	127.6	126.1
0.0	99.5	98.0		

RADIAL PROFILES			DIAMETRICAL PROFILES		
RADIUS	---Position---		RADIUS	---Position---	
(M)	EL.50	EL.123	(M)	EL.50	EL.123
0.00	142.0	51.3	1.11	105.9	108.0
0.13	177.1	207.7	0.58	162.2	186.4
0.25	153.8	175.3	0.25	171.9	203.6
0.38	172.7	203.7	0.09	175.7	209.4
0.49	153.7	175.8	-0.09	177.1	207.7
0.61	162.3	194.3	-0.58	163.6	180.8
0.75	133.5	147.7	-1.11	110.8	115.2
1.11	103.8	108.4	AMB.	21.9	21.9

SURFACE TEMPERATURE PROFILE			
-----Position-----			
ANGLE	EL.50	EL.123	EL.169
-45	107.8	107.7	69.0
0	110.8	108.0	88.9
45	106.5	114.9	76.2
90	104.6	108.8	97.4
135	103.8	108.4	73.0
180	105.9	115.2	41.6



TABLE G.17. Insulated Vertical Vacuum Run

GENERAL RUN CONDITIONS			
Run No.	14	Date:	Mar 19, 1985
Loading	Full	Temp.	23.5 C
Wind Sp.	0	Solar	0
Cask P	Vacuum	Power	14.3 KW

AXIAL PROFILE DATA				
ELEV	Basket Locations			
(M)	2J	4J SURFACE	1A	2A
4.9	62.7	60.4		
4.5	120.2	70.7	112.2	115.6
3.8	179.8	110.4		
3.3	216.6	220.7	110.9	201.2
2.8	229.8	110.6		
2.0	236.2	100.0	226.4	210.4
1.4	231.2	236.1	106.9	218.7
0.7	194.8	98.0		
0.2	124.3	86.3	121.6	119.5
0.0	99.8	98.2		

RADIAL PROFILES			DIAMETRICAL PROFILES		
RADIUS	Position		RADIUS	Position	
(M)	EL.50	EL.123	(M)	EL.50	EL.123
0.00	184.4		1.11	104.0	110.0
0.13	231.2	216.6	0.58	218.7	201.2
0.25	200.8	185.8	0.25	233.7	212.8
0.38	231.2	211.6	0.09	236.1	220.7
0.49	204.5	186.5	-0.09	231.2	216.6
0.61	224.2	207.9	-0.58	209.2	187.6
0.75	153.0	149.6	-1.11	104.7	108.4
1.11	106.9	110.9	AMB.	23.5	23.5

SURFACE TEMPERATURE PROFILE			
Position			
ANGLE	EL.50	EL.123	EL.169
-45	106.2	109.5	76.5
0	104.7	110.0	76.6
45	108.9	112.8	56.0
90	106.5	108.7	88.0
135	106.9	110.9	70.7
180	104.0	108.4	72.9



APPENDIX H

CASK RADIATION MEASUREMENT DATA AND INSTRUMENTATION



## APPENDIX H

### CASK RADIATION MEASUREMENT DATA AND INSTRUMENTATION

This appendix contains a description of the instruments and devices used to obtain gamma and neutron dose rate measurements. It also contains the data obtained with these devices.

#### GAMMA AND NEUTRON INSTRUMENTATION

The thermoluminescent and track etch dosimeters were used to measure gamma and neutron dose rate profiles, respectively. A  $^3\text{He}$  spectrometer, a tissue equivalent proportional counter, and a multisphere spectrometer measured neutron dose equivalent rate and average energy. The intrinsic germanium gamma spectrometer measured the gamma spectrum.

#### Thermoluminescent Dosimeter

The axial and radial gamma dose rate profiles of the cask were measured using thermoluminescent dosimeters (TLDs). Each dosimeter consisted of four  $^7\text{LiF}$  chips placed in a gelatin capsule. The capsule was attached to a 1-in. square styrofoam cube to protect the dosimeter from the high temperatures expected at the surface of the cask. When heated, the TLDs emit light in quantities proportional to the energy deposited in the material by the incident radiation; hence, the need to use the styrofoam cubes to protect the dosimeters from high temperatures. The four chips per dosimeter were used to give good statistical results.

The dosimeters were left on for 2 to 3 days; the dates and times on and off were recorded for each dosimeter. The first set of measurements for a partially loaded cask consisted of 30 locations; the second set of measurements with a fully loaded cask consisted of 54 locations. After exposure of the TLDs from the storage cask, the chips were removed from the gelatin capsules and read out on a Harshaw 2000A detector.

The gamma dose for the TLD is calculated using a calibration factor derived by exposing a set of calibration dosimeters to 100 mR of radiation from a 10-Ci  $^{137}\text{Cs}$  documented source. The average of the readouts from all the calibration chips was used to convert the TLD reader output from nanocoulombs to mR. The results for the four chips in a given dosimeter capsule were averaged and then the background given by a set of control TLDs was subtracted out. The resulting total dose equivalent in mR was divided by the length of time the TLD was on the cask to determine dose rate.

#### Track Etch Dosimeter

The track etch dosimeters (TEDs) were used during the full load of the performance tests to improve the definition of the neutron dose rate profile. The track etch dosimeters were used on only the fully loaded cask, and the measurement locations consisted of 21 points along the side of the cask, 4 on the top, and 8 on the bottom. The dosimeters were left on the cask for a total of about 2 days and then returned and processed.

The track etch dosimeters were made of 1.125-in. by 0.625-in. by 0.07-in. strips of CR-39 plastic, allyl diglycol polycarbonate. They were covered with a 3-mil layer of polyethylene to protect them from background alpha radiation. The dosimeters were also wrapped in aluminum foil during the trip to and from the test site. During the dose rate measurements, the dosimeters were taped directly to the surface of the cask, and the times and locations were individually recorded. Upon exposure to radiation, damage sites are created through neutron bombardment of the polymer, causing proton recoil interactions and breaking some of the polymer crosslinkages. The dosimeters were analyzed using a caustic solution and electrochemical etching to produce visible tracks of the damage sites. The number of tracks were counted and the visible track density was related to the dose rate.

Several track etch dosimeters designated as controls were taken to the site and stored away from the cask to provide an indication of the background radiations received by the dosimeters. The neutron doses for the track etch dosimeters were calculated from the track density (tracks/cm<sup>2</sup>) using the energy response curve at an average neutron energy of 200 keV as given by the  $^3\text{He}$  spectrometer data analysis. The calibration factor was  $5.0 \times 10^{-6}$  tracks/

neutron to convert tracks /cm<sup>2</sup> to neutron fluence (n/cm<sup>2</sup>). The neutron dose was calculated from the fluence using  $6.11 \times 10^{-6}$  mrem/(n/cm<sup>2</sup>). The total dose in mrem was then divided by the time the dosimeter was on the cask to get the dose equivalent rate.

### <sup>3</sup>He Spectrometer

The <sup>3</sup>He spectrometer provides a direct measurement of neutron flux as a function of energy. The detector itself consists of a proportional counter filled with a mixture of <sup>3</sup>He and argon. The neutrons interact with the <sup>3</sup>He to produce a triton and a proton. These charged particles are slowed down by the fill gas and deposit some or all of their energy in the detector. When the charged particles are completely stopped in the sensitive volume of the tube, the energy absorbed is directly proportional to the energy of the incident neutron plus 764 keV, the energy released by the nuclear reaction. The <sup>3</sup>He detector is most sensitive to thermal neutrons due to the 1/v cross section of <sup>3</sup>He for neutron absorption. This results in a large peak at 764 keV, which is used to calibrate the spectrometer.

The data accumulated with the <sup>3</sup>He spectrometer is analyzed using an unfolding code called HESTRIP3 (Brackenbush, Reece, and Tanner 1984), which converts counts/channel into neutron dose equivalent as a function of energy and calculates an average neutron energy. The <sup>3</sup>He spectrometer can be used to determine the neutron energy spectrum for neutrons with energies between thermal and 5 MeV, although it is most accurate between 50 keV and 1 MeV.

### Tissue Equivalent Proportional Counter

The tissue equivalent proportional counter (TEPC) is used to directly measure the neutron dose rate. The TEPC also provides information about the linear energy transfer and quality factor of the incident neutrons. It consists of a hollow sphere or cylinder of tissue equivalent plastic filled with a low pressure tissue equivalent gas. Neutrons interacting within the wall of the TEPC produce recoil protons and heavy ions that travel through the fill gas causing ionization. The electronic pulses created by the charged particles are collected on the counter anode. Because energy deposited in the gas divided by



the mass of the gas is the absorbed dose that would be received by an equivalent volume of tissue in air, it is possible to determine dose equivalent rates directly from the TEPC data. As a result, the TEPC is an absolute dosimeter and does not require independent calibration, so long as the size of the gas cavity is accurately known. The data taken with the tissue equivalent proportional counter is analyzed with the computer code TACI (Cummings 1984), which is run on an HP-87 desktop computer.

#### Multisphere Spectrometer

The multisphere spectrometer is used for determining neutron dose equivalent and spectra for intermediate and high energy neutrons. The detector is a lithium-6 iodide (LiI) scintillation crystal optically coupled to a photomultiplier tube. The detector is used in conjunction with a cadmium cover and five high density polyethylene spheres of varying sizes. For a single location, count rate measurements are taken with the bare detector, with a cadmium cover on the detector, and with a 3-in., 5-in., 8-in., 10-in., and 12-in. diameter polyethylene sphere on the detector. The polyethylene moderates the neutrons, and the resulting slow neutrons produce a distinct peak that can be measured. The incident neutron energy spectrum can be estimated by using the differences in slow neutron count rates given by the different sizes of moderator.

The multisphere spectrometer data is analyzed with the unfolding code SPUNIT (Brackenbush and Scherpelz 1984). The number of counts and the live time for each detector configuration are entered into the code. The code then calculates neutron flux, dose rate, dose equivalent rate, quality factor, and average neutron energy. However, the response function contained in SPUNIT is for a 12.7-mm x 12.7-mm LiI crystal; the crystal used in the measurements was a 4-mm x 4-mm crystal. Therefore, based on the ratio of the volumes of the crystals, a correction factor of 10.1 was used on the SPUNIT results for flux and dose equivalent rate.

#### Intrinsic Germanium Spectrometer

The intrinsic germanium spectrometer was used to provide gamma spectral information. The spectrometer is a semiconductor-type radiation detector and

consists of a germanium crystal operated as a reverse biased diode. Gamma rays that interact within the crystal cause ionization, and the resulting charged particles produce an electron current that is collected at the electrodes. The electron current is proportional to the energy deposited within the crystal. The detector is also useful in identifying source radionuclides. The source radionuclides can be identified by their characteristic photopeaks that are measured by the germanium detector. The magnitude of the peaks can also be compared to estimated relative quantities of radionuclides. Before taking any measurements of the gamma radiation around the cask, calibration runs were made with a  $^{60}\text{Co}$  and a  $^{137}\text{Cs}$  source at the site. Data from the intrinsic germanium detector was analyzed on a Canberra Series 85 multichannel analyzer. The Series 85 has a resident library that contains nuclear decay data from Kocher (1977).

#### Survey Instruments

The PNL neutron survey was performed using a SNOOPY, which consists of a BF3 detector moderated by an 8-1/2 in. polyethylene cylinder. GE-MO used an Eberline Model PNR-4. The SNOOPY provided simple dial readouts for dose equivalent, and was used to check neutron spectrometer and TED results and to locate points where streaming occurred. The PNL gamma survey readings were taken with a standard Hanford Cutie Pie (Eberline RO-3B). GE-MO used an Eberline Model RO-3. Both instruments utilize ion chambers. The PNL survey instruments are described in BNWL-MA-62 PT 2 (Pacific Northwest Laboratory 1973). Information on the Eberline instruments can be obtained from the vendor.

#### SHIELDING DATA

The radiation measurements consisted of a general survey of the cask with the portable survey instruments, a set of measurements with neutron and gamma spectrometers at four locations, and profiles obtained with TLDs and TEDs. The four spectrometer locations were the center of the top lid, center of the bottom, the side of the cask at an elevation of 150 cm with respect to the bottom of the cask at an angle of 90 degrees, and at the top of the neutron shield at an angle of 90 degrees as shown in Figure H.1. The survey and profile points

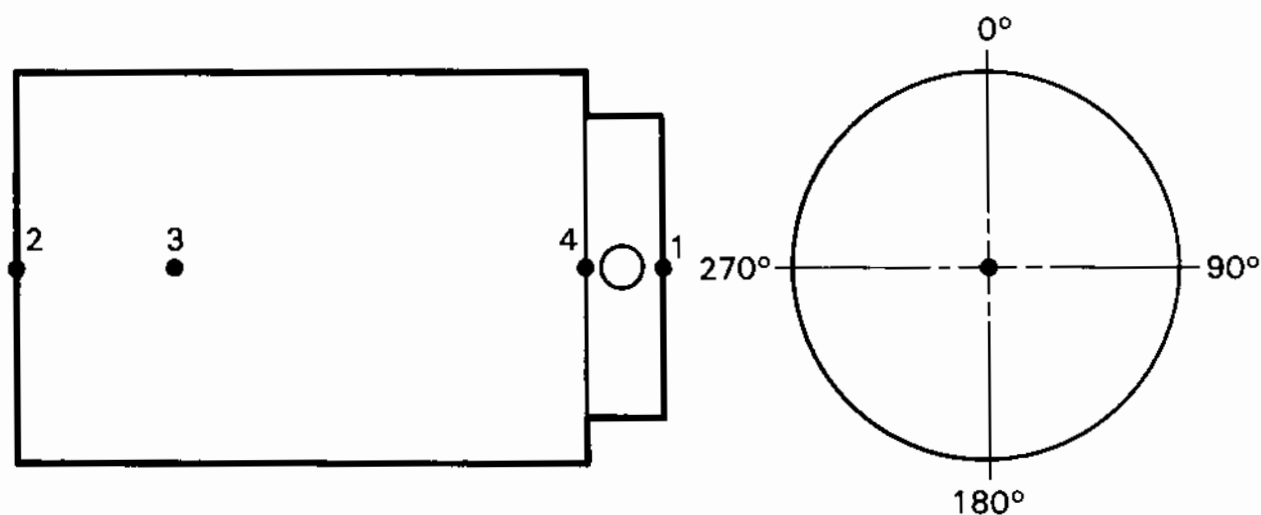


FIGURE H.1. REA 2023 Spent Fuel Storage Cask Spectral Radiation Measurement Location

included the four main locations plus additional points along the side, top, and bottom. A set of measurements was made for both the partially and the fully loaded cask.

#### Gamma Dose Measurements

The gamma dose rates estimated using the TLDs are presented in Tables H.1 and H.2 for the partial and full loads, respectively. The uncertainty in a measurement is the spread in the readings from the four TLD chips contained in a single gelatin capsule. Prior to the TLDs being put on the cask, GE-MO had surveyed the cask at various locations determined by dividing the cask into eight sections and elevations as shown in Figure H.2. Readings were taken by GE-MO personnel with portable instruments (Eberline RO-3) at the intersections of the grid thus created. These readings are found in Table H.3. Similar but fewer gamma dose rates measurements were made by PNL personnel with a Cutie Pie and are given in Table H.4. The GE-MO measurements were taken inside on the decontamination pad; the PNL measurements were taken outside at the test site. The PNL measurements should be adjusted to compensate for overresponse at cold temperatures. Figure H.3 shows the temperature response of the Cutie Pie.



TABLE H.1. Thermoluminescent Dosimeter Results for the REA  
Spent Fuel Storage Cask (Partial Loading)

<u>Side Elevation, cm</u>	<u>Angle, degrees</u>	<u>Dose Rate, mR/hr</u>	<u>Uncertainty, mR/hr</u>
40	45	11.45	0.35
46	45	5.17	0.17
60	45	5.33	0.28
100	45	6.67	0.41
150	0	8.49	0.11
223.1	26.5	8.88	0.60
223.1	45	8.31	0.30
223.1	45	7.99	0.21
300	45	8.32	0.42
350	45	6.64	0.25
380	45	5.46	0.22
408.5	45	6.33	0.34
420	45	6.84	0.16
440	45	12.17	0.57
450	45	11.27	0.44
460	45	8.28	0.50
470	45	14.78	0.97
480	45	19.38	1.95
490	45	3.83	0.05

<u>Top Radius, cm</u>	<u>Angle, degrees</u>	<u>Dose Rate, mR/hr</u>	<u>Uncertainty, mR/hr</u>
0.0	0	26.82	0.77
13.0	45	25.31	0.83
13.0	225	19.97	0.75
37.6	45	20.68	0.42
61.0	45	18.34	0.32
64.5	24.5	13.18	0.30
80.0	26.5	31.10	0.77
80.0	45	28.36	1.40
90.0	26.5	16.38	0.47
90.0	45	19.28	1.85

<u>Bottom Radius, cm</u>	<u>Angle, degrees</u>	<u>Dose Rate, mR/hr</u>	<u>Uncertainty, mR/hr</u>
0.0	0	68.57	2.34

**TABLE H.2.** Thermoluminescent Dosimeter Results for the REA Spent Fuel Storage Cask (Full Loading)

Side Elevation, cm	Angle, degrees	Dose Rate, mR/hr	Uncertainty, mR/hr
20	26.5	21.27	0.63
30	26.5	26.89	1.64
40	26.5	22.84	1.15
46	26.5	9.14	0.50
53	26.5	9.07	0.27
60	26.5	9.02	0.31
100	26.5	11.66	0.44
150	26.5	13.57	0.99
223.1	0	10.47	0.54
223.1	4	11.38	0.67
223.1	26.5	14.43	0.28
223.1	41	12.81	0.60
223.1	45	11.61	0.49
300	26.5	13.36	0.67
380	26.5	9.08	0.16
400	26.5	10.77	0.42
420	26.5	14.27	0.19
435	26.5	9.17	0.31
440	26.5	26.64	0.64
445	26.5	24.99	1.52
450	26.5	20.33	0.35
455	26.5	17.62	0.49
460	26.5	14.59	0.71
465	26.5	16.83	0.87
470	26.5	26.40	1.73
475	26.5	36.79	1.37
480	26.5	34.79	0.63
485	26.5	14.52	0.37
490	26.5	5.20	0.41

TABLE H.2. (contd)

Top Radius, cm	Angle, degrees	Dose Rate, mR/hr	Uncertainty, mR/hr
0.0	0	28.64	1.29
13.0	45	26.92	1.75
13.0	225	24.11	4.95
25.3	45	31.54	1.19
37.6	45	30.86	1.64
49.3	45	37.28	1.29
61.0	45	33.08	1.01
63.5	24.5	32.34	0.95
71.0	45	35.93	1.82
75.0	45	47.86	2.43
77.5	45	61.59	3.41
80.0	45	60.66	3.44
82.5	26.5	71.26	1.04
82.5	45	57.04	3.04
85.0	45	49.90	0.84
90.0	26.5	29.95	2.47
90.0	45	26.41	0.18
95.0	45	11.64	0.23
Bottom Radius, cm	Angle, degrees	Dose Rate, mR/hr	Uncertainty, mR/hr
0.0	0	69.67	1.42
13.0	45	64.40	4.05
37.6	45	84.17	3.78
61.0	45	83.20	3.23
71.0	45	50.82	1.47
80.0	45	23.59	0.50
90.0	45	7.19	0.52



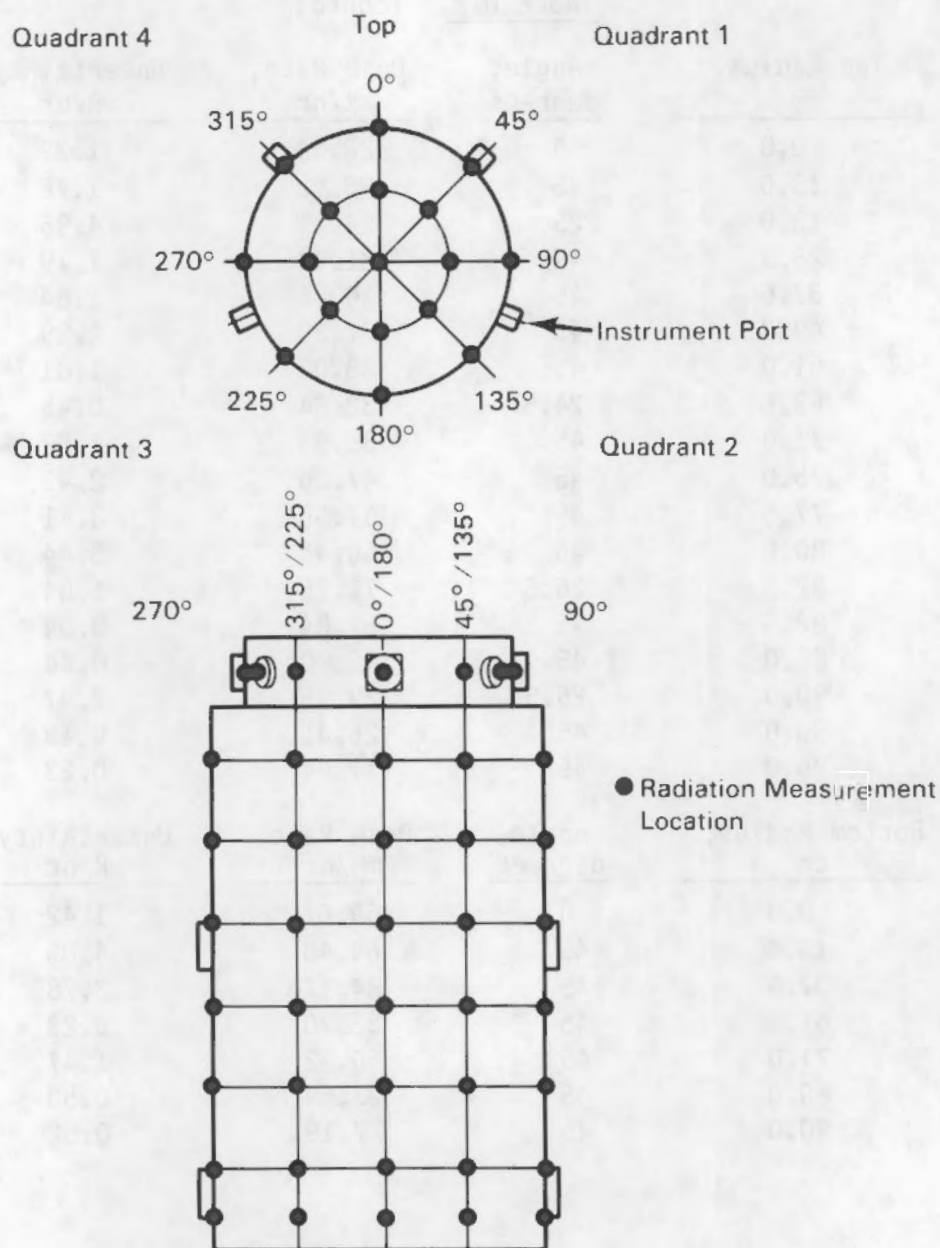


**FIGURE H.2.** Cask Radiation Measurement Locations

The information collected with survey instruments and TLDs provided the shape of the gamma dose rate profile. Additional measurements were taken with an intrinsic germanium spectrometer to determine the gamma spectrum. These measurements were taken at four locations: top center of the cask, bottom center of the cask, side of the cask at an elevation of 150 cm, and top of the

TABLE H.3. REA Cask Radiation Survey Data Taken by General Electric

Location	Partial Loading		Full Loading	
	Gamma Dose Rate, mR/hr	Neutron Dose Rate, mrem/hr	Gamma Dose Rate, mR/hr	Neutron Dose Rate, mrem/hr
Top Center	32	35	30	30
Top 0° 19"	28	30	34	38
Top 0° 38" (Edge)	9	5	18	15
Top 45° 19"	25	33	40	28
Top 45° 38" (Edge)	10	5	28	18
Top 45° High (0 in.)	32	35	60	32 @ 6"
Top 45° Low (38 in.)	10	5	28	18 @ 38"
Top 90° 19"	25	33	36	30
Top 90° 38" (Edge)	8	20	13	18
Top 135° 19"	27	33	36	29
Top 135° 19" (Edge)	8	10	24	12
Top 180° 19"	22	33	29	27
Top 180° 38" (Edge)	6	13	12	15
Top 225° 19"	21	25	31	28
Top 225° 38" (Edge)	8	5	21	5
Top 270° 19"	25	35	29	28
Top 270° 38" (Edge)	11	20	17	15
Top 315° 19"	18	33	28	26
Top 315° 38" (Edge)	9	5	33	14
Trunnion Mount D	5.5	23	5.5	15
Instrument Port 1	15	20	20	25
Upper Trunnion A	2	4	2	4
Instrument Port 2	10	22	10	25
Upper Side 135°	10	30	12	26
Trunnion Mount C	3	23	3.5	19
Upper Side 225°	8	25	15	25
Instrument Port 3	10	20	13	25
Upper Trunnion B	2	3.5	2.3	3.3
Instrument Port 4	9	20	12	24
Vent Port	15	25	10	23
Side 12'-0°	14	1.5	9.5	1.3
Side 12'-45°	10	1.5	12	0.8
Side 12'-90°	11	1.0	9	0.8
Side 12'-135°	8	1.3	9	1
Side 12'-180°	10	1.5	7	1
Side 12'-225°	9	1.0	11	0.9
Side 12'-270°	14	1.0	10	1
Side 12'-315°	11	1.3	12	1.2



TABLE H.3. (contd)

Location	Partial Loading		Full Loading	
	Gamma Dose Rate, mR/hr	Neutron Dose Rate, mrem/hr	Gamma Dose Rate, mR/hr	Neutron Dose Rate, mrem/hr
Side 10'-0°	11	2.5	12	2.3
Side 10'-45°	11	2.0	15	3
Side 10'-90°	11	1.5	11.5	2.4
Side 10'-135°	9	1.5	12	2.1
Side 10'-180°	9	2.3	9	2.1
Side 10'-225°	10	2.5	13	2.3
Side 10'-270°	12	2.5	13	2.2
Side 10'-315°	12	2.5	16	2.8
Side 8'-0°	12	1.8	12	2.5
Side 8'-45°	12	2.3	15	2.6
Side 8'-90°	6	3.5	6	4
Side 8'-135°	10	2.5	13	3.3
Side 8'-180°	10	1.5	10	2.5
Side 8'-225°	11	2.0	14	2.3
Side 8'-270°	6	3.2	6.5	4
Side 8'-315°	14	2.0	17	2.7
Side 6'-0°	12	1.5	12	2.5
Side 6'-45°	12	1.8	15.5	2.5
Side 6'-90°	13	1.7	12.5	2.5
Side 6'-135°	11	2.0	14	3.3
Side 6'-180°	10	2.0	10	2.8
Side 6'-225°	11	2.0	14	3.2
Side 6'-270°	12	1.5	12	2.1
Side 6'-315°	14	2.5	12	2.5
Side 4'-0°	13	1.7	13	2.2
Side 4'-45°	12	2.0	15	2.5
Side 4'-90°	13	2.0	13	2.1
Side 4'-135°	10	1.8	14	2.1
Side 4'-180°	10	1.5	11	2
Side 4'-225°	10	1.5	14	2
Side 4'-270°	13	1.5	13	1.5
Side 4'-315°	13	1.5	16	1.7
Side 2'-0°	8	2.5	8	2.4
Side 2'-45°	9	3.0	11	2.5
Side 2'-90°	4	2.7	4.5	2.6
Side 2'-135°	7	2.0	9	2.4
Side 2'-180°	6	2.0	6	2.1
Side 2'-225°	6	1.5	9	2.3



TABLE H.3. (contd)

Location	Partial Loading		Full Loading	
	Gamma Dose Rate, mR/hr	Neutron Dose Rate, mrem/hr	Gamma Dose Rate, mR/hr	Neutron Dose Rate, mrem/hr
Side 2'-270°	4	1.8	4.5	2.3
Side 2'-315°	9	2.0	11	2.1
Side 1'-0°	10	25.0	11.5	25
Side 1'-45°	16	25.0	24	23
Side 1'-90°	14	23.0	16	25
Side 1'-135°	6	20.0	14	23
Side 1'-180°	11	25.0	11.5	20
Side 1'-225°	13	25	20	25
Side 1'-270°	17	25	17.5	30
Side 1'-315°	16	23	21	25
45° Plane High (Ft In)	18 (189")	30	25	30
45° Plane Low (Ft In)	8.5 (170")	0.75	7	0.8
Drain Port #1	10	22	11	2.7
Drain Port #2	7	23	7.5	27
Bottom Center	78	55	68	50
Bottom Center 0° 19"	40	40	80	50
Bottom Center 0° 38"	4	15	4	7
Bottom Center 45° 19"	54	45	80	45
Bottom Center 45° 38"	5	18	5	10
Bottom Center 90° 19"	38	40	65	47
Bottom Center 90° 38"	4	4	3.2	4.5
Bottom Center 135° 19"	30	45	70	49
Bottom Center 135° 38"	3	20	3.3	10
Bottom Center 180° 19"	48	45	85	49
Bottom Center 180° 38"	4	15	3.9	5
Bottom Center 225° 19"	66	45	120	49
Bottom Center 225° 38"	4	20	4.2	10
Bottom Center 270° 19"	115	47	145	50
Bottom Center 270° 38"	4	5	3.9	7
Bottom Center 315° 19"	76	45	110	50
Bottom Center 315° 38"	5	20	4.5	10

TABLE H.4. PNL Cutie Pie Measurements for REA Cask

Location	Measured Gamma Dose Rates, mR/hr (a)	
	Partial Loading	Full Loading
Top Center	34	40
Top 0 19"	26	44
Top 0 38" (Edge)	14	3
Top 45 38" (Edge)		10
Top 90 19"		48
Top 90 39" (Edge)	8	7
Top 270 38" (Edge)		38
Side 1'-45	16.5	32.5
Side 1'-90		21
Side 2'-45	7	12.5
Side 2'-90		3.4
Side 4'-45	10.5	18
Side 4'-90	12	
Side 6'-45	10.5	18.5
Side 6'-90	12.5	
Side 8'-45		18.5
Side 10'-45	10	12
Side 10'-90	11	
Side 12'-45	7.5	13
Side 12'-90	8	9
Bottom Center	90	75
Bottom 0 19"	43	100
Bottom 45 19"		80
Bottom 90 38" (Edge)	1.6	3
Bottom 270 19"	115	165
Bottom 270 38" (Edge)		40

(a) Readings were taken at a temperature of about  $-6^{\circ}\text{C}$ . At this temperature the Cutie Pie overresponds. To compensate for the overresponse of the instrument, the values in this table should be multiplied by 0.82 to give actual dose rate.

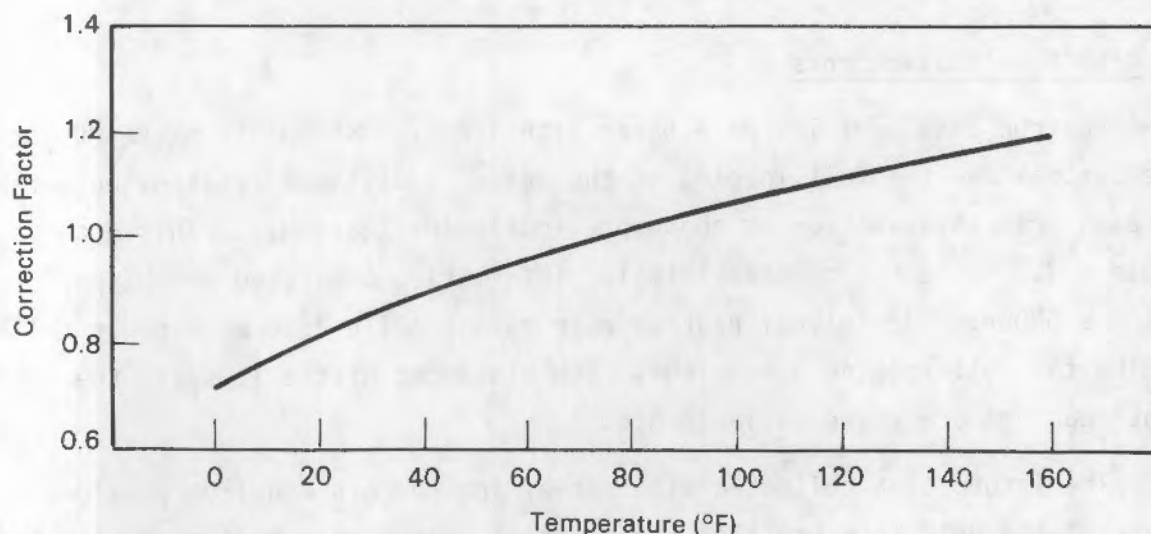


FIGURE H.3. Temperature Response of the Cutie Pie

neutron shield as was shown in Figure 5.26. Gamma spectral information had to be taken 2.5 m away from the surface of the cask due to the high sensitivity of the detector. At each location, three measurements were taken, each at a different detector gain to cover the energy range up to 10 MeV. During the measurements at the top of the cask, the detector was shielded with lead bricks to prevent possible gamma interference from filter units located approximately 200 ft away. For measurements at the bottom and the side, the cask provided the necessary shielding (the side measurement was taken at a 270 degree rather than a 90 degree angle).

The major radionuclides identified were  $^{60}\text{Co}$  and  $^{144}\text{Ce/Pr}$  at the top and bottom of the cask and  $^{144}\text{Ce/Pr}$ ,  $^{154}\text{Eu}$ ,  $^{134}\text{Cs}$ ,  $^{137}\text{Cs}$ ,  $^{106}\text{Ru/Rh}$ , and  $^{60}\text{Co}$  at the side. The differences between the major radionuclides identified at the top and bottom and those identified at the side are caused by the variations in radionuclide distribution along the fuel assembly and shielding materials. The dominance of  $^{60}\text{Co}$  at the top and bottom is due to the activated stainless steel, which is heavily concentrated at the ends of the assemblies. Along the side of the cask the source of radionuclides is almost entirely the spent fuel. The primary contributor at the side is  $^{144}\text{Ce/Pr}$ . The gamma spectra did not vary between the partial loading and the full loading.



### Neutron Dose Measurements

Neutron dose profiles were taken with survey instruments by GE-MO for both the partial and the full loading of the cask. Individual readings were taken at each grid intersection as shown previously in Figure H.2. This data is in Table H.3. Table H.5 contains similar information collected by PNL personnel using a SNOOPY. Additional neutron dose rate profile information was collected during the full loading using TEDs. The placement of the TEDs and the resultant readings are given in Table H.6.

The information collected with survey instruments and TEDs provides the shape of the dose rate profiles. Additional measurement were made with a  $^3\text{He}$  spectrometer, a tissue equivalent proportional counter, and a multisphere spectrometer, to determine neutron dose rate and spectral information. These measurements were taken at four locations previously identified in Figure H.1. The neutron measurements were made at the surface of the cask. Measurements were also taken 1 m from the surface of the cask with the TEPC and the multisphere spectrometer at those same four locations, to provide information on how the dose rates varied with distance from the cask.

TABLE H.5. PNL SNOOPY Measurement for REA Cask

Location	Neutron Dose Rate Gamma Dose Rates, mrem/hr	
	Partial Loading	Full Loading
Top Center	20	19
Top D 19"	19	
Top 90 19"		17
Top 90 38" (Edge)	5	6
Side 6"-90		7
Side 1'-90		14.5
Side 2'-45		1.7
Side 2'-90		4.5
Side 10'-45	1.5	
Side 12'-90		1.6
Bottom Center	50	60
Bottom 90 19"		45
Bottom 270 19"		45
Bottom 90 38" (Edge)	10	



TABLE H.6. Track Etch Dosimeter Results for the REA Spent Fuel Storage Cask (Full Loading)

Side Elevation, cm	Angle, degrees	Tracks/cm <sup>2</sup> -hr, adjusted	Dose Rate, mR/hr
0	26.5	4.10	5.0
20	26.5	11.70	14.3
30	26.5	13.30	16.2
40	26.5	7.50	9.2
50	26.5	0.99	1.2
60	26.5	1.20	1.5
100	26.5	1.20	1.5
150	26.5	2.81	3.4
223.1	0	3.17	3.8
223.1	4	2.96	3.6
223.1	26.5	5.03	6.2
223.1	41	0.22	2.8
223.1	45	2.11	2.6
300	26.5	2.61	3.2
380	26.5	1.41	1.7
420	26.5	0.00	0.0
430	26.5	0.70	0.9
440	26.5	7.62	9.3
450	26.5	4.91	6.0
460	26.5	5.72	7.0
470	26.5	3.51	4.3
480	26.5	3.80	4.6
490	26.5	1.70	2.1
Top Radius, cm	Angle, degrees	Tracks/cm <sup>2</sup> -hr, adjusted	Dose Rate, mR/hr
0.0	45	10.33	12.6
60.0	45	10.02	12.3
80.0	45	4.74	5.8
95.0	45	2.22	2.7
Bottom Radius, cm	Angle, degrees	Tracks/cm <sup>2</sup> -hr, adjusted	Dose Rate, mR/hr
0.0	45	26.86	32.8
0.0	135	24.41	29.8
0.0	225	27.97	34.2
0.0	315	19.37	23.7
60.0	45	16.80	20.5
80.0	45	12.72	15.5
95.0	45	3.67	4.5
97.5	45	4.94	6.0
100.0	45	3.25	4.0
105.0	45	4.32	5.3
107.5	45	2.95	3.6
110.0	45	2.15	2.6



The neutron dose rate measurements for the partial and full loading are given in Tables H.7 and H.8 for the  $^3\text{He}$  spectrometer ( $^3\text{He}$ ), tissue equivalent proportional counter (TEPC), the multisphere spectrometer (M/S), the pocket rem meter (PRM), and the SNOOPY survey instrument.

The neutron energy spectra measured by the  $^3\text{He}$  spectrometer at the top, bottom, and side of the cask are given in Figure H.4. The neutron flux distribution is given in 20 keV energy bins for energies between 30 keV and 1 MeV. The minima in the spectra for the top and bottom measurements correspond to absorption resonances in the neutron cross sections for iron and oxygen. Due to the poor resolution in the data along the side, it is difficult to identify any real minima in the neutron energy spectrum at that location. The flux weighted average neutron energy as estimated in the analysis is around 200 keV for the top and bottom, and 150 keV for the two measurements along the side.

TABLE H.7. Neutron Dose Rate Measurements at Partial Loading

Location	Dose Rate, mrem/hr				
	He-3	TEPC	M/S	PRM	SNOOPY <sup>(b)</sup>
Top of Cask-CL					
@ contact	17.0	13.6 <sup>(a)</sup>	17.3	16.4	20
@ 1 meter			6.92	5.93	7.5
Bottom of Cask-CL					
@ contact	39.9	41.8	34.3	49.0	50
@ 1 meter		15.0	15.3	14.6	18
Side of Cask-90 (el. = 150 cm)					
@ contact	1.22	1.50	1.33	1.92	1.7
Top of Neutron Shield					
@ contact	8.14			11.8	12

(a) The TEPC detector blew over during the night at an undeterminate time; therefore, the time of the run during which the detector was at the measurement location is unknown. The location at which the TEPC was found was at the edge of the cask, which has a much lower dose rate than at the center.

(b) The dose rate as converted from counts/second from a scaler attached to the SNOOPY using 1.44-4 mrem/count from  $^{252}\text{Cf}$  calibration run.



TABLE H.8. Neutron Dose Rate Measurements at Full Loading

Location	Dose Rate, mrem/hr				
	He-3	TEPC	M/S	PRM	SNOOPY(a)
Top of Cask-CL					
@ contact	13.7	13.1	12.2	16.9	19 (16)
@ 1 meter		4.33	5.2	6.65	6.5 (5.2)
Bottom of Cask-CL					
@ contact	32.9	44.0	32.2	60.6	60 (47)
@ 1 meter		11.8	11.2	19.8	18 (15)
Side of Cask-90 (el. = 150 cm)					
@ contact	1.84	1.46	1.51	3.40	2.0 (1.5)
@ 1 meter		0.87	0.97	2.30	1.4 (1.1)
Top of Neutron Shield					
@ contact	11.3	8.9		17.8	13.5 (11)

(a) The dose rate as converted from counts/second from a scaler attached to the SNOOPY using 1.44-4 mrem/count from  $^{252}\text{Cf}$  calibration run.

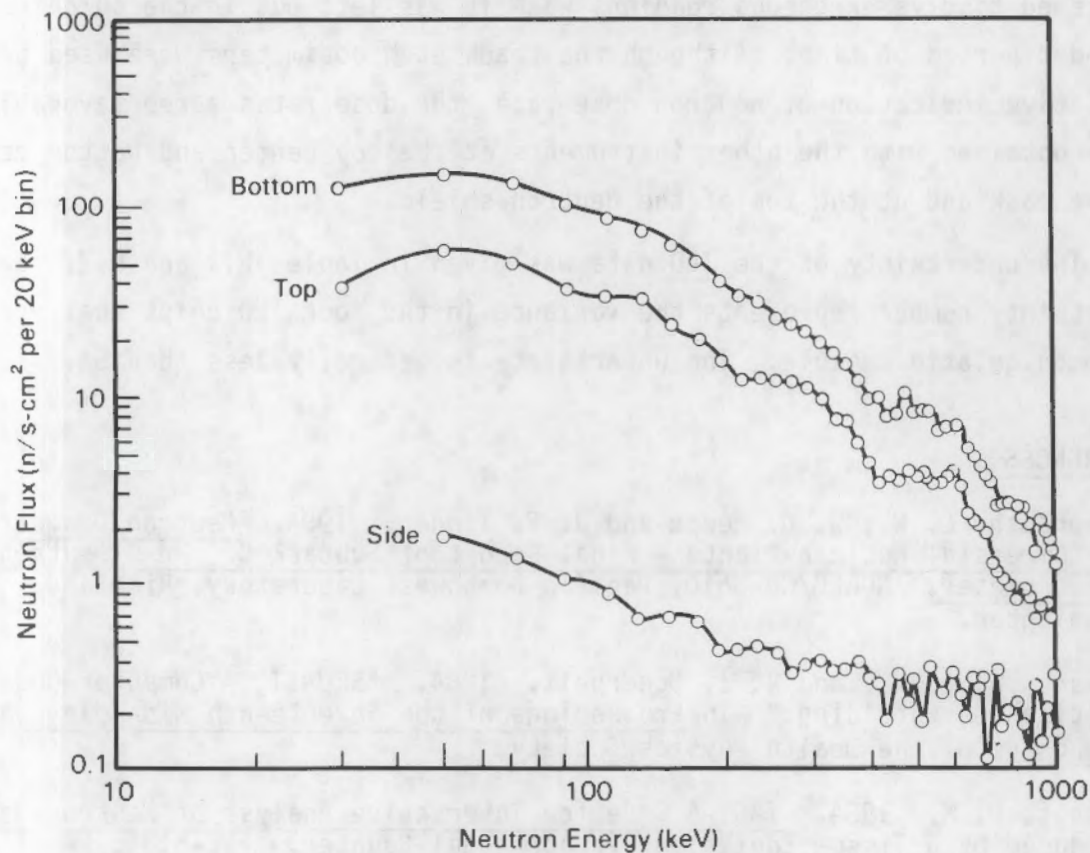


FIGURE H.4.  $^3\text{He}$  Spectrometer Results

The average neutron energy decreased slightly from the partial loading to the full loading. This is due to the self-shielding of the fuel, especially on the ends where there would tend to be less streaming and reflection when the cask was fully loaded.

#### DATA PRECISION

The results of the  $^3\text{He}$  spectrometer, the TEPC, and the multisphere spectrometer are within 5% to 20% of each other, which is very good when measuring neutron dose equivalents. The SNOOPY results are higher than the  $^3\text{He}$ , the TEPC, and the multispheres, which is to be expected. Survey instruments are energy-dependent and are usually calibrated in a hard spectrum, such as PuBe or  $^{252}\text{Cf}$ , which causes the instrument to read high in a softer spectrum. The pocket rem meter (PRM) is an experimental instrument which is still in the developmental stage. The PRM seemed to perform adequately in most cases, but it seemed to give erroneous readings when it was left out in the cold for any extended period of time. Although the track etch dosimeters were used only as a relative indication of neutron dose rate, the dose rates agree favorably with those obtained with the other instruments at the top center and bottom center of the cask and at the top of the neutron shield.

The uncertainty of the TLD data was given in Tables H.1 and H.2. Each uncertainty number represents the variance in the four TLD chips that occupied a common gelatin capsule. The uncertainty is generally less than 5%.

#### REFERENCES

- Brackenbush, L. W., W. D. Reece and J. E. Tanner. 1984. Neutron Dosimetry at Commercial Nuclear Plants - Final Report of Subtask C: He-3 Neutron Spectrometer. NUREG/CR-3610, Pacific Northwest Laboratory, Richland, Washington.
- Brackenbush, L. W., and R. I. Scherpelz. 1984. "SPUNIT, A Computer Code for Multisphere Unfolding." In Proceedings of the Seventeenth Mid-Year Topical Symposium of the Health Physics Society.
- Cummings, F. M. 1984. TACI-A Code for Interactive Analysis of Neutron Data Produced by a Tissue Equivalent Proportional Counter. PNL-5136, Pacific Northwest Laboratory, Richland, Washington.



Kocher, D. C. 1977. Nuclear Decay Data for Radionuclides Occuring in Routine Releases from Nuclear Fuel Cycle Facilities. ORNL/NUREG/TM-102, Oak Ridge National Laboratory, Oak Ridge, Tennessee.

Pacific Northwest Laboratory. 1973. Portable Radiation Survey Instrument Manual. BNWL-MA-62 PT2, Richland, Washington.



Report of the Joint Fact-Finding Commission on the  
Activities of the Central Intelligence Agency in  
the United States, 1975-1976

Executive Summary  
The Joint Fact-Finding Commission was established by the  
House of Representatives in 1975 to investigate the  
activities of the Central Intelligence Agency in the  
United States.

1. Introduction  
2. Background  
3. Findings  
4. Conclusions  
5. Recommendations

DISTRIBUTION

<u>No. of Copies</u>		<u>No. of Copies</u>	
	<u>OFFSITE</u>		
110	DOE Technical Information Center		W. Stringfield U.S. Department of Energy Office of Civilian Radioactive Waste Management Washington, DC 20545
	R. Bown U.S. Department of Energy Office of Civilian Radioactive Waste Management RW-30 Washington, DC 20545		C. P. Gertz U.S. Department of Energy Idaho Operations Office 550 2nd Street Idaho Falls, ID 83401
	J. Epstein U.S. Department of Energy Office of Civilian Radioactive Waste Management RW-30 Washington, DC 20545		K. G. Golliher U.S. Department of Energy Albuquerque Operations Office P.O. Box 5400 Albuquerque, NM 87115
	J. R. Hilley U.S. Department of Energy Office of Storage and Transportation Systems Washington, DC 20545		L. Lanni U.S. Department of Energy Magnetic Fusion and Nuclear Division San Francisco Operations Office 1333 Broadway Oakland, CA 94612
	D. E. Shelor U.S. Department of Energy Office of Civilian Radioactive Waste Management RW-32 Washington, DC 20545		C. Matthews U.S. Department of Energy Oak Ridge National Laboratory P.O. Box E Oak Ridge, TN 37830
	H. Steinburg U.S. Department of Energy Office of Storage and Transportation Systems RW-33 1000 Independence Ave. Washington, DC 20585		D. Veith U.S. Department of Energy Nevada Operations Office P.O. Box 14100 Las Vegas, NV 89114



No. of  
Copies

N. H. Davison  
U.S. Nuclear Regulatory  
Commission  
Office of Nuclear Materials  
Safety and Safeguards  
Washington, DC 20555

C. Feldman  
U.S. Nuclear Regulatory  
Commission  
Office of Nuclear Regulatory  
Research  
MS 5650 NL  
Washington, DC 20555

W. Lake  
U.S. Nuclear Regulatory  
Commission  
Office of Nuclear Materials  
Safety and Safeguards  
Washington, DC 20555

C. H. Peterson  
U.S. Nuclear Regulatory  
Commission  
Office of Nuclear Material  
Safety and Safeguards  
MS 62355  
Washington, DC 20555

J. A. Carr  
Battelle Memorial Institute  
Office of Nuclear Waste  
Isolation  
505 King Avenue  
Columbus, OH 43201

B. A. Rowles  
Battelle Memorial Institute  
Office of Nuclear Waste  
Isolation  
505 King Avenue  
Columbus, OH 43201

W. R. Juergens  
Brooks & Perkins  
12633 Inkster Road  
Livonia, MI 48150

No. of  
Copies

R. Kunita  
Carolina Power & Light Co.  
P.O. Box 1551  
Raleigh, NC 27602

C. K. Anderson  
Combustion Engineering, Inc.  
1000 Prospect Hill Road  
Windsor, CT 06095

Ebasco Services Incorporated  
Two World Trade Center  
New York, NY 10048

D. H. Schoonen  
EG&G  
P.O. Box 1625  
Idaho Falls, ID 83415

P. E. Eggers  
Eggers Ridihalgh Partners, Inc.  
1445 Summit Street  
Columbus, OH 43201

FLUOR Engineers, Inc.  
Advanced Technology Division  
P.O. Box C-11944  
Santa Anna, CA 92711-1944

J. W. Doman  
Morris Operation  
General Electric Company  
7555 E. Collins Road  
Morris, IL 60450

E. E. Voiland  
General Electric Company  
Nuclear Fuel & Services  
Division  
7555 E. Collins Road  
Morris, IL 60450

R. Anderson  
General Nuclear Services, Inc.  
135 Darling Drive  
Avon, CT 06001



No. of  
Copies

V. J. Barnhart  
General Nuclear Services, Inc.  
135 Darling Drive  
Avon, CT 06001

J. D. Rollins  
General Nuclear Services, Inc.  
135 Darling Drive  
Avon, CT 06001

L. B. Ballou  
Lawrence Livermore National  
Laboratory  
P.O. Box 808  
Livermore, CA 94550

M. W. Schwartz  
Lawrence Livermore National  
Laboratory  
P.O. Box 808  
Livermore, CA 94550

C. F. Smith  
Lawrence Livermore National  
Laboratory  
P.O. Box 808  
Livermore, CA 94550

G. Bosler  
Los Alamos National Laboratory  
Los Alamos, NM 87545

P. Rinard  
Los Alamos National Laboratory  
Los Alamos, NM 87545

H. Lowenburg  
Lowenburg Associates  
1091 Rosemont Drive  
Rockville, MD 20852

J. Houston  
Nuclear Assurance Corporation  
5720 Peach Tree Parkway  
Norcross, GA 30092

No. of  
Copies

R. T. Haelsig  
Nuclear Packaging Inc.  
1010 S. 336th Street  
Federal Way, WA 98003

L. E. Wiles  
Numerical Applications, Inc.  
825 Goethals Drive  
Richland, WA 99352

J. V. Massey  
NUTECH Engineers  
145 Martinvale Lane  
San Jose, CA 95116

C. E. Parks  
Oak Ridge National Laboratory  
P.O. Box X  
Oak Ridge, TN 37831

D. Woods  
Ralph M. Parsons Co.  
100 West Walnut Street  
Pasadena, CA 91124

T. L. Sanders  
Sandia National Laboratory  
Albuquerque, NM

M. E. Mason  
Transnuclear, Inc.  
1 N. Broadway  
White Plains, NY 10601

B. R. Teer  
Transnuclear, Inc.  
1 N. Broadway  
White Plains, NY 10601

TRW, Inc.  
Energy Development Group  
Suite 201  
200 Union Blvd.  
Denver, CO 80228

No. of  
Copies

No. of  
Copies

C. E. King  
Uranium Mgt. Corp.  
175 Curtner Ave. MC 620  
San Jose, CA 95125

M. L. Smith  
Virginia Power Co.  
P.O. Box 26666  
Richmond, VA 23261

A. R. Hakl  
Westinghouse Electric Corp.  
Waste Technology Services  
Division  
P.O. Box 10864  
Pittsburg, PA 15236

J. H. Saling  
Westinghouse Electric Corp.  
Waste Technology Services  
Division  
P.O. Box 10864  
Pittsburg, PA 15236

ONSITE

2 DOE Richland Operations Office

R. D. Izatt  
J. P. Collins

2 Rockwell Hanford Operations

C. L. Brown  
G. T. Harper

51 Pacific Northwest Laboratory

G. H. Beeman  
L. W. Brackenbush  
B. M. Cole  
J. M. Cuta  
J. M. Creer (10)  
M. D. Freshley  
E. R. Gilbert  
R. J. Guenther  
R. L. Goodman  
R. J. Hall  
C. M. Heeb  
U. P. Jenquin  
A. B. Johnson, Jr.  
D. K. Kreid  
N. J. Lombardo  
R. A. McCann  
J. L. McElroy  
M. A. McKinnon (10)  
T. E. Michner  
D. F. Newman  
D. R. Oden, Jr.  
D. R. Rector  
R. A. Stokes  
J. E. Tanner  
D. S. Trent  
C. L. Wheeler  
Technical Information (5)  
Publishing Coordination (2)